

A MULTI-PROXY APPROACH CONSIDERING REEF, SAND
APRON AND LAGOON DEVELOPMENT IN RESPONSE TO
LATE QUATERNARY GEOMORPHOLOGICAL AND
ENVIRONMENTAL CHANGES

(186 SEITEN, 54 ABBILDUNGEN,
17 TABELLEN, 59 ANHÄNGE)

DISSERTATION
ZUR ERLANGUNG DES DOKTORGRADES
DER NATURWISSENSCHAFTEN

VORGELEGT BEIM FACHBEREICH 11
DER JOHANN WOLFGANG GOETHE–UNIVERSITÄT
IN FRANKFURT AM MAIN

VON
ANJA ISAACK
AUS TÜBINGEN

FRANKFURT (2016)
(D 30)

vom Fachbereich 11 Geowissenschaften/Geographie der
Johann Wolfgang Goethe Universität als Dissertation angenommen.

Dekan: Prof. Dr. Peter Lindner

Gutachter:

Prof. Dr. Eberhard Gischler

Institut für Geowissenschaften, Goethe Universität, Frankfurt am Main, Deutschland

Dr. Gilbert F. Camoin

Centre Européen de Recherche et d'Enseignement de Géosciences de l'Environnement
(CEREGE), Aix-en-Provence, France

Datum der Disputation: 16.06.2017

TABLE OF CONTENTS

Acknowledgements	b
Dedication	c
Abstract	1
Chapter 1: Introduction	3
Chapter 2: The Significance of Sand Aprons in Holocene Atolls and Carbonate Platforms ...	12
Chapter 3: Late Quaternary Barrier and Fringing Reef Development of Bora Bora (Society Islands, South Pacific): first Subsurface Data from the Darwin-type Barrier-Reef System	34
Chapter 4: A new model evaluating Holocene sediment dynamics: insights from a mixed carbonate-siliciclastic lagoon (Bora Bora, Society Islands, French Polynesia, South Pacific)	77
Chapter 5: Facies variations in the mixed carbonate-siliciclastic lagoon of Bora Bora, French Polynesia: the influence of Holocene sea-level and climate change in the South Pacific	136
Chapter 6: Summary and Outlook	177
Zusammenfassung	182
List of Notations and Abbreviations	d
Supplemental material	e
Appendix	j
Curriculum Vitae	rrr

Anyone who has ever passed over a reef in a boat or in an airplane or seen a reef underwater cannot fail to have been impressed by the ever present beautiful play of colors. It is probably this beauty, as much as anything, that has stimulated man's curiosity as to the how and why of reef development [...]

Edward Purdy, 1974

ABSTRACT

In light of the global sea-level rise and climate change of the 21th century, it is important to look back into the recent past in order to understand what the future might hold. A multi-proxy data set was compiled to evaluate the influence of geomorphological and environmental factors, such as antecedent topography, subsidence, sea level and climate, on reef, sand apron and lagoon development in modern carbonate platforms through the Holocene. Therefore, a combination of remote sensing and morphological data from 122 modern carbonate platforms and atolls in the Atlantic, Indian and Pacific Oceans were conducted, along with a case study from the oceanic (Darwinian) barrier-reef system of Bora Bora, French Polynesia, South Pacific.

The influence of antecedent topography and platform size as factors controlling Holocene sand apron development and extension in modern atolls and carbonate platforms is hypothesized. Antecedent topography describes the elevation and relief of the underlying Pleistocene topography (karst) and determines the distance from the sea floor to the rising postglacial sea level. Maximum lagoon depth and marginal reef thickness, when available in literature, were used as proxies for antecedent topography. Sand apron proportions of 122 atolls and carbonate platforms from the Atlantic, Indian and Pacific Oceans were quantified and correlated to maximum lagoon depth, total platform area and marginal reef thickness. This study shows that sand apron proportions increase with decreasing lagoon depths. Sand apron proportions also increase with decreasing platform area. The interaction of antecedent topography and Holocene sea-level rise is responsible for variations in accommodation space and at least determines the extension of the lateral expansion of sand aprons. In general, sand apron formation started when marginal reefs approached relative sea level. Spatial and regional variations in sea-level history let sand apron formation start earlier in the Indo-Pacific region (transgressive-regressive) than in the Western Atlantic Ocean (transgressive).

The influence of sea level, antecedent topography and subsidence of a volcanic island on late Quaternary reef development was evaluated based on six rotary core transects on the barrier and fringing reefs of Bora Bora. This study was designed to revalue the Darwinian model, the subsidence theory of reef development, which genetically connects fringing reef, barrier reef and atoll development by continuous subsidence of the volcanic basement. Postglacial sea-level rise, and to a minor degree subsidence, were identified as major factors controlling Holocene reef development in that they have created accommodation space and controlled reef architecture. Antecedent topography was also an important factor because the

Holocene barrier reef is located on a Pleistocene barrier reef forming a topographic high. Pleistocene soil and basalt formed the pedestal of the fringing reef. Uranium-Thorium dating shows that barrier and fringing reefs developed contemporaneously during the Holocene.

In the barrier-reef lagoon of Bora Bora, the influence of environmental factors, such as sea level and climate, tsunamis and tropical cyclones controlling Holocene sediment dynamics was evaluated based on sedimentological, paleontological, geochronological and geochemical data. The lagoonal succession comprises mixed carbonate-siliciclastic sediments overlying peat and Pleistocene soil. The multi-proxy data set shows variations in grain-size, total organic carbon (proxy for primary productivity), Ca and Cl element intensities (proxies for carbonate availability and lagoonal salinity) during the mid-late Holocene. These patterns could result from event sedimentation during storms and correlate to event deposits found in nearby Tahaa, probably induced by elevated cyclone activity. Accordingly, elevated erosion and runoff from the volcanic island and lower lagoonal salinity would be a result of rainfall during repeated cyclone landfall. However, Ti/Ca and Fe/Ca ratios as proxies for terrigenous sediment delivery peaked out in the early Holocene and declined since the mid-Holocene. Benthic foraminifera assemblages do not indicate reef-to-lagoon transport. Alternatively, higher and sustained hydrodynamic energy is probably induced by stronger trade winds and a higher-than-present sea level during the mid-late Holocene. The increase in mid-late Holocene sediment dynamics within the back-reef lagoon is supposed to display sediment-load shedding of sand aprons due to the oversteepening of slopes at sand apron/lagoon edges during their progradation rather than an increase in tropical storm activity during that time.

The influence of sea-level and climate changes on sediment import, composition and distribution in the Bora Bora lagoon during the Holocene is validated. Lagoonal facies succession comprises siderite-rich marly wackestones, foraminifera-siderite wackestones, mollusk-foraminifera marly packstones and mollusk-rich wackestones during the early-mid Holocene, and mudstones since the mid-late Holocene. During the early Holocene, enhanced weathering and iron input from the volcanic island due to wetter climate conditions led to the formation of siderite within the lagoonal sediments. The geochemical composition of these siderites shows that precipitation was driven by microbial activity and iron reduction in the presence of dissolved bicarbonate. Chemical substitutions at grain margins illustrate changes in the oxidation state and probably reflect changes in pore water chemistry due to sea-level rise and climate change (rainfall). In the late Holocene, sediment transport into the lagoon is hampered by motus on the windward side of the lagoon, which led to early submarine lithification within the lagoon.

CHAPTER 1

INTRODUCTION

1.1 Scientific rationale

Coral-reefs systems and modern carbonate platforms have already been subject to the impact of sea-level and climate change, and they will be subject to the effects of future sea-level and climate change (Woodroffe and Webster, 2014, and references therein).

As global sea-level rise and climate change have been accelerating during the last few centuries (ICPP, 2014), a better understanding of how sea-level and climate change had affected coral reef and lagoon development during the recent past will be crucial in understanding how these systems will react in terms of future sea-level and climate changes. In this context, a multidisciplinary and multifaceted view regarding investigations on coral-reef systems is important in order to fully understand their complexity in time and space (Hubbard, 2016). The potential of coral reef and lagoon systems as recorders and archives for palaeo-environmental and climate changes is known for a long time and scientific drilling into modern coral reefs and lagoons is challenging (fig. 1/1; Camoin and Webster, 2015; Braithwaite, 2016, and references therein).

In general, modern carbonate platforms such as fringing reefs, barrier reefs and atolls are built ups consisting of different integral geomorphological elements, such as the marginal (and fringing) reefs, sand aprons and the lagoon (e.g., Rankey et al., 2011; fig. 1/2). In case of fringing and barrier reef settings, a central volcanic island is also present (fig. 1/2). Within the platform system, every geomorphological element has its own function: the marginal reefs represent the highly productive areas where the main carbonate production takes place and carbonate sediment is generated (e.g., Burne, 1991). In the back-reef area, sand aprons form sediment pathways from the reef crest into the lagoon (Marshall and Davies, 1982; Woodroffe et al., 1994; Purdy and Gischler, 2005; Harris et al., 2014a). The lagoon itself acts as a sediment trap (e.g., Hopley, 2011) and receives carbonate sediments from the outer reef area, as well as from in situ carbonate production (Stoddart, 1969; Scoffin and Tudhope, 1988; Kench, 2011). Particularly in fringing and barrier-reef settings, a volcanic hinterland represents a further sediment source and imports siliciclastic material into the lagoon (e.g., Zinke et al., 2003a).

The structure of atolls and modern carbonate platforms has been linked to a bucket with marginal reefs holding a pile of unconsolidated sediment (Ladd, 1949). In the late Quaternary,



Fig. 1/1: Scientific drilling into reefs and the lagoon; a) Rotary drilling into the barrier reef, an elevated Holocene reef terrace; b) Rotary drilling into the barrier reef, the yellow arrow marks the reef terrace from (a), photo: S. Haber; c) Rotary drilling into the fringing reef; d) Vibrocoring equipment; e) Preparation for vibrocoring on board, photo G Meyer; f) Rossfelder vibrocoring device floating in water, photo G. Meyer

marginal reefs frequently kept pace with the postglacial sea-level rise, however, the sedimentation of back-reef areas and lagoonal infill lagged behind and created “empty buckets” geometries (high reef rim and deep lagoon; Schlager, 1993; Purdy and Gischler, 2005).

There is still an ongoing debate regarding which geologic process, i.e., subsidence (Darwin, 1842), meteoric dissolution and antecedent topography (MacNeil, 1954; Purdy, 1974; Purdy

and Winterer, 2001, 2006), sea-level variability (Daly, 1915), biotic self-organisation (Schlager and Purkis, 2013, 2015) led to the formation of these empty bucket structures. Recently published results on numerical modeling suggest that a combination of these factors drove development of the modern platform morphologies (e.g., Toomey et al., 2013, 2016). The interpretations of unfilled buckets (meaning unfilled accommodation space) would have important implications for the conceptual methods of sequence stratigraphy, e.g., in that cycle thickness equals accommodation space or not, and represents a valid proxy for the reconstruction of sea-level variations through time (Purdy and Gischler, 2005).

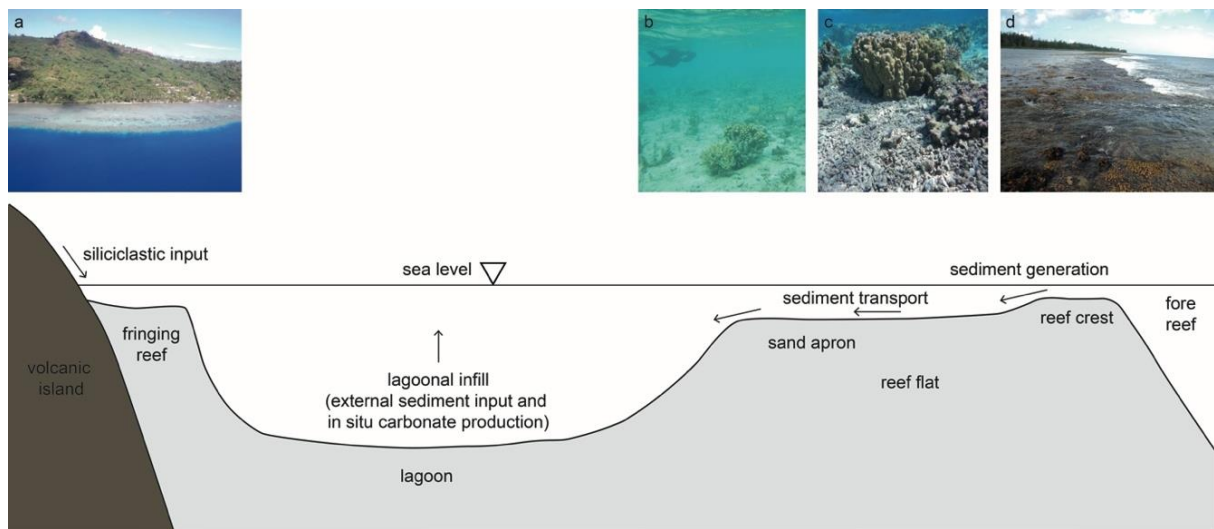


Fig. 1/2: Schematic cross section of the barrier-reef system of Bora Bora, South Pacific showing the geomorphological platform elements and observations of the study area: **a)** Aerial photograph, view to W, with the volcanic island, fringing reef and deep blue lagoon; **b)** Underwater photograph showing the back-reef area. Coral cover is sparse and the turbidity indicates (fine-)sediment transport across the reef flat towards the lagoon; **c)** Underwater photograph, with corals and coral rubble close to the reef crest; **d)** Photograph, view to SW, showing the reef crest at low tides, with a wave-breaking spur and groove system towards the open ocean

Environmental changes such as short-term climate fluctuations during the late Quaternary are orbitally driven, i.e., reflecting periodicities of 23,000 years (precession), 41,000 years (obliquity), and 100,000 years (eccentricity), as proposed by Milankovitch in 1941 (e.g., Woodroffe and Webster, 2014). Since the last glacial maximum (ca. 23,000 yrs BP), postglacial sea-level rise was mainly driven by the melting of land-based ice sheets (e.g., Camoin and Webster, 2015). When deglaciation ended in the mid-late Holocene, sea level was above modern level. Evidence for this sea-level highstand is obvious throughout the Indo-Pacific region (Pirazzoli et al., 1987; Pirazzoli and Montaggioni, 1988; Pirazzoli, 1991; Hallmann et al., 2013). In Bora Bora, elevated coral reef terraces occur on the outer reef flat (fig. 1/3).

The variability in the course of the Holocene sea level is contributed to regional disparities in the pattern of relative sea-level history, primarily caused by glacio and hydro-isostatic effects, i.e., Earth's return to equilibrium after the exchange of water mass between the

continents and ocean, otherwise known as the so-called glacial isostatic adjustment (GIA, Lambeck et al., 2010, 2014), and the redistribution of water masses in the global ocean, otherwise known as so-called equatorial oceanic siphoning (Mitrovica and Peltier, 1991; Mitrovica and Milne, 2002; Milne and Mitrovica, 2008).



Fig. 1/3: Elevated reef terrace in Bora Bora indicating the mid-late Holocene sea-level highstand

According to these authors, two physical mechanisms are responsible for the equatorial oceanic siphoning effect and dominated the mid-late Holocene sea-level highstand and fall. The ice-sheet loading of continents caused a subsidence in the landmass and, in return, an uplift of the peripheral seafloor. Due to the loss of massive land-based ice sheets into adjacent ocean basins, the continental landmasses rebound. An associated influx of meltwater into the ocean basins results in the collapse of peripheral forebulges and fall of sea level in equatorial (far-field) regions (fig. 1/3a; Mitrovica and Milne, 2002). The second process is linked to the ocean load-induced levering of continental margins and describes the addition of meltwater to offshore ocean regions of subsidence, which produces a global drop in sea surface and induces a sea-level fall (fig. 1/3b; Mitrovica and Milne, 2002). In summary, the mid-late Holocene sea-level fall is caused by water masses drawn from equatorial regions to fill accommodation caused by collapsing peripheral forebulges and continental levering (Mitrovica and Milne, 2002).

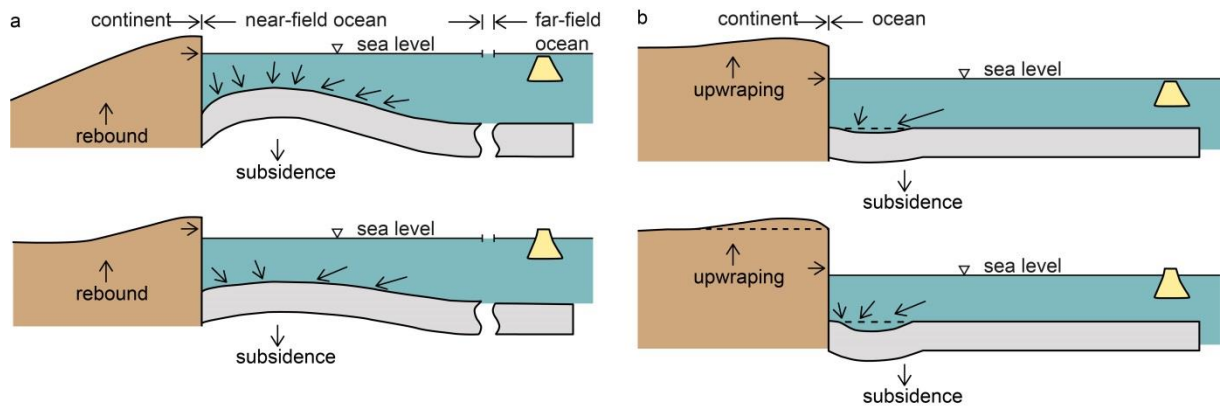


Fig. 1/4: Schematic illustration of the equatorial oceanic siphoning effect (modified after Mitrovica and Milne, 2002); **a**) collapse of forebulges; **b**) continental levering (see text)

1.2 Objectives

The present doctoral thesis comprises a multi-proxy approach considering late Quaternary reef, sand apron and lagoon development in order to improve our understanding of long term environmental and geomorphological changes in these systems. Particular attention is paid to the interaction of reef accretion, lagoonal sedimentation, sediment transport mechanisms and controlling factors of reef and lagoon development in the barrier-reef system of Bora Bora, South Pacific (Chapters 3, 4 and 5). The objectives of this study are as follows:

- 1) Evaluation of the influence of geomorphological platform features and sea-level variations in the accretion and lateral extensions of sand aprons
- 2) Evaluation of the influence of antecedent topography, subsidence, sea level, climate and siliciclastic input on barrier and fringing-reef development
- 3) Evaluation of the same factors controlling sediment dynamics (short-term event deposition versus long-term sedimentary processes) and driving mechanisms of lagoonal sediment accumulation through the Holocene
- 4) Reconstruction of the Holocene evolution of the oceanic barrier-reef lagoon of Bora Bora, considering facies distribution, lagoonal infill, and the role of siliciclastic input regarding the formation of symsedimentary siderite

These objectives are addressed in Chapters 2, 3, 4 and 5:

Chapter 2 focuses on the influence of antecedent topography and platform size as factors controlling the lateral extension of sand aprons in modern carbonate platforms and atolls is examined based on the statistical assessment of remote sensing data combined with geomorphological parameters. In Chapter 3, the influence of sea level, antecedent topography and subsidence to late Quaternary development of the barrier and fringing reef sections of

Bora Bora, South Pacific is investigated. Chapter 4 comprises a multi-proxy study including sedimentological, palaeontological, geochemical and geochronological data of sediment cores from the barrier-reef lagoon of Bora Bora and shows the reaction of the sedimentary system with regard to morphological and environmental changes. Chapter 5 presents temporal and spatial facies variations in the Bora Bora lagoon in response to sea-level and climate change. Furthermore, palaeo-environmental conditions during the formation of syndepositional siderite are elucidated.

1.3 Thesis outline

The present doctoral thesis is submitted in fulfillment of the requirements for a cumulative dissertation for the degree of *Doctor rerum naturalium (Dr. rer. nat.)* at the *Institut für Geowissenschaften, Goethe Universität Frankfurt am Main*. Requirements for the submission of a cumulative PhD-thesis to the *Institut für Geowissenschaften, Goethe Universität* include two papers published in peer-reviewed journals and one submitted to a peer-reviewed journal. The PhD candidate must be the first author of at least two of them.

This thesis is based on four manuscripts. Three of them have been published in peer-reviewed journals (Chapter 2: *Carbonates and Evaporites*; Chapter 3: *Sedimentology*; Chapter 4: *Sedimentary Geology*) and one has been submitted to a peer-reviewed journal (Chapter 5: *Marine Geology*). The introduction in the first chapter gives a short overview of the general topic and consolidates the following chapters. The last chapters comprise a concluding summary and outlook in both English and German, along with datasets of the presented studies.

1.4 References

- Braithwaite, C.J.R., 2016. Coral-reef records of Quaternary changes in climate and sea-level. *Earth-Science Rev.* 156, 137–154. doi:10.1016/j.earscirev.2016.03.002
- Burne, R. V., 1991. Carbonate sediment budgets and coastal management in South Pacific Island nations. *Work. Coast. Processes South Pacific Isl. Nations SOPAC Tech. Bull.* 7, 45–53.
- Camoin, G.F., Webster, J.M., 2015. Coral reef response to Quaternary sea-level and environmental changes: State of the science. *Sedimentology* 62, 401–428. doi:10.1111/sed.12184
- Daly, R.A., 1915. The Glacial-Control Theory of Coral Reefs. *Proc. Am. Acad. Arts Sci.* 51, 157–251.

- Hallmann, N., Camoin, G., Eisenhauer, A., Vella, C., Samankassou, E., Fietzke, J., Milne, G.A., 2013. Sea-level changes over the past 6,000 years in the Society and Tuamotu Islands, French Polynesia, in: *Book of Abstracts, American Geophysical Union, Fall Meeting 2013*.
- Harris, D.L., Vila-Concejo, A., Webster, J.M., 2014. Geomorphology and sediment transport on a submerged back-reef sand apron: One Tree Reef, Great Barrier Reef. *Geomorphology* 222, 132–142. doi:10.1016/j.geomorph.2014.03.015
- Hopley, D., 2011. Lagoons, in: Hopley, D. (Ed.), *Encyclopedia of Modern Coral Reefs: Structure, Form and Process*. Springer Netherlands, Dordrecht, pp. 617–618. doi:10.1007/978-90-481-2639-2_224
- Hubbard, D.K., 2016. Coral Reefs at the Crossroads – An Introduction, in: Hubbard, D.K., Rogers, C.S., Lipps, J.H., Stanley, G.D. (Eds.), *Coral Reefs of the World 6: Coral Reefs at the Crossroads*. Springer-Verlag, p. 314.
- ICPP, 2014. Summary for Policymakers, in: *Climate Change 2014: impacts, adaptation, and vulnerability. Part A: Global and sectoral aspects. Contribution of Working Group II to the Fifth Assessment Report of the Intergovernmental Panel on Climate Change* (Field, C.B., V.R. Barros, D.J. Dokken, K.J. Cambridge University Press, Cambridge, United Kingdom and New York, NY, USA, pp. 1–32.
- Kench, P.S., 2011. Sediment dynamics, in: Hopley, D. (Ed.), *Encyclopedia of Modern Coral Reefs*. Springer Netherlands, pp. 994–1005.
- Ladd, H.S., 1949. The problem of coral reefs. *Sci. Mon.* 69, 297–305.
- Lambeck, K., Rouby, H., Purcell, A., Sun, Y., M., S., 2014. Sea level and global ice volumes from the Last Glacial Maximum to the Holocene. *PNAS* 111, 15296–15303.
- Lambeck, K., Woodroffe, C.D., Antonioli, F., Anzidei, M., Gehrels, W.R., Laborel, J., Wright, A.J., 2010. Paleoenvironmental records, geophysical modeling, and reconstruction of sea-level trends and variability on centennial and longer timescales, in: J. Church, P.L., Aarup, W.T., Wilson, W.S. (Eds.), *Understanding Sea- Level Rise and Variability*. Blackwell, Chichester, pp. 61–121.
- MacNeil, F.S., 1954. The shape of atolls; an inheritance from subaerial erosion forms. *Am. J. Sci.* 252, 402–427.
- Marshall, J.F., Davies, P.J., 1982. Internal structure and Holocene evolution of One Tree Reef, Southern Great Barrier Reef. *Coral Reefs* 1, 21–28.
- Milankovitch, M.M., 1941. *Kanon der Erdbestrahlungen und seine Anwendung auf das*

- Eiszeitenproblem. Serb. Acad. Beorg. Spec. Pub. 132 p.
- Milne, G.A., Mitrovica, J.X., 2008. Searching for eustasy in deglacial sea-level histories. *Quatern. Sci. Rev.* 27, 2292–2302.
- Mitrovica, J.X., Milne, G.A., 2002. On the origin of late Holocene sea-level highstands within equatorial ocean basins. *Pergamon* 21, 2179–2190.
- Mitrovica, J.X., Peltier, W.R., 1991. On postglacial subsidence over the equatorial oceans. *J. Geophys. Res.* 96, 20,053–20,071.
- Pirazzoli, P.A., 1991. *World atlas of Holocene sea-level changes*. Elsevier Science.
- Pirazzoli, P.A., Montaggioni, L.F., 1988. Holocene sea-level changes in French Polynesia. *Palaeogeogr. Palaeoclimatol. Palaeoecol.* 68, 153–175.
- Pirazzoli, P.A., Montaggioni, L.F., Vergnaud-Grazzini, C., Saliege, J.F., 1987. Late Holocene sea level and coral reef development in Vahitahi atoll, eastern Tuamotu Islands, Pacific Ocean. *Mar. Geol.* 76, 105–116.
- Purdy, E.G., 1974. Reef configurations: cause and effect, in: Laporte, L.F. (Ed.), *Reefs in Time and Space*. pp. 9–76.
- Purdy, E.G., Gischler, E., 2005. The transient nature of the empty bucket model of reef sedimentation. *Sediment. Geol.* 175, 35–47. doi:10.1016/j.sedgeo.2005.01.007
- Purdy, E.G., Gischler, E., Lomando, A.J., 2003. The Belize margin revisited. 2. Origin of Holocene antecedent topography. *Int. J. Earth Sci.* 92, 552–572. doi:10.1007/s00531-003-0325-z
- Purdy, E.G., Winterer, E.L., 2006. Contradicting barrier reef relationships for Darwin's Evolution of reef types. *Int. J. Earth Sci.* 95, 143–167. doi:10.1007/s00531-005-0511-2
- Purdy, E.G., Winterer, E.L., 2001. Origin of atoll lagoons. *GSA Bull.* 113, 837–854.
- Rankey, E.C., Reeder, S.L., Garza-Perez, J.R., 2011. Controls on links between geomorphical and surface sedimentological variability: Aitutaki and Maupiti Atolls, South Pacific Ocean. *J. Sediment. Res.* 81, 885–900. doi:10.2110/jsr.2011.73
- Schlager, W., 1993. Accommodation and supply - a dual control on stratigraphic sequences. *Sediment. Geol.* 86, 111–136.
- Schlager, W., Purkis, S.J., 2015. Reticulate reef patterns - antecedent karst versus self-organization. *Sedimentology* 62, 501–515. doi:10.1111/sed.12172
- Schlager, W., Purkis, S.J., 2013. Bucket structure in carbonate accumulations of the Maldives, Chagos and Laccadive archipelagos. *Int. J. Earth Sci.* 102, 2225–2238.

doi:10.1007/s00531-013-0913-5

- Scoffin, T.P., Tudhope, A.W., 1988. Shallowing-upwards sequences in reef lagoon sediments: examples from the Holocene of the Great Barrier Reef of Australia and the Silurian of Much Wenlock, Shropshire, England. *Proc. 6th Int. Coral Reef Symp. Aust.* 3, 479–484.
- Stoddart, D., 1969. Ecology and morphology of recent coral reefs. *Biol. Rev.* 44, 433–498.
- Toomey, M., Ashton, A.D., Perron, J.T., 2013. Profiles of ocean island coral reefs controlled by sea-level history and carbonate accumulation rates. *Geology* 41, 731–734. doi:10.1130/G34109.1
- Toomey, M.R., Ashton, A.D., Raymo, M.E., Perron, J.T., 2016. Late Cenozoic sea level and the rise of modern rimmed atolls. *Palaeogeogr. Palaeoclimatol. Palaeoecol.* 451, 73–83. doi:10.1016/j.palaeo.2016.03.018
- Woodroffe, C.D., Mclean, R.E., Wallensky, E., 1994. Geomorphology on the Cocos (Keeling) Islands. *Atoll Res. Bull.* 402, 1–33.
- Woodroffe, C.D., Webster, J.M., 2014. Coral reefs and sea-level change. *Mar. Geol.* 352, 248–267. doi:10.1016/j.margeo.2013.12.006
- Zinke, J., Reijmer, J.J.G., Thomassin, B.A., 2003. Systems tracts sedimentology in the lagoon of Mayotte associated with the Holocene transgression. *Sediment. Geol.* 160, 57–79. doi:10.1016/S0037-0738(02)00336-6

CHAPTER 2

THE SIGNIFICANCE OF SAND APRONS IN HOLOCENE ATOLLS AND CARBONATE PLATFORMS

Anja Isaack, Eberhard Gischler

Institut für Geowissenschaften, J.W. Goethe-Universität, Altenhöferallee 1,
60438 Frankfurt am Main, Germany

Keywords: sand apron, antecedent topography, atoll, progradation, lagoon depth,
Holocene

Published 2015: Carbonates and Evaporites, pp 1–13. doi:10.1007/s13146-015-0268-z

Abstract

Sand aprons are located in the back-reef area of atolls and carbonate platforms and form transport pathways of reef-derived sediment into adjacent lagoons and platform interiors. Even though there are studies focussing on sand apron sediment dynamics, the knowledge of Holocene sand apron evolution is limited, because hardly any subsurface data is available. In our model, antecedent topography, i.e., the elevation of the underlying Pleistocene karst surface and platform area are major factors controlling Holocene sand apron development. Because data on marginal reef thickness in Holocene atolls and carbonate platforms is limited, we also used maximum lagoon depth as proxy for the depth to the underlying Pleistocene surface. Sand apron proportions of 122 atolls and carbonate platforms from the Atlantic, Indian and Pacific Oceans were quantified and correlated to maximum lagoon depth, total platform area and marginal reef thickness, when available. Our analyses show significant correlations between sand apron proportions and both maximum lagoon depth ($r = -0.420$; $p = 0.000$) and total platform area ($r = -0.226$; $p = 0.012$). There is no statistically significant correlation ($r = -0.364$; $p = 0.165$) between sand apron proportions and depth to Pleistocene surface at platform margins. We assume that the lacking correlation can be explained by the limited data set of 16 atolls. Principle component analyses might allow the separation of Atlantic (Caribbean) from Indo-Pacific atolls, which probably arise from spatial and regional variations in sea-level history, i.e., in the Atlantic (transgressive) and Indo-Pacific region

(transgressive-regressive), but more subsurface data are necessary to confirm our interpretation. In general, Holocene sand apron formation has started when marginal reefs approached relative sea level some 6000-3000 yrs BP. Because accommodation space started to be limited, depositional systems of sand aprons prograded towards the lagoon. Estimated sedimentation-rate data of atoll lagoons show that accumulation of sand aprons is up to three times higher than lagoonal background sedimentation and therefore suited to fill lagoonal accommodation space and to create "filled buckets" in small and intermediately sized platforms (up to hundreds of km² size), even during times of high-amplitude sea-level fluctuations of an icehouse world. Although we postulate an application of the antecedent topography model to Holocene sand apron development, further factors controlling reef development such as hydrodynamics and carbonate production still influence sand apron development and pattern. Our study shows the need for further work and knowledge of the subsurface of carbonate platforms and reef sand aprons, which is still limited. Collectively, hydrodynamic (waves, tides and currents), biologic (carbonate production and distribution of organisms) as well as geomorphological (present-day and antecedent topography) factors should be combined, when generating new models for sand apron development to better understand sand apron history in the geologic past.

2.1 Introduction

Sand aprons are deposits of carbonate sand located leeward of the reefal margin and extend towards the interior of atolls and carbonate platforms (fig. 2/1). They form integral geomorphological elements of modern and ancient reefs and carbonate platforms (e.g., Rankey and Garza-Peréz 2012). On satellite images, sand aprons can easily be identified by their typical light blue to turquoise color.

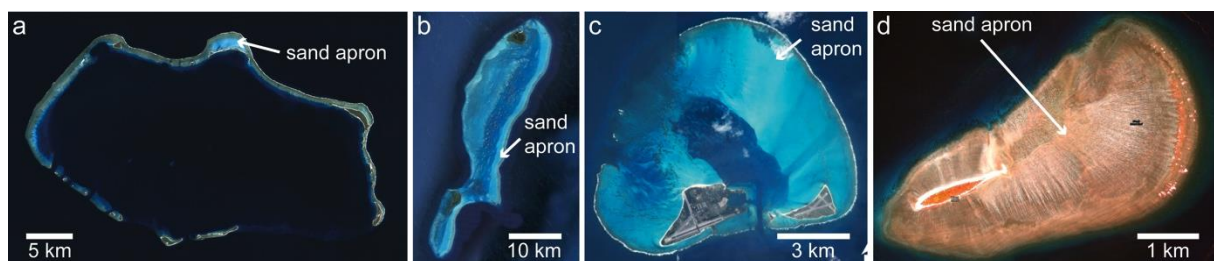


Fig. 2/1: Satellite images of four atolls that exhibit various degrees of lagoonal infilling by sand aprons; **a**) Bikini Atoll, Marshall Islands, with narrow sand aprons; **b**) Lighthouse Reef Atoll, Belize, with well-developed sand aprons; **c**) Midway Atoll, Hawaiian Islands, an almost filled bucket; **d**) Wreck Reef, Great Barrier Reef, in which sand apron has virtually filled lagoonal accommodation space completely. Satellite images are from Google Earth (Data SIO, U.S. Navy, NGA, GEBCO)

Sand aprons usually deepen from < 1 m to ca. 5 m away from the reef margin. Their widths range from tens of meters to several kilometers. Sand apron sediment is produced

at the reef margin with subsequent transport in back-reef direction (e.g., Stoddart, 1969; Marshall and Davies, 1982; Hopley et al., 2007). Sand apron sediments are characterized by gradation in grain size, the sorting usually improving away from the reef margin (Macintyre et al., 1987; Kench, 1997; Rankey et al., 2011; Harris et al., 2014).

Deposits of sand aprons can form extensive facies bodies, which provide excellent hydrocarbon storage properties in the fossil record (Wasserman and Rankey 2014). Therefore, the understanding of sand apron development and controlling factors is of fundamental importance, e.g., for petroleum exploration. It has long been considered that factors responsible for sediment transport are of physical origin, with waves, currents and tides causing variations in the energy level (e.g., Kench, 1998b; O'Leary et al., 2009). The movement of sediment forces the progradation of sand aprons towards the lagoon (Marshall and Davies, 1982; Purdy and Gischler, 2005). Kench (1998a) examined sand apron dimensions on the Cocos (Keeling) Islands Atoll, Indian Ocean, and postulated that physical processes have controlled the areal extent and development of sand aprons. Harris et al. (2011, 2014) showed on One Tree Reef, southern Great Barrier Reef that sediment pathways of sand aprons occur under moderate energy conditions with waves being the main force entraining sediment. On Aranuka Atoll, Gilbert Islands, Wasserman and Rankey (2014) detailed texture of sediments along sand aprons to refer to the hydrodynamic regime. On a global scale, Rankey and Garza-Peréz (2012) focused on 60 Holocene isolated carbonate platforms and tested oceanographic parameters such as waves and tides as responsible factors for sand apron dimensions. However, there were no systematic relationships between these parameters and sand apron extent.

Lagoon infill with sediments derived from reef flats is the major constructional process for coral reefs once they attain a stable elevation with respect to sea level (Marshall and Davies, 1982; Kench, 1998a). With regard to the "empty bucket" model (see Schlager, 1993; and references therein), Purdy and Gischler (2005) described partly filled lagoons of modern carbonate platforms as a transitional stage, not as an end member of carbonate accumulation geometry and postulated that atoll lagoons are suited to be infilled by sand aprons. Although many studies have concentrated on the variability of present-day sediment dynamics of sand aprons, the influence of antecedent topography controlling Holocene sand apron formation and development has been largely neglected thus far.

The purpose of this study is the evaluation of the relationship between sand apron extensions and geomorphological platform features: we hypothesize that Holocene sand apron development is controlled to a large part by antecedent topography and platform size.

Antecedent topography describes the elevation and relief of the underlying Pleistocene karst surface and determines the distance from the sea floor to the rising postglacial sea level. Together with platform size, it is a measure of accommodation space. Because of the difficulty to core several meter thick sand deposits and the penetration limits of seismics in shallow sand areas, hardly any subsurface data of Holocene sand aprons exist (fig. 2/2). Therefore, maximum lagoon depth and Holocene reef thickness data, when available, were used as proxies for antecedent topography.

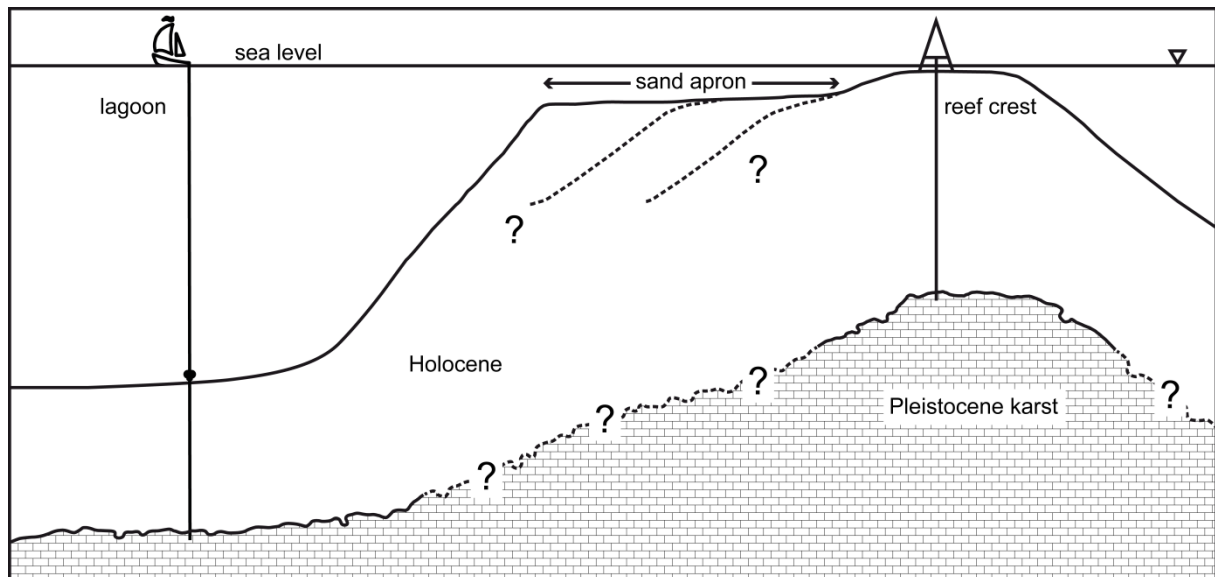


Fig. 2/2: Schematic transect through reef margin showing the depth of the underlying antecedent Pleistocene topography extending to the lagoon. Typical rotary drill location on the reef crest and vibrocore site in the lagoon are drawn to visualize the limitations of sampling. Because of limited subsurface data of sand aprons, elevation and shape of underlying Pleistocene is usually enigmatic

2.2 Data set and method

A total of 122 atolls and carbonate platforms in the Atlantic, Indian and Pacific Oceans were included in this analysis. They comprise the Tuamotu Archipelago (29 atolls), Caroline Islands (26), Marshall Islands (24), Maldives (21), Gilbert Islands (9), Caribbean (7), Great Barrier Reef (3), Hawaiian Islands (2) and Cocos (Keeling) Islands Atoll (1) (fig. 2/3; tab. 2/1). The proportions of sand aprons were quantified by using satellite images in Google Earth (fig. 2/1) and the open source software ImageJ. Areas of sand aprons and total platform area were measured in ImageJ (fig. 2/4). In the next step, the percentaged sand apron proportions were calculated by dividing sand apron size and atoll size, under the assumption that the total platform area reflects 100%.

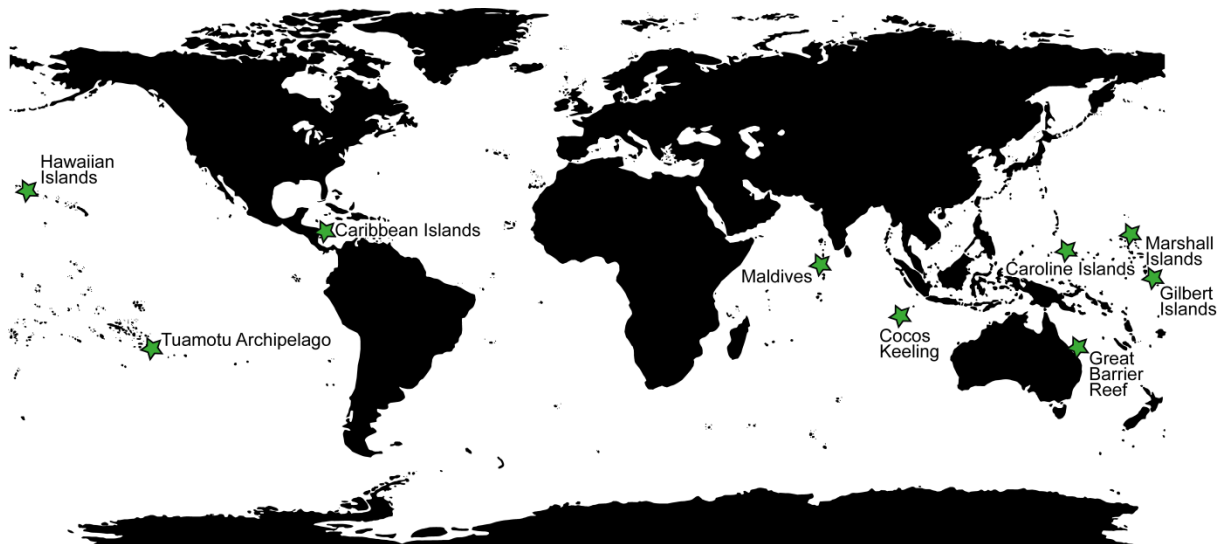


Fig. 2/3: Location map showing the position of atolls and carbonate platforms analyzed in this study

Sand apron proportions were correlated to maximum lagoon depths in meters and total platform areas in square kilometers (tab. 2/2) using the comprehensive data set of Purdy and Winterer (2001). Their database relies on hydrographic charts and other published data (see Purdy and Winterer, 2001; GSA data repository item 2001075). Lagoon floor topography can be quite irregular and therefore lagoonal depth also varies. We decided to use maximum lagoon depth from the database of Purdy and Winterer (2001), following their recommendation "to use maximum lagoon depth as the only meaningful depth attribute available".



Fig. 2/4: Satellite images of **a**) Makunudu Atoll, Maldives, illustrating **b**) the mapped sand apron areas (gray) and the atoll's perimeter (yellow), which encircles total atoll area (from Google Earth; Data SIO, U.S. Navy, NGA, GEBCO)

Table 2/1: Summary of geomorphological data acquired and data from rotary drilling. Total platform area and maximum lagoon depth according to Purdy and Winterer (2001). GBR = Great Barrier Reef

Atoll	Atoll Group	Total platform area (km²)	Maximum lagoon depth (m)	Sand apron proportion (%)	Depth to Pleistocene (m)	References	Drill hole location
Ihavandiffulu	Maldives	286	49	12.96			
Tiladummali-Miladummadu	Maldives	3850	58	3.33			
Makunudu	Maldives	139	31	29.54			
Gaha (Gaafaru)	Maldives	82	40	15.28			
N Malosmadulu	Maldives	1168	49	4.45			
Fadiffolu	Maldives	699	55	6.72			
S Malosmadulu	Maldives	1075	55	4.27	14	Kench et al. 2009	Reef (close to island)
Horsburgh (Goidoo)	Maldives	105	42	27.41			
N Male	Maldives	1565	69	3.68	20	Woodroffe 2005	?
Rasdho	Maldives	59	37	21.72	13.5	Gischler et al. 2008	W reef
S Male	Maldives	535	58	8.09			
Felidu	Maldives	1021	68	6.24			
Ari	Maldives	2252	69	3.13			
Wataru	Maldives	43	35	15.28			
N Nilandu	Maldives	594	66	6.61			
Mulaku	Maldives	956	73	6.48			
S Nilandu	Maldives	739	68	5.77			
Kolumadulu	Maldives	1617	79	3.80			
Haddummati	Maldives	881	73	6.34			
Suvadiva	Maldives	3152	82	1.73			
Addu	Maldives	158	79	4.93	20	Woodroffe 2005	?
Manihi	Tuamotus	201	37	1.60			
Ahe	Tuamotus	171	54	1.41			
Takaroa	Tuamotus	114	39	1.98			
Takapoto	Tuamotus	114	60	3.05			
Matahiva	Tuamotus	34	8	7.88	10	Pirazzoli and Montaggioni 1986	Outer lagoon

Continue on next page

Atoll	Atoll Group	Total platform area (km ²)	Maximum lagoon depth (m)	Sand apron proportion (%)	Depth to Pleistocene (m)	References	Drill hole location
Tikahau	Tuamotus	351	40	1.98			
Rangiroa	Tuamotus	1762	70	1.60			
Arutua	Tuamotus	437	19	3.77			
Apataki	Tuamotus	723	50	0.98			
Aratika	Tuamotus	175	30	1.35			
Taiaro	Tuamotus	14	27	3.23			
Kauehi	Tuamotus	343	60	1.72			
Toau	Tuamotus	489	24	9.11			
Raroia	Tuamotus	367	50	1.37			
Fakarava	Tuamotus	1245	60	3.21			
Taenga	Tuamotus	173	14	1.79			
Katiu	Tuamotus	207	20	4.02			
Makemo	Tuamotus	716	60	6.97			
Faaite	Tuamotus	197	20	3.16			
Tuanake	Tuamotus	25	20	5.05			
Hiti	Tuamotus	20	20	13.68			
Tepoto	Tuamotus	3	10	29.63			
Tahanea	Tuamotus	469	24	5.68			
Anaa	Tuamotus	632	10	5.84			
Amanu	Tuamotus	242	62	1.15			
Hao	Tuamotus	578	61	1.58			
Nukutipipi	Tuamotus	26	17	14.04			
Mururoa	Tuamotus	137	52	5.19	24	Camoin et al. 2001	Reef crest
Fangatau	Tuamotus	47	42	3.21			
Pokaakku (Taongi)	Marshalls	129	15	15.49			
Bikar	Marshalls	5	20	19.03			
Bikini	Marshalls	799	60	2.53	31.5	Emery et al. 1954	Island
Enewetak	Marshalls	1084	62	4.98	12	Ladd and Schlanger 1960	?
Rongelap	Marshalls	1146	62	2.95			

Continue on next page

Atoll	Atoll Group	Total platform area (km ²)	Maximum lagoon depth (m)	Sand apron proportion (%)	Depth to Pleistocene (m)	References	Drill hole location
Rongerik	Marshalls	209	49	7.15			
Ulirik (Utirik)	Marshalls	91	49	8.12			
Ailinganae	Marshalls	157	31	8.39			
Talu (Taka)	Marshalls	154	51	6.04			
Ailieik	Marshalls	238	53	3.64			
Wotho	Marshalls	468	37	6.20			
Likiep	Marshalls	489	56	1.83			
Ujelang	Marshalls	107	49	3.39			
Kwajalein	Marshalls	2304	61	0.47			
Lae	Marshalls	34	66	3.57			
Aur	Marshalls	285	82	1.41			
Maloelap	Marshalls	1068	81	0.75			
Namu	Marshalls	462	49	12.29			
Ailinglapalap	Marshalls	819	62	1.08			
Majuro	Marshalls	383	82	1.08			
Arno	Marshalls	437	62	5.02			
Mili	Marshalls	899	71	1.85			
Jaluit	Marshalls	855	49	1.51			
Ebon	Marshalls	129	33	8.00			
Kure Atoll	Hawaii	58	15	70.83			
Midway Atoll	Hawaii	83	6	57.54			
Cocos (Keeling) Islands Atoll		130	15	17.29	15.8	Woodroffe 2005	Island
Alacran Reef	Caribbean	221	23	9.57	33.5	Macintyre et al. 1977	Island
Hogsty Reef	Caribbean	28	8	12.68			
Chinchorro Bank	Caribbean	550	8	14.75			
Turneffe Islands	Caribbean	525	8	3.32	3.8	Gischler and Hudson 1998	Cay Bokel, reef
Lighthouse Reef	Caribbean	200	8	13.67	7.9	Gischler and Hudson 1998	Windward, reef flat
Glovers Reef	Caribbean	260	18	5.31	11.7	Gischler and Hudson 1998	Leeward, reef flat
Roncador Bank	Caribbean	19	18	4.24			

Continue on next page

Atoll	Atoll Group	Total platform area (km ²)	Maximum lagoon depth (m)	Sand apron proportion (%)	Depth to Pleistocene (m)	References	Drill hole location
Butaritari (Makin)	Gilberts	446	38	2.29			
Abaiang	Gilberts	313	27	3.10			
Tarawa	Gilberts	421	25	0.96	20	Marshall and Jacobsen 1985	Island
Maiana	Gilberts	107	16	5.31			
Abemama	Gilberts	292	22	5.57			
Aranuka	Gilberts	113	18	12.03			
Nonouti	Gilberts	668	20	2.87			
Tabiteuea	Gilberts	648	0	4.33			
Onotoa	Gilberts	110	15	2.86			
Ulithi	Carolines	361	64	0.97			
Namonuito	Carolines	2267	65	0.16			
Murilo	Carolines	414	51	0.42			
Nomwin	Carolines	318	52	0.80			
Kayangel	Carolines	21	5	13.44			
Sorol	Carolines	2	45	5.19			
West Fayu	Carolines	11	38	5.54			
Olimarao	Carolines	11	31	4.86			
Pulap	Carolines	43	35	0.00			
Elato	Carolines	11	27	5.58			
Lamotrek	Carolines	41	50	1.89			
Oroluk	Carolines	453	75	1.05			
Woleai	Carolines	43	53	0.34			
Uranie (Puluwat)	Carolines	332	60	5.96			
Ifalik	Carolines	6	20	9.09			
Pakin	Carolines	24	55	5.69			
Losap	Carolines	40	67	2.24			
Ant	Carolines	99	67	4.85			
Mokil	Carolines	6	60	4.15			
Pingelap	Carolines	29	42	7.67			

Continue on next page

Atoll	Atoll Group	Total platform area (km ²)	Maximum lagoon depth (m)	Sand apron proportion (%)	Depth to Pleistocene (m)	References	Drill hole location
Namoluk	Carolines	13	77	2.61			
Ngatik	Carolines	114	159	1.30			
Lukunor	Carolines	67	57	1.10			
Satawan	Carolines	419	77	2.59			
Nukuoro	Carolines	40	99	0.08			
Kapingamarangi	Carolines	74	79	1.79			
Lady Musgrave	GBR	6	9	15.76			
One Tree Reef	GBR	13	10	14.45	12.5	Davies and Hopley 1983	Windward margin, coral flat, close to Capricornia Cay
Wreck Reef	GBR	4	1	72.10	7.5	Davies and Hopley 1983	Windward margin, reef flat close to crest

Furthermore, available data from rotary drilling on depth to Pleistocene surface at reef margins (depth equals distance from the local sea-level datum to the top of Pleistocene bedrock) from 16 atolls (for references see tab. 2/1) were correlated to sand apron proportions and to maximum lagoon depths and total platform areas of these 16 atolls (tab. 2/3). Correlation and principle component analyses (tab. 2/4) were made using the PAST software (Hammer et al., 2001).

Table 2/2: Correlation table of geomorphological parameters of all data. Note that r-values are plotted in lower left and p-values in upper right corners. R-values are statistically significant if $p < 0.05$ and are marked bold

	Total platform area (km ²)	Maximum lagoon depth (m)	Sand apron proportion (%)
Total platform area (km²)	—	0.0001	0.0122
Maximum lagoon depth (m)	0.3498	—	0.0000
Sand apron proportion (%)	-0.2263	-0.4208	—

2.3 Results

Correlation analyses show statistically significant negative correlations between sand apron proportions and both maximum lagoon depth ($r = -0.420$; $p = 0.000$; fig. 2/5a; tab. 2/2) and total platform area ($r = -0.226$; $p = 0.012$; fig. 2/5b; tab. 2/2). There is a significant positive

correlation between total platform area and maximum lagoon depth ($r = 0.349$; $p = 0.000$; tab. 2/2), respectively. The strongest correlations between sand apron and maximum lagoon depth can be found in the Maldives ($r = -0.799$; $p = 0.000$); the Tuamotu Archipelago ($r = -0.493$; $p = 0.006$); the Marshall Islands ($r = -0.815$; $p = 0.000$) and the Caroline Islands ($r = -0.563$; $p = 0.002$) when looking at individual atoll groups, i.e., archipelagoes.

Sand apron proportions decrease with increasing depth to Pleistocene surface at reef margins of 16 atolls, however, there is no statistically significant correlation ($r = -0.364$; $p = 0.165$; fig. 2/6a; tab. 2/3). Considering only these 16 atolls, a statistically significant correlation exists between total platform area and maximum lagoon depth ($r = 0.611$; $p = 0.011$; tab. 2/3). Furthermore, maximum lagoon depth covaries with depth to the Pleistocene surface at reef margins ($r = 0.594$; $p = 0.015$).

Table 2/3: Correlation table of geomorphological parameters including marginal reef thickness of 16 atolls. Note that r-values are plotted in lower left and p-values in upper right corners. R-values are statistically significant if $p < 0.05$ and are marked bold

	Total platform area (km ²)	Maximum lagoon depth (m)	Sand apron proportion (%)	Depth to Pleistocene surface at margin (m)
Total platform area (km²)	—	0.0117	0.1230	0.2802
Maximum lagoon depth (m)	0.6118	—	0.085561	0.0152
Sand apron proportion (%)	-0.4016	-0.4431	—	0.1657
Depth to Pleistocene surface at margin (m)	0.2875	0.5941	-0.3640	—

Principle component analyses (PCA) were used for the determination of the influence of the different geomorphological parameters (sand apron size, platform size, max. lagoon depth, depth to Pleistocene) and to decipher similarities between investigated platforms and regions. The results of the PCAs (eigenvalues, total variances and loadings) are given in table 2/4. 99.82% (fig. 2/5c); 87.21% (fig. 2/5d) and 83.56% (fig. 2/6b) of the variance, respectively, could be explained by principle component 1. Cross plots of component 1 and 2 exhibit considerable overlap but there is also clustering by region (fig. 2/5c, d; fig. 2/6b). For example, atolls from the Maldives, Marshalls, and Tuamotus cluster together, as an expression of their geomorphological similarity.

Table 2/4: Results of the principle component analyses: eigenvalues, total variances and loading matrices. Note that the plots for each table block are shown in figures 5c, d and figure 6b

Sand apron proportion; maximum lagoon depth; total platform area (plot shown in Fig. 5c)

PC	Eigenvalue	% variance
1	388451	99.82
2	586.58	0.15
3	98.15	0.03

	Component 1	Component 2	Component 3
Maximum lagoon depth (m)	0.014	0.979	0.203
Sand apron proportion (%)	-0.004	-0.203	0.979
Total platform area (km ²)	0.999	-0.015	0.001

Sand apron proportion; maximum lagoon depth (plot shown in Fig. 5d)

PC	Eigenvalue	% variance
1	671.74	87.21
2	98.53	12.79

	Component 1	Component 2
Maximum lagoon depth (m)	0.977	0.213
Sand apron proportion (%)	-0.213	0.977

Sand apron proportion; depth to Pleistocene surface at reef margins (plot shown in Fig. 6b)

PC	Eigenvalue	% variance
1	303.43	83.56
2	59.70	16.44

	Component 1	Component 2
Sand apron proportion (%)	-0.221	0.975
Depth to Pleistocene surface at reef margin (m)	0.975	0.221

2.4 Discussion

Marginal reefs of carbonate platforms represent the primary source of sediments (Burne, 1991), which are transported lagoonwards via sand aprons, contributing significantly to the infill of platform interior accommodation space (Marshall and Davies, 1982; Woodroffe et al., 1994; Purdy and Gischler, 2005). The results of this study indicate a covariance of sand apron proportions and maximum lagoon depth, i.e., an increase in sand apron proportions with decreasing maximum lagoon depth (fig. 2/5a). Maximum lagoon depth is to a large part the result of subaerial solution (karstification) of Pleistocene limestone during sea-level

lowstands and differential accretion rates at platform margins and interiors (Schlager, 1993; Purdy and Winterer, 2001; Gischler, 2015). During repeated ups and downs of Pleistocene sea level, the relief between lagoon depth and marginal reef elevation has been increasing, because reef accretion exceeds lagoonal sedimentation severalfold. Hermatypic corals grow preferentially on geomorphological highs at platform margins, whereas unconsolidated sediment accumulates in topographic lows of the Pleistocene pedestal such as atoll lagoons (Purdy, 1974).

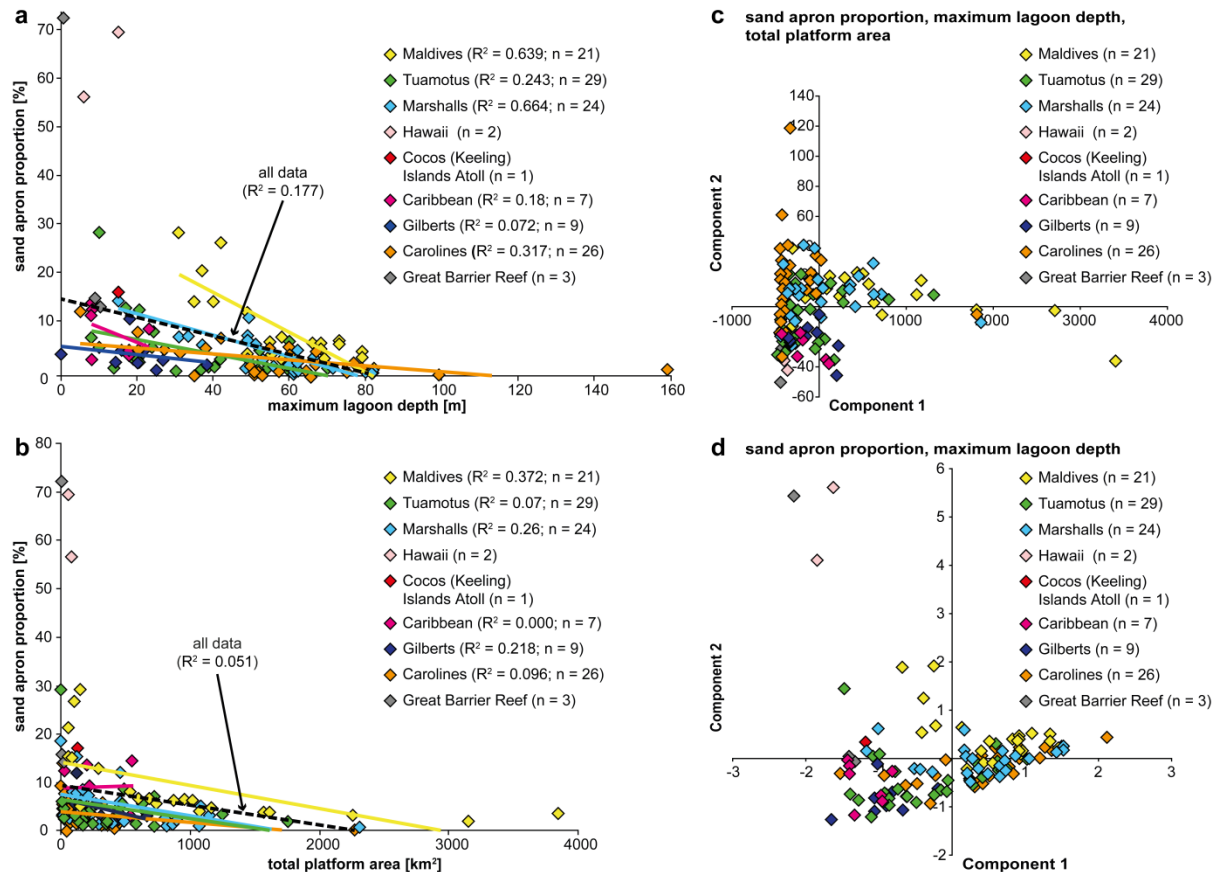


Fig. 2/5: **a)** Correlation between sand apron proportions versus maximum lagoon depth; **b)** Sand apron proportions versus total platform area. Parameters used are all data (dashed line) and regional atoll groups. Plots **c** and **d** show the results of principle component analyses. Parameters used in analyses include sand apron proportions, maximum lagoon depth and total platform area in **c**, and sand apron proportions and maximum lagoon depth in **d**

Carbonate production provides the material for sediment transport and lagoonal infill. Smithers et al. (1994) were able to distinguish between two types of sedimentation on the Cocos (Keeling) Islands Atoll; a muddy facies leeward of the islands accumulating between 0.25–0.5 m/kyr and sand aprons with accumulation rates between 0.5–1.0 m/kyr. In the Maldives, mean lagoonal background sedimentation rates in the Holocene were measured to 0.9 m/kyr (Klostermann and Gischler, 2015), as compared to average marginal reef accretion rates of 3.3 m/kyr (Gischler et al., 2008). Holocene sedimentation rates in the three Belize atoll lagoons amount to 0.6 m/kyr (Gischler, 2003) on average; reef accumulation rate

averages some 3.0 m/kyr (Gischler and Hudson, 1998). The supply of allochthonous sediment, which is transported via sand apron pathways into the lagoon is much higher than autochthonous sediment produced within the lagoon. Woodroffe et al. (1994) estimated sand apron progradation to 1000 m of lateral extension per kyr in Cocos (Keeling) Islands Atoll. Klostermann and Gischler (2015) calculated lateral lagoonal infill by sand aprons in a small Maldivian atoll to 250 m per kyr in the late Holocene. Given the same amount of reef-derived sediment, the lagoonal infilling process is faster in a hypothetical smaller atoll with a shallow lagoon than in larger ones with a deeper lagoon (Purdy and Winterer, 2001). Perry et al. (2013) recently presented quantitative evidence for this relationship in lagoonal infill of faroes, circular reef structures common in the Maldives' archipelago.

The rate of lagoon filling via sand aprons is not solely a function of sediment delivery by lateral extent on a decadal or daily scale (Vila-Concejo et al., 2013). On the lagoonward side of the sand apron of Aranuka Atoll, Kiribati, sediments are poorly sorted (Wasserman and Rankey, 2014). The results of these authors suggest *in situ* carbonate production as responsible factor urging variations in sedimentation patterns along reef sand aprons during their progradation. On the Dry Tortugas, an isolated carbonate ramp in south Florida, geomorphologic zonations, i.e., a continuous reef rim and sand aprons are lacking and lagoonal infill is mainly driven by autochthonous carbonate production within the shallow lagoon (Isaack, 2013). The sediments within the lagoon are poorly sorted (Isaack, 2013), as in the Kiribati example.

Analyses from the Maldives, Marshall Islands, Caroline Islands and the Tuamotu Archipelago show the highest correlations between sand apron proportions and maximum lagoon depth (fig. 2/5a; tab. 2/2). In our study, nearly all atolls of these archipelagoes were analyzed; e.g., all 21 atolls of the Maldives were considered, while only 4 reef-fringed islands were excluded from the analysis. There are no statistically significant signals in the data from the Gilbert Islands and the Great Barrier Reef, which might be explained by the much more limited data sets (Gilbert Islands $n = 9$; Great Barrier Reef $n = 3$). The correlation pattern of the two Hawaiian atolls Kure and Midway is reversed as compared to the overall trend. Although Kure has a greater lagoon depth (15 m) than Midway (6 m), its sand apron covers almost 70% of the platform area (almost filled bucket), as opposed to 57% in Midway. However, total lagoon area in Kure is smaller than in Midway, which underlines the importance of platform size. Also, the continuity of the peripheral reef rim of Kure atoll is greater than that on Midway, and results in significant sediment transport towards the inner atoll area (Purdy and Gischler, 2005). The pattern of lagoon infill likely depends on the nature

of the reef rim and sediment production may be proportional to the atoll's perimeter (Tudhope, 1989). The Caribbean atolls show reversed correlations between sand apron proportion, lagoon depth and total platform area (fig. 2/5), however, statistically insignificant. Notwithstanding being described as atolls, Caribbean examples such as Hogsty Reef in the Bahamas and Roncador Bank off the east coast of Nicaragua and three atolls off the Belize Barrier Reef clearly differ in origin and morphology from Indo-Pacific atolls (Woodroffe and Biribo, 2011) in that they are mostly located on continental crust and lack deep lagoons.

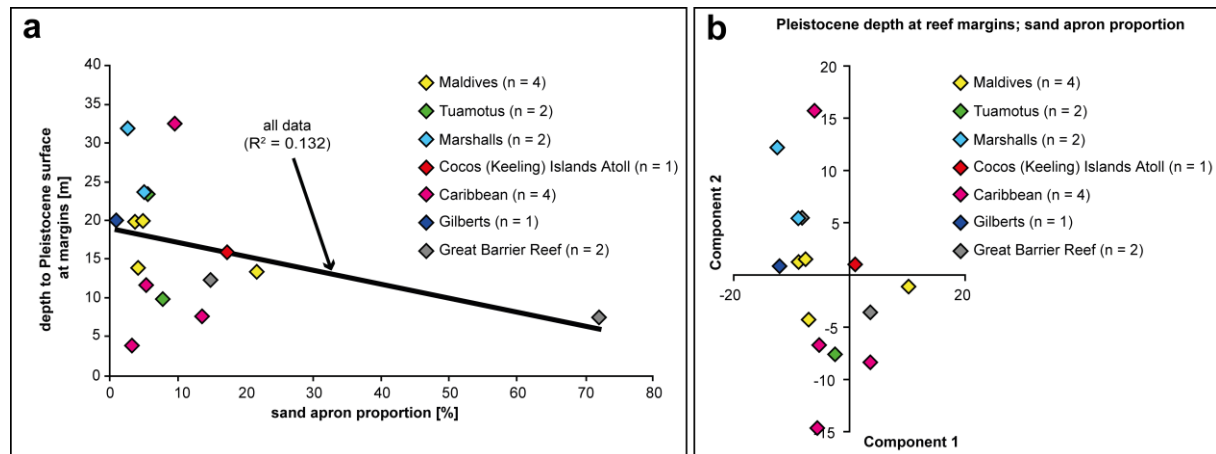


Fig. 2/6: **a**) Correlation between sand apron proportions and depth to Pleistocene surface at reef margins. Correlation is statistically insignificant likely due to limited data set; **b**) Results of principle component analysis. Parameters used in analyses include sand apron proportions and Pleistocene depth at reef margins

In modern atolls and carbonate platforms, the elevation of the underlying Pleistocene bedrock occurs at different depths depending on the geological setting. Rates of subsidence and variations in environmental parameters such as precipitation, which are crucial for reef geomorphology, are different in mid-oceanic and continental settings; they may also vary along individual reef locations. For example, differential subsidence and karst dissolution along the Belize coast has resulted in differences in elevation of antecedent topography, successive platform flooding, reef initiation and eventually led to differences in lagoon depths (e.g., Gischler and Hudson, 1998, 2004). Even if topographic features such as changes in slope and palaeo-channels are suggested to be more important in facilitating coral settlement than overall shelf architecture (Webster, 1999; Grossman and Fletcher, 2004), antecedence has affected early stages of reef development and locally determines gross atoll morphology (Purdy, 1974; Montaggioni, 2005). In the oceanic barrier reef systems of Mayotte, Indian Ocean, Zinke et al. (2003) identified the depth of the marginal reef passages, which formed since the last interglacial, to be crucial for lagoonal development. Harris et al. (2011) assumed that long-term gross progradation of sand aprons occurs, with sand apron sediment transport along morphological formations such as ebb channels.

Acting as sediment conduits, sand aprons form a transitional zone between the high-productive reef flat areas and atoll lagoons. The atoll lagoon provides accommodation space for the exported material. Because of the virtual absence of subsurface data of sand aprons, depth and shape of the Pleistocene topography underlying Holocene sand aprons is largely unknown (see fig. 2/2). Rotary drilling is usually made at or near reef crests or on reef islands and reveals information about the elevation of the underlying Pleistocene surface at platform margins (fig. 2/2; tab. 2/1). Vibrocoreing in atoll lagoons discloses Holocene successions often including the Pleistocene-Holocene transition, e.g., in Belize (Gischler, 2003) and in the Maldives (Klostermann and Gischler, 2015). The elevation of the pedestal under sand aprons lies in-between marginal reef and lagoonal Pleistocene elevation, however, hardly any core data are available (fig. 2/2). The shape of Pleistocene sand aprons is presumably comparable to modern sand aprons in platforms and atolls, however, like in modern examples, their extent and size has certainly varied considerably. The measured correlation between sand apron proportions and depth to Pleistocene surface at reef margins is believed to be statistically insignificant because of the limited data set ($n = 16$) and the fact that the depth to Pleistocene surface at reef margins is just an approximation of the elevation of the Pleistocene surface underlying adjacent sand aprons. All the same, the cross plots of the two parameters exhibits a negative trend as expected based on our assumptions. Clearly, more subsurface data from Holocene margins and sand aprons will be necessary to support the interpretations put forward here.

The interplay of antecedent topography and the rising post-glacial sea level is of crucial importance because both parameters determine variations in accommodation space for given reefs (Woodroffe and Webster, 2014; and references therein). The history and pattern of Holocene sea-level change throughout the Indo-Pacific (transgressive-regressive curves) is in contrast to the Western Atlantic region (transgressive curves). For the Indo-Pacific realm, it is postulated that there has been a widespread mid-to-late Holocene sea-level highstand (Pirazzoli and Montaggioni, 1986; Camoin et al., 2004; Woodroffe, 2005; Kench et al., 2009), while the Western Atlantic sea level has been rising continuously to its present level (Adey, 1978; Lighty et al., 1982; Toscano and Macintyre, 2003). This led to spatial and regional variations in the time at which reefs reached modern sea level (Hopley et al., 2007). However, the initiation of Holocene reef growth above the Pleistocene karst surface on platform tops occurred at ca. 10000–8000 kyrs BP in the Indian Ocean (Camoin et al., 2004; Gischler et al., 2008; Kench et al., 2009), in the Pacific Ocean (Marshall and Davies, 1982; Montaggioni, 1988) as well as in the Caribbean region (Gischler & Hudson, 1998; Gischler, 2015).

Holocene sea-level curves indicate a period of rapid sea-level rise before reefs approaching relative sea level ca. 7500 yrs BP in the western Indian Ocean (Camoin et al., 1997, 2004), the position of the modern sea level was reached ca. 4500 kyrs BP in the central Indian Ocean (Kench et al., 2009; Klostermann and Gischler, 2015) and ca. 6000–5500 kyrs BP in the central Pacific (Pirazzoli and Montaggioni, 1986; Rashid et al., 2014). In the western Pacific (Great Barrier Reef), sea-level highstand was reached ca. 7000 yr BP, oscillated and fell to its present position ca. 2000 yrs BP (Lewis et al., 2008). When Holocene sea level stabilized close to its present position, accommodation space started to become limited and sand aprons were forced to change from aggradation in a transgressive system tract to progradation in a highstand system tract (Purdy and Gischler, 2005). Therefore, lateral extension of sand aprons and infill of platform lagoons should have started earlier in the Indo-Pacific realm than in the Western Atlantic, and, accordingly, Indo-Pacific sand aprons proportions should be higher than Western Atlantic ones. On the other hand, lagoon depths are generally shallower in Western Atlantic as compared to Indo-Pacific platforms, i.e., accommodation space is lower and, hence, sand aprons should be larger in the former as compared to the latter. Results of principle component analyses show that atolls from the Caribbean region tend to plot at the margins of the data clouds, possibly as a consequence of their geomorphological dissimilarity with the Indo-Pacific examples, but the cross plots also exhibit considerable overlap of data points (fig. 2/5c, d). Clearly, a limitation of this study is the need for more subsurface data to validate the interpretations put forward here, and, to be able to better distinguish between geomorphological factors such as antecedent topography, platform size and the course of Holocene sea level.

2.5 Conclusions

Our hypothesis of antecedent topography being a fundamental factor controlling Holocene sand apron development and extension is supported by the covariance of sand apron proportions and maximum lagoon depth (as a proxy for antecedent topography). Sand apron proportions increase with decreasing lagoon depths. Sand apron proportions also increase with decreasing platform area, underlining the importance of platform size. The interplay of antecedent topography and Holocene sea-level rise determines variations in accommodation space and is responsible for the lateral expansion of sand aprons. The formation of sand aprons has started when marginal reefs approached relative sea level. Regional variability in Holocene sea-level history presumably let sand apron formation start earlier in the Indo-Pacific region than in the Western Atlantic Ocean, and of course subsurface data of reefs sand

aprons are needed to support this assumption. The mid- to late-Holocene sea-level highstand and fall in the Indo-Pacific realm restricted vertical accretion of sand aprons by the constriction of accommodation space thereby constraining lateral extent of sand aprons. Carbonate production at reef margins (and to a lesser extent on sand aprons) is responsible for the amount of sediment supply, which is transported to atoll lagoons by reef sand aprons. Sedimentation rates of sand aprons are estimated to be up to three times higher than those of lagoonal background sedimentation and therefore suited to infill lagoonal accommodation space and create "filled buckets" in small and intermediately sized carbonate platforms. The combination of physical, biological and geomorphological parameters as controlling factors for sand apron development should be kept in mind, when applying these analogs to the stratigraphic record.

Acknowledgements

We thank the Alfons and Gertrud Kassel-Stiftung for financial support (fellowship to AI). The constructive criticisms of Erdal Koşun (Antalya) and an anonymous journal reviewer helped to improve this publication and are gratefully acknowledged.

References

- Adey, W.H. 1978. Coral reef morphogenesis: a multidimensional model. *Science* 202:831-837. doi:10.1126/science.202.4370.831
- Burne, R. 1991. Carbonate sediment budgets and coastal management in South Pacific Island nations. Workshop on Coastal Processes in South Pacific Island Nations SOPAC Technical Bulletin 7:45-53
- Camoin, G.F., Colonna, M., Montaggioni, L.F., Casanova, J., Faure, G. and Thomassin, B.A. 1997. Holocene sea level changes and reef development in southwestern Indian Ocean. *Coral Reefs* 16: 247-259. doi:10.1007/s003380050080
- Camoin, G.F., Ebren, P., Eisenhauer, A., Bard, E. and Faure, G. 2001. A 300,000-yr coral reef record of sea level changes, Mururoa Atoll (Tuamotu archipelago, French Polynesia). *Palaeogeography Palaeoclimatology Palaeoecology* 175:325-341
- Camoin, G., Montaggioni, L.F. and Braithwaite, C.J.R. 2004. Late glacial to postglacial sea levels in the Western Indian Ocean. *Marine Geology* 206:119-46. doi:10.1016/j.margeo.2004.02.003
- Davies, P.J. and Hopley, D. 1983. Growth fabrics and growth rates of Holocene reefs in the Great Barrier Reef. *BMR Journal of Australian Geology Geophysics* 8:237-252

- Emery, K.O., Tracey, J.L. and Ladd, H.S. 1954. Geology of Bikini and nearby atolls. U.S. Geological Survey Professional Paper 260-A:1-265
- Gischler, E. 2003. Holocene lagoonal development in the isolated carbonate platforms off Belize. *Sedimentary Geology* 159:113-132. doi:10.1016/S0037-0738(03)00098-8
- Gischler, E. 2015. Quaternary reef response to sea level and environmental change in the western Atlantic. *Sedimentology* 62:429-465. doi:10.1111/sed.12174
- Gischler, E. and Hudson, J.H. 1998. Holocene development of three isolated carbonate platforms, Belize, Central America. *Marine Geology* 144:333-347
- Gischler, E. and Hudson, J.H. 2004. Holocene development of the Belize barrier reef. *Sedimentary Geology* 164:223-236
- Gischler, E., Hudson, J.H. and Pisera, A. 2008. Late Quaternary reef growth and sea level in the Maldives (Indian Ocean). *Marine Geology* 250:104-113. doi:10.1016/j.margeo.2008.01.004
- Grossman, E.E. and Fletcher, C.H. 2004. Holocene reef development where wave energy reduces accommodation space, Kailua Bay, Windward Oahu, Hawaii, USA. *Journal of Sedimentary Research* 74:49-63. doi:10.1306/070203740049
- Hammer, Ø., Harper, D.A.T. and Paul, D.R. 2001. PAST: Paleontological Statistics Software Package for education and data analysis. *Palaeontologica Electronica* 4:4-9, 178kb
- Harris, D.L., Vila-Concejo, A., De Carli, E.V. and Webster, J.M. 2011. Geomorphology and morphodynamics of a sand apron, One Tree reef, southern Great Barrier Reef. *Proceedings of the 11th International Coastal Symposium, Journal of Coastal Research* SI 64:760-764
- Harris, D.L., Vila-Concejo, A. and Webster, J.M. 2014. Geomorphology and sediment transport on a submerged back-reef sand apron: One Tree Reef, Great Barrier Reef. *Geomorphology* 222:132-142. doi:10.1016/j.geomorph.2014.03.015
- Hopley, D., Smithers, S. and Parnell, K. 2007. *The Geomorphology of the Great Barrier Reef, development, diversity and change*. Cambridge University Press
- Isaack, A. 2013. *Rezente Sedimentfazies der Dry Tortugas, Südflorida, USA*. Unpublished M.Sc. thesis, Goethe Universität Frankfurt
- Kench, P.S. 1997. Currents of removal analysis of carbonate sediments. *Proceedings of the 8th International Coral Reef Symposium, Panama* 1:503-508
- Kench, P.S. 1998a. Physical controls on development of lagoon sand deposits and lagoon infilling in an Indian Ocean atoll. *Journal of Coastal Research* 14:1014-1024

- Kench, P.S. 1998b. A currents of removal approach for interpreting carbonate sedimentary processes. *Marine Geology* 145:197-323
- Kench, P.S., Smithers, S.G., McLean, R.F. and Nichol, S.L. 2009. Holocene reef growth in the Maldives: Evidence of a mid-Holocene sea level highstand in the central Indian Ocean. *Geology* 37:455-458. doi:10.1130/G25590A.1
- Klostermann, L. and Gischler, E. 2015. Holocene sedimentary evolution of a mid-ocean atoll lagoon, Maldives, Indian Ocean. *International Journal of Earth Science* 104:289–307. doi:10.1007/s00531-014-1068-8
- Ladd, H.S. and Schlanger, S.O. 1960. Drilling Operations on Eniwetok Atoll. U.S. Geological Survey Professional Paper 260-Y:863-899
- Lighty, R.G., Macintyre, I.G. and Stukenrath, R. 1982. *Acropora palmata* reef framework: a reliable indicator of sea level in the Western Atlantic for the past 10,000 years. *Coral Reefs* 1:125-130
- Macintyre, I.G., Burke, R.B., Stuckenrath, R. 1977. Thickest recorded Holocene reef section, Isla Pérez core hole, Alacran Reef, Mexico. *Geology* 5:749-754
- Macintyre, I.G., Graus, R., Reinthal, P.N., Littler, M.M. and Littler, D.S. 1987. The barrier reef sediment apron: Tobacco Reef, Belize. *Coral Reefs* 6:1-12. doi:10.1007/BF00302206
- Marshall, J.F. and Davies, P.J. 1982. Internal structure and Holocene evolution of One Tree Reef, southern Great Barrier Reef. *Coral Reefs* 1:21-28. doi:10.1007/BF00286536
- Marshall, J.F. and Jacobsen, G. 1985. Holocene growth of a mid-Pacific atoll: Tarawa, Kiribati. *Coral Reefs* 4:11-17
- Montaggioni, L.F. 1988. Holocene reef growth history in mid-plate high volcanic islands. *Proceedings of the 6th International Coral Reef Symposium Townsville, Australia* 3:455-460
- Montaggioni, L.F. 2005. History of Indo-Pacific reef systems since the last glaciation: Development patterns and controlling factors. *Earth-Science Reviews* 71:1-75. doi:10.1016/j.earscirev.2005.01.002
- O’Leary, M.J., Perry, C.T., Beavington-Penney, S.J. and Turner, J.R. 2009. The significant role of sediment bio-retexturing within a contemporary carbonate platform system: Implications for carbonate microfacies development. *Sedimentary Geology* 219:169-179. doi:10.1016/j.sedgeo.2009.05.005

- Pirazzoli, P.A. and Montaggioni, L.F. 1986. Late Holocene sea level changes in the Northwest Tuamotu Islands, French Polynesia. *Quaternary Research* 25:350-368. doi:10.1016/0033-5894(86)90006-2
- Perry, C.T., Kench, P.S., Smithers, S.G., Yamano, H., O'Leary, M. and Gulliver, P. 2013. Time scales and modes of reef lagoon infilling in the Maldives and controls on the onset of reef island formation. *Geology* 41:1111-1114. doi:10.1130/G34690.1
- Purdy, E.G. 1974. Reef configurations: Cause and effect, in: Laporte LF (ed) *Reefs in time and space*, SEPM Special Publication 18:9-76
- Purdy, E.G. and Gischler, E. 2005. The transient nature of the empty bucket model of reef sedimentation. *Sedimentary Geology* 175:35-47. doi:10.1016/j.sedgeo.2005.01.007
- Purdy, E.G. and Winterer, E.L. 2001. Origin of atoll lagoons. *GSA Bulletin* 113:837-854
- Rankey, E.C. and Garza-Peréz, J.R. 2012. Seascape metrics of shelf-margin reef and reef sand aprons of Holocene carbonate platforms. *Journal of Sedimentary Research* 82:53-71. doi:10.2110/jsr.2012.7
- Rankey, E.C., Reeder, S.L. and Garza-Peréz, J.R. 2011. Controls on links between geomorphology and surface sedimentological variability: Aitutaki and Maupiti Atolls, South Pacific Ocean. *Journal of Sedimentary Research* 81:885-900. doi:10.2110/jsr.2011.73
- Rashid, R., Eisenhauer, A., Stocchi, P., Liebetrau, V., Fietzke, J., Rüggeberg, A. and Dullo, W.C. 2014. Constraining mid to late Holocene relative sea level change in the southern equatorial Pacific Ocean relative to the Society Islands, French Polynesia. *Geochemistry Geophysics Geosystems* doi:10.1002/2014GC005272
- Schlager, W. 1993. Accommodation and supply - a dual control on stratigraphic sequences. *Sedimentary Geology* 86:111-136
- Smithers, S.G., Woodroffe, C.D., McLean, R.F. and Wallensky, E.P. 1994. Lagoonal sedimentation in the Cocos (Keeling) Islands, Indian Ocean. *Proceedings of the 7th International Coral Reef Symposium* 1:273-288
- Stoddart, D.R. 1969. Ecology and morphology of recent coral reefs. *Biological Reviews* 44:433-498
- Toscano, M., Macintyre, I.G. 2003. Corrected western Atlantic sea-level curve for the last 11,000 years based on calibrated ¹⁴C dates from *Acropora palmata* framework and intertidal mangrove peat. *Coral Reefs* 22:257-270

- Tudhope, A.W. 1989. Shallowing-upwards sedimentation in a coral reef lagoon, Great Barrier Reef of Australia. *Journal of Sedimentary Petrology* 59:1036-1051
- Vila-Concejo, A., Harris, D.L., Webster, J.M. and Power, H.E. 2013. Coral reef sediment dynamics: evidence of sand apron evolution on a daily and decadal scale, in: Conley DC, Masselink G, Russel PE, O'Hare TJ (eds) *Proceedings Coastal Research*, SI 65:606-611. doi:10.2112/SI65-103.1
- Wasserman, H.N. and Rankey, E.C. 2014. Physical oceanographic influences on sedimentology of reef sand aprons: Holocene of Aranuka Atoll (Kiribati), Equatorial Pacific. *Journal of Sedimentary Research* 84:586-604. doi:10.2110/jsr.2014.50
- Webster, J.M. 1999. The response of coral reefs to sea level change: Evidence from the Ryukyu Islands and the Great Barrier Reef. Unpublished PhD thesis, University of Sydney
- Woodroffe, C.D. 2005. Late Quaternary sea level highstands in the central and eastern Indian Ocean: A review. *Global and Planetary Change* 49:121-138. doi:10.1016/j.gloplacha.2005.06.002
- Woodroffe, C.D. and Biribo, N. 2011. Atolls, in: Hopley D (ed) *Encyclopedia of modern coral reefs, structure, form and process*. Springer, pp 1-21. doi:10.1016/j.margeo.2013.12.006
- Woodroffe, C.D., McLean, R.F. and Wallensky, E. 1994. Geomorphology of the Cocos (Keeling) Islands. *Atoll Research Bulletin* 402:1-33
- Woodroffe, C.D. and Webster, J.M. 2014. Coral reefs and sea-level change. *Marine Geology* 352:248-267. doi:org/10.1016/j.margeo.2013.12.006
- Zinke, J., Reijmer, J.J.G., Thomassin, B.A., Dullo, W.C., Grootes, P.M. and Erlenkeuser, H. 2001. Postglacial flooding history of Mayotte lagoon (Comoro archipelago, southwest Indian Ocean). *Marine Geology* 194:181-196. doi:10.1016/S0025-3227(02)00705-3

CHAPTER 3

LATE QUATERNARY BARRIER AND FRINGING REEF DEVELOPMENT OF BORA BORA (SOCIETY ISLANDS, SOUTH PACIFIC): FIRST SUBSURFACE DATA FROM THE DARWIN-TYPE BARRIER-REEF SYSTEM

Eberhard Gischler¹, J. Harold Hudson², Marc Humblet³, Juan Carlos Braga⁴,
Anton Eisenhauer⁵, **Anja Isaack**¹, Flavio S. Anselmetti⁶ and Gilbert F. Camoin⁷

¹Institut für Geowissenschaften, J.W. Goethe-Universität, Frankfurt am Main,
Germany

²ReefTech Inc., Miami, Florida, USA

³Department of Earth and Planetary Sciences, Nagoya University, Nagoya,
Japan

⁴Departamento de Estratigrafía y Paleontología, Universidad de Granada,
Granada, Spain

⁵GEOMAR, Helmholtz-Zentrum für Ozeanforschung Kiel, Kiel, Germany

⁶Institute of Geological Sciences & Oeschger Centre for Climate Change
Research, University of Bern, Bern, Switzerland

⁷Aix-Marseille Université, CNRS, IRD, CEREGE UM34, Aix-en-Provence &
Europôle Méditerranéen de l'Arbois, BP 80, Aix-en-Provence cedex 4, France

Keywords: barrier reef, fringing reef, Quaternary, U-series dating, Bora Bora,
Pacific

*Published 2016: **Sedimentology**, 63:1522–1549. doi:10.1111/sed.12272*

*(Contributions of A. Isaack: acquisition of rotary drill cores, assessment of XRD
and calcimeter data and final approval of the version to be submitted.)*

Abstract

Darwin's universally-known subsidence theory, based on Bora Bora as a model, was developed without information from the subsurface. To evaluate the influence of environmental factors on reef development, two traverses with three cores, each on the barrier and the fringing reefs of Bora Bora, were drilled and 34 uranium-series dates obtained and

subsequently analyzed. Sea-level rise and, to a lesser degree, subsidence were crucial for Holocene reef development in that they have created accommodation space and controlled reef architecture. Antecedent topography played a role as well, because the Holocene barrier reef is located on a Pleistocene barrier reef forming a topographic high. The pedestal of the fringing reef was Pleistocene soil and basalt. Barrier and fringing reefs developed contemporaneously during the Holocene. The occurrence of five corallgal assemblages indicate an upcore increase in wave energy. Age-depth plots suggest that barrier and fringing reefs have prograded during the Holocene. The Holocene fringing reef is up to 20 m thick and comprises corallgal and microbial reef sections, and abundant unconsolidated sediment. Fringing reef growth started 8780 ± 50 yr BP; accretion rates average 5.65 m/kyr. The barrier reef consists of > 30 m thick Holocene corallgal and microbial successions. Holocene barrier reef growth began $10,030 \pm 50$ yr BP and accretion rates average 6.15 m/kyr. The underlying Pleistocene reef formed $116,900 \pm 1100$ yr BP, *i.e.*, during marine isotope stage 5e. Based on Pleistocene age, depth, and corallgal palaeobathymetry, the subsidence rate of Bora Bora was estimated to 0.05-0.14 m/kyr. In addition to subsidence, reef development on shorter timescales like in the late Pleistocene and Holocene, has been driven by glacioeustatic sea-level changes causing alternations of periods of flooding and subaerial exposure. Comparisons with other oceanic barrier reef systems in Tahiti and Mayotte exhibit more differences than similarities.

3.1 Introduction

In the widely known subsidence theory of reef development, Darwin (1842) used Bora Bora as type barrier reef to explain the genetic connection between shoreline-attached fringing reefs, barrier reefs (detached from shore by lagoon), and atolls (annular reefs with deep central lagoon). Darwin (1842, his figs 5; 6) showed that due to subsidence of a volcanic island and contemporaneous reef aggradation and slight retrogradation, fringing reefs develop into barrier reefs, and eventually into atolls. Likewise, Dana (1875, p. 287) and Davis (1928, p. 302-306) argued that Bora Bora was an ideal example of a barrier-reef structure originating from subsidence of a volcanic island. Opposing the subsidence theory, Agassiz (1903, p. 161-164) interpreted the reefs of the Society Islands, including Bora Bora, as remnants of denudation and erosion resting on larger platforms. Crossland (1928) also favored erosion as crucial factor in the development of reefs of the archipelago. These early discussions were based only on surface and geomorphological observations.

The significance of subsidence of volcanic islands for the development of isolated reefs in the open ocean was proven for the first time by drilling on Enewetak Atoll, Marshall Islands (Ladd et al., 1953), which recovered 1.25-1.4 km of reefal limestone overlying Eocene basalt. However, Saller and Koepnick (1990) showed that reef facies in Enewetak had not simply aggraded and slightly retrograded as predicted by Darwin's model, but significantly prograded; furthermore, major unconformities were identified in the drill cores. The progradation is a consequence of an overall falling trend of Neogene sea level, which resulted in carbonate accumulation rates exceeding the rate of creation of accommodation space. The unconformities resulted from repeated subaerial exposure during sea-level lowstands. Comparable observations were made in Mururoa Atoll, Tuamotu archipelago, in which stacked, aggrading and prograding Pleistocene reef units separated by karst surfaces have been identified in core and by forward modelling (Camoin et al., 2001; Montaggioni et al., 2015). Antecedent karst topography (Purdy, 1974), formed during sea-level lowstands, appears to be an important control on modern reef geomorphology. Barrier and atoll reef geomorphologies can apparently be produced by meteoric dissolution during sea-level lowstands as shown by Purdy (1974) and Purdy and Winterer (2001, 2006). However, alleged karst geomorphologies such as the principal bucket or saucer shape of coral reefs may also be a consequence of biotic self-organization as recently demonstrated by Schlager and Purkis (2013, 2015).

Scientific drilling in the Society Islands started on Moorea and Tahiti (Montaggioni 1988; Bard et al., 1996; Montaggioni et al., 1997) and underlined the importance of postglacial sea-level rise for late Quaternary reef development. Thick successions (> 80 m) of late Pleistocene and Holocene reef limestone were recovered from the barrier reef of Papeete, Tahiti (Bard et al., 1996; Montaggioni et al., 1997; Cabioch et al., 1999a). Sea-level data show a rapid rise from 13,800 yrs until ca. 6000 yrs BP and a subsequent slow rise approaching modern level (Bard et al., 1996). During the late Holocene, from ca. 6000-1000 yrs BP, sea level is thought to have exceeded modern level by about 1.5 m, based on sedimentological and chronological studies of exposed reef limestones collected in various areas of French Polynesia (Montaggioni and Pirazzoli, 1984; Pirazzoli et al., 1985a, b, 1987; Pirazzoli and Montaggioni, 1988a; Rashid et al., 2014). Additional drill cores from the barrier reef at Papeete, Tahiti, were used to constrain sea level during the time window 14,000-9000 yrs BP around meltwater pulse 1B (Bard et al., 2010). Recently, IODP Expedition 310 recovered 37 cores in three traverses in the fore-reef area (42-118 m water depth) around Tahiti with the aim of reconstructing post-glacial sea-level rise starting from the maximum of the last glaciation

some 20,000 yrs BP until the early Holocene (Deschamps et al., 2012; Camoin et al., 2012). Post-glacial sea-level rise was rapid and reefs accreted with 10 m/kyr. A very rapid rise during meltwater pulse 1A punctuated continuous reef development and led to reef backstepping and incipient drowning (Camoin et al., 2012). Interestingly, no indications for meltwater pulse 1B were found, like in the postglacial reef record of Barbados in the western Atlantic (Fairbanks, 1989). Based on core data from IODP Expedition 310, Blanchon et al., (2014) revisited Darwin's subsidence model, and suggested that in Tahiti a fringing to barrier reef transformation occurred during ca. 14000-12300 yrs BP. The former fringing reef had transformed into a barrier reef only when it became stranded at the edge of an older Pleistocene reef platform. These authors postulated that the reef was isolated from the coast and terrigenous influx and a transition to fast-growing acroporids increased barrier reef accretion. However, the fringing-to-barrier transition was not recovered and could not be dated exactly. Likewise, there are no age data of the top of the Pleistocene platform. Also, it is unknown when and how the modern fringing reefs around the island of Tahiti came into existence and developed, because they have not been drilled thus far. Data from a core on Motu Uta in Papeete harbor also indicated that the back reef lagoon acted as sink of siliciclastic sediment, however, a lagoonal patch reef started to develop on top of the siliciclastics some 7700 yrs BP (Cabioch et al., 1999a; their figs 4; 9).

A further critical issue concerns the accuracy of subsidence rates of Tahiti and especially the other islands and reefs in the Society archipelago. Studies of the geomorphology of shorelines resulted in estimates of 0.15 m/kyr subsidence for Tahiti and 0.05 m/kyr for Bora Bora and other islands in the western part of the archipelago (Pirazzoli and Montaggioni, 1985; Pirazzoli et al., 1985b). The island of Huahine did not fit this model of decreasing subsidence away from the hotspot though (Pirazzoli et al., 1985b). Fadlil et al. (2011) measured the recent subsidence rate of Tahiti by geodetic means and calculated a mean of 0.5 m/kyr. Subsidence evaluations based on core studies in Tahiti arrived at consistent rates. Bard et al. (1996) estimated long-term subsidence in Tahiti to 0.25 m/kyr based on a 549,000 yr BP K-Ar-age of basalt recovered 114 m downcore below a Pleistocene reef unit. Likewise, Thomas et al. (2012) identified 0.25 m/kyr as a minimum and 0.4 m/kyr as a maximum subsidence rate based on dated Pleistocene corals from IODP Expedition 310. Deschamps et al. (2012) concluded that 0.25 m/kyr was a value in agreement with various estimates obtained by different methods and assumed the true value to be between 0.2-0.4 m/kyr. These consistent estimates have recently been challenged by Blanchon et al. (2014), who argued that a subsidence of 0.5-0.6 m/kyr in Tahiti would be necessary to

account for the elevation of last interglacial corals at 115-120 m in IODP 310 cores dated by Thomas et al. (2009). No new subsidence data for the Leeward Islands in the Society archipelago have been published since the work by Pirazzoli and Montaggioni (1985) and Pirazzoli et al. (1985b).

Only a very few oceanic (Darwinian) barrier reef systems have been investigated by core studies in general. Examples include Tahiti (south Pacific) and Mayotte (Indian Ocean). Apart from Tahiti and nearby Moorea, no subsurface data exist from other reefs in the Society Island archipelago. Regarding the other archipelagoes in French Polynesia, scientific drilling was performed only on Mataiva Atoll (Pirazzoli and Montaggioni, 1986) and on Mururoa Atoll (Camoin et al., 2001) in the Tuamotus. Shallow holes drilled on Tikehau Atoll in the same archipelago were used to study reef hydrology but not sedimentology and chronology (Rougerie and Wauthy, 1993). To the knowledge of the authors, no fringing reefs were drilled in the region, which potentially have been subject to stronger siliciclastic and nutrient input and experienced weaker exposure to waves and currents as compared to barrier reefs. Therefore this study was designed to obtain subsurface data from both barrier and fringing reefs of Bora Bora, the type barrier reef of Darwin's subsidence theory. The aim of this study is to evaluate the influence of Holocene sea level, subsidence, antecedent topography, and other environmental factors such as siliciclastic input and exposure on barrier and fringing reef development.

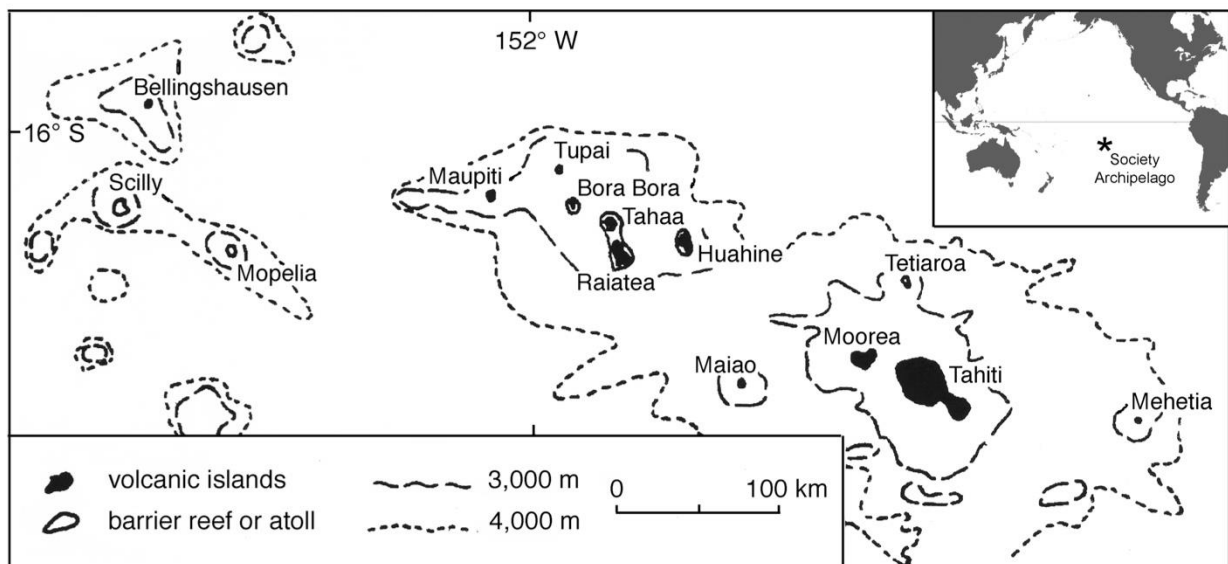


Fig. 3/1: Location of Bora Bora in the Society Islands (map modified from Gabriele and Salvat, 1985) and in the south Pacific. The location of the Society hotspot is between Mehetia and Tahiti

3.2 Study Area

Bora Bora is located in the western part of the Society archipelago in the central south Pacific Ocean (fig. 3/1). Together with the nearby Austral, Gambier, Tuamotu, and Marquesas islands, the archipelago is part of French Polynesia. The Society archipelago comprises nine islands and five atolls, and is 720 km long (fig. 3/1). Ages of the volcanic islands (4.3-0.3 Ma) increase from southeast (Mehetia) to northwest (Bellingshausen), and suggest a plate movement of 11 cm/yr over the Society hotspot (Blais et al. 2000; Guillou et al., 2005). The volcanic island of Bora Bora and the nearby island of Toopua are 3.45-3.10 Ma old based on radiometric (K/Ar) dating of basalts (Blais et al., 2000). The islands are composed of alkali basalt, rare hawaiites, intrusive gabbros, and a volcanic breccia. The Baie de Povai between Bora Bora and Toopua outlines the former caldera (fig. 3/2).

The climate of Bora Bora is tropical and characterized by a hot and wet season during the austral summer from November to April, and a colder and drier period in the austral winter from May to October

(Gabri  and Salvat, 1985). Trade winds are blowing from the northeastern to southeastern directions (Pirazzoli et al., 1985a). Eleven major cyclones have hit the Society Islands during 1901 to 1968. Major storms Lisa, Reva, and Veena have passed during 1982 to 1983 (Pirazzoli et al., 1985a). In February 2010, category 4 cyclone Oli made landfall on the Society Islands.

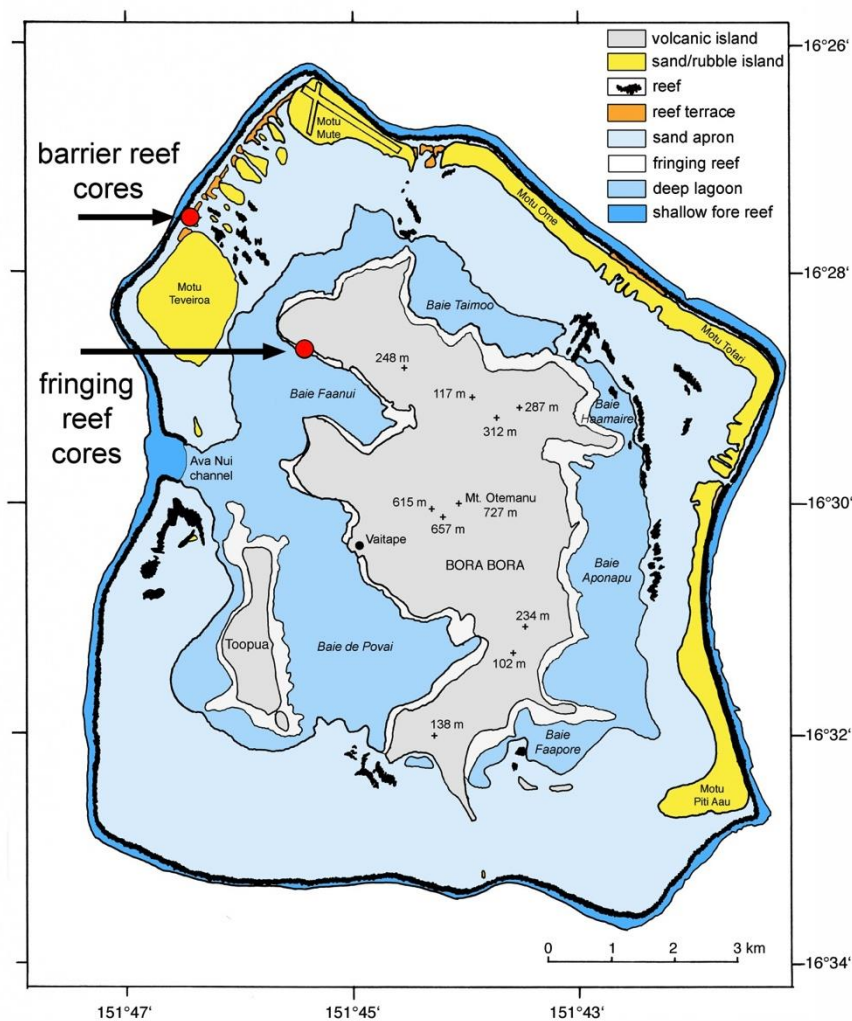


Fig. 3/2: Map of Bora Bora (after Gischler, 2011; modified) indicating locations of rotary core traverses on barrier and fringing reefs

Annual average air temperatures in French Polynesia decrease from 27 °C in the north to 21 °C in the south. Monthly air-temperature extremes in the Society Islands range from 24 to 28°C (Gabrié and Salvat, 1985). The spring tidal range is up to 40 cm (Pirazzoli et al., 1985a). Annual precipitation in Bora Bora, as measured from 1951 to 1961 (Guilcher et al., 1969), averages 2000 mm/yr. Measurements of sea-surface temperatures in the lagoon ranged from 23.8-26.7 °C in August 1963; salinity was slightly elevated above normal marine and ranged from 36.7-36.9‰ during the same time period (Guilcher et al. 1969).

The volcanic island of Bora Bora has an area of ca. 30 km² with a 32 km long and complex coastline creating extensive bays and long peninsulas (fig. 3/2). The highest point, Mt. Otemanu, rises 727 m above sea level. The island is densely wooded. There is one ephemeral water course that is draining into Faanui Bay. The barrier-reef system surrounding the volcanic island has an area of ca. 70 km². The shoreline is almost completely lined by fringing reefs. The lagoon floor is quite irregular and includes six basins (areas of Baie de Povai, Baie Faanui, Baie Taimoo, Baie Haamaire, Baie Aponapu, and Baie Faapore) up to 40 m deep (Guilcher et al., 1969; Gabrié et al., 1994). Lagoonal patch reefs are lacking. One break in the barrier reef (Ava Nui channel, in the west) is up to 48 m deep and connects the lagoon with the surrounding ocean. The barrier reef, including the reef crest and the extensive sand apron, is 1-2 km wide. The reef crest consists largely of coralline algae (*Porolithon*) and the brown alga *Turbinaria* (Gabrié et al., 1994). Water depth on sand aprons usually does not exceed 3.5 m. Sand aprons are wider in the south and southwest, where no motus (elongated sand and rubble islands) exist, as compared to the north and east. Motus apparently act as barriers of sediment transport from the marginal reefs to the lagoon. Coral patch reefs on the sand apron are most extensive in the northeastern and eastern part of Bora Bora, usually in the lee of narrow, shallow waterways (hoa) through the motus. On the eastern, northern, and northwestern sides of the island, long and continuous motus are developed. They are interrupted by a few very shallow hoa. Lagoonal circulation is sustained by water entering through the hoas on the eastern reef and leaving through Ava Nui channel in the west (Gabrié et al., 1994). The lack of motus on the southwestern and southern reef margin was suggested to be an expression of a southwestward tilt of the volcanic edifice (Blais et al., 2000), *i.e.*, a deeper position of the antecedent topography. On the ocean sides of the motus, coral rubble conglomerate, beachrock, and fossil elevated reef terraces (feo) occur (Pirazzoli et al., 1985b, 1988; Pirazzoli and Montaggioni, 1988a, b; Rashid et al., 2014). The terraces are Holocene in age and present evidence of a higher-than-present Holocene sea level. On the seaward side of the reef crest, a well-developed spur and groove system can be found (Gabrié et al., 1994;

Gischler, 2010). The shallow outer reef is characterized by few corals including *Acropora* and *Pocillopora* as well as pavements of crustose coralline algae.

3.3 Methods

Six rotary cores were drilled during April 2014 using a hydraulic drill fixed to a tripod with wireline core barrel. Barrel length was 1.5 m. One traverse of three cores was drilled on the northwestern barrier reef and one traverse of the cores on the fringing reef in Baie Faanui (figs 3/2; 3/3). Coordinates were recorded with GPS. Elevation was measured to mean sea level (MSL). Barrier reef cores include TEV1 ($16^{\circ}27'27.8''\text{S}$; $151^{\circ}46'31.8''\text{W}$; drilled at MSL), TEV2 ($16^{\circ}27'26.8''\text{S}$; $151^{\circ}46'33.1''\text{W}$; drilled 1 m above MSL), and TEV3 ($16^{\circ}27'26.0''\text{S}$; $151^{\circ}46'35.0''\text{W}$; drilled 0.5 m below MSL). Fringing reef cores comprise FAA1 ($16^{\circ}28'37.2''\text{S}$; $151^{\circ}45'30.3''\text{W}$; drilled at MSL), FAA2 ($16^{\circ}28'38.4''\text{S}$; $151^{\circ}45'30.9''\text{W}$; drilled 1 m below MSL), and FAA3 ($16^{\circ}28'37.7''\text{S}$; $151^{\circ}45'30.7''\text{W}$; drilled 0.5 m below MSL). Core recovery ranged from 0-87% and averaged 25-41% in barrier reef and 4-36% in fringing reef cores (tab. 3/1).

Depths of samples in cores including error ranges were calculated based on recovery in individual core barrels. Snorkel trips around the two drill sites were undertaken to collect qualitative data regarding bottom characteristics.

In the home laboratory, cores were cut with a rock saw and subsequently studied with regard to sedimentology including diagenesis, taxonomy, and age. Eighty-one thin sections from samples taken from cores TEV1-3 and FAA1 were qualitatively studied under a

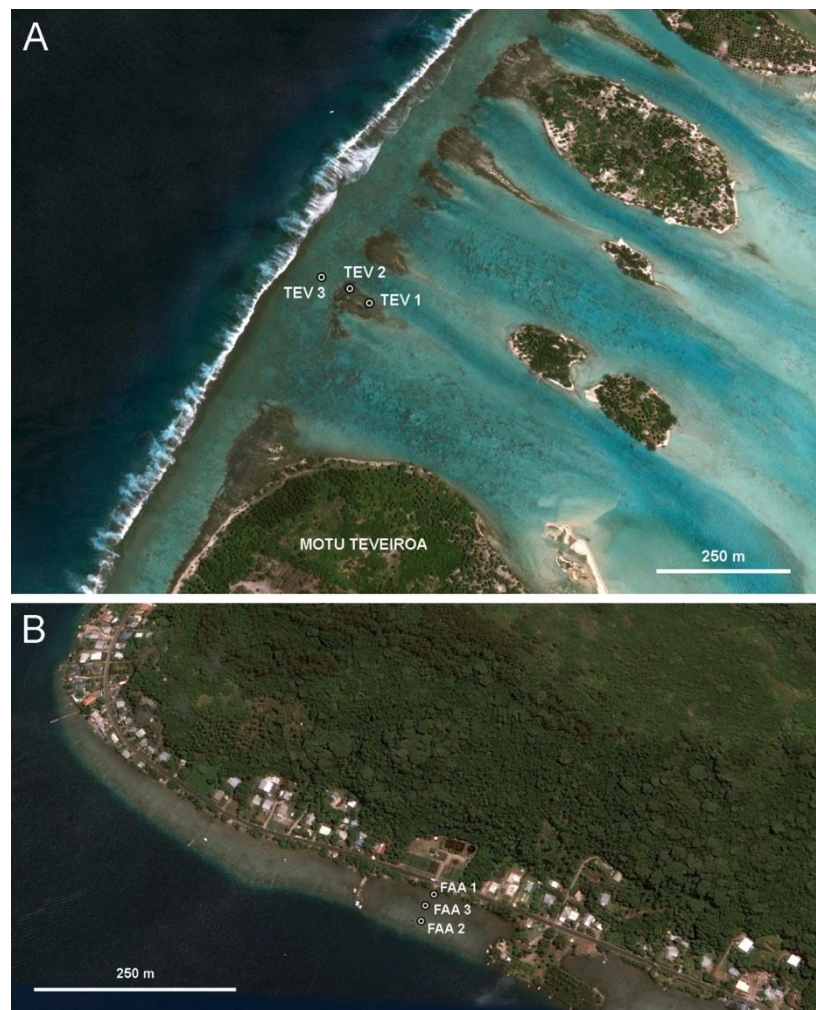


Fig. 3/3: Satellite images with barrier and fringing reef drilling locations (from GoogleEarth); a) Barrier reef; b) Fringing reef

Table 3/1: Recovery in barrier and fringing reef cores of Bora Bora

barrel	recovery (cm)	recovery (%)	barrel	recovery (cm)	recovery (%)	barrel	recovery (cm)	recovery (%)
TEV 1			TEV 3			FAA 1		
1	87.0	58.0	1	120.0	80.0	1	130.0	86.7
2	125.0	83.3	2	75.0	50.0	2	50.0	33.3
3	110.0	73.3	3	10.0	6.7	3	60.0	40.0
4	115.0	76.7	4	15.0	10.0	4	70.0	46.7
5	70.0	46.7	5	20.0	13.3	5	130.0	86.7
6	60.0	40.0	6	40.0	26.7	6	80.0	53.3
7	60.0	40.0	7	50.0	33.3	7	30.0	20.0
8	50.0	33.3	8	70.0	46.7	8	0.0	0.0
9	50.0	33.3	9	70.0	46.7	9	0.0	0.0
10	20.0	13.3	10	15.0	10.0	10	0.0	0.0
11	25.0	16.7	11	20.0	13.3	11	10.0	6.7
12	30.0	20.0	12	60.0	40.0	12	80.0	53.3
13	15.0	10.0	13	70.0	46.7	mean	53.3	35.5
14	40.0	26.7	14	75.0	50.0	FAA 2		
15	40.0	26.7	15	55.0	36.7	1	35.0	23.3
16	120.0	80.0	16	50.0	33.3	2	0.0	0.0
17	120.0	80.0	17	95.0	63.3	3	0.0	0.0
18	25.0	16.7	18	60.0	40.0	4	0.0	0.0
19	30.0	20.0	19	0.0	0.0	5	10.0	6.7
20	55.0	36.7	20	15.0	10.0	6	0.0	0.0
21	27.0	18.0	mean	49.3	32.9	7	0.0	0.0
mean	60.7	40.5	mean barrier reef	48.9	32.6	mean	6.4	4.3
TEV 2						FAA 3		
1	110.0	73.3				1	25.0	16.7
2	45.0	30.0				2	0.0	0.0
3	0.0	0.0				3	0.0	0.0
4	0.0	0.0				4	0.0	0.0
5	45.0	30.0				5	0.0	0.0
6	80.0	53.3				6	0.0	0.0
7	60.0	40.0				7	5.0	3.3
8	70.0	46.7				8	5.0	3.3
9	60.0	40.0				9	0.0	0.0
10	20.0	13.3				10	5.0	3.3
11	8.0	5.3				11	5.0	3.3
12	15.0	10.0				12	0.0	0.0
13	25.0	16.7				13	0.0	0.0
14	40.0	26.7				14	95.0	63.3
15	60.0	40.0				15	95.0	63.3
16	35.0	23.3				mean	15.7	10.5
17	15.0	10.0				mean fringing reef	27.1	18.1
18	30.0	20.0						
19	20.0	13.3						
20	17.0	11.3						
21	20.0	13.3						
mean	36.9	24.6						

polarization microscope. Subsamples were powderized and relative amounts of carbonate minerals measured by XRD following the method Milliman (1974, p. 22-27). The same method was used to assess the aragonite content of corals selected for age dating; see below. In several samples from FAA1, the ratio of carbonates and siliciclastics was measured using a Scheibler calcimeter (Müller, 1967).

Table 3/2: Results of XRD analyses in samples that were also used for thin-section preparation. Results of XRD analyses of corals for age dating are not shown because they all consisted of 100% aragonite. Calcium carbonate content was measured only for some of the samples from core FAA 1

sample	depth in core (m)	aragonite (%)	high-Mg-calcite (%)	low-Mg-calcite (%)	CaCO ₃ (%)	remarks
TEV 1 b 1-1	1.00	93.57	6.22	0.21		
TEV 1 b 2-1	1.85	80.76	18.67	0.58		
TEV 1 b 2-2	2.75	74.18	24.87	0.95		
TEV 1 b 3-1	3.35	91.39	8.19	0.43		
TEV 1 b 4-1	5.15	88.54	10.89	0.57		
TEV 1 b 4-2	5.60	88.63	3.51	7.86		
TEV 1 b 6-1	7.75	91.27	8.47	0.26		
TEV 1 b 6-2	8.30	98.56	1.26	0.18		
TEV 1 b 7-1	9.25	68.28	30.41	1.31		
TEV 1 b 8-1	11.55	88.22	11.18	0.60		
TEV 1 b 9-1	12.55	56.70	43.30	0.00		
TEV 1 b11-1	15.60	90.63	8.81	0.56		
TEV 1 b11-2	16.20	66.40	31.67	1.93		
TEV 1 b12-1	17.10	76.90	23.10	0.00		
TEV 1 b13-1	18.50	71.81	28.19	0.00		
TEV 1 b13-2	19.00	76.20	22.87	0.92		
TEV 1 b14-1	20.05	44.74	53.76	1.50		microbialite
TEV 1 b16-1	23.50	65.48	32.36	2.16		
TEV 1 b18-1	26.50	96.76	3.01	0.23		
TEV 1 b19-1	27.60	99.81	0.05	0.14		
TEV 1 b20-1	29.05	86.54	11.18	2.28		
TEV 1 b20-2	29.60	52.12	44.49	3.39		
TEV 1 b20-3	30.00	31.88	63.34	4.78		red algal crust
TEV 1 b21-1	30.60	36.64	1.12	62.24		Pleistocene
TEV 1 b21-2	31.50	58.00	0.98	41.02		Pleistocene
TEV 2 b 1-1	0.20	97.17	2.69	0.14		
TEV 2 b 1-2	0.70	34.18	65.05	0.77		microbialite
TEV 2 b 2-1	2.35	64.23	34.60	1.18		
TEV 2 b 5-1	7.00	95.41	4.31	0.27		
TEV 2 b 7-1	9.40	89.81	9.83	0.36		

Continue on next page

sample	depth in core (m)	aragonite (%)	high-Mg-calcite (%)	low-Mg-calcite (%)	CaCO ₃ (%)	remarks
TEV 2 b 8-1	10.85	86.30	13.34	0.36		
TEV 2 b 8-2	11.90	70.07	29.38	0.55		
TEV 2 b 9-1	12.50	65.28	32.61	2.12		
TEV 2 b10-1	14.60	57.11	41.14	1.75		
TEV 2 b13-1	18.60	69.40	29.08	1.51		
TEV 2 b14-1	20.50	68.04	29.91	2.05		
TEV 2 b15-1	22.20	62.03	36.34	1.63		
TEV 2 b16-1	23.45	57.15	41.43	1.42		
TEV 2 b18-1	26.00	81.32	17.93	0.76		
TEV 2 b18-2	26.25	73.86	24.56	1.58		
TEV 2 b19-1	27.90	85.18	14.21	0.61		
TEV 2 b21-1	30.60	90.05	9.53	0.42		
TEV 2 b21-2	30.90	83.85	15.67	0.48		
TEV 3 b 1-1	0.65	97.79	2.06	0.16		
TEV 3 b 1-1	0.65	97.79	2.06	0.16		
TEV 3 b 2-1	1.75	65.27	33.02	1.72		
TEV 3 b 3-1	2.80	22.79	74.77	2.43		red algal crust
TEV 3 b 5-1	6.65	82.70	16.59	0.71		
TEV 3 b 6-1	8.80	71.54	27.59	0.86		
TEV 3 b 7-1	9.60	66.35	32.45	1.21		
TEV 3 b 7-2	9.75	93.34	6.43	0.23		
TEV 3 b 8-1	10.60	70.69	28.29	1.02		
TEV 3 b 8-2	10.80	78.28	20.98	0.73		
TEV 3 b 9-1	12.95	73.94	24.96	1.09		
TEV 3 b 9-2	13.30	91.51	7.98	0.51		
TEV 3 b10-1	14.25	74.83	24.09	1.08		
TEV 3 b11-1	16.15	66.85	32.10	1.04		
TEV 3 b12-1	17.55	78.46	20.17	1.37		
TEV 3 b13-1	19.20	35.06	61.35	3.58		red algal crust
TEV3 b 14-1	20.50	47.75	50.91	1.34		microbialite
TEV3 b 15-1	21.45	65.51	32.31	2.18		
TEV3 b 16-1	22.95	75.52	23.04	1.44		
TEV3 b 16-2	23.50	57.18	40.79	2.02		
TEV3 b 17-1	24.25	41.95	55.50	2.55		
TEV3 b 17-2	24.95	58.74	39.15	2.11		
TEV3 b 17-3	25.10	74.43	23.25	2.32		
TEV3 b 17-4	25.40	68.71	30.09	1.20		
TEV3 b 18-1	26.60	77.88	21.05	1.07		
TEV3 b 18-2	26.80	70.96	27.98	1.07		
FAA 1 b1-1	1.25	79.66	19.83	0.51	98.04	

Continue on next page

sample	depth in core (m)	aragonite (%)	high-Mg-calcite (%)	low-Mg-calcite (%)	CaCO ₃ (%)	remarks
FAA 1 b1-2	1.40	83.68	15.63	0.70	98.04	
FAA 1 b2-1	2.40	82.62	12.33	5.05	99.67	
FAA 1 b3-1	3.25	72.79	26.30	0.91	99.67	
FAA 1 b4-1	4.90	78.96	19.76	1.28		
FAA 1 b4-2	5.60	57.84	40.95	1.20	99.67	
FAA 1 b5-1	6.35	20.11	69.12	10.77	97.55	microbialite
FAA 1 b6-1	8.05	23.76	74.70	1.54	99.84	microbialite
FAA 1 b6-2	8.35	50.48	47.95	1.57	94.44	
FAA 1 b6-3	8.70	83.79	15.37	0.84	94.60	
FAA 1 b7-1	9.60	44.14	53.91	1.95	95.58	
mean	14.46	71.10	26.23	2.67	97.71	

Corals in cores were identified using the standard publications of Wallace (1999), Veron (2000), and the new guide of Humblet et al., (2015). Corals were identified at the lowest taxonomic level possible. Morphogroups were defined when several species in the same genus could not be distinguished (e.g., *Acropora* gr. *humilis*). Coral colonies described as massive are 5 cm in thickness or more. The width of coral branches was measured and they were categorized as fine (< 1 cm), medium-size (1-1.5 cm), or robust (> 1.5 cm). Coralline algae were identified in thin-sections. Thickness of coralline algal crusts was measured. The occurrences of vermetids and the encrusting foraminifer *Homotrema rubrum* was noted. Thirty-four uranium-series measurements of coral ages were performed following standard procedures for coral carbonate material. For U/Th dating, only corals with no indications of early diagenesis and an aragonite content of 100% were selected. Separation of uranium and thorium from the sample matrix was done using Eichrom-UTEVA resin following previously published methods (Fietzke et al. 2005). Determination of uranium and thorium isotope ratios were done using the multi-ion-counting inductively coupled plasma mass spectroscopy (MIC-ICP-MS) approach using the method of Fietzke et al., (2005). For isotope dilution measurements, a combined ²³³U/²³⁶U/²²⁹Th spike was used with stock solutions calibrated for concentration using NIST-SRM 3164 (U) and NIST-SRM 3159 (Th) as combi-spike, calibrated against CRM-145 uranium standard solution (formerly known as NBL-112A) for uranium isotope composition and against a secular equilibrium standard (HU-1, uranium ore solution) for the precise determination of ²³⁰Th/²³⁴U activity ratios. In clean room labs usually whole-procedure blank values of these kind of samples were measured between 0.5 and 1 pg for thorium and between 10 and 20 pg for uranium. Both values are in the range typical of this method and the laboratory (Fietzke et al., 2005). Based on the ²³⁰Th/²³²Th and ²³⁴U/²³⁸U

ratios, ages were calculated using the U-half-lives and Th-half-lives published by Cheng et al., (2000). Two additional samples from reef terraces of the northwestern barrier reef (BB27: 16°27'36.0"S; 151°46'39.0"W) and the eastern barrier reef (BB31: 16°30'15.0"S; 151°41'55.0"W) were dated with the radiocarbon method by Beta Analytic Inc., Miami, Florida. Sample elevation above mean sea level was assessed with a measuring tape during high and low tides.

3.4 Results

3.4.1 Sedimentology and diagenesis

Average recovery in barrier reef core TEV1 was 40.5%, amounted to 24.6% in TEV2, and reached 32.9% in TEV3. The cores consist of buff-colored, coral-rich Holocene limestones (fig. 3/4). Holocene reef successions are > 30 m thick. At the base of core TEV1, a section of Pleistocene limestone was recovered.

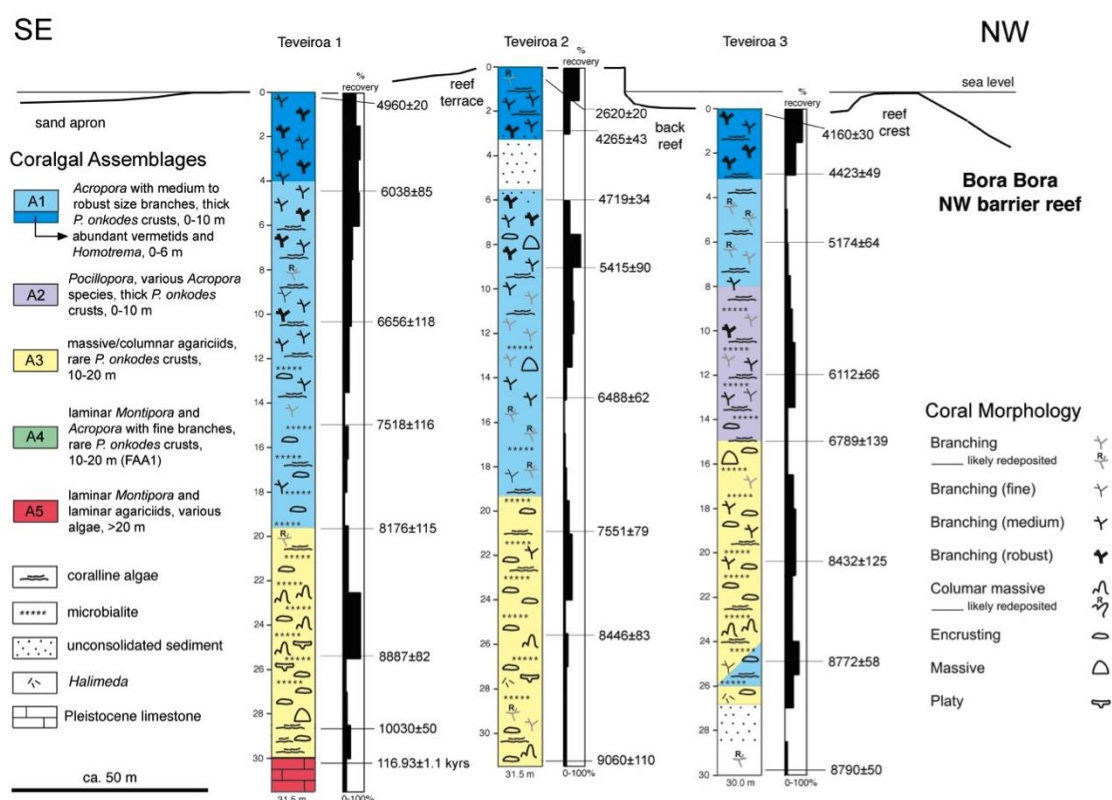


Fig. 3/4: Cross-section through barrier reef near Tevairoa island with interpreted core logs and palaeobathymetric interpretation. Low-recovery core sections were not included in palaeobathymetric considerations and left white

Pleistocene age could be inferred directly in the field from the dense texture, dark grey colors, and abundant recognizable blocky low-magnesium-calcite crystals. Cores TEV2 and TEV3 contained a 2-3 m thick sand-rich section at the top and the base, respectively. Fringing reef core FAA1 is composed of brownish-buff colored, coral-rich limestone in the upper part and a

sand-rich section in the lower part. The core had a recovery of 35.5% (fig. 3/5). Cores FAA2 and FAA3 are composed of very thick sand-rich sections with interspersed corals that produced low core recovery (fig. 3/5). Because of the large amounts of sand, problems with friction and water circulation were encountered so that hole FAA2 had to be abandoned before reaching the underlying Pleistocene section. At the bases of cores FAA1 and FAA3, brownish to reddish late Pleistocene soil and fragments of basalt were recovered. The late Pleistocene age was inferred based on the fact that terrestrial sediment must have been deposited during subaerial exposure prior to the Holocene. Holocene reef thickness ranged from 16-19 m. No underlying Pleistocene fringing reef was encountered.

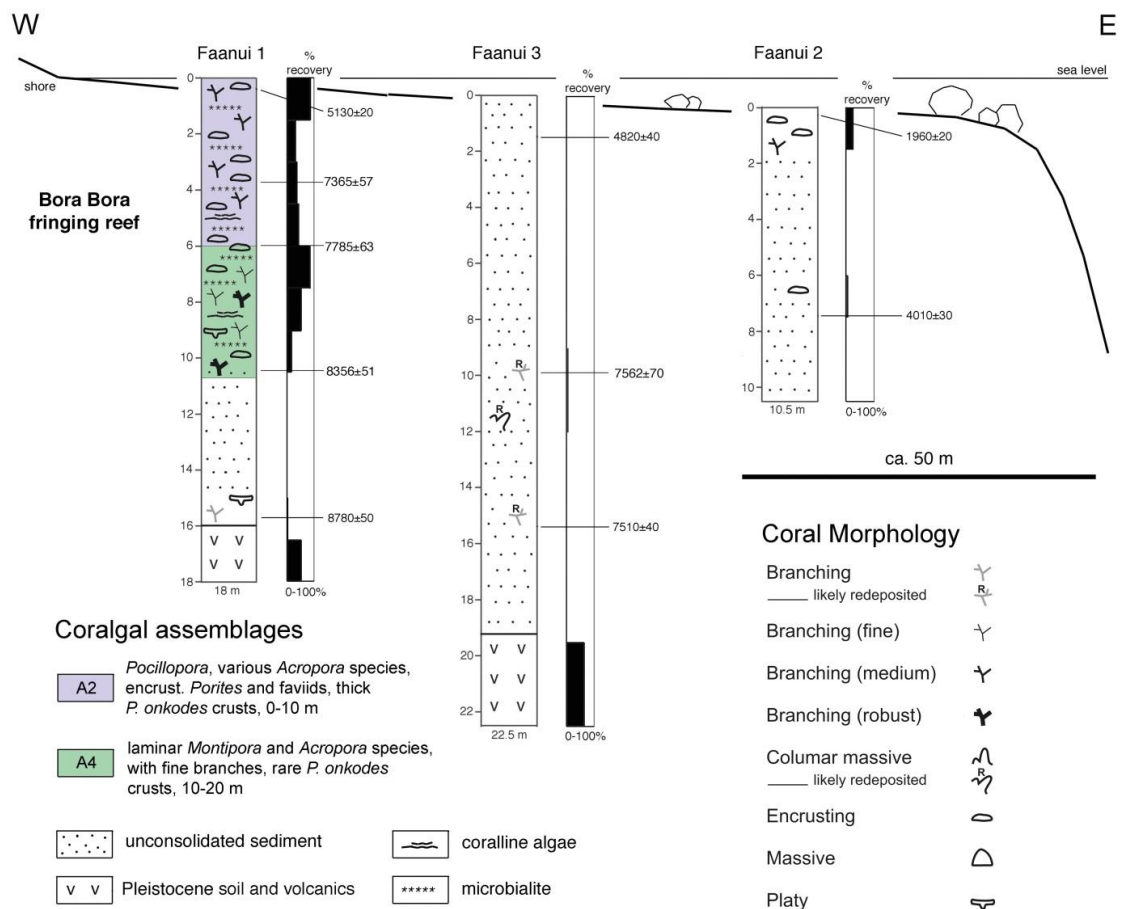


Fig. 3/5: Cross-section through fringing reef in Faanui Bay with interpreted core logs and palaeobathymetric interpretation. Low-recovery core sections were not included in palaeobathymetric considerations and left white

Corals are volumetrically the most abundant components in the cores (figs 3/6-3/8). Crustose coralline algae and *Halimeda* fragments are very common. Coralline algal crusts can be several centimeters thick. Coral and red algal distributions are described in more detail below. Shells of mollusks including vermetid gastropod encrustations are found commonly. Foraminiferal tests (miliolids and rotaliids) and the encrusting *Homotrema rubrum* and *Carpentaria* sp. occur. Both vermetids and *Homotrema* are more abundant towards core tops

(see below). Echinoderm fragments, mostly echinoid spines, are moderately abundant. Fine-grained carbonate sediment ("mud") as matrix with recognizable skeletal components is common (figs 3/9d; 3/10a).

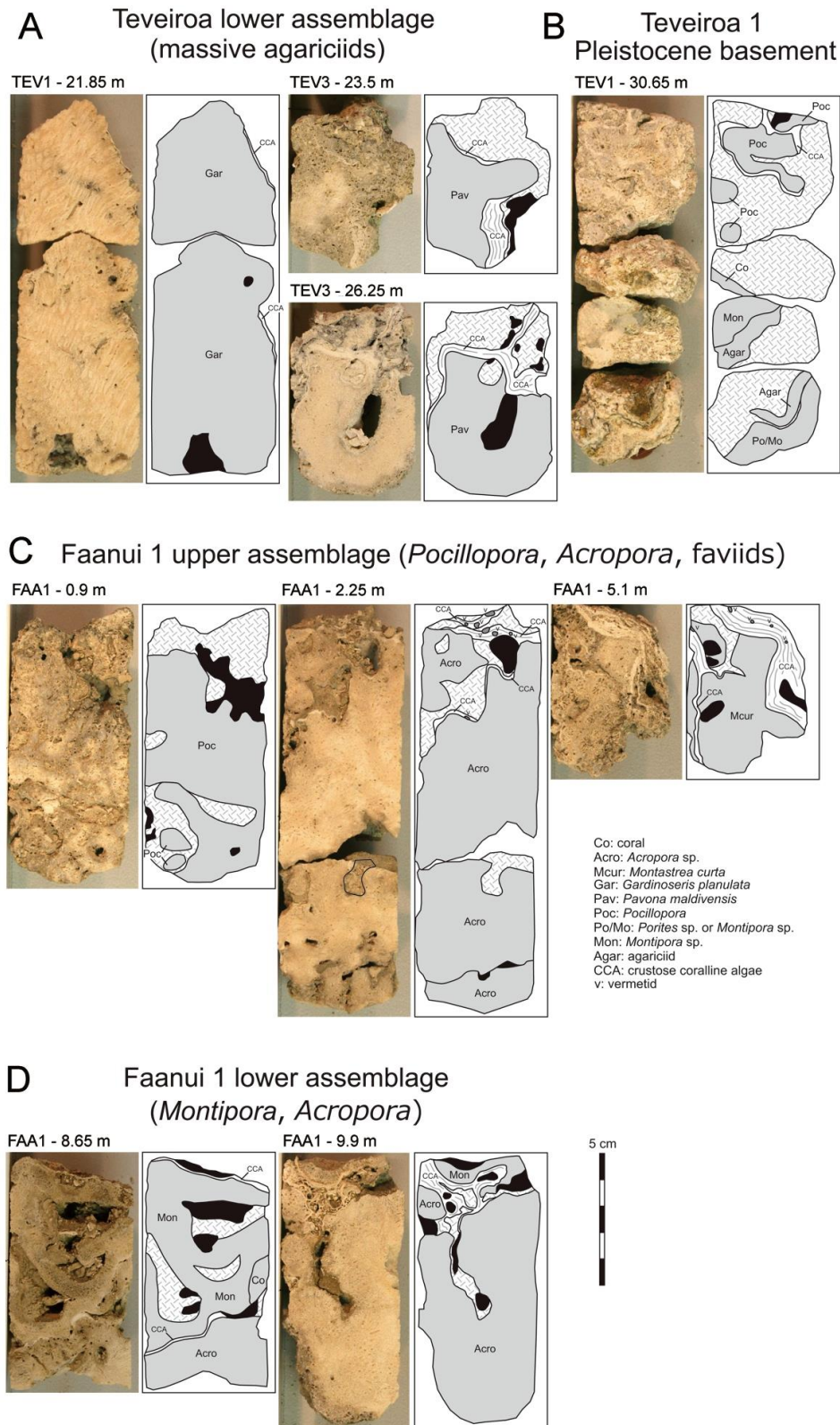


Fig. 3/6: Core sections showing characteristic corals from barrier reef. Upper assemblage with medium to robust branching *Acropora* and *Pocillopora*

Teveiroa upper assemblage
(*Acropora* -medium/robust branching-, *Pocillopora*)

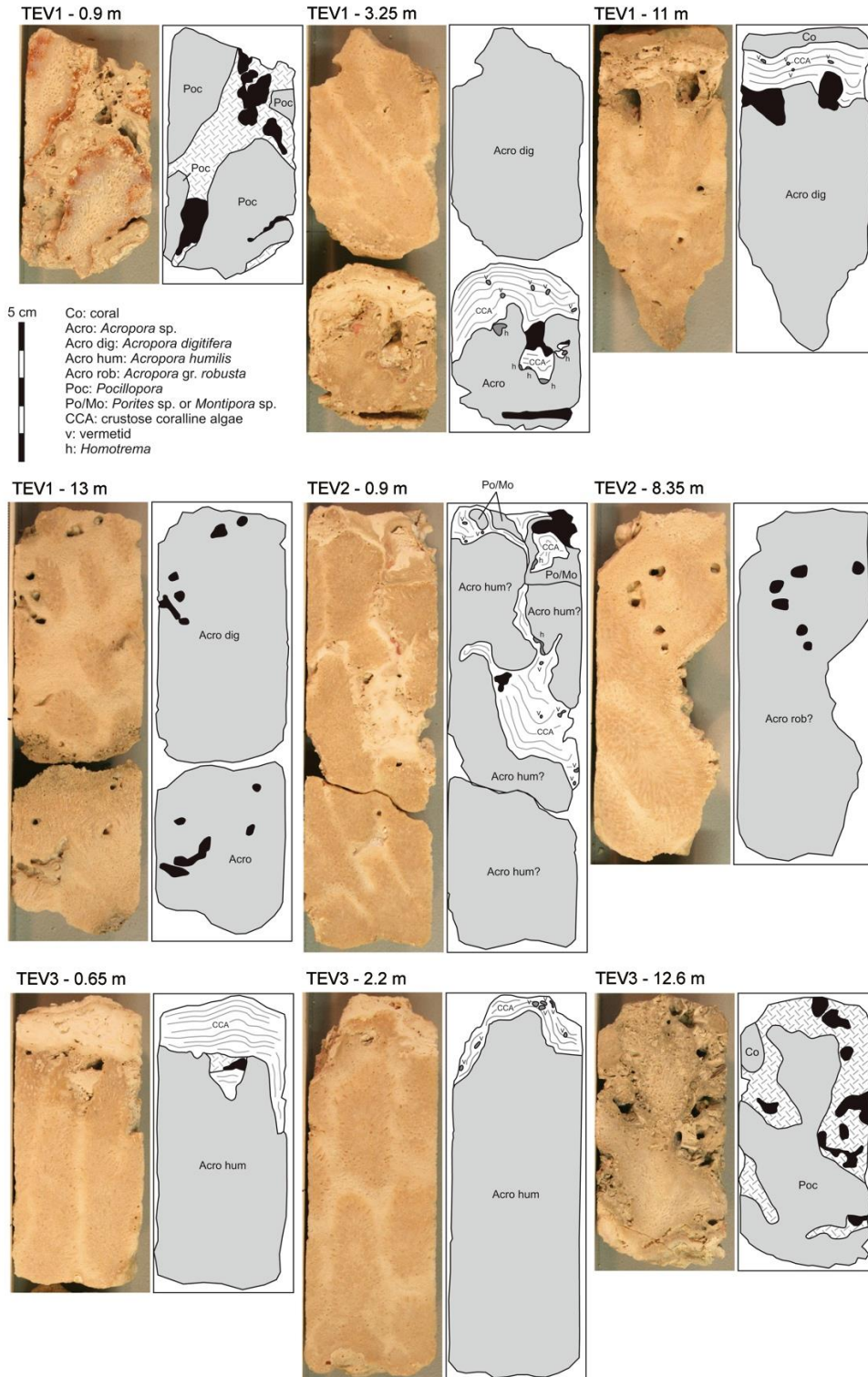


Fig. 3/7: Core sections showing characteristic corals from barrier and fringing reefs; **a)** Lower assemblage of barrier reef with massive agariciids; **b)** Pleistocene assemblage of barrier reef; **c)** Fringing reef upper assemblage with *Pocillopora*, *Acropora*, and faviids; **d)** Fringing reef lower assemblage with *Montipora* and *Acropora*

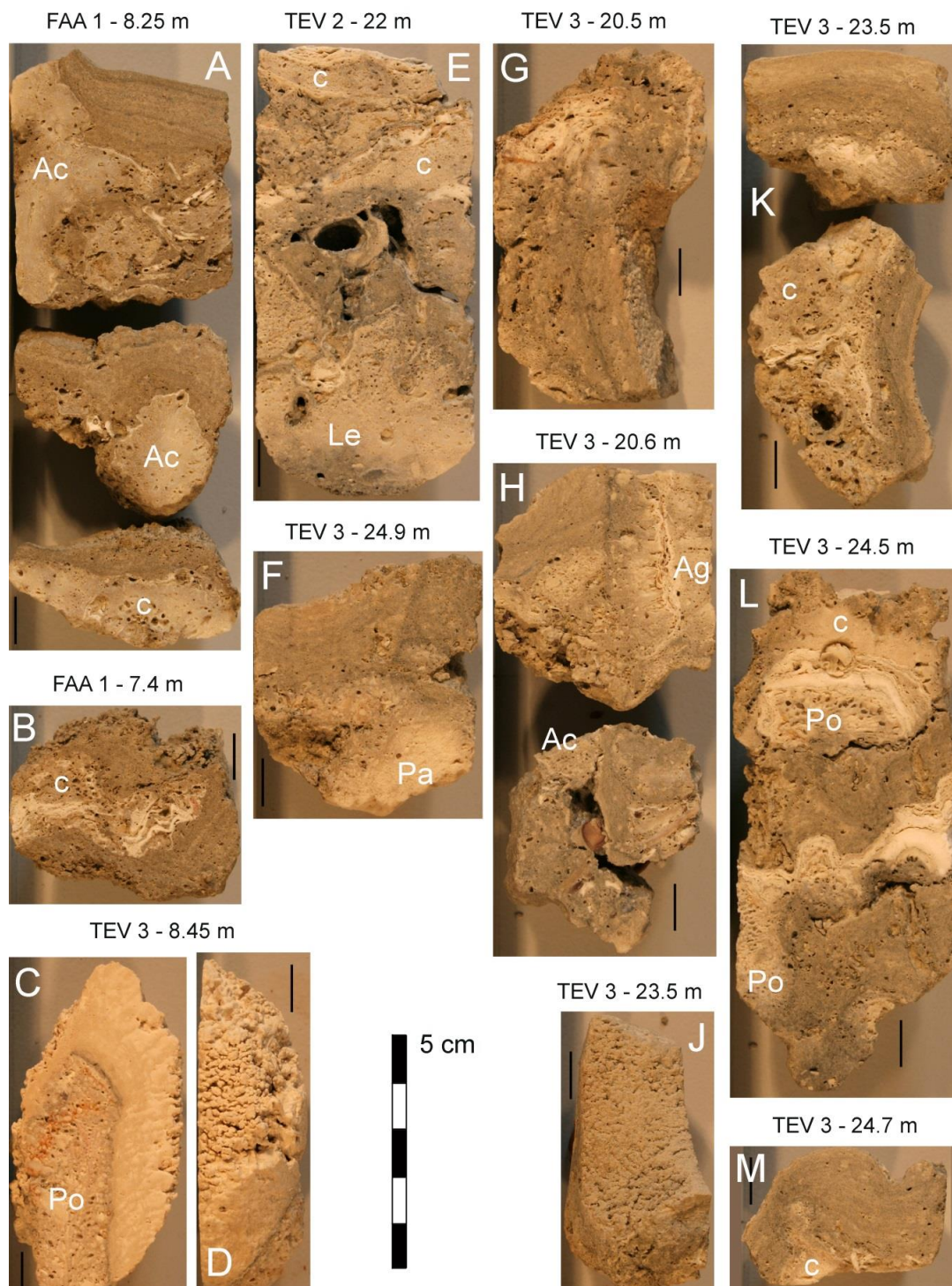


Fig. 3/8: Core specimens from barrier and fringing reefs that contain abundant microbialites: **a)** Laminated microbialite crusts on acroporid corals (Ac) and unidentified coral (c). Note thin crustose coralline algal crust (white) between coral and microbialite; **b)** Stick of branched coral encrusted by crustose coralline algae (white; with red *Homotrema*) and unlaminated microbialite; **c)** Buff-colored, laminated microbialite crust on pocilloporid coral (Po); **d)** Knobby surface of microbialite; **e)** Cavity among corals filled in with crustose coralline algae and microbialite crust. Le = *Leptoseris*; **f)** Laminated microbialite crust on *Pavona* (Pa) coral; **g)** Thick microbial crust and coralline algal crust with vermetids; **h)** Microbial crusts among corals (Ac = *Acropora*; Ag = agaricid); **j)** Knobby surface of laminated microbialite; **k)** Coral (c) encrusted by coralline algae and laminated microbialite; **l)** Alteration of corals (Po = *Pocillopora*), coralline algae, and microbialite; **m)** Laminated microbialite on coral (c)

Microbialite crusts occur frequently and are more common and thicker in lower core sections (figs 3/4, 3/5; 3/8). In many cases, microbialite overlies coralline algae, which in turn overlie coral (figs 3/8a, b, l). Microbialites are usually brown and can be up to several centimeters thick (figs 3/8a, c, m). Their macroscopic texture is either laminated or unlaminated. Microbialite surfaces are usually knobby. Microscopic textures are mostly clotted and peloidal, less frequently laminated (figs 3/10b, d). In cores TEV1 and TEV2, microbialites become abundant below 12 m, in core TEV3 below 9 m core depth (fig. 3/4). In core FAA1, they are common starting from the core top down to the top of the sandy section (fig. 3/5). Microbialites are texturally similar to the ones described from the barrier reef cores of Tahiti but not as thick (Montaggioni and Camoin, 1993; Camoin and Montaggioni 1994; Westphal et al., 2010; Seard et al., 2011). Microbialite abundance apparently ceased after *ca.* 6000 yrs BP (figs 3/4; 3/5). This is in accordance with observations in Tahiti (Camoin et al. 1999; Camoin et al. 2006; Seard et al. 2011), and in Holocene reef cores from the Atlantic and Indian Oceans where microbialite crust abundance also decreases upcore (Gischler and Hudson 2004; Gischler et al. 2008; Heindel et al. 2012). The apparent late Holocene decrease in reefal microbialite abundance has been attributed to changes in environmental parameters such as nutrient content, alkalinity, and light and energy conditions (Camoin et al. 1999, 2006; Seard et al. 2011). Similar causes, especially a decrease in alkalinity during the glacial-interglacial transition have been invoked by Riding et al. (2014) to explain the fading of microbial fabrics in reef framework in the mid-late Holocene.

Typical early marine and meteoric phreatic cements (e.g., Longman, 1980; Macintyre and Marshall, 1988) have been identified in the cores. Marine cements are usually found in open spaces within skeletons and shells and less common on grain surfaces. They comprise aragonite needle (acicular) cement (figs 3/9a, c; 3/10a), and high-magnesium-calcite peloidal and microcrystalline cements (fig. 3/9a, e). Early marine micrite envelopes are common and best visible at the rim of mollusk shells. In the upper part of core TEV2, isopachous aragonite cement crusts are abundant (fig. 3/9b). Here, cement crusts get as thick as 1 mm. Meteoric cements are common in the Pleistocene section of core TEV1 (fig. 3/10e, f). They include blocky and dogtooth (scalenohedral) low-magnesium-calcite cements. Recrystallization of aragonite components such as corals and *Halimeda* frequently occurs. However, in many examples, recrystallization did not completely affect grains and parts of the precursor textures are still preserved. Some corals still have parts that consist completely of aragonite. Dissolution and moldic porosity are rare in the Pleistocene section.

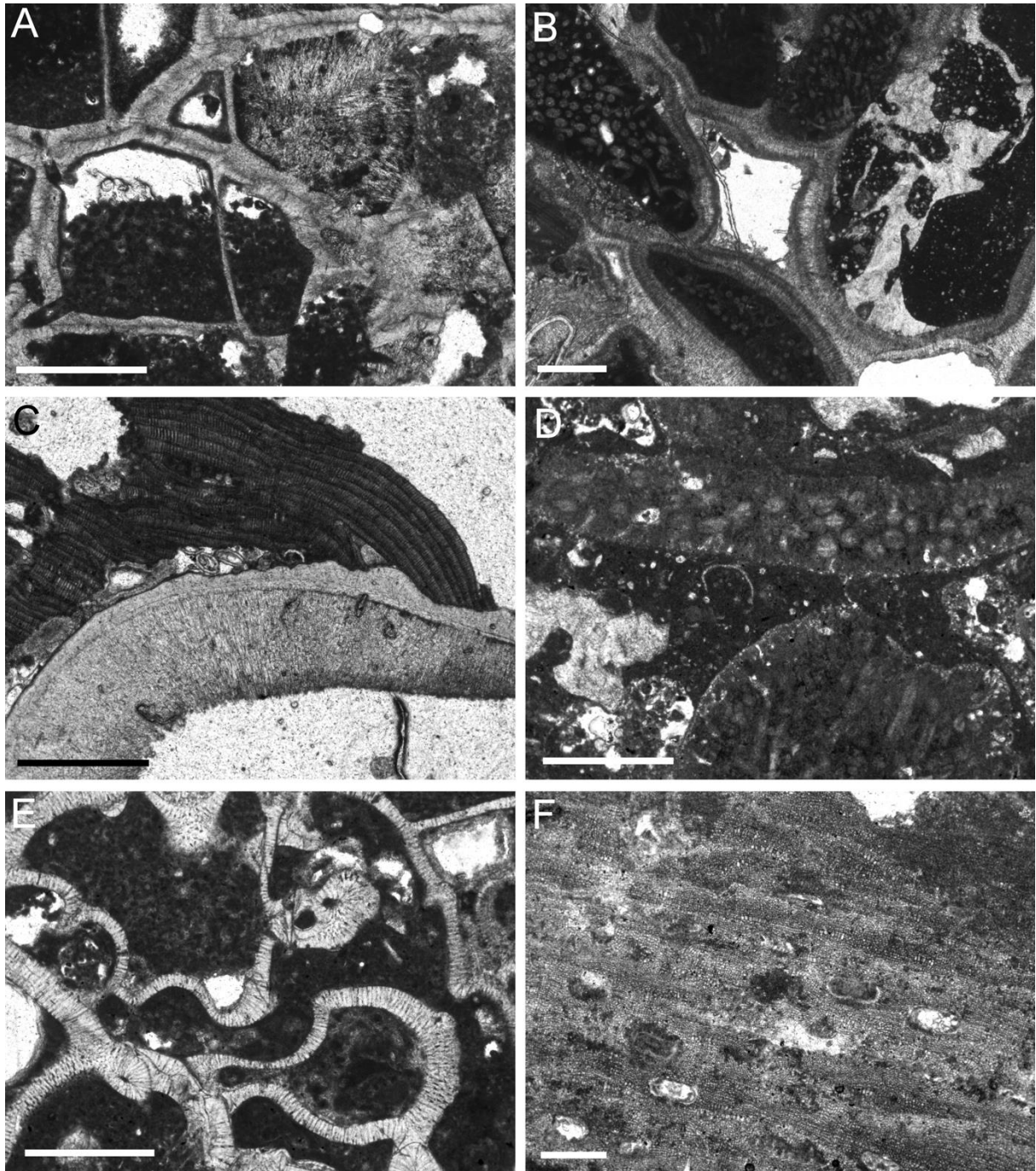


Fig. 3/9: Thin-section micrographs of Holocene samples showing diagenetic features and coralline algae. Scale bar is 1 mm long; **a)** Intraparticle cavities in coral skeleton filled with aragonite needle and high-magnesium-calcite peloidal cements. TEV3, 8.8 m; **b)** Fragments of *Halimeda* and coral lined by isopachous crusts of aragonite needle cement. TEV2, 0.2 m; **c)** Mollusk shell encrusted by coralline alga (*Lithophyllum* gr. *prototypum*; above) and lined by aragonite needle cement (below). TEV3, 26.8 m; **d)** *Halimeda* fragments in fine-grained sediment matrix. FAA1, 8.35 m; **e)** *Carpentaria* sp. (encrusting foraminifer) and peloidal high-magnesium-calcite cement. FAA1, 1.25 m; **f)** Coralline algal crust of *Porolithon onkodes*. TEV1, 15.6 m

The Holocene core sections are composed almost entirely of calcium carbonate with aragonite and high-magnesium-calcite predominating (tab. 3/2). Average aragonite content is 71%, high-magnesium-calcite 26%, and low-magnesium-calcite 3%. In cores with abundant red coralline algae and microbialites, high-magnesium-calcite content was higher than aragonite content. In the Pleistocene reef, contents of low-magnesium-calcite are much higher (41-62%)

due to meteoric diagenesis. Because of the somewhat darker color of fringing reef core FAA1 as compared to barrier reef cores TEV1-3, the amount of siliciclastics was measured in samples from the former core. Carbonate content ranged from 94.6-99.7% (tab. 3/2), i.e., fine siliciclastic material usually does not exceed 5%.

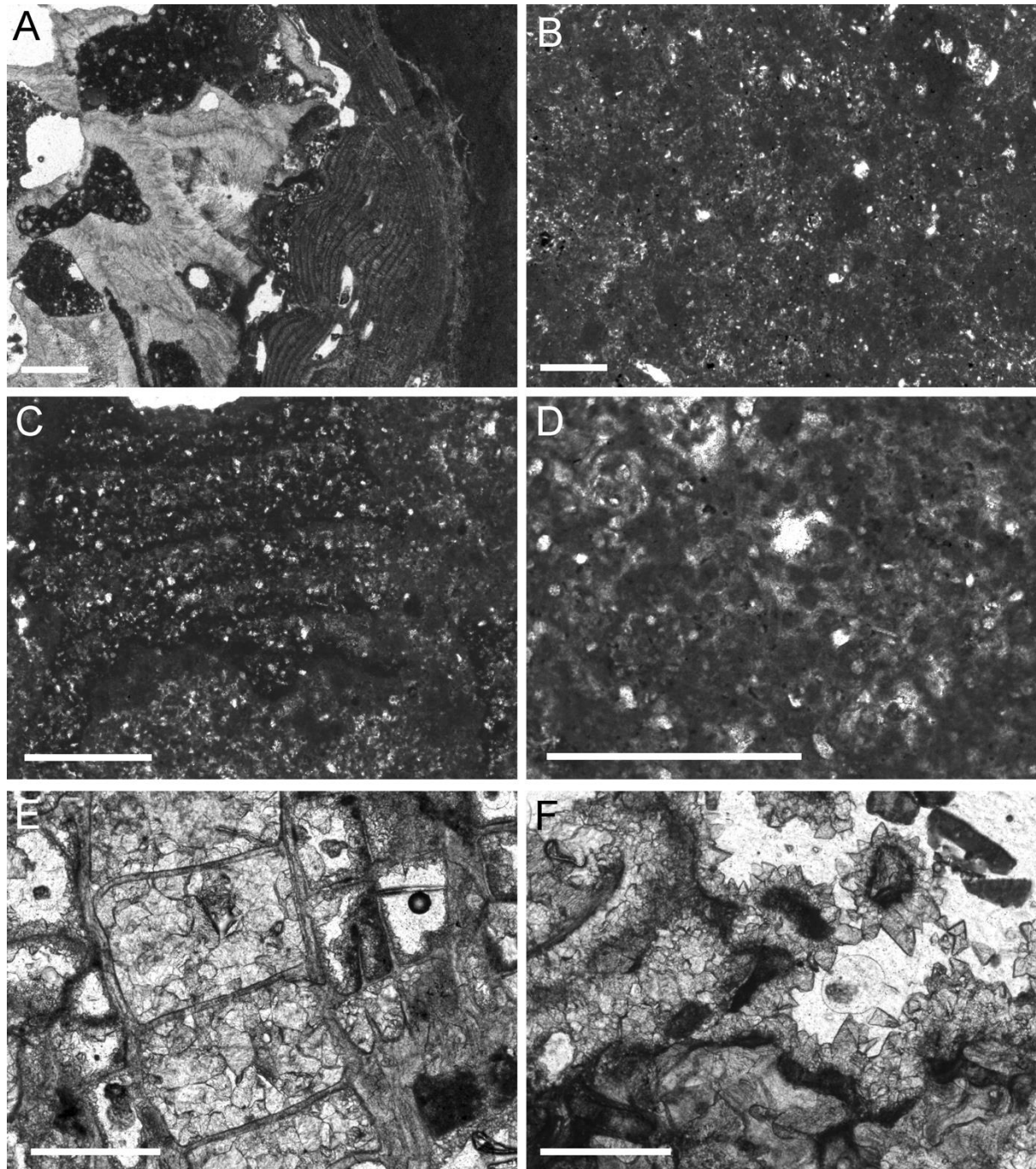


Fig. 3/10: Thin-section micrographs of Holocene microbialites and Pleistocene samples. Scale bar is 1 mm long; a) Succession, from left to right, of coral, coralline algal crust (*Lithophyllum* gr. *prototypum*), and microbialite. Cavities in coral filled in with fine-grained detritus. TEV3, 24.25 m; b) Clotted texture in microbialite. FAA1, 8.05 m; c) Irregular lamination in microbialite. TEV3, 10.6 m; d) Peloidal texture in microbialite. TEV3, 9.6 m; e) Coral skeleton filled in with blocky low-magnesium-calcite cement. TEV1, 30.6 m; f) Coral skeleton lined with blocky and dogtooth (skalenohedral) cements of low-magnesium-calcite. TEV1, 31.5 m

3.4.2 Distribution of corals, coralline algae, and other taxa

The most abundant corals include digitate and robust branching *Acropora*, other species of *Acropora*, *Montipora*, *Pocillopora*, agariciids (*Gardinoseris*, *Leptoseris*, *Pavona*), *Porites*, and faviids (suppl. fig. 3/1). In the upper ca. 15 m of the barrier reef cores, digitate and robust branching and corymbose *Acropora* and *Pocillopora* are common. In lower core sections below ca. 15 m, massive and columnar agariciids dominate. In core TEV3, an intermediate section with abundant *Pocillopora* occurs from ca. 8-15 m core depth. In the Pleistocene section of core TEV1, laminar *Montipora* and agariciids are common. Fringing reef core FAA1 exhibits abundant *Pocillopora* and encrusting faviids and *Porites* down to ca. 6 m depth, and *Montipora* and various *Acropora* below that core depth. In both barrier and fringing reef cores, the abundances of vermetids and the encrusting foraminifer *Homotrema rubrum* increase upcore (suppl. fig. 3/1).

The distribution of red coralline algae and the thickness of algal crusts is shown on suppl. figure 3/2. Thick crusts (up to 30 mm) of *Porolithon onkodes* (fig. 3/9f) may be seen in upper core sections. Lower core sections are characterized by the occurrence of thinner crusts (ca. 10 mm) of various coralline algae. In the barrier reef cores TEV1 and TEV2, the transition was observed in ca. 19 m depth. In core TEV3, the change to thinner algal crusts occurs at ca. 15 m, below which *P. onkodes*, occasionally in the form of thick crusts (24-25 m core depth), is still present. In fringing reef core FAA1, the abundance of thick *P. onkodes* crusts decreases significantly below ca. 5 m core depth.

Based on these observations, five coralgal assemblages have been identified (see figs 3/4; 3/5). These include (1) assemblage A1 dominated by *Acropora* with medium-sized to robust branches, including *A. gr. humilis* and *A. gr. robusta*, associated with thick *Porolithon onkodes* crusts in upper sections of the barrier reef cores down to 19 m. *Pocillopora* is present in various proportions but is most abundant in the upper 8 m of core TEV1. This assemblage is characteristic of the high-energy reef flat (Montaggioni et al., 1997; Cabioch et al., 1999a; Montaggioni, 2005), and probably formed in water depths less than 10 m. The upcore increase in the abundances of *A. gr. humilis* and *A. gr. robusta*, vermetids and *Homotrema* as well as the thickness of *P. onkodes* crusts probably reflects a shallowing to water depths less than 6 m in the upper 4 m of the barrier reef cores (Cabioch et al., 1999b; Montaggioni, 2005; Abbey et al., 2011). (2) Assemblage A2 is dominated by *Pocillopora* and various *Acropora* species, with *Porolithon onkodes* crusts in core TEV3 between 8-4 m and in the upper 8 m of core FAA1. The latter section is further characterized by a relatively high abundance of encrusting *Porites* and faviids. The assemblage indicates a water depth of 0-10 m. (3)

Assemblage A3 is dominated by agariciids, mainly massive to columnar *Gardinoseris planulata* and *Pavona maldivensis*, characterized by a lack of thick *P. onkodes* crusts and present only in the lower sections of the barrier reef cores. The assemblage is indicative of an intermediate energy environment of the fore reef, the sheltered reef flat or back reef. The corals indicate a wide depth range of 0-30 m (Abbey et al., 2011; IUCN red list website), which can be further constrained to a maximum depth of 20 m based on the occurrences of *Lithophyllum* gr. *pustulatum*, *Peyssonnelia*, and occasionally thin crusts of *P. onkodes* (e.g., Abbey et al., 2011). The proportion of *P. maldivensis* relative to *G. planulata* and that of corymbose *Acropora* with medium-size branches increase distally which may reflect variable hydrodynamic conditions across the barrier reef (Veron, 2000). (4) Assemblage A4 is dominated by laminar *Montipora* and *Acropora* with fine branches, associated with *Lithophyllum* gr. *prototypum*, *L.* gr. *pustulatum*, *Lithoporella*, *Amphiroa*, and occasional thin crusts of *P. onkodes*, present in the lower section of core FAA1. The coralgal association is consistent with a relatively protected setting at depths of 10-20 m (Cabioch et al., 1999b) (5) Assemblage A5 consists of laminar *Montipora* and laminar agariciids, with *Lithophyllum* gr. *pustulatum* and *Lithoporella* and occurs in the Pleistocene section of core TEV1. The assemblage characterizes low-energy reef settings at estimated depths of at least 20 m (Abbey et al., 2011) or shallower, under turbid conditions (Done, 1982).

3.4.3 Chronology and reef accretion

Absolute ages obtained from corals are listed in table 3/3. Holocene uranium-series-ages range from 1956 ± 18 to $10,033 \pm 54$ yrs BP. No age reversals occur. Similar ages in core FAA3 at -10 m and -15 m are a consequence of the low recovery and uncertainties in the exact elevation of dated corals. All initial $^{234}\text{U}/^{238}\text{U}$ activity ratios fall in the range of modern seawater values indicating no diagenetic alteration. In this regard, all U/Th data can be considered to be strictly reliable. This is in particular true for sample TEV 1-30.6 m (*Pocillopora*) showing a Pleistocene age of $116,900 \pm 1100$ yrs BP, corresponding to the late part of marine isotope stage 5e. Its $^{234}\text{U}/^{238}\text{U}$ initial ratio is in full accord with the modern value and can hence also be considered strictly reliable.

Holocene reef accretion rates were calculated between absolute uranium series dates of cores TEV1-3 and FAA1 (fig. 3/11). They range from 1.39-13.84 m/kyr and show an average of 6.03 m/kyr. Accretion rates decrease during the course of the Holocene. No statistically significant differences in accretion rate between barrier (average 6.15 m/kyr) and fringing reef (5.65 m/kyr) were detected. Age-depth plots suggest that fringing and barrier reefs prograded

Table 3/3: U-series data of coral samples from the six cores, ^{14}C ages (from BETA ANALYTIC INC.) of two samples taken on outcrops of fossil Holocene reef terraces are added at the bottom. BB 31 was taken on the eastern barrier reef at the northern end of Motu Piti Aau; BB 27 was collected at the northern tip of Motu Teveiroa (see fig. 3/2). Minimum subsidence: 0.05 m/kyr; maximum subsidence: 0.14 m/kyr. Elevation error was calculated based on recovery in individual core barrels

core	material/coral	^{238}U (ppm)	^{232}Th (ppb)	$^{230}\text{Th}/^{232}\text{Th}$ (dpm/dpm)	$^{230}\text{Th}/^{238}\text{U}$ (dpm/dpm)	$^{234}\text{U}/^{238}\text{U}$ (dpm/dpm)	$^{234}\text{U}/^{238}\text{U}$ (dpm/dpm)	Age (kyrs)	core depth (m)	depth relative to sea level (SL)	corr. depth to SL min. subsidence	corr. depth to SL max. subsidence
TEV 1	<i>Acropora</i>	3.690 ± 0.005	0.083 ± 0.000	10549 ± 1663	0.0502 ± 0.0001	1.143 ± 0.002	1.145 ± 0.002	4963 ± 0.023	-0.45 ± 0.45	-0.45 ± 0.45	-0.20	0.24
TEV 1	<i>Acropora</i>	3.330 ± 0.007	0.595 ± 0.004	1099 ± 19	0.0611 ± 0.0006	1.148 ± 0.004	1.150 ± 0.004	6038 ± 0.085	-4.28 ± 0.23	-4.28 ± 0.23	-3.98	-3.43
TEV 1	<i>Acropora</i>	2.966 ± 0.005	0.093 ± 0.001	8663 ± 804	0.0675 ± 0.0010	1.154 ± 0.003	1.157 ± 0.003	6656 ± 0.118	-9.95 ± 0.45	-9.95 ± 0.45	-9.62	-9.02
TEV 1	<i>Porites</i>	3.102 ± 0.007	0.714 ± 0.012	1044 ± 17	0.0753 ± 0.0008	1.145 ± 0.004	1.148 ± 0.004	7518 ± 0.116	-15.63 ± 0.63	-15.63 ± 0.63	-15.25	-14.58
TEV 1	<i>Pavona</i>	3.009 ± 0.007	1.470 ± 0.012	525 ± 7	0.0817 ± 0.0008	1.144 ± 0.004	1.147 ± 0.004	8176 ± 0.115	-20.05 ± 0.55	-20.05 ± 0.55	-19.64	-18.91
TEV 1	<i>Gardineroseris</i>	2.960 ± 0.006	0.093 ± 0.001	11446 ± 1100	0.0882 ± 0.0005	1.141 ± 0.003	1.144 ± 0.003	8887 ± 0.082	-25.35 ± 0.15	-25.35 ± 0.15	-24.91	-24.11
TEV 1	<i>Montipora</i>	3.550 ± 0.004	0.215 ± 0.001	5862 ± 277	0.0991 ± 0.0003	1.142 ± 0.002	1.146 ± 0.002	10.033 ± 0.054	-28.98 ± 0.48	-28.98 ± 0.48	-28.48	-27.58
TEV 1	<i>Pocillopora</i>	2.056 ± 0.003	0.161 ± 0.001	35181 ± 2307	0.7299 ± 0.0017	1.108 ± 0.003	1.151 ± 0.004	116,925 ± 1.101	-30.6 ± 0.60	-30.6 ± 0.60		
TEV 2	<i>Acropora</i>	3.993 ± 0.006	0.070 ± 0.000	7860 ± 1576	0.0268 ± 0.0001	1.144 ± 0.002	1.145 ± 0.002	2618 ± 0.018	-0.20 ± 0.20	0.80 ± 0.20	0.93	1.17
TEV 2	acroporid	3.281 ± 0.007	0.102 ± 0.001	5681 ± 523	0.0436 ± 0.0003	1.151 ± 0.004	1.153 ± 0.004	4265 ± 0.043	-2.48 ± 0.53	-1.48 ± 0.53	-1.27	-0.88
TEV 2	<i>Acropora</i>	3.167 ± 0.006	0.073 ± 0.001	10058 ± 1713	0.0479 ± 0.0002	1.147 ± 0.003	1.149 ± 0.003	4719 ± 0.034	-6.53 ± 0.53	-5.53 ± 0.53	-5.29	-4.87
TEV 2	<i>Acropora</i>	3.323 ± 0.007	0.207 ± 0.002	3151 ± 154	0.0549 ± 0.0007	1.148 ± 0.004	1.151 ± 0.004	5.415 ± 0.09	-9.45 ± 0.45	-8.45 ± 0.45	-8.18	-7.69
TEV 2	<i>Acropora</i>	3.650 ± 0.007	0.062 ± 0.001	19209 ± 3849	0.0655 ± 0.0004	1.149 ± 0.003	1.152 ± 0.004	6488 ± 0.062	-14.35 ± 0.65	-13.35 ± 0.65	-13.03	-12.44
TEV 2	<i>Acropora</i>	3.588 ± 0.008	0.532 ± 0.004	1661 ± 28	0.0759 ± 0.0005	1.149 ± 0.004	1.152 ± 0.004	7551 ± 0.079	-20.48 ± 0.53	-19.48 ± 0.53	-19.10	-18.42

Continue on next page

core	material/coral	²³⁸ U (ppm)	²³² Th (ppb)	²³⁰ Th/ ²³² Th (dpm/dpm)	²³⁰ Th/ ²³⁸ U (dpm/dpm)	²³⁴ U/ ²³⁸ U (dpm/dpm)	²³⁴ U/ ²³⁸ U initial (dpm/dpm)	Age (kyrs)	core depth (m)	depth relative to sea level (SL)	corr. depth to SL min. subsidence	corr. depth to SL max. subsidence
TEV 2	<i>Pocillopora</i>	2.166 ± 0.005	0.458 ± 0.003	1308 ± 26	0.0845 ± 0.0005	1.147 ± 0.004	1.150 ± 0.004	8446 ± 0.083	-26.08 ± 0.58	-25.08 ± 0.58	-24.66	-23.90
TEV 2	<i>Porites</i>	2.829 ± 0.003	0.165 ± 0.001	5793 ± 372	0.0903 ± 0.0009	1.146 ± 0.002	1.150 ± 0.002	9063 ± 0.110	-30.88 ± 0.63	-29.88 ± 0.63	-29.43	-28.61
TEV 3	<i>Acropora</i>	2.947 ± 0.005	0.189 ± 0.001	2401 ± 130	0.0423 ± 0.0002	1.144 ± 0.003	1.146 ± 0.003	4161 ± 0.028	-0.25 ± 0.25	-1.25 ± 0.25	-1.04	-0.67
TEV 3	<i>Acropora</i>	3.388 ± 0.007	0.171 ± 0.002	3210 ± 159	0.0451 ± 0.0003	1.149 ± 0.004	1.151 ± 0.004	4423 ± 0.049	-2.63 ± 0.38	-3.63 ± 0.38	-3.41	-3.01
TEV 3	<i>Acropora</i>	3.627 ± 0.007	0.048 ± 0.000	25661 ± 8327	0.0526 ± 0.0004	1.150 ± 0.004	1.152 ± 0.004	5174 ± 0.064	-6.65 ± 0.65	-6.65 ± 0.65	-6.39	-5.93
TEV 3	<i>Acropora</i>	3.051 ± 0.007	0.031 ± 0.000	79171 ± 75735	0.0618 ± 0.0004	1.149 ± 0.004	1.152 ± 0.004	6112 ± 0.066	-11.60 ± 0.40	-12.60 ± 0.40	-12.29	-11.74
TEV 3	faviid	3.107 ± 0.008	3.261 ± 0.041	204 ± 4	0.0686 ± 0.0011	1.148 ± 0.004	1.151 ± 0.004	6789 ± 0.139	-15.65 ± 0.65	-16.65 ± 0.65	-16.31	-15.70
TEV 3	<i>Acropora</i>	3.593 ± 0.008	0.142 ± 0.001	7885 ± 495	0.0839 ± 0.0009	1.142 ± 0.004	1.145 ± 0.004	8432 ± 0.125	-20.33 ± 0.38	-21.33 ± 0.38	-20.91	-20.15
TEV 3	<i>Acropora</i>	2.720 ± 0.004	0.146 ± 0.001	5958 ± 338	0.0871 ± 0.0003	1.141 ± 0.003	1.145 ± 0.003	8772 ± 0.058	-24.78 ± 0.28	-25.78 ± 0.28	-25.34	-24.55
TEV 3	<i>Pocillopora</i>	2.382 ± 0.003	0.183 ± 0.001	4183 ± 237	0.0876 ± 0.0003	1.145 ± 0.002	1.149 ± 0.002	8793 ± 0.047	-29.35 ± 0.65	-30.35 ± 0.65	-29.91	-29.12
FAA 1	<i>Acropora</i>	5.489 ± 0.005	8.208 ± 0.012	108.18 ± 0.29	0.0521 ± 0.0001	1.142 ± 0.002	1.144 ± 0.002	5128 ± 0.024	-0.20 ± 0.20	-0.20 ± 0.20	0.06	0.52
FAA 1	<i>Acropora</i>	3.591 ± 0.005	0.431 ± 0.002	2017 ± 39	0.0738 ± 0.0004	1.144 ± 0.003	1.147 ± 0.003	7365 ± 0.057	-3.8 ± 0.45	-3.80 ± 0.45	-3.43	-2.77
FAA 1	<i>Pocillopora</i>	2.700 ± 0.005	0.971 ± 0.004	689 ± 7	0.0781 ± 0.0004	1.146 ± 0.003	1.150 ± 0.003	7785 ± 0.063	-6.10 ± 0.10	-6.10 ± 0.10	-5.71	-5.01
FAA 1	<i>Acropora</i>	3.640 ± 0.005	0.336 ± 0.001	2994 ± 69	0.0830 ± 0.0003	1.139 ± 0.003	1.142 ± 0.003	8356 ± 0.051	-9.93 ± 0.58	-9.93 ± 0.58	-9.51	-8.76
FAA 1	<i>Acropora</i>	3.414 ± 0.004	1.532 ± 0.003	616 ± 4	0.0877 ± 0.0003	1.147 ± 0.002	1.151 ± 0.002	8782 ± 0.047	-15.80 ± 0.70	-15.8 ± 0.70	-15.36	-14.57

Continue on next page

core	material/coral	^{238}U (ppm)	^{232}Th (ppb)	$^{230}\text{Th}/^{232}\text{Th}$ (dpm/dpm)	$^{230}\text{Th}/^{238}\text{U}$ (dpm/dpm)	$^{234}\text{U}/^{238}\text{U}$ (dpm/dpm)	$^{234}\text{U}/^{238}\text{U}$ initial (dpm/dpm)	Age (kyrs)	core depth (m)	depth relative to sea level (SL)	corr. depth to SL min. subsidence	corr. depth to SL max. subsidence
FAA 2	faviid	5.801 ± 0.008	11.755 ± 0.012	31.34 ± 0.14	0.0205 ± 0.0001	1.145 ± 0.002	1.146 ± 0.002	1956 ± 0.018	-0.58 ± 0.58	-1.58 ± 0.58	-1.48	-1.31
FAA 2	<i>Porites</i>	7.714 ± 0.009	16.326 ± 0.003	60.16 ± 0.24	0.0411 ± 0.0002	1.140 ± 0.002	1.142 ± 0.002	4012 ± 0.027	-6.80 ± 0.70	-7.80 ± 0.70	-7.60	-7.24
FAA 3	faviid	3.364 ± 0.004	1.071 ± 0.004	489 ± 5	0.0488 ± 0.0003	1.142 ± 0.002	1.144 ± 0.002	4824 ± 0.037	-0.88 ± 0.63	-1.38 ± 0.63	-1.14	-0.71
FAA 3	<i>Acropora</i>	3.769 ± 0.006	13.063 ± 0.050	68.2 ± 0.5	0.0763 ± 0.0005	1.139 ± 0.003	1.146 ± 0.003	7562 ± 0.070	-9.75 ± 0.75	-10.25 ± 0.75	-9.87	-9.19
FAA 3	<i>Pocillopora</i>	2.159 ± 0.003	0.680 ± 0.002	775 ± 11	0.0756 ± 0.0003	1.150 ± 0.002	1.153 ± 0.002	7509 ± 0.042	-15.0 ± 3.00	-15.50 ± 3.00	-15.12	-14.45
BB 31 - E barrier reef	<i>Acropora</i>							3035 ± 0.195	outcrop	1.00 ± 0.30	1.15	1.42
BB 27 - Teveitroa N	<i>Porites</i>							0.770 ± 0.120	outcrop	1.00 ± 0.30	1.04	1.11

during the course of the Holocene (fig. 3/12). Away from the coast and towards the sea, respectively, ages of individual cores get increasingly younger. This is especially well recognizable in the fringing reef core traverse.

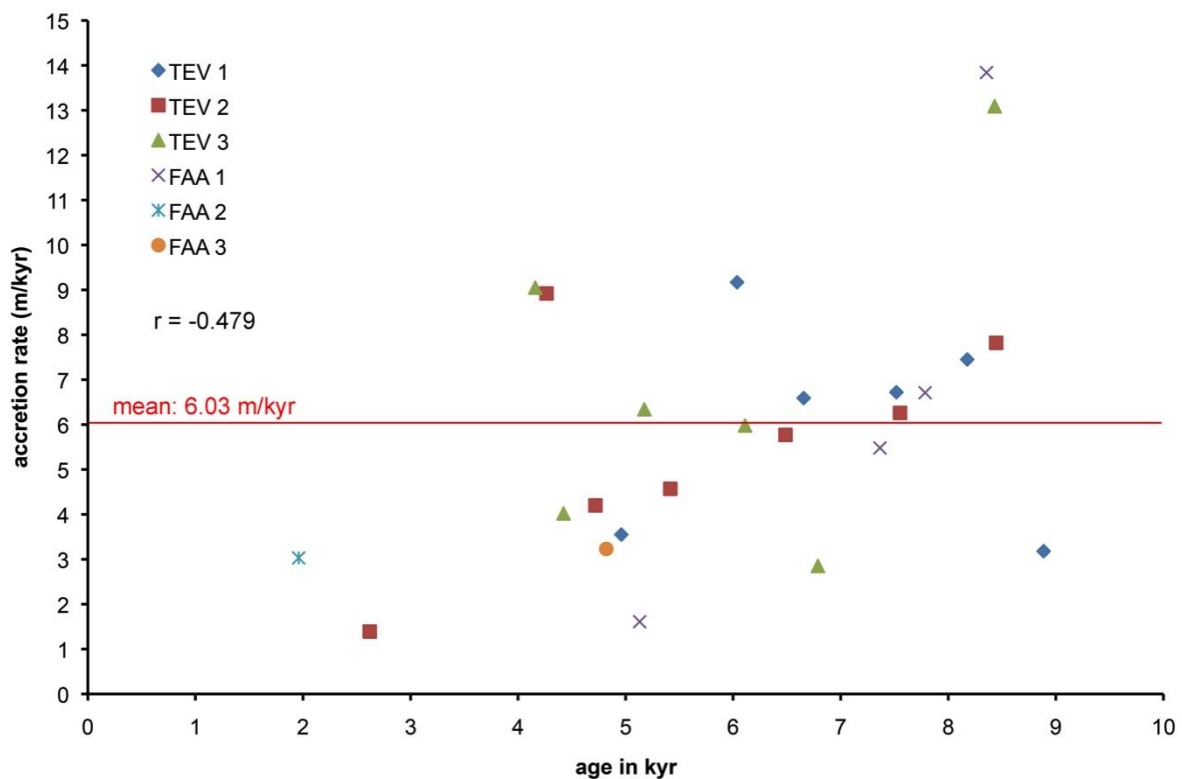


Fig. 3/11: Variation of barrier and fringing reef-accretion rates during the Holocene

3.3 Discussion

3.3.1 Holocene reef development and comparison with Tahiti and other reef sites

Coral reefs are excellent archives of environmental change and former sea level (Davies and Montaggioni, 1985; Woodroffe and Webster, 2014; Camoin and Webster, 2015, and references therein). In the case of Bora Bora, both fringing and barrier reefs apparently were initiated in water depths of around 10 m and approached sea level during the course of the Holocene. The barrier reef was established ca. 10000 yrs BP, only slightly earlier than the fringing reef (8800 yrs BP). The consistent upcore successions of assemblages of corals, coralline algae, and other bathymetric indicators such as vermetid gastropods and *Homotrema rubrum* in both barrier and fringing reef cores supports the interpretation of shallowing during the Holocene. These consistent observations and the fact that core traverses have been investigated, largely excludes the possibility of catch-up artefacts that may potentially be seen in isolated reef cores (Blanchon and Blakeway, 2003). Further afield in the Indo-Pacific realm, upcore shallowing in postglacial and Holocene reefs can be found, e.g., in a fringing reef in Vanuatu (Cabioch et al., 1998), in atoll-like reefs of the southern Great Barrier Reef

(Dechnik et al., 2015), in a Holocene fringing reef in the Seychelles (Braithwaite et al., 2000), and an atoll lagoon reef in the Maldives (Gischler et al., 2008), respectively. During the late Holocene, rates of creation of accommodation space were outpaced by rates of sediment production, i.e., reef accretion in Bora Bora. Vertical accretion rates decrease during the Holocene (fig. 3/11), and barrier and fringing reefs show indications of progradation as a consequence of reduction in accommodation space during the late Holocene (figs 3/4; 3/5; 3/12). In their review of fringing reef growth, Kennedy and Woodroffe (2002) have stressed the importance of accommodation space for reefal growth and geomorphological development. A prominent example of fringing reef progradation is Hanauma reef on Oahu, Hawaii (Easton and Olson, 1976). Likewise, the fringing reef of Galeta Point, Panama, exhibits progradation of the marginal *Acropora* facies over the deeper-water massive coral facies during the Holocene (Macintyre and Glynn, 1976). Kennedy and Woodroffe (2002) also discussed the width of the underlying platform as controlling factor of the degree of progradation. The pedestal of the Bora Bora fringing reef was presumably rather narrow as no underlying Pleistocene reef was recovered.

The style of barrier reef development in Bora Bora appears to be somewhat different from that in Tahiti where the Papeete barrier reef persisted in high-energy environments with water depths of less than 6 m throughout the Holocene (Montaggioni et al., 1997; Cabioch et al., 1999a). However, domal *Porites* occurrences at the bases of Tahiti cores P7 and P8 possibly indicate somewhat deeper water conditions during 13500-12000 yrs BP (Cabioch et al., 1999a). Average Holocene reef accretion rates of the Bora Bora and Tahiti barrier reefs are comparable though and amount to 6.15 m/kyr and 6.10-6.56 m/kyr, respectively. Subsurface data of Tahiti fringing reefs are not available. The slightly higher accretion rate of the Bora Bora barrier as compared to the fringing reef could be a consequence of a higher siliciclastic input and elevated nutrient concentrations in the latter coastal setting. However, the high carbonate contents measured in the nearshore fringing reef core FAA1 do not support this argument (tab. 3/2).

In general, siliciclastic input in the Bora Bora lagoon is rather limited (Gischler, 2011), and the significance of the lagoon as siliciclastic sink does not appear to be as important as in Tahiti barrier reef system (Camoin et al. 1999; Cabioch et al., 1999a; Blanchon et al., 2014). The relatively late occurrence of the robust *Acropora* coral community in the Bora Bora cores would also support this contention. In the Indian Ocean, the oceanic (Darwinian) barrier reef of Mayotte exhibits geomorphological similarity with Bora Bora, but like the Tahiti barrier

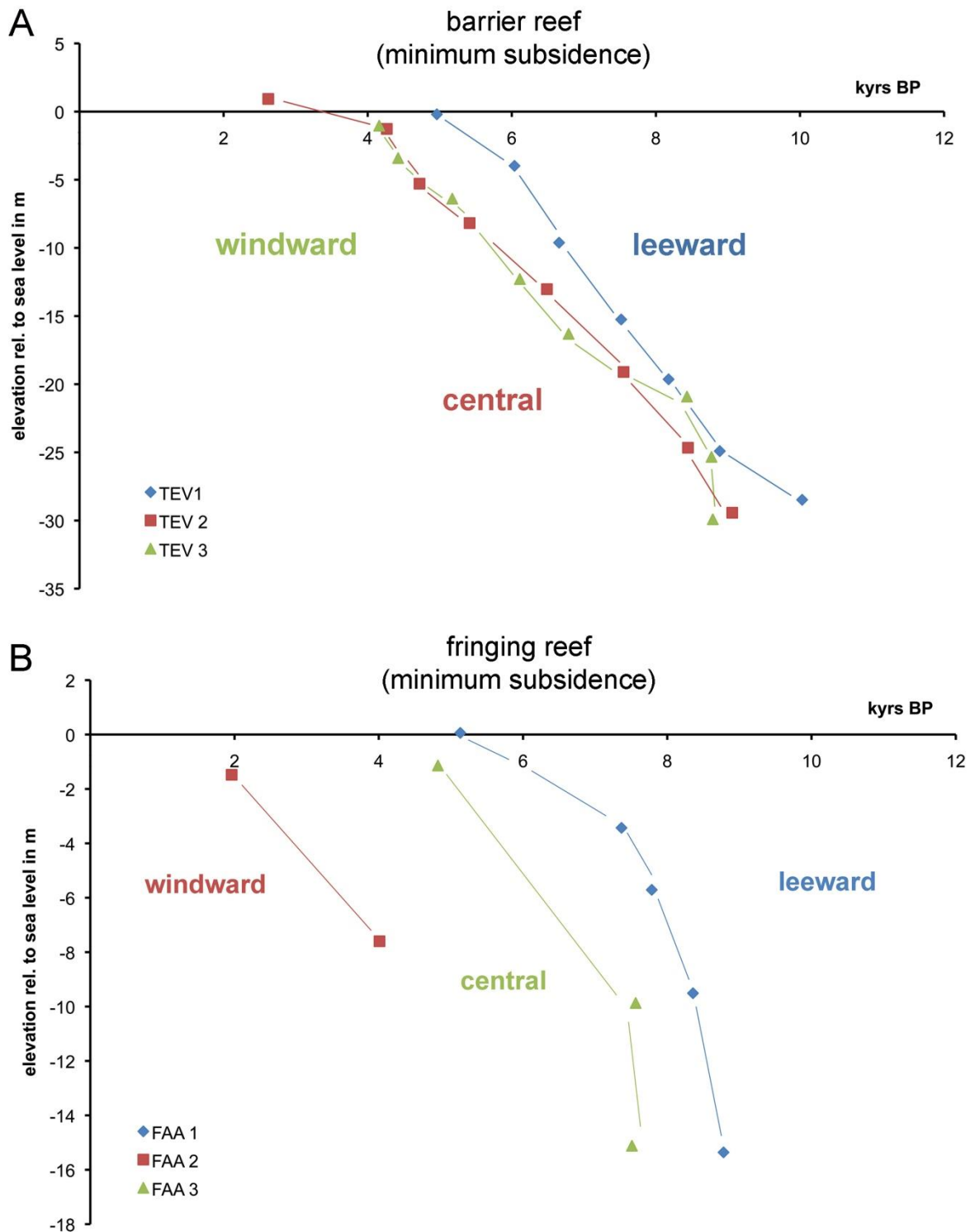


Fig. 3/12: Sea-level data per location suggests that both barrier and fringing reefs prograded during the Holocene. Depths have been corrected for minimum subsidence of 0.05 m/kyr. Note that interim rise of values for core TEV3 from 9-8 kyrs BP corresponds to shallowing of corallgal facies; see fig. 3/4

reef appears to have a different style of reef accretion. In a barrier reef core, a 21 m thick *Acropora*-rich Holocene succession overlies a Pleistocene reef unit. The Mayotte barrier reef was initiated 9600 yrs BP and apparently kept up with sea-level rise (Camoin et al., 1997). The Mayotte fringing reefs, composed of massive and branched corals and bioclastic sand and

gravel, were established ca. 8000 yrs BP and reach thicknesses of up to 10 m, but it is not entirely clear whether they accreted in keep-up or catch-up modes (Zinke et al., 2003). The barrier reef lagoon of Mayotte, Indian Ocean, also acts as a sink of significant amounts of siliciclastics (Masse et al., 1989; Zinke et al., 2003).

Comparisons with other late Quaternary reef systems, occurring in the central Pacific region and further afield, exhibit comparable ranges of reef thickness and accretion rates. However, massive coral facies appear to be more common, and the mode of reef accretion (e.g., keep-up versus catch-up) as well as reef architecture (e.g., aggrading, prograding, retrograding) is not always entirely clear because isolated cores rather than core traverses were drilled in some settings. Thickness of Holocene reefs in the adjacent Cook Islands (Aitutaki barrier reef, Pukapuka Atoll, Rakahanga Atoll) to the south of the Society Islands ranged from 10-30 m; reefs were initiated ca. 8000 yrs BP (Gray and Hein, 2005). According to the core logs, massive coral facies appear to predominate over branched coral facies. Sand facies and sections without recovery, which probably also represent unconsolidated sediment, are very common. On an atoll margin of Kiribati, further to the NW from the Society Islands, Holocene reef thickness reached 12-17 m and reef growth set in as early as 8800 yrs BP (Marshall and Jacobson, 1985). Once more, massive corals are apparently much more common than branched corals and sand facies. Holocene fringing reefs in New Caledonia accreted up to 10 m since ca. 7000 yrs BP (Cabioch et al., 1995). Massive coral (*Porites*) facies and rubble facies are more common than branched (*Acropora*) facies that largely occurs in lower core units. In the Great Barrier Reef, highest Holocene reef thickness is seen in the central region. Marginal and fringing reefs get as thick as 25 m and were initiated 8000-9000 yrs BP (Davies and Hopley, 1983). Both massive and branched coral facies as well as detrital facies occur on windward reefs; fringing reefs are dominated by massive coral and detrital facies. In a Maldives atoll example, Indian Ocean, Holocene marginal reefs exhibit keep-up modes of reef accretion during the Holocene with abundant branched acroporid coral facies. A lagoonal reef in the same atoll was largely composed of massive corals (Gischler et al., 2008). Likewise, massive corals prevailed in the cores taken in another atoll of the Maldives by Kench et al., (2009). Marginal Holocene reef thickness ranged from 14 to >20 m (Gischler et al., 2008; Kench et al., 2009). In the Atlantic, where no true oceanic (Darwinian) barrier reef systems occur, comparable Holocene reef thicknesses were only found in the western Caribbean. The reef margin of Alacran Atoll, Yucatán shelf, has a Holocene thickness of at least 22.7 m, probably as much as 33.5 m (Macintyre et al., 1976). The age of the reef base is unknown. The cored section is composed of massive and branched coral

facies. The lowest age data were collected at 23 m depth (5440 yrs BP). The section from 25.5-33.5 m above Pleistocene bedrock had virtually no recovery and possibly represents a section of unconsolidated Holocene sediment. Maximum Holocene thickness of the Belize Barrier Reef, the largest reef structure in the Atlantic, exceeds 21 m. The barrier reef was initiated before 8260 yrs BP, which was the oldest Holocene age obtained (Gischler and Hudson, 2004). Massive coral, branched coral, and unconsolidated sand facies were recovered.

3.3.2 The influence of sea level, subsidence, and antecedent topography

Sea-level fluctuations, subsidence, and antecedent topography are of importance for Indo-Pacific and Atlantic reef building during the Holocene (Montaggioni, 2005; Toomey et al., 2013; Camoin and Webster, 2015; Gischler, 2015; and references therein). The coral age-depth plot of the new Bora Bora data shows that sea level in the early Holocene has been rising rapidly and approached modern level ca. 6000 yrs BP (fig. 3/13).

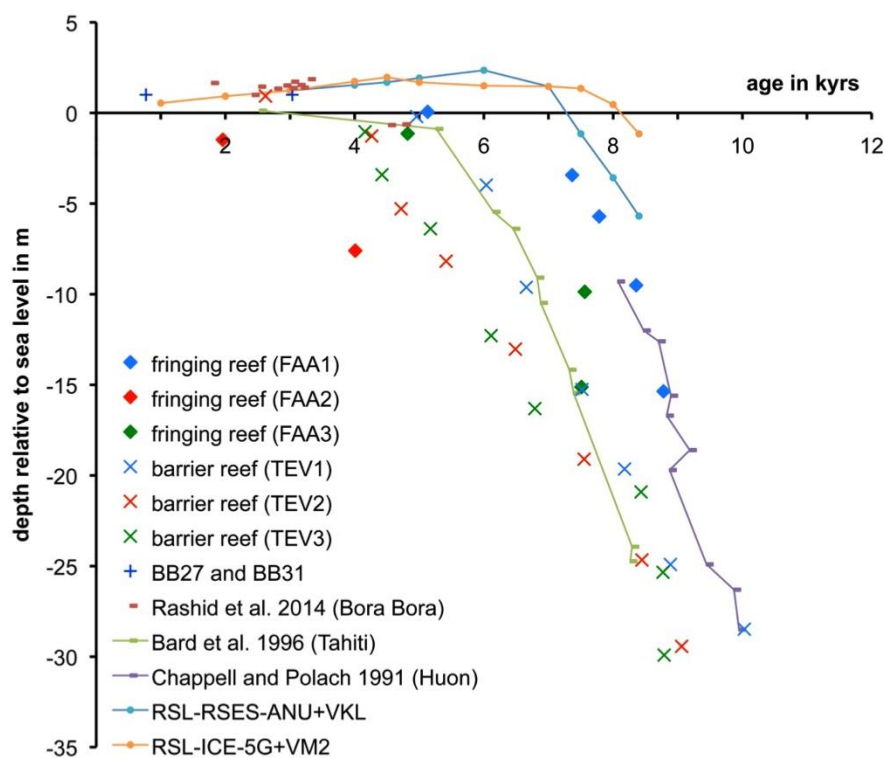


Fig. 3/13: Sea-level data in comparison to other data from Bora Bora (Rashid et al., 2014; U-series ages), data from Tahiti (Bard et al., 1996; calibrated radiocarbon ages from upper 30 m of core P6), data from Papua New Guinea (Chappell and Polach 1991; calibrated radiocarbon ages from upper 30 m of their core), and two modelled sea-level curves for French Polynesia (Rashid et al., 2014). Depths of Bora Bora data have been corrected for minimum subsidence of 0.05 m/kyr. Elevation and age error ranges are smaller than the data points (Table 3). The ^{14}C -data from Bard et al., (1996) and Chappell and Polach (1991) were calibrated based on the Marine13 database (Talma and Vogel 1993; Reimer et al., 2013)

Data from fossil reef terraces of Bora Bora indicate a higher-than-present sea level during the late Holocene (ca. 6000-1000 yrs BP) that has been estimated to be up to 1.8 m (Rashid et al., 2014). Figure 3/14 shows the new sea-level data with palaeobathymetrical error bars added, which allows the tentative construction of a sea-level curve for Bora Bora. The curve has been drawn as an approximate mean of

the palaeo-depth ranges, provided that no data point lies above the curve. The rate of rise during 10000-6000 yrs BP was around 5 m/kyr. The Holocene sea-level record of Tahiti (Bard et al., 1996) does only fit the new Bora Bora data in parts. Fifteen of the 34 dates (44%) from the Bora Bora barrier and fringing reefs plot above the Tahiti sea-level curve. However, the palaeo-depth range of dated Holocene corals in Tahiti by Bard et al., (1996) amounts to ca. 4-11 m as discussed in detail by Cabioch et al., (1999b, fig. 3/5), i.e., most of the new Bora Bora age data would certainly fall within this range. Only two age dates obtained from core FAA1 and one from core TEV1 would slightly lie outside this range. In addition, it should be kept in mind that the resulting uranium-series ages are systematically older as compared to ^{14}C ages of the same samples. With one exception at -27 m, Bard et al. (1996) had only dated the samples of core depths greater than 30 m by both uranium-series and ^{14}C methods; for the shallower core depth range considered here (< 30 m), only ^{14}C ages are available. The upper part of the sea-level data from the Huon Peninsula, Papua New Guinea (Chappell and Polach, 1991), exhibits a good fit with the new Bora Bora age data, as virtually all data obtained during this study fall on or below the curve (figs 3/13; 3/14). The calculated sea-level curves based on the ICE-5G and RSES-ANU geophysical models (Rashid et al., 2014) also appear to fit the new data of this study (fig. 3/13), because the new Bora Bora data plot below the curves. The RSES-ANU-curve, which assumes a continued meltwater input from Antarctica, apparently exhibits a better fit than the ICE-5G-curve.

Probably due to lower subsidence rates and, possibly, the different geomorphologies of the reef pedestals, e.g., differences in island slopes, Holocene reefs in Bora Bora are considerably thinner and were initiated later as compared to Tahiti. In Bora Bora, maximum subsidence may be calculated to 0.14 m/kyr, based on the 116900 yrs age from a Pleistocene pocilloporid coral located 30.6 m below present sea level, an assumed MIS 5e sea level of +6 m (Hearty et al., 2007), and a minimum Pleistocene palaeo-water depth of 20 m. It has to be kept in mind that a 2-4 m error may be inherent in the commonly used MIS 5e peak level due to glacial isostatic adjustment (Creveling et al., 2015). The subsidence rate of 0.14 m/kyr is in fact a maximum value, because the palaeo-water depth was probably higher than 20 m based on the coralgal assemblage, including laminar *Montipora*, laminar agariciids, and a lack of *P. onkodes* in the Pleistocene section in core TEV1. Assuming a palaeo-water depth of 30 m, which was well possible based on the coralgal assemblage, the calculated subsidence rate would amount to 0.05 m/kyr. This value is similar to the estimate of Pirazzoli and Montaggioni (1985) and Pirazzoli et al. (1985b), which was determined based on Holocene shoreline geomorphology, i.e., the comparison of degrees of emergence of Holocene reef

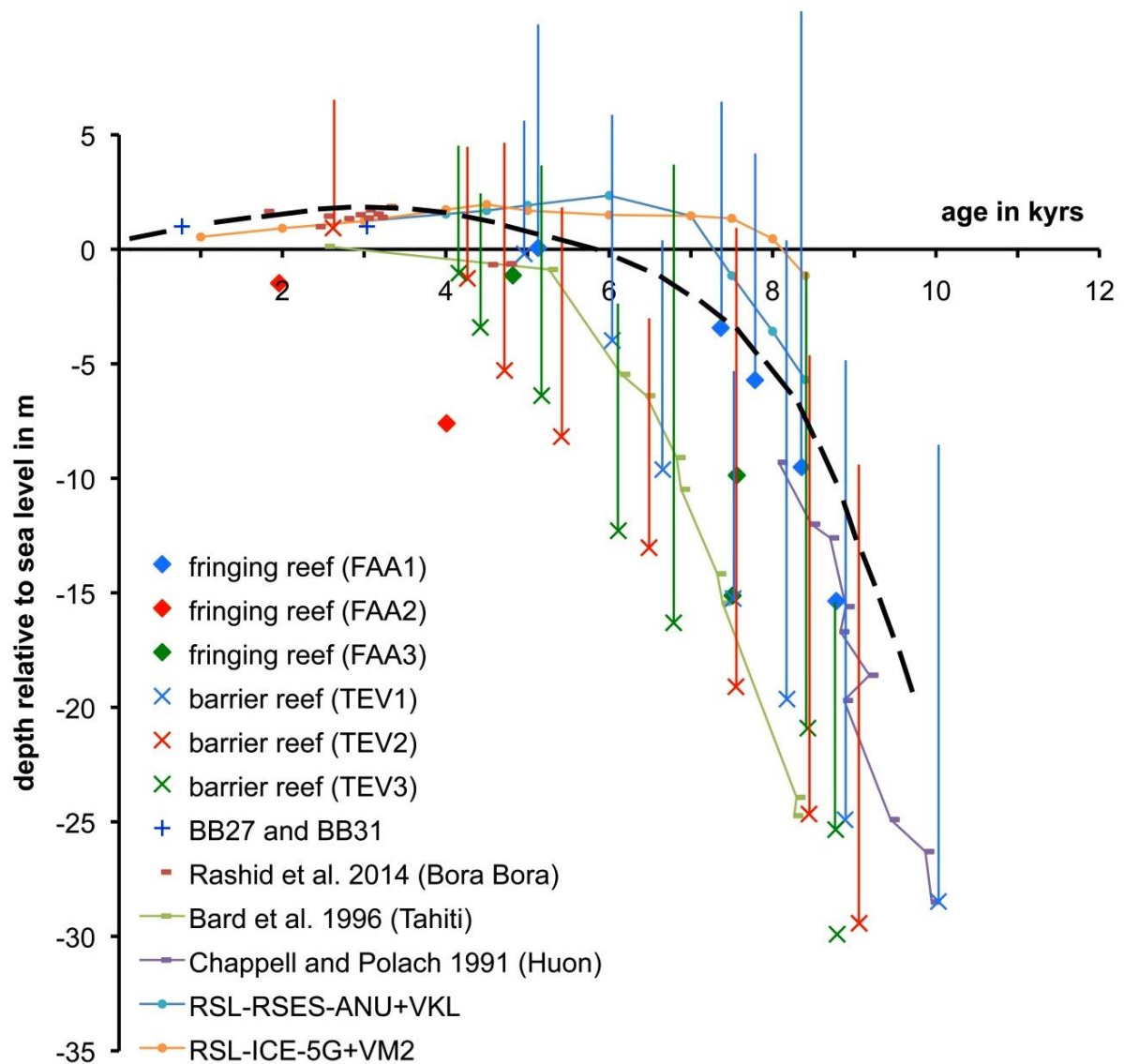


Fig. 3/14: Bora Bora sea-level data (corrected for minimal subsidence) with palaeo-bathymetrical error bars, based on depth ranges of coralgal associations. Tentative sea-level curve (black dashed line) is no mathematical function, but is intended to represent a mean of the elevation data thereby excluding that data points lie above the curve

platforms in the Society archipelago. A significantly lower subsidence in Bora Bora, a significantly smaller island and some 270 km away from the Society Islands hot spot as compared to Tahiti located close to the hot spot, would agree with geotectonic and isostatic considerations (Rashid et al., 2014). Based on the minimum subsidence rate for Bora Bora of 0.05 m/kyr and the established rate of Tahiti of 0.25 m/kyr (Deschamps et al., 2012), absolute subsidence values since the end of marine isotope stage 5e some 1150000 yrs BP would amount to 5.75 m in Bora Bora and to 28.75 m in Tahiti. Subsidence alone presumably created considerably less accommodation space in Bora Bora as compared to Tahiti.

The influence of antecedent topography for Quaternary reef development was systematically investigated by Purdy (1974). He argued that topographic highs of a limestone

karst relief, produced during sea-level lowstands, were the sites of reef growth during subsequent sea-level highstands, whereas topographic lows would become locations of sediment accumulation. With regard to oceanic (Darwinian) barrier reefs and atolls, Purdy and Winterer (2001, 2006) analyzed global data sets and showed that lagoon depths were statistically correlated with precipitation rates, thereby stressing the dissolution-shape relationship. Purdy and Winterer (2006) also discussed examples of both barrier and atoll reef geomorphologies in emergent Neogene limestone islands such as Mangaia, Cook Islands, supposedly created by limestone dissolution. However, new data from Schlager and Purkis (2013, 2015) have shown that apparent karst geomorphology such as the bucket or saucer shape of reefs and reticulate reef patterns may result from biotic self-organization rather than from meteoric limestone dissolution.

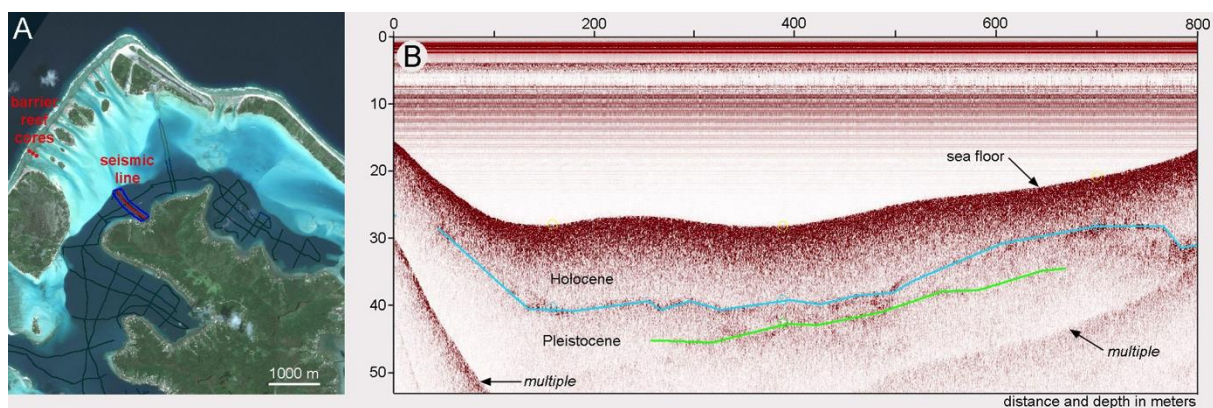


Fig. 3/15: Representative seismic line along deep lagoon SE of the barrier reef core traverse. Blue-marked reflection is interpreted as Holocene-Pleistocene boundary. Holocene lagoon deposits have 10 to 12 m thickness. Green line highlights second reflection within the Pleistocene, possibly subaerial exposure horizon between older Pleistocene units. Pleistocene reef limestone was reached at barrier reef core TEV1 at 30 m below present sea level, i.e., Pleistocene relief between reef margin and deep lagoon approximates 10 m

The reef drill-core data discussed here is complemented by seismic data collected in the Bora Bora lagoon (fig. 3/15). The seismic reflection indicating the base of the Holocene sequence reaches as deep as ca. 40 m below modern sea level, marking on this transect the deepest point of the Pleistocene lagoon east of Motu Teveiroa (fig. 3/15). These data indicate that the Pleistocene reef underlying the Holocene barrier reef of Bora Bora forms a topographic high ca. 10 m above the adjacent Pleistocene lagoon floor resulting in a relief considerably less than the ca. 40 m relief that is seen in the modern. The difference in Pleistocene and Holocene reliefs may be due to (1) karst dissolution and erosion in Pleistocene reefal and lagoonal limestone and (2) the higher Holocene accretion/sedimentation rate in the reef when compared to the lagoon. Similar Pleistocene reef-lagoon reliefs and up to three times higher accretion/sedimentation rates were encountered in reefs versus lagoons in western Atlantic (Gischler, 2015) and Indian Ocean reef systems (Gischler et al., 2008; Klostermann and

Gischler, 2015). The fact that there is a ca. 10 m of Pleistocene relief between the platform margin and the lagoon in Bora Bora also suggests that the MIS 5e-reef recovered in core TEV1 probably represents the top of a Pleistocene barrier reef rather than a fringing reef. A lagoon depth of about 10 m has been suggested as divide between fringing and barrier reefs (Milliman, 1974, p. 157; Kennedy and Woodroffe, 2002). Additional drilling and age-dating of Pleistocene deposits at the marginal reef and in the lagoon would be necessary to validate the barrier-reef character of the recovered MIS 5e-reef with certainty.

3.4 Conclusions

The following conclusions may be drawn based on the analysis of a barrier reef and a fringing reef core traverse drilled in the oceanic barrier reef system of Bora Bora and 34 new, reliable uranium-series dates from corals. Sea level, and to a lesser extent subsidence and antecedent topography, controlled Holocene barrier and fringing reef development. Subsidence alone cannot explain the development of late Quaternary reefs in Bora Bora, which was used as model of the subsidence theory. Fringing and barrier reefs developed more or less contemporaneously. A more than 30 m thick Holocene barrier reef accreted on top of a Pleistocene (marine isotope stage 5e) barrier reef with an average rate of 6.15 m/kyr during the past 100300 yrs. The Holocene barrier reef consists of > 30 m thick Holocene coralgall and microbial successions, characterized by an upcore transition from a massive to columnar agaricid-rich to an *Acropora-Pocillopora* assemblage, and a robust-branching *Acropora* assemblage with thick *P. onkodes* crusts, vermetids, and *Homotrema*.

The underlying Pleistocene reef is composed largely of corals with laminar *Montipora* and agaricids. The fringing reef was initiated on Pleistocene soil 8780 yrs BP and accreted with an average rate of 5.65 m/kyr. An *Acropora-Montipora* assemblage transitions upcore to an *Acropora-Pocillopora*-faviid assemblage with thick crusts of *Porolithon onkodes*, vermetids, and *Homotrema*. Both barrier and fringing reefs in Bora Bora exhibit evidence for shallowing during the Holocene, based on coralgall palaeo-bathymetry data. In the course of the Holocene, barrier and fringing reefs prograded seaward and away from the coast, respectively. The subsidence of Bora Bora is estimated to range from a minimum of 0.05 m/kyr to a maximum of 0.14 m/kyr, based on an absolute Pleistocene age-depth datum and on coralgall palaeo-bathymetry. The Holocene reef-lagoon relief of ca. 40 m is much higher as compared to the Pleistocene relief of ca. 10 m, due to differential accretion in the Holocene and possibly erosion/karst dissolution in the Pleistocene. Comparisons with other oceanic barrier reef systems such as Tahiti and Mayotte show more differences than

similarities. In both Tahiti and Mayotte, barrier reefs apparently accreted in the keep-up mode. Reef thickness is significantly higher in Tahiti and much lower in Mayotte. Siliciclastic input from the central island was more important in Tahiti and Mayotte as compared to Bora Bora. Holocene reef accretion rates among the three locations are comparable. Comparisons with other major reef systems also exhibit more differences than similarities. In general, massive coral facies appear to be more common in the other reef systems discussed in the comparison for reasons not entirely clear.

Acknowledgements

We are grateful to the Deutsche Forschungsgemeinschaft (DFG) who has been funding the Bora Bora research project (Gi 222/23-1). Stefan Haber and Gabriela Meyer were hard-working helpers during field-work. We thank S.A.R.L. Ti Ai Moana (Paea, Tahiti), Captain Yann Paureau, and his first mate Sebastien for logistic support. Our host Gérard Bion in Bora Bora supported us in many ways. The mayor of Bora Bora and the Ministère du Logement, des Affaires Foncières, de l'Économie Numérique et de l'Artisanat (Papeete) kindly issued research permits. LPL Group (Hamburg), SDV (Papeete), and C.H. Robinson (Houston) organized equipment and sample transportation around the globe. Two anonymous reviewers and the associate editor made critical comments that helped to improve this paper.

References

- Abbey, E., Webster, J.M., Braga, J.C., Sugihara, K., Wallace, C., Iryu, Y., Potts, D., Done, T., Camoin, G. and Seard, C. 2011. Variation in deglacial coralgall assemblages and their paleoenvironmental significance: IODP Expedition 310, "Tahiti Sea Level". *Global Planet. Change*, 76, 1-15.
- Agassiz, A. 1903. *The Coral Reefs of the Tropical Pacific*. Harvard Univ. Mus. Comp. Zool. Mem., 28, 410 p.
- Bard, E., Hamelin, B., Arnold, M., Montaggioni, L.F., Cabioch, G., Faure, G. and Rougerie, F. 1996. Deglacial sea-level record from Tahiti corals and the timing of global meltwater discharge. *Nature*, 382, 241-244.
- Bard, E., Hamelin, B. and Delanghe-Sabatier, D. 2010. Deglacial meltwater pulse 1B and Younger Dryas sea levels revisited with boreholes at Tahiti. *Science*, 327, 1235-1237.
- Blais, S., Guille, G., Guillou, H., Chauvel, C., Maury, R.C. and Caroff, M. 2000. Géologie, géochimie et géochronologie de l'île de Bora Bora (Société, Polynésie Française). *Acad. Sci. (Paris) Comptes Rendus, Sci. de la Terre et des Planètes*, 331, 579-585.

- Blanchon, P. and Blakeway, D. 2003. Are catch-up reefs an artefact of coring? *Sedimentology*, 50, 1271-1282.
- Blanchon, P., Granados-Corea, M., Abbey, E., Braga, J.C., Braithwaite, C., Kennedy, D.M., Spencer, T., Webster, J.M. and Woodroffe, C.D. 2014. Postglacial fringing-reef to barrier-reef conversion on Tahiti links Darwin's reef types. *Sci. Rep.*, 4, 4997.
- Braithwaite, C., Montaggioni, L.F., Camoin, G.F., Dalmaso, H., Dullo, W.C. and Mangini, A. 2000. Origins and development of Holocene coral reefs: a revisited model based on reef boreholes in the Seychelles, Indian Ocean. *Int. J. Earth Sci.*, 89, 431-445.
- Cabioch, G., Camoin, G.F. and Montaggioni, L.F. 1999a. Postglacial growth history of a French Polynesian barrier reef tract, Tahiti, central Pacific. *Sedimentology*, 46, 985-1000.
- Cabioch, G., Montaggioni, L.F. and Faure, G. 1995. Holocene initiation and development of New Caledonian fringing reefs, SW Pacific. *Coral Reefs*, 14, 131-140.
- Cabioch, G., Montaggioni, L.F., Faure, G. and Ribaud-Laurenti, A. 1999b. Reef coralgal assemblages as recorders of paleobathymetry and sea level changes in the Indo-Pacific province. *Quat. Sci. Rev.*, 18, 1681-1695.
- Cabioch, G., Taylor, F.W., Récy, J., Edwards, R.L., Gray, S.C., Faure, G., Burr, G.S. and Corrège, T. 1998. Environmental and tectonic influence on growth and internal structure of a fringing reef at Tasmaloum (SW Espiritu Santo, New Hebrides island arc, SW Pacific), In Camoin, G.F. and Davies, P.J. (eds.) *Reefs and carbonate platforms in the Pacific and Indian Oceans*. IAS Spec. Publ., 25, 261-277.
- Camoin G., Cabioch G., Eisenhauer A., Braga J.C., Hamelin, B. and Lericolais, G. 2006. Environmental significance of microbialites in reef environments during the last deglaciation. *Sed. Geol.*, 185, 277-295
- Camoin, G.F., Colonna, M., Montaggioni, L.F., Casanova, J., Faure, G. and Thomassin, B.A. 1997. Holocene sea level changes and reef development in the southwestern Indian Ocean. *Coral Reefs*, 16, 247-259.
- Camoin, G.F., Ebren, P., Eisenhauer, A., Bard, E. and Faure, G. 2001. A 300,000 years record of sea-level changes, Mururoa atoll (French Polynesia). *Palaeogeogr. Palaeoclimatol. Palaeoecol.*, 175, 325-341.
- Camoin, G.F., Gautret, P., Montaggioni, L.F. and Cabioch, G. 1999. Nature and environmental significance of microbialites in Quaternary reefs: the Tahiti paradox. *Sed. Geol.*, 126, 271-304.

- Camoin, G.F. and Montaggioni, L.F. 1994. High energy coralgall-stromatolite frameworks from Holocene reefs (Tahiti, French Polynesia). *Sedimentology*, 41, 655-676.
- Camoin, G.F., Searl, C., Deschamps, P., Webster, J.M., Abbey, E., Braga, J.C., Iryu, Y., Durand, N., Bard, E., Hamelin, B., Yokoyama, Y., Thomas, A.L., Henderson, G.M. and Doussoulliez, P. 2012. Reef response to sea-level and environmental changes during the last deglaciation: Integrated Ocean Drilling Program Expedition 310, Tahiti Sea Level. *Geology*, 40, 643-646.
- Camoin, G.F. and Webster, J.M. 2015. Coral reef response to Quaternary sea-level and environmental changes: state of the science. *Sedimentology*, 62, 401-428.
- Chappell, J. and Polach, H. 1991. Post-glacial sea-level rise from a coral record at Huon Peninsula, Papua New Guinea. *Nature*, 349, 147-149.
- Cheng, H., Edwards, R., Hoff, J., Gallup, C., Richards, D. and Asmerom, Y. 2000. The half-lives of uranium-234 and thorium-230. *Chem. Geol.*, 169, 17-33.
- Creveling, J.R., Mitrovica, X., Hay, C.C., Austermann, J. and Kopp, R.E. 2015. Revisiting tectonic corrections applied to Pleistocene sea-level highstands. *Quat. Sci. Rev.*, 111, 72-80.
- Crossland, C. 1928. Coral reefs of Tahiti, Moorea, and Rarotonga. *J. Linnean Soc. London, Zool.*, 36, 577-620.
- Dana, J.D. 1875. *Corals and Coral Islands*. London, Sampson Low, Marston, Low & Searle, 348 p.
- Darwin, C.R. 1842. *The Structure and Distribution of Coral Reefs*. London, Smith Elder, 214 p.
- Davies, P.J. and Montaggioni, L.F. 1985. Reef growth and sea-level change: the environmental signature. *Proc. 5th Int. Coral Reef Symp.*, 3, 477-515.
- Davies, P.J. and Hopley, D. 1983. Growth fabrics and growth rates of Holocene reefs in the Great Barrier Reef. *BMR J. Austral. Geol. Geophys.*, 8, 237-251.
- Davis, W.M. 1928. *The Coral Reef Problem*. Amer. Geogr. Soc. Spec. Publ., 9, 596 p.
- Dechnik, B., Webster, J.M., Braga, J.C. and Reimer, P.J. 2015. Holocene "turn-on" and evolution of the southern Great Barrier Reef: revisiting reef cores from the Capricorn Bunker Group. *Mar. Geol.*, 363, 174-190.

- Deschamps, P., Durand, N., Bard, E., Hamelin, B., Camoin, C., Thomas, A.L., Henderson, G.M., Okuno, J. and Yokoyama, Y. 2012. Ice-sheet collapse and sea-level rise at the Bølling warming 14,600 years ago. *Nature*, 483, 559-564.
- Done, T.J. 1982. Patterns in the distribution of coral communities across the central Great Barrier Reef. *Coral Reefs*, 1, 95-107.
- Easton, W.H. and Olson, E.A. 1976. Radiocarbon profile of Hanauma Reef, Oahu, Hawaii. *Geol. Soc. Amer. Bull.*, 87, 711-719.
- Fadlil, A., Sichoix, L., Barriot, J.-P., Ortéga, P. and Willis, P. 2011. Evidence for a slow subsidence of the Tahiti island from GPS, DORIS, and combined satellite altimetry and tide gauge sea level records. *Comptes Rendus Geosci.*, 34, 331-341.
- Fairbanks, R.G. 1989. A 17,000-year glacio-eustatic sea level record: influence of glacial melting rates on the Younger Dryas event and deep-water circulation. *Nature*, 342, 637-642.
- Fietzke, J., Liebetrau, V., Eisenhauer, A. and Dullo, W.C. 2005. Determination of uranium isotope ratios by multi-static MIC-ICP-MS, method and implementation for precise U- and Th-series isotope measurements. *J. Anal. Atomic Spectr.*, 20, 395-401.
- Gabrié, C. and Salvat, B. 1985. General features of French Polynesian islands and their coral reefs. *Proc. 5th Int. Coral Reef Symp.*, 1, 3-15.
- Gabrié, C., Planes, S., Baldwin, J., Bonvallet, C., Chauvet, C., Vernaudeau, Y., Payri, C., and Galzin, R. 1994. Study of the coral reefs of Bora-Bora (Society archipelago, French Polynesia) for the development of a conservation and management plan. *Ocean & Coastal Manag.*, 25, 189-216.
- Gischler, E. 2010. Indo-Pacific and Atlantic spurs and grooves revisited: the possible effects of different Holocene sea-level history, exposure, and reef accretion rate in the shallow fore reef. *Facies*, 56, 173-176.
- Gischler, E. 2011. Sedimentary facies of Bora Bora, Darwin's type barrier reef (Society Islands, south Pacific): the unexpected occurrence of non-skeletal grains. *J. Sed. Res.*, 81, 1-17.
- Gischler, E. 2015. Quaternary reef response to sea-level and environmental change in the western Atlantic. *Sedimentology*, 62, 429-465.
- Gischler, E and Hudson, J.H. 2004. Holocene development of the Belize Barrier Reef. *Sed. Geol.*, 164, 223-236.

- Gischler, E., Hudson, J.H. and Pisera, A. 2008. Holocene reef development in the Maldives, Indian Ocean. *Mar. Geol.*, 250, 104-113.
- Gray, S.C. and Hein, J.R. 2005. Lagoonal reef accretion and Holocene sea-level history from three atolls in the Cook Islands, central south Pacific. *J. Coast. Res.*, 42, 253-264.
- Guilcher, A., Berthois, L., Doumenge, F., Michel, A., Saint-Requier, A. and Arnold, R. 1969. Les récifs et lagons coralliens de Mopelia et de Bora-Bora (îles de la Société). *Mém. Orstrom*, 38, 103 p.
- Guillou, D., Maury, R.C., Blais, S., Cotten, J., Legendre, C., Guille, G. and Caroff, M. 2005. Age progression along the Society hotspot chain (French Polynesia) based on new unspiked K-Ar ages. *Soc. Géol. France Bull.*, 176, 135-150.
- Hearty, P.J., Hollin, J.T., Neumann, A.C., O'Leary, M.J. and McCulloch, M. 2007. Global sea-level fluctuations during the last interglacial (MIS 5e). *Quat. Sci. Rev.*, 26, 2090-2112.
- Heindel, K., Birgel, D., Brunner, B., Thiel, V., Westphal, H., Ziegenbalg, S.B., Gischler, E., Cabioch, G. and Peckmann, J. 2012. Post-glacial microbialite formation in coral reefs in the Pacific Ocean, Caribbean, and Indian Ocean. *Chem. Geol.*, 304-305, 117-130.
- Humblet, M., Hongo, C. and Sugihara, K. 2015. An identification guide to some major Quaternary fossil reef-building coral genera (*Acropora*, *Isopora*, *Montipora*, and *Porites*). *Island Arc*, 24, 16-30.
- Kennedy, D.M. and Woodroffe, C.D. 2002. Fringing reef growth and morphology: a review. *Earth-Sci. Rev.*, 57, 255-277.
- Klostermann, L. and Gischler, E. 2015. Holocene sedimentary evolution of a mid-ocean atoll lagoon, Maldives, Indian Ocean. *Int. J. Earth Sci.*, 104: 289-307.
- Ladd, H.S., Ingerson, E., Townsend, R.C., Russell, M. and Stephenson, H.K. 1953. Drilling on Eniwetok Atoll, Marshall Islands. *Amer. Assoc. Petrol. Geol. Bull.*, 37, 2257-2280.
- Kench, P.S., Smithers, S.G., McLean, R.F. and Nichol, S.L. 2008. Holocene reef growth in the Maldives: evidence of a mid-Holocene sea-level highstand in the central Indian Ocean. *Geology*, 37, 455-458.
- Longman, M.W. 1980. Carbonate diagenetic textures from near-surface diagenetic environments. *Amer. Assoc. Petrol. Geol. Bull.*, 64, 461-487.
- Macintyre, I.G., Burke, R.B. and Stuckenrath, R. 1976, Thickest recorded Holocene reef section, Isla Pérez core hole, Alacran reef, Mexico. *Geology*, 5, 749-754.

- Macintyre, I.G. and Glynn, P.W. 1976. Evolution of modern Caribbean fringing reef, Galeta Point, Panama. *Amer. Assoc. Petrol. Geol. Bull.*, 60, 1054-1072.
- Macintyre, I.G. and Marshall, J.F. 1988. Submarine lithification in coral reefs: some facts and misconceptions. *Proceedings 6th International Coral Reef Symposium*, 1, 263-272.
- Marshall, J.F. and Jacobson, G. 1985. Holocene growth of a mid Pacific atoll: Tarawa Kiribati. *Coral Reefs*, 4, 11-17.
- Masse, J.-P., Thomassin, B.A. and Acquaviva, M. 1989. Bioclastic sedimentary environments of coral reefs and lagoon around Mayotte Island (Comoro Archipelago, Mozambique Channel, SW Indian Ocean). *J. Coast. Res.*, 5, 419-432.
- Milliman, J.D. 1974. *Marine Carbonates. Recent Sedimentary Carbonates. Part 1.* New York, Springer, 375 p.
- Montaggioni, L.F. 1988. Holocene reef growth history in mid-plate high volcanic islands. *Proc. 6th Int. Coral Reef Symp.*, 3, 455-460.
- Montaggioni, L.F. 2005. History of Indo-Pacific coral reef systems since the last glaciation: development patterns and controlling factors. *Earth-Sci. Rev.*, 71, 1-75.
- Montaggioni, L.F., Borgomano, J., Fournier, F. and Granjeon, D. 2015. Quaternary atoll development: new insights from the two-dimensional stratigraphic forward modelling of Mururoa island (central Pacific Ocean). *Sedimentology*, 62, 466-500.
- Montaggioni, L.F., Cabioch, G., Camoin, G.F., Bard, E., Ribaud-Laurenti, A., Faure, G., Déjardin, P. and Récy, J. 1997. Continuous record of reef growth over the past 14 k.y. on the mid-Pacific island of Tahiti. *Geology*, 25, 555-558.
- Montaggioni, L.F. and Camoin, G.F. 1993. Stromatolites associated with coralgal communities in Holocene high-energy reefs. *Geology*, 21, 149-152.
- Montaggioni, L.F. and Pirazzoli, P.A. 1984. The significance of exposed coral conglomerates from French Polynesia (Pacific Ocean) as indicators of recent relative sea-level changes. *Coral Reefs*, 3, 29-42.
- Müller, G. 1967. *Methods in Sedimentary Petrology, Part 1.* Stuttgart, Schweizerbart, 283 p.
- Pirazzoli, P.A. and Montaggioni, L.F. 1985. Lithospheric deformation in French Polynesia (Pacific Ocean) as deduced from Quaternary shorelines. *Proc. 5th Int. Coral Reef Symp.*, 3, 195-200.
- Pirazzoli, P.A. and Montaggioni, L.F. 1986. Late Holocene sea-level changes in the northwest Tuamotu islands, French Polynesia, *Quat. Res.*, 25, 350-368.

- Pirazzoli, P.A. and Montaggioni, L.F. 1988a. Holocene sea-level changes in French Polynesia. *Palaeogeogr. Palaeoclimatol. Palaeoecol.* 68, 153-175.
- Pirazzoli, P.A. and Montaggioni, L.F. 1988b. The 7000 yr sea level curve in French Polynesia: geodynamic implication for mid-plate volcanic islands. *Proc. 6th Int. Coral Reef Symp.*, 3, 467-477.
- Pirazzoli, P.A., Brousse, R., Delibras, G., Montaggioni, L.F., Sachet, M.H., Salvat, B. and Sinoto, Y.H. 1985a. Leeward islands, Maupiti, Tupai, Bora Bora, Huahine, Society archipelago. *Proc. 5th Int. Coral Reef Symp.*, 1, 17-72.
- Pirazzoli, P.A., Montaggioni, L.F., Delibras, G., Faure, G. and Salvat, B. 1985b. Late Holocene sea-level changes in the Society Islands and in the northwest Tuamotu Atolls. *Proc. 5th Int. Coral Reef Symp.*, 3, 131-136.
- Pirazzoli, P.A., Montaggioni, L.F., Salvat, B. and Faure, G. 1988. Late Holocene sea level indicators from twelve atolls in the central and eastern Tuamotus (Pacific Ocean). *Coral Reefs*, 7, 57-68.
- Pirazzoli, P.A., Montaggioni, L.F., Vergnaud-Grazzini, C. and Saliege, J.F. 1987. Late Holocene sea levels and coral reef development in Vahitahi Atoll, eastern Tuamotu Islands, Pacific Ocean. *Mar. Geol.*, 76, 105-116.
- Purdy, E.G. 1974. Reef configurations: cause and effect, In Laporte, L.F. (ed.) *Reefs in Time and Space*. *SEPM Spec. Publ.*, 18, 9-76.
- Purdy, E.G. and Winterer, E.L. 2001. Origin of atoll lagoons. *Geol. Soc. Amer. Bull.*, 113, 837-854.
- Purdy, E.G. and Winterer, E.L. 2006. Contradicting barrier reef relationships for Darwin's evolution or reef types. *Int. J. Earth Sci.*, 95, 143-167.
- Rashid, R., Eisenhauer, A., Stocchi, P., Liebetrau, V., Fietzke, J., Rüggeberg, A. and Dullo W.C. 2014. Constraining mid to late Holocene relative sea level change in the southern equatorial Pacific Ocean relative to the Society Islands, French Polynesia. *Geochem. Geophys. Geosyst.*, 15, 2601-2615.
- Reimer, P.J. and 30 others 2013. IntCal13 and Marine13 radiocarbon age calibration curves 0-50,000 years cal BP. *Radiocarbon*, 55, 1869-1887.
- Riding, R., Liang, L. and Braga, J.C. 2014. Millennial-scale ocean acidification and late Quaternary decline of cryptic bacterial crusts in tropical reefs. *Geobiology*, 12, 387-405.

- Rougerie, F. and Wauthy, B. (1993) The endo-upwelling concept: from geothermal convection to reef construction. *Coral Reefs*, 12, 19-30.
- Saller, A.H. and Koepnick, R.B. 1990. Eocene to early Miocene growth of Enewetak Atoll: insight from strontium-isotope data. *Geol. Soc. Amer. Bull.*, 102, 381-390.
- Schlager, W. and Purkis, S.J. 2013. Bucket structure in carbonate accumulations of the Maldives, Chagos and Laccadive archipelago. *Int. J. Earth Sci.*, 102, 2225-2238.
- Schlager, W. and Purkis, S. 2015. Reticulate reef patterns - antecedent karst versus self-organization. *Sedimentology*, 62, 501-515.
- Seard, C., Camoin, G., Yokoyama, Y., Matsuzaki, H., Durand, N., Bard, E., Sepulcre, S. and Deschamps, P. 2011. Microbialite development patterns in the last deglacial reefs from Tahiti (French Polynesia; IODP Expedition #310): implications on reef framework architecture. *Mar. Geol.*, 279, 63-86.
- Steers, J.A. and Stoddart, D.R. 1977. The origin of fringing reefs, barrier reefs, and atolls. In Jones, O.A. and Endean, R. (eds.), *Biology and Geology of Coral Reefs*. Academic Press, New York, p. 21-57.
- Talma, A.S. and Vogel, J.C. 1993. A simplified approach to calibrating C14 dates. *Radiocarbon*, 35, 317-322.
- Thomas, A.L. and 25 others 2012. Assessing subsidence rates and paleo water-depths for Tahiti reefs using U-Th chronology of altered corals. *Mar. Geol.*, 295-298, 86-94.
- Thomas, A.L., Henderson, G.M., Deschamps, P., Yokoyama, Y., Mason, A.J., Bard, E., Hamelin, B., Durand, N. and Camoin, G. 2009. Penultimate deglacial sea-level timing from uranium/thorium dating of Tahitian corals. *Science*, 324, 1186-1189.
- Toomey, M., Ashton, A.D. and Perron, J.T. 2013. Profiles of ocean island coral reefs controlled by sea-level history and carbonate accumulation rates. *Geology*, 41, 731-734.
- Veron, J.E.N. (2000) *Corals of the world*. Australian Institute of Marine Science and CRR Qld Pty Ltd, Townsville, Australia, 3 volumes.
- Wallace, C.C. 1999. *Staghorn corals of the world*. Museum of Tropical Queensland; CSIRO Publishing, Collingwood, Australia, 421 p.
- Westphal, H., Heindel, K., Brandano, M. and Peckmann, J. 2010. Genesis of microbialites as contemporaneous framework components of coral reefs, deglacial of Tahiti (IODP 310). *Facies*, 56, 337-352.

Woodroffe, C.D. and Webster, J.M. 2014. Coral reefs and sea-level change. *Mar. Geol.*, 352, 248-267.

Zinke, J., Reijmer, J.J.G., Thomassin, B., Dullo, W.C., Grootes, P.M. and Erlenkeuser, H. 2003. Postglacial flooding history of the Mayotte lagoon (Comoro archipelago, SW Indian Ocean). *Mar. Geol.*, 194, 181-196.

CHAPTER 4

A NEW MODEL EVALUATING HOLOCENE SEDIMENT DYNAMICS: INSIGHTS FROM A MIXED CARBONATE-SILICICLASTIC LAGOON (BORA BORA, SOCIETY ISLANDS, FRENCH POLYNESIA, SOUTH PACIFIC)

Anja Isaack¹, Eberhard Gischler¹, J. Harold Hudson², Flavio S. Anselmetti³,
Andreas Lohner³, Hendrik Vogel³, Eva Garbode¹, Gilbert F. Camoin⁴

¹Institut für Geowissenschaften, Goethe-Universität, Frankfurt/Main, Germany

²Reef Tech Inc., Miami, Florida, USA

³Institute of Geological Sciences and Oeschger Centre for Climate Change
Research, University of Bern, Bern, Switzerland

⁴Aix-Marseille Université, CNRS, IRD, CEREGE UM34, Aix-en-Provence &
Europôle Méditerranéen de l'Arbois, BP 80, Aix-en-Provence cedex 4, France

Keywords: barrier-reef lagoon; sediment dynamics; mixed carbonate-siliciclastic
sediments, sand apron slumping, Holocene; benthic foraminifera

*Published 2016: **Sedimentary Geology**, 343:99–118.*

doi:10.1016/j.sedgeo.2016.08.002

Abstract

Mixed carbonate-siliciclastic lagoons of barrier reefs provide great potential as sedimentary archives focusing on palaeoenvironmental and palaeoclimatic changes as well as on event deposition. Sediment sources include lagoonal carbonate production, the marginal reef and the volcanic hinterland. Mixed carbonate-siliciclastic continent-attached coastal lagoons have been intensively studied, however, their isolated oceanic counterparts have been widely disregarded. Here, we present a new model of Holocene sediment dynamics in the barrier-reef lagoon of Bora Bora based on sedimentological, palaeontological, geochronological and geochemical data. The lagoonal succession started with a Pleistocene soil representing the Lowstand Systems Tract. As the rising Holocene sea inundated the carbonate platform, peat accumulated locally ~10650-9400 yrs BP. Mixed carbonate-siliciclastic sedimentation started ca. 8700-5500 yrs BP and represents the Transgressive Systems Tract. During that time,

sediments were characterized by relatively coarse grain size and contained high amounts of terrestrial material from the volcanic hinterland as well as carbonate sediments mainly produced within the lagoon. Siliciclastic content decreases throughout the Holocene. After the rising sea had reached its modern level, sand aprons formed between reef crest and lagoon creating transport pathways for reef-derived material leading to carbonate-dominated sedimentation ca. 6000-3000 kyrs BP during the Highstand Systems Tract. However, mainly fine material was transported and accumulated in the lagoon while coarser grains were retained on the prograding sand apron. From ca. 4500-500 yrs BP, significant variations in grain-size, total organic carbon as indicator for primary productivity, Ca and Cl element intensities as qualitative indicators for carbonate availability and lagoonal salinity are seen. Such patterns could indicate event (re-)deposition and correlate with contemporaneous event deposits found in the lagoon of nearby Tahaa, which are supposed to be induced by elevated cyclone activity. Correspondingly, enhanced erosion and run-off from the volcanic hinterland as well as lower lagoonal salinity would be associated with intense rainfall during repeated cyclone landfall. Increased amounts of coarse-grained sediment from marginal reef areas would be transported into the lagoon. However, Ti/Ca and Fe/Ca ratios as proxies for terrigenous sediment delivery have incessantly declined since the mid-Holocene. Also, benthic foraminiferal faunas do not validate reef-to-lagoon transport of sediment. Alternatively, the apparent onset of higher hydrodynamic energy conditions can be explained by more permanent southeast trade winds and higher-than-present sea level, which are supposed for the mid-late Holocene in the south Pacific. Sustained winds would have flushed higher amounts of open ocean water into the lagoon enhancing primary productivity and the amount of pelagic organisms within the lagoon while lowering lagoonal salinity. We propose the shift towards coarser-grained sedimentation patterns during the mid-late Holocene to reflect sediment-load shedding of sand aprons due to oversteepening of slopes at sand apron/lagoon edges during times of stronger trades and higher-than-present sea level of the Highstand Systems Tract, which led to redeposition of sediment even within the lagoon center. Modern conditions including a sea-level fall to modern level were reached ca. 1000 yrs BP, and lagoonal infill has been determined to a large part by fine-grained carbonate-dominated sediments produced within the lagoon and derived from the marginal reef. Infill of lagoonal accommodation space via sand aprons is estimated to be up to six times higher than infill by lagoonal background sedimentation and emphasizes the importance of the progradation of sand aprons. Contrary to the commonly supposed assumption that coarse-grained sediment layers within fine-grained lagoonal successions represent overwash events

induced by storms or periods of higher storm activity, we postulate a new model of long-term lagoonal sediment dynamics including sea level, climatic change and geomorphological variation of the barrier reef lagoon.

4.1 Introduction

The potential of coral reef systems as key recorders for palaeo-environmental changes has been known for long time and applied to fossil and modern carbonate platforms worldwide (e.g., Camoin and Webster, 2015, and references therein). While most of the studies focused on the investigation of the corals and the coral-reef record, back-reef lagoons have rarely been used as sedimentary archives for palaeoenvironmental changes and event deposition.

Variations in distribution of sediment texture reflect variations in the hydrodynamic energy system of reefs and carbonate platforms, shown for example by Gischler (2011) at the study site, in the Great Barrier Reef, Pacific Ocean (Frith, 1983), in Cocos (Keeling) Islands Atoll, Indian Ocean (Kench, 1998a) and in the Florida Reef Tract, western Atlantic Ocean (Ginsburg, 1956). Storms or tsunamis are important sporadic high-energy events that lead to significant sediment transport and sorting in distal areas of back-reef lagoons and can therefore not be excluded in sediment studies (Harris et al., 2015; Kench et al., 2008; Scoffin, 1992).

In general, back-reef lagoons act as sediment traps; i.e., carbonate sediment mainly produced on the reef flat undergoes subsequent and continuous transport across the reef flat and sand apron before it finally accumulates in the lagoon (Kench, 2011; Stoddart, 1969; Scoffin and Tudhope, 1988). Hence, sedimentation patterns should result in lagoonward fining of sediments. Even if lagoonal carbonate production occurs, it is predicted to be less significant than allochthonous transport and accumulation of sand apron sediments (e.g., Woodroffe et al., 2004). For those reasons, back-reef lagoons provide not only information of variations of sedimentation and ecology of sediment-producing organisms in the platform interior, but also detect variations and changes of the coral reef and reef-associated organisms from the reef crest and immediate back-reef areas.

Oceanic (Darwinian) barrier-reef lagoons represent mixed carbonate-siliciclastic systems, which also receive weathered materials from the volcanic hinterland and are therefore well suited for the application of different proxies to detect environmental variations and changes in sea level and climate. Still, studies investigating oceanic barrier-reef lagoons are rare. Zinke et al. (2005, 2003a, 2000) investigated sediment facies and faunal composition associated with the Holocene transgression in sediment cores from the mixed carbonate-

siliciclastic barrier reef lagoon of Mayotte, Indian Ocean. Furthermore, Zinke et al. (2003b, 2001) interpreted lagoonal successions in terms of sequence stratigraphy and delineated lowstand, transgressive and highstand deposits based on seismic and core data. In Tahaa, French Polynesia, South Pacific, Toomey et al. (2013) used grain-size variability in sediment cores from the barrier-reef lagoon to identify high-energy event deposits induced by tropical cyclones during the last 5000 yrs.

The number of studies focusing on oceanic barrier-reef lagoon systems is limited; therefore we also consulted investigations of atoll lagoons for comparison. For the reconstruction of palaeo-storm and tsunami history over the past 4000 yrs, Yu et al. (2009) dated several sedimentary events in atoll lagoon cores from Yungshu Reef, south China Sea, based on a study of redeposited coral blocks and grain-size variability. However, these authors could not distinguish between storm and tsunami deposits. Klostermann and Gischler (2015) used vibrocores to detail Holocene sedimentary facies and evolution of a Maldivian atoll lagoon (Indian Ocean) with regard to sequence stratigraphy. In addition, Klostermann et al. (2014) identified six sedimentary events induced by tsunamis using grain-size variability and the presence of shallow-water organisms such as corals, coralline algae and reef-associated foraminifera deposited within the lagoon. Because of the close position to the equator, the authors were able to exclude storms as trigger for event deposition.

Modern and innovative methods such as non-destructive x-ray fluorescence (XRF) core scanning provide a quick, inexpensive and accurate high-resolution record, which helps to identify sedimentological and environmental changes (Röhl and Abrams, 2000). Gregory et al. (2015) combined benthic foraminiferal and high-resolution XRF analyses in two coastal lagoon cores from Cuba to examine climatic variability. The authors found decreasing Ti/Ca ratios over the past 4000 yrs and interpreted this observation to be a consequence of declined precipitation and the onset of a long-term dry period in the Caribbean region. In shallow marine sediment cores of Charlotte Harbor, southwest Florida, van Soelen et al. (2012) used XRF core scanning and biomarker analysis to identify periods with increased runoff and primary productivity during the mid-late Holocene supposing that these were induced by long-term hydrodynamic and atmospheric changes involving shifts of the Intertropical Convergence Zone (ITCZ), the Bermuda-Azores High and the Polar Front. Coarser-grained layers consisting of quartz sands and shell debris are present throughout the core record, but are very common during the late Holocene, which might result from an increase in tropical cyclone activity in the Gulf of Mexico.

In order to add to the limited knowledge on oceanic barrier-reef lagoon development in general, we investigated sediment cores from the lagoon of Bora Bora to unravel sediment dynamics during the evolution of the barrier-reef complex in response to the early Holocene sea-level transgression and subsequent fluctuations during the mid-late Holocene as well as Holocene climate variability. Our multi-proxy approach includes sedimentological, palaeontological, geochemical and geochronological data to evaluate factors controlling sedimentary patterns (short-term event deposition vs. long-term sedimentary processes) and driving mechanisms of sediment dynamics through the Holocene in a mixed carbonate-siliciclastic lagoon system.

4.2 Study area

The oceanic barrier-reef system of Bora Bora is located in the northwestern part of the Society archipelago in the South Pacific Ocean (fig. 4/1). The Society islands and nearby Austral, Gambier, Tuamotu and Marquesas islands belong to the overseas territory of French Polynesia. Increasing ages of volcanic islands from southwest (Mehetia; 0.3 Ma) to northwest (Bellingshausen; 4.3 Ma) suggest a plate movement of 11 cm/yr over the Society hotspot (Blais et al., 2000; Guillou et al., 2005). According to radiometric (K/Ar) dating of basalts, the volcanic island of Bora Bora and nearby island of Toopua formed 3.45-3.10 Ma ago. These edifices consist of alkali basalt, rare hawaiites, intrusive gabbros, and volcanic breccia (Blais et al., 2000; Uto et al., 2007). The Bay the Povai between the two volcanic islands is supposed to outline the caldera.

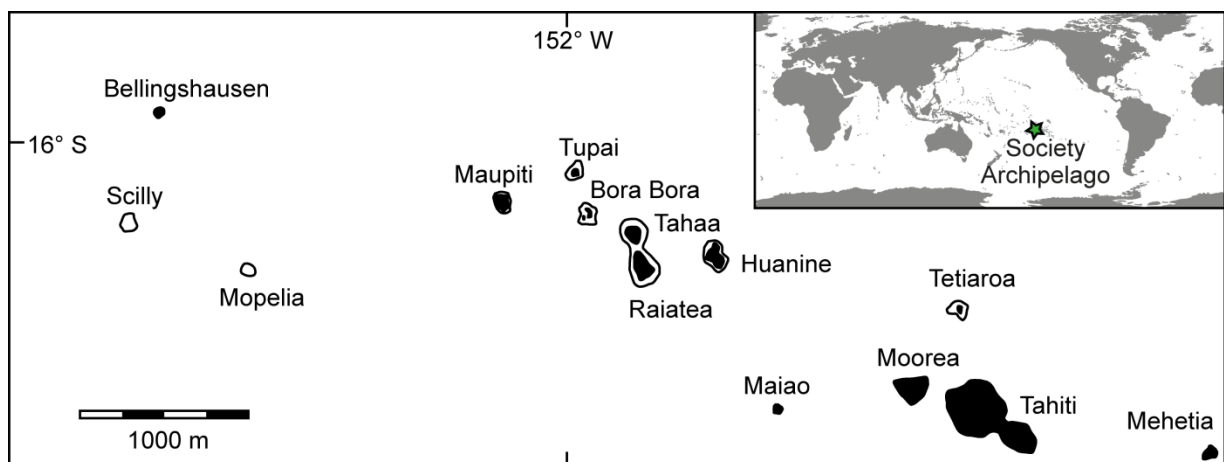


Fig. 4/1: Location of Bora Bora in the Society archipelago and in the South Pacific Ocean

The volcanic island of Bora Bora is densely wooded and covers an area of about 30 km² with the highest point Mount Otemanu rising up to 727 m above sea level. The irregular coastline forms peninsulas and six extensive bays: Baie Faanui, Baie Tamoo, Baie Haamaire, Baie Aponapu, Baie Faapore and Baie de Povai (clockwise, beginning in the west; fig. 4/2). The

lagoon floor has a high relief and is up to 45 m deep (Baie Aponapu). Bora Bora has an extensive barrier reef system, which covers an area of ca. 70 km². Fringing reefs encircle the volcanic island (fig. 4/3a). Pinnacle and patch reefs are situated in the deeper parts of the sand apron and are nearly absent within the lagoon.

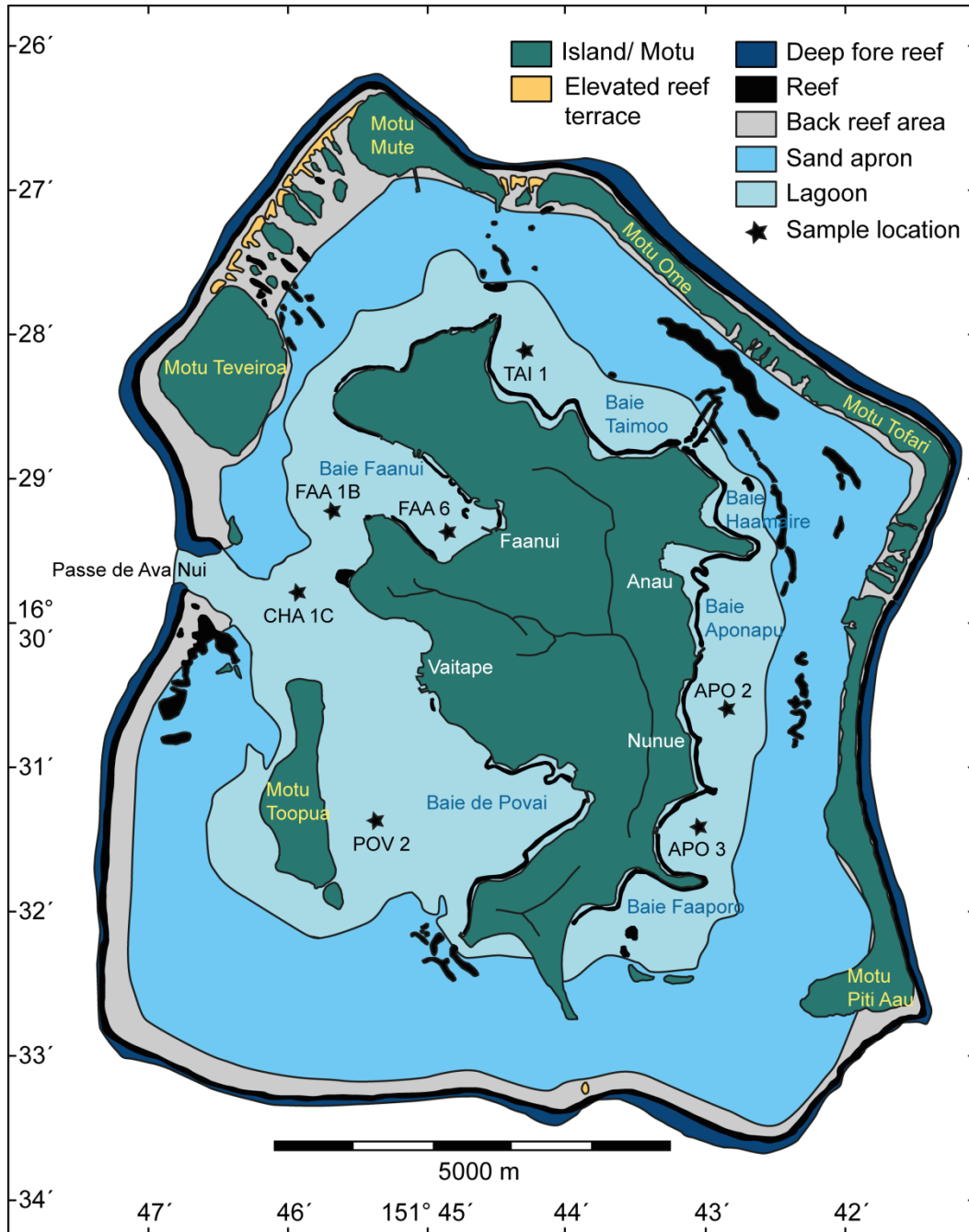


Fig. 4/2: Geomorphological map of Bora Bora showing the location of analysed vibrocores in the lagoon (black stars). This map is based on the British Admiralty Chart 1107 (1:25,000) and satellite images

A wide and shallow sand apron extends towards the lagoon forming sediment transport pathways from the reef crest into the adjacent lagoon (fig. 4/3c, d). The extension of the sand apron reaches its maximum in the southern part of the lagoon (fig. 4/3d). The sand apron has its minimum width in the eastern side of the lagoon, where sediment supply is restricted by

motus (narrow elongated sand islands), acting as natural barriers of sediment transport from the reef crest into the lagoon (figs. 4/2; 4/3c). Motus predominantly occur on the windward side of the barrier reef and are interrupted by small passages called hoas. The lack of motus on the southwestern and southern reef margin could be an expression of a southwestward tilt of the volcanic edifice (Blais et al., 2000), i.e., a deeper position of the antecedent topography (Gischler, 2011). The channel Passe de Ava Nui is up to 48 m deep connecting the lagoon with the open ocean in the western part of the platform. Lagoon circulation is characterized by water entering the hoas in the east and leaving the lagoon in the west through the channel Ava Nui (Gabrié et al., 1994). Coral rubble conglomerate, beachrock and fossil elevated reef terraces occur on the ocean sides of the motus (Gischler et al., 2016; Pirazzoli et al., 1988, 1985b; Pirazzoli and Montaggioni, 1988). Coral reef blocks can rarely be found at the shore of Bora Bora. A well-developed spur and groove system can be found on seaward side of the reef crest (Gabrié et al., 1994; Gischler, 2010).



Fig. 4/3: Aerial photographs of Bora Bora showing **a**) view into Baie Faanui with distinctive fringing reef encircling the volcanic island; **b**) Motu Mute with air strip in background and the back-reef area behind the reef crest with extensive sand apron indicating lagoonward sediment transport; **c**) Motu Piti Aau, sand aprons and eastern lagoon, sediment transport from reef margin via sand apron into the lagoon probably restricted by motus on the windward margin; **d**) southern end of Bora Bora, Toopua in the background, with barrier reef and wide sand apron suggesting extensive sediment transport into the lagoon

The climate of Bora Bora is tropical with a hot and rainy (austral summer) season from November to April and a relatively dry and cool season (austral winter) from May to October (Gabrié and Salvat, 1985). Trade winds prevail and blow from northeastern to southeastern

directions (Pirazzoli et al., 1985b). Major storms Lisa, Reva, and Veena have passed the Society Islands during 1982-1983 (Pirazzoli et al., 1985b). The most intense tropical cyclone (TC) in French Polynesia was TC Oli (category 4), which hit the Society Islands in February 2010. In January 2015, TC Niko formed north of the Leeward Islands of French Polynesia and intensified while moving southwards. In French Polynesia, annual average air temperatures decrease from 27 °C to 21 °C from north to south. Monthly air-temperature extremes range from 24 °C to 28 °C in the Society Islands (Gabrié and Salvat, 1985). The spring tidal range can be up to 40 cm (Pirazzoli et al., 1985a). Measurements of precipitation from 1951 to 1961 show that in Bora Bora annual precipitation rates averages 2000 mm/yr (Guilcher et al., 1969). Measurements of sea-surface temperatures in the lagoon ranged from 23.8 °C to 26.7 °C in August 1963; during the same time period, salinity was slightly elevated above normal and ranged from 36.7‰ to 36.9‰ (Guilcher et al., 1969).

4.3 Methods

During field work in Bora Bora from 4-30 May 2014, thirteen vibrocore stations were selected in the deep barrier reef lagoon based on shallow reflection seismic data, which will be published in detail elsewhere. Vibrocores were taken using a Rossfelder P3 vibrocorer connected with an aluminum pipe measuring 6 m length and 7.5 cm in diameter. Following core recovery, water-filled parts of the aluminum pipes were cut off, cores were sectioned and sealed at the tops with plastic caps and shipped to the Institute of Geosciences, Frankfurt am Main, for further processing.

Seven cores from the eastern and western sides of the lagoon (fig. 4/2; APO 2; APO 3; CHA 1C; FAA 1B; FAA 6; POV 2; TAI 1, tab. 4/1) were opened, photographed and described. Samples and subsamples were taken in one half of the core; the other half was archived. For detailed grain-size analyses, samples were taken at high resolution every 2.5 cm, wet sieved through a 0.125 mm sieve and after drying through 2 mm and 0.25 mm sieves, respectively. The relative proportions (weight percentages) of each sediment fraction were calculated based on total dry weights of the samples. The degree of sorting of the sediment was calculated with Gradistat (Blott and Pye, 2001).

Bulk sediment samples were pulverized in order to measure carbonate content using a Scheibler-type calcimeter, following the simple reaction of carbonate solution with hydrochloric acid (Müller, 1964). X-ray powder diffraction (XRD) was performed in order to quantify carbonate phases of the bulk sediments and determine qualitative mineralogy (Milliman, 1974). Because of the low content of terrestrial mineral composition in upper core

Table 4/1: Locations and depths of the vibrocores investigated in the Bora Bora lagoon

Location	Vibrocore	Water depth (m)	Core length (m)	Long W (decimal degrees)	Lat S (decimal degrees)
Baie de Aponapu	APO 2	35	4.60	151.7176208	16.50801277
	APO 3	32	3.52	151.7203827	16.52214622
Passe de Ava Nui	CHA 1 C	38	4.04	151.7680969	16.49309731
Baie de Faanui	FAA 1 B	27	3.92	151.7616425	16.48695564
	FAA 6	24	2.64	151.7516479	16.48764992
Baie de Povai	POV 2	31	3.73	151.7600555	16.52108955
Baie de Taimoo	TAI 1	29	3.38	151.7407532	16.46811676

samples, bulk sediment content was measured only in three basal samples. Each sample was measured using a Panalytical X'Pert Pro diffractometer. For the identification of mineral phases, the software X'Pert HighScore Plus and MacDiff were used (Petschick et al., 1996).

Based on the 2-0.25 mm sediment fraction of cores APO 2 and POV 2, 11 samples for the identification of foraminifera species were selected and 200 individuals per sample identified using the descriptions of Cushman (1942, 1933, 1932); Cushman et al. (1954); Debenay (2012); Loeblich and Tappan (1988); Parker (2009) and Todd (1965);. For comparison of specimens, the collection of Maldivian foraminifera published by Parker and Gischler (2011) was consulted. Additionally, specimens of foraminifera were glued on aluminum stubs and coated with gold/paladium for 4 minutes for SEM imaging with a Jeol JSM 6490 LV scanning electron microscope at the Senckenberg Research Institute, Frankfurt am Main.

Preliminary facies were defined based on visual inspection and sedimentological and mineralogical analyses using the classification of limestones by Dunham (1962) and the extended version of Embry and Klovan (1972). Grain-supported and mud-supported sediment textures were differentiated based on either more or less than 50% fines (< 0.125 mm fraction).

Core APO 2 from the eastern lagoon was selected for more detailed analyses based on sedimentary features. A representative split of the grain-size fraction 0.25-0.125 mm of 5 samples was investigated under a binocular microscope and relative percentages of pelagic organisms (pteropods, planktonic foraminifera) were quantified. Detailed textural analysis of the fine fraction every 2.5 cm was made using a HORIBA Laser Scattering Particle Size Distribution Analyzer LA-950 from the Institute of Physical Geography, Frankfurt am Main. Non-destructive x-ray fluorescence core scanning (XRF) was done with an ITRAX core scanner (Cox Ltd.) at the Institute of Geological Sciences and Oeschger Centre for Climate

Change Research, University of Bern, Switzerland. The sediment was irradiated on the core surface with x-ray every 5 mm for 10 seconds (Lohner, 2015). A silicon drift detector allows the detection of elements from Al to U. For this study, the elements Al, Cl, Ca, Ti, Fe and Cu were considered. Measurements of total organic carbon were done within a sample distance of 10 cm using a Bruker G4 Icarus CS analyzer (Lohner, 2015).

A total of 25 samples of mollusk shell fragments from the > 2 mm sediment fraction and from peat were selected for radiometric age dating with accelerated mass spectroscopy (AMS) (after Bard, 1998) by Beta Analytic Inc., Miami, Florida, USA. Ages were calibrated (2-sigma) and corrected for the local reservoir effect (Talma and Vogel, 1993). Therefore, the MARINE13 (Reimer et al., 2013) and SHCAL13 (Hogg et al., 2013) databases were applied. Parameters used for the calculation of the marine reservoir effect in mollusk shells are $\Delta R = 17 \pm 21$ and $\text{Glob res} = -200$ to 500.

Statistical testing of data and the calculation of diversity indices was made using the PAST software (Hammer et al., 2001). The software Analyseries (Paillard et al., 1996) was used to interpolate between unequal sample distances. Graphical presentations were made using the Panplot software (Sieger and Grobe, 2005).

4.4 Results

4.4.1 Sedimentology

Lagoonal succession

A loamy reddish-brown to bluish-gray soil forms the base of cores APO 3, CHA 1C, FAA 1B and POV 2. All cores show extensive bioturbation at the base (fig. 4/4). The soil in a very proximal core (FAA 6) is rusty-red to bluish-gray (fig. 4/4). Recovered soil thicknesses reach 12-55 cm in the vibrocores. The same type of soil was recovered also below a Holocene fringing reef on the northwestern shore of Bora Bora during rotary drilling (Gischler et al. 2016). A dark brown peat was recovered in core APO 2, more than 30 cm thick (fig. 4/4). Peat fragments were found also in core CHA 1C, incorporated in younger, basal mixed carbonate-siliciclastic sediments. The corebase of TAI 1 consists of a yellowish-gray serpulid-rich rudstone, ca. 70 cm thick (fig. 4/4). Packstones, wackestones and mudstones accumulated above soil and peat during the Holocene without a prominent transition in color (fig. 4/4). Sediment colors change from gray close to the base to light yellowish gray towards the top of each core.

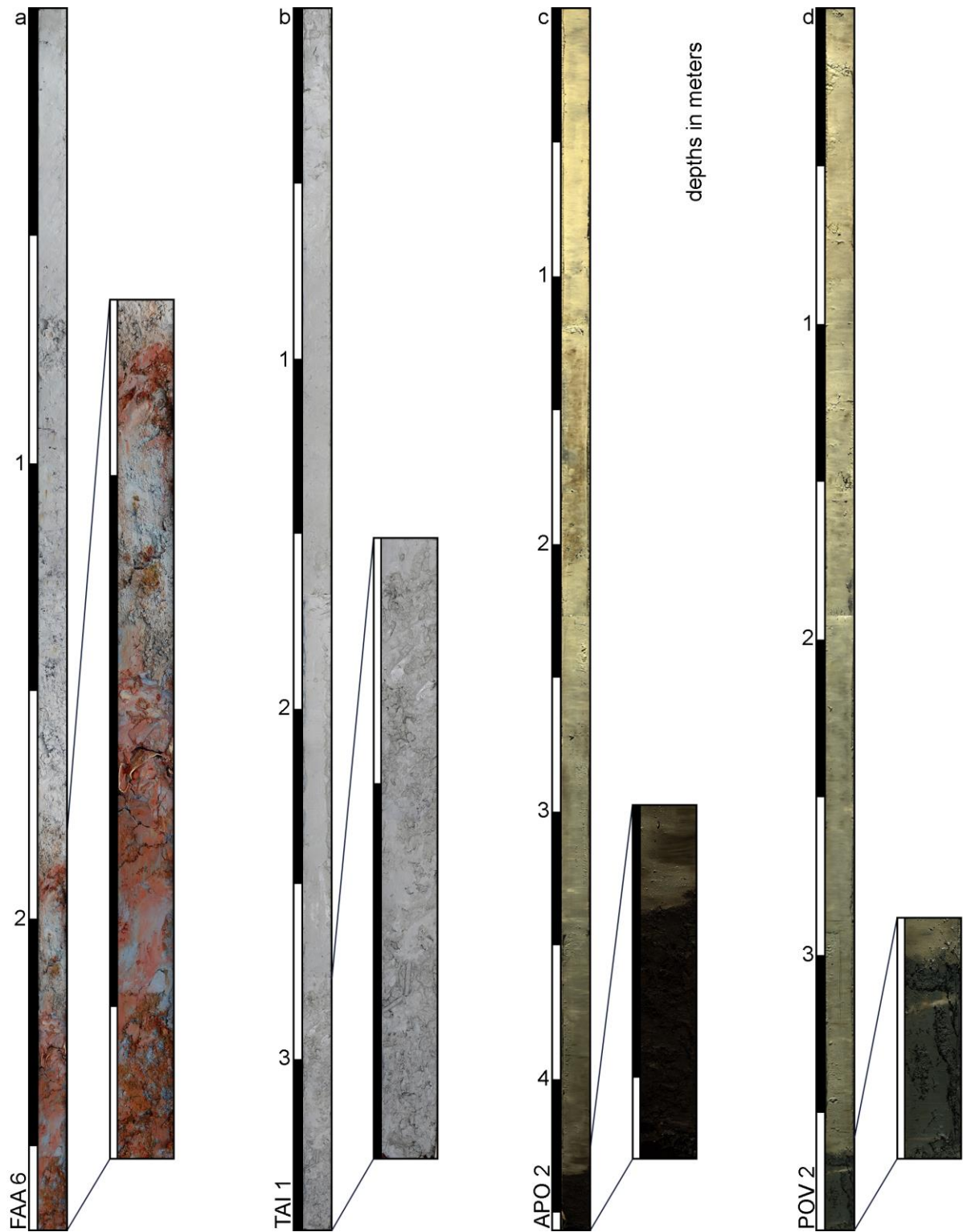


Fig. 4/4: Photos of selected vibrocores **a**) FAA 6 (proximal western lagoon), corebase showing rusty-red to blueish-gray soil; **b**) TAI 1 (northern lagoon), a serpulid-rudstone dominates the corebase; **c**) APO 2 (eastern lagoon), black peat is present at corebase; **d**) POV 2 (distal western lagoon), corebase comprises brown soil. Photos of cores FAA 6 and TAI 1 were taken using a Nikon camera, cores APO 2 and POV 2 were scanned using a GEOTEK Multi-Sensor Core Logger (MSCL)

Texture and sorting

In general, all sediment cores show upcore fining from packstones to wackestones to mudstones. However, vibrocore records reveal substantial trends in grain-size variability over the Holocene. For the development of a reliable indicator of sediment dynamics, we excluded the > 2 mm fraction, because it often consists of isolated, large serpulid tube fragments and mollusk shells.

The coarse-grained sediment fraction 2-0.25 mm displays upcore fining as well, except for cores CHA 1C, FAA 1B and FAA 6. Cores APO 2, POV 2 and TAI 1 show similar sedimentary pattern with grain-size peaks at 97.5-207.5 cm core depth (APO 2; fig. 4/5) and at 60-155 cm core depth (POV 2; fig. 4/6a). The sediment fraction 2-0.25 mm of core APO 3 shows a similar trend, but less clearly defined (within the interval of the standard deviation), probably due to the increased amount of coarse-grained sediment at the core base (fig. 4/6b). The coarse fraction of core CHA 1C decreases upcore to ca. 70 cm core depth (fig. 4/6c). A coarser-grained interval in core TAI 1 occurs from 20-120 cm core depth (fig. 4/6d). Grain size of core FAA 1B decreases steadily upcore without significant peaks (fig. 4/6e). Apparently, a shell layer between 69-80 cm core depth and a coarse-grained layer at ca. 102.5 cm core depth are present in core FAA 6 (fig. 4/6f). The shell layer mostly consists of shelly remains from mollusks, crustacean and serpulid tube fragments. The coarse-grained sediment fraction decreases upcore (fig. 4/6f). Detailed grain-size analysis of core APO 2 reveals an interval of increased amount of the clay-size fraction between 100-290 cm core depth (fig. 4/5). In core APO 2, the degree of sorting changes from moderately well sorted and moderately sorted sediments to poorly sorted sediments at the corebase to very well sorted sediment towards the core top. Sediments of core APO 3 are poorly to moderately well sorted at the corebase and well to very well sorted towards the coretop. Core CHA 1C consists predominantly of moderately to moderately well sorted sediments. Core POV 2 is poorly to moderately well sorted. From base to top, the sorting of core FAA 1B changes from poorly sorted to moderately sorted and well sorted. Sediments of core TAI 1 are moderately sorted to well sorted, except for poorly sorted sediments at the corebase. The sorting of FAA 6 starts with poorly sorted sediments at the base and changes to moderately sorted and well sorted sediments at the core top.

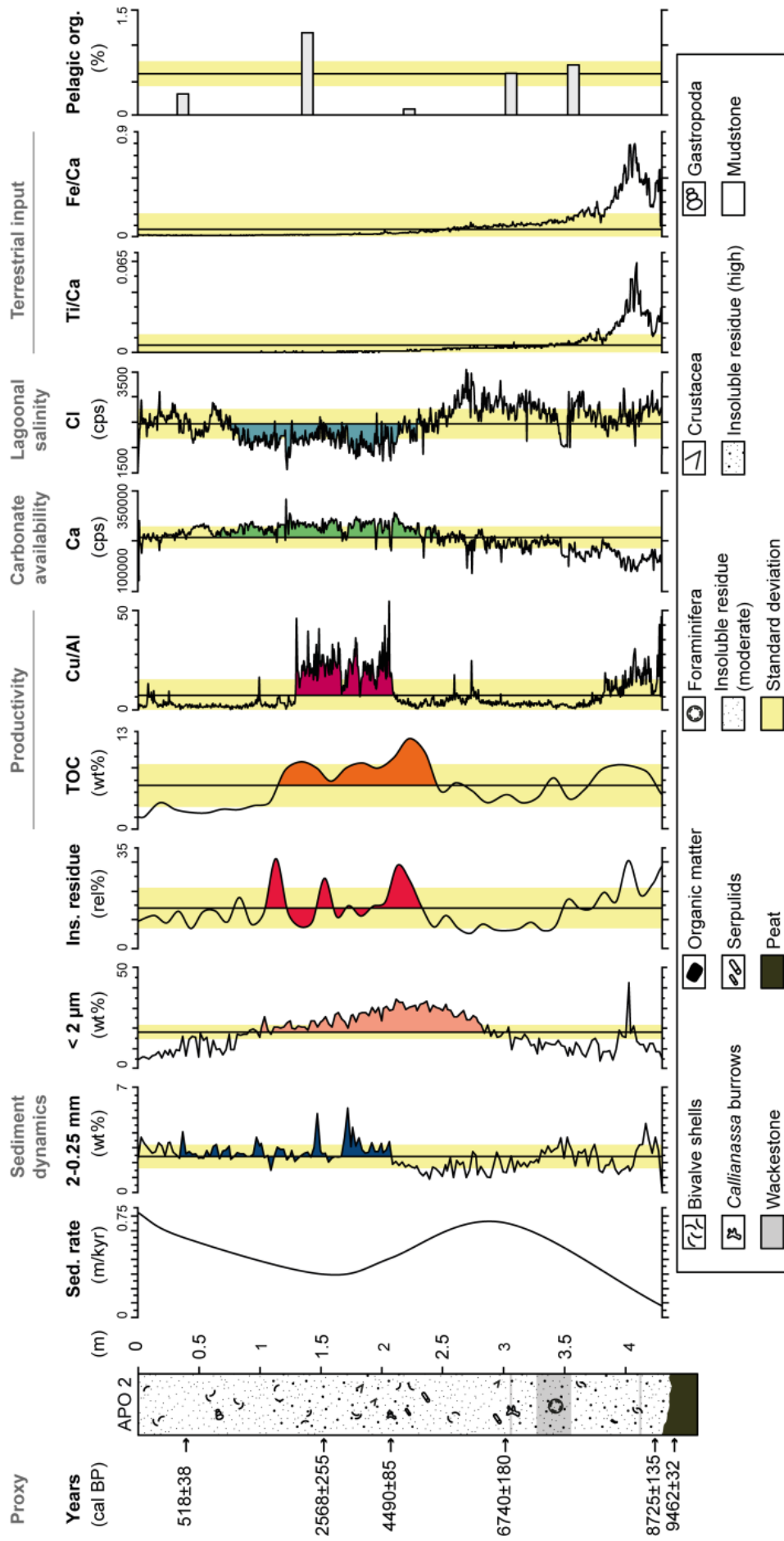


Fig. 4/5: Log, sedimentation rates and multi-proxy data set of core APO 2. Please note that XRF data are recorded in cps = counts per second or as element ratios and do not represent absolute values. Percentages of pelagic organism (planktonic foraminifera, pteropods) refer to the 0.25-0.125 mm sediment fraction. Ins. residue = insoluble residue, TOC = total organic carbon, org. = organism. Yellow bars are the standard deviation

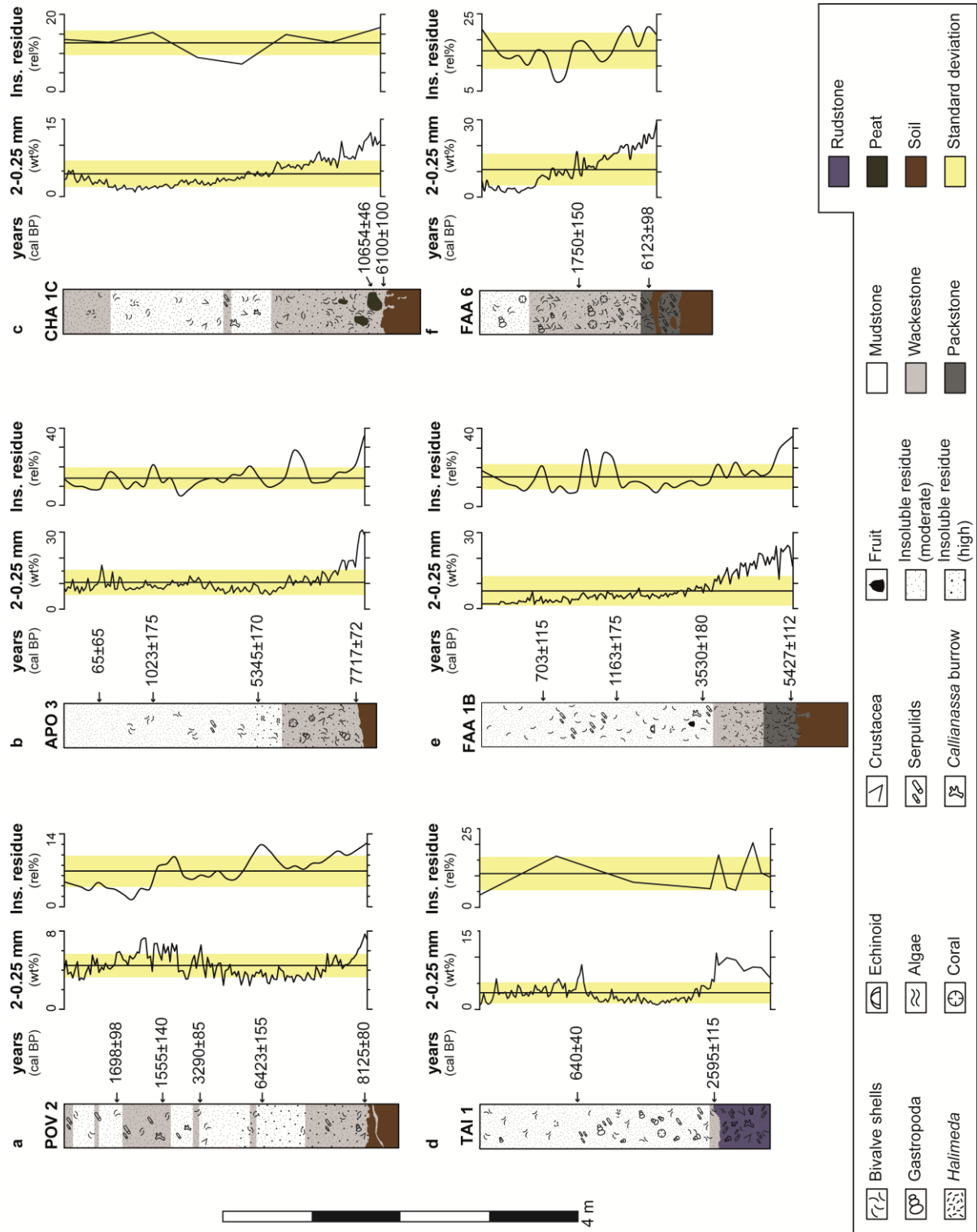


Fig. 4/6: Logs of vibrocores, coarse-grained sediment fraction (2-0.25 mm) and relative content of insoluble residue (ins. residue). a) POV 2, western lagoon; b) APO 3, eastern lagoon; c) CHA 1C, channel, western lagoon; d) TAI 1, northern lagoon; e) FAA 1B, western lagoon; f) FAA 6, proximal western lagoon. Yellow bars are the standard deviation

Mineralogy

Sediments are mainly composed of calcium carbonate and to a lesser degree of siliciclastic and organic material (insoluble residue) (suppl. tab. 4/1). In general, all cores show an upcore increase in carbonate content and a decrease in insoluble residue (figs. 4/5; 4/6). The amount of insoluble residue varies between 5.1-30.2% (mean 13.7%) in core APO 2; between 5.3-34.7% (mean 14.2%) in core APO 3; 7.2-16.2% (mean 12.7%) in core CHA 1C and between 7.1-34.2% (mean 15.3%) in core FAA 1B. The amount of insoluble residue fluctuates between 7.2-20.5 % (mean 14.6%) in core FAA 6; 1.3-12.1% (mean 6.8%) in core POV 2 and between 5.4-20.7% (mean 11.3%) in core TAI 1. In core APO 2, an increase in insoluble residue in the upper core sections between ca. 100-190 cm core depth can be observed (fig. 4/5).

Regarding carbonate phases, aragonite is most abundant in the sediments varying 84.6-89.2% on average (suppl. tab. 4/2). The average abundance of high-magnesium calcite measures 8.5-13.11% and low-magnesium calcite 2.1-2.9% (suppl. tab. 4/2).

Full-angle XRD analyses reveal relative proportions of mineralogical components. Soil is composed of goethite (54.9%), halloysite (28.3%), anatase (12.7%) and to a lesser degree of low-magnesium calcite (4.1%). In addition to the carbonate phases, basal sediment samples consist of goethite (0.6-1.6%), halloysite (1-1.2%), siderite (0.5-1.9%) and pyrite (0.8-0.9%).

4.4.2 Foraminifera

The most abundant foraminifera species in samples from core APO 2 are *Textularia agglutinans* (mean 43.4%), *Spiroloculina subimpressa* (mean 20.4%), *Textularia porrecta* (mean 8.4%) and *Textularia candeiana* (mean 4.8%) with only two exceptions (figs. 4/7; 4/8).

The sample at 270 cm core depth is characterized by *Elphidium excavatum* (20%), *Textularia agglutinans* (20%) and to lesser parts by *Spiroloculina subimpressa* (6.5%), *Operculina ammonoides* (6%), *Quinqueloculina agglutinans* (5%), *Quinqueloculina* sp.1 (6%) and other species (occurrence < 5%), and reflects a high diversity (fig. 4/7; 4/8). The samples from core POV 2 contain *Textularia agglutinans* (mean 21.3%), *Elphidium excavatum* (mean 19.5%), *Textularia pseudogramen* (mean 11%), *Textularia porrecta* (mean 9.7%), *Textularia candeiana* (mean 9.6%), *Textularia foliacea* (mean 5%), and *Spiroloculina subimpressa* (mean 7.8%) at 137.5 cm and 155 cm core depth (fig. 9; 8). The upper core sample consists predominantly of *Textularia agglutinans* (24.5%), *Elphidium excavatum* (22.5%), *Textularia candeiana* (11.5%) and *Textularia pseudogramen* (10%) with a decreased diversity (fig. 4/8; 4/9). Specimen of *Amphistegina* spp. and *Sorites* sp. were rarely

dispersed within the lagoon sediments (fig. 4/7). Both cores show a decreasing upcore trend in diversity (Shannon index; fig. 4/8; 4/9).

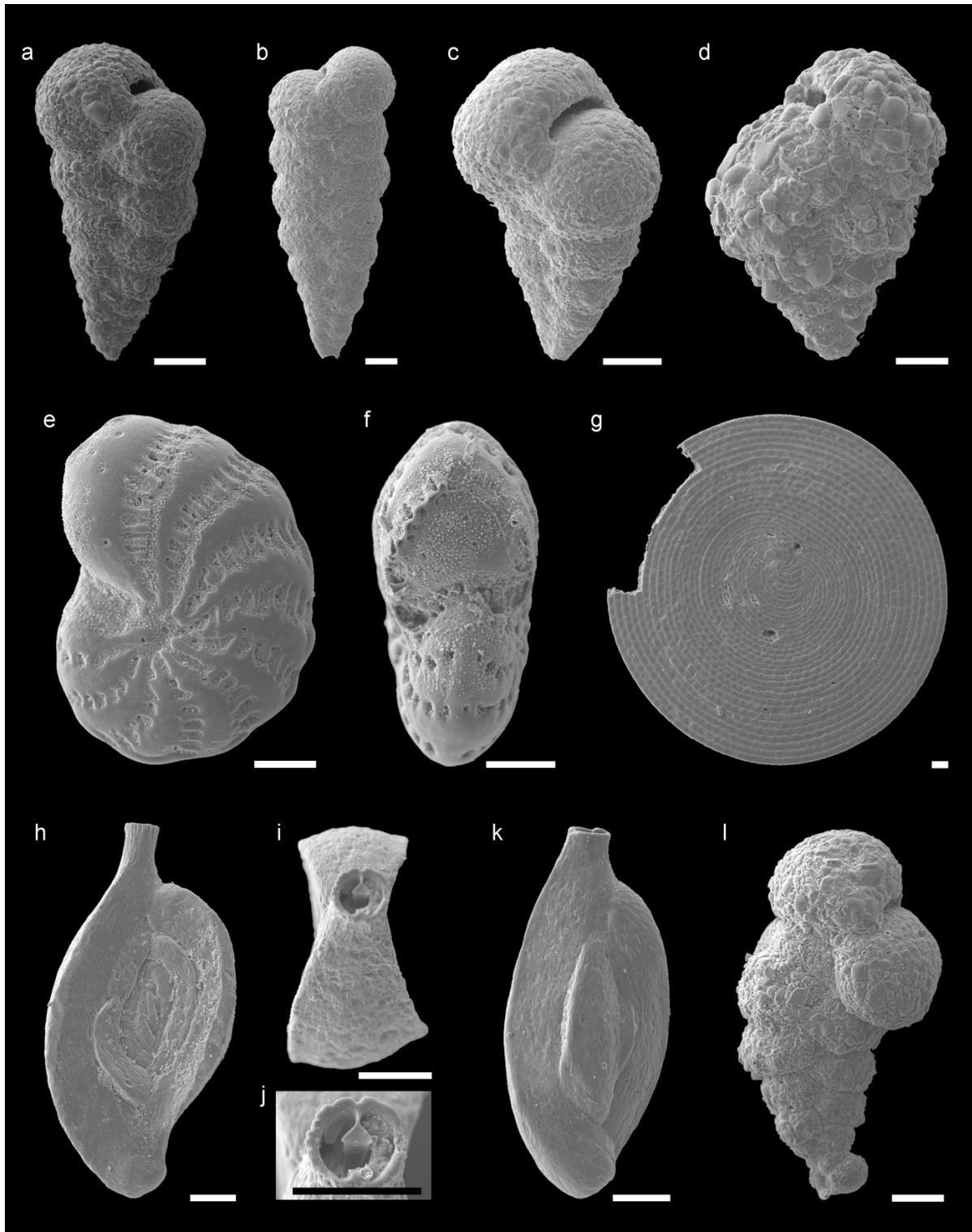


Fig. 4/7: Scanning Electron Microscope images of selected foraminifera taxa **a)** *Textularia agglutinans*; **b)** *Textularia porrecta*; **c)** *Textularia candeiana*; **d)** *Textularia foliacea*; **e)** *Elphidium excavatum*; **f)** *Elphidium excavatum*, apertural view; **g)** *Sorites* sp.; **h)** *Spiroloculina subimpressa*; **i)** *Spiroloculina subimpressa*, apertural view; **j)** *Spiroloculina subimpressa*, enlarged apertural view showing bifid teeth; **k)** *Quinqueloculina polyгона*; **l)** *Textularia* sp.; scale-bars are 100 μ m

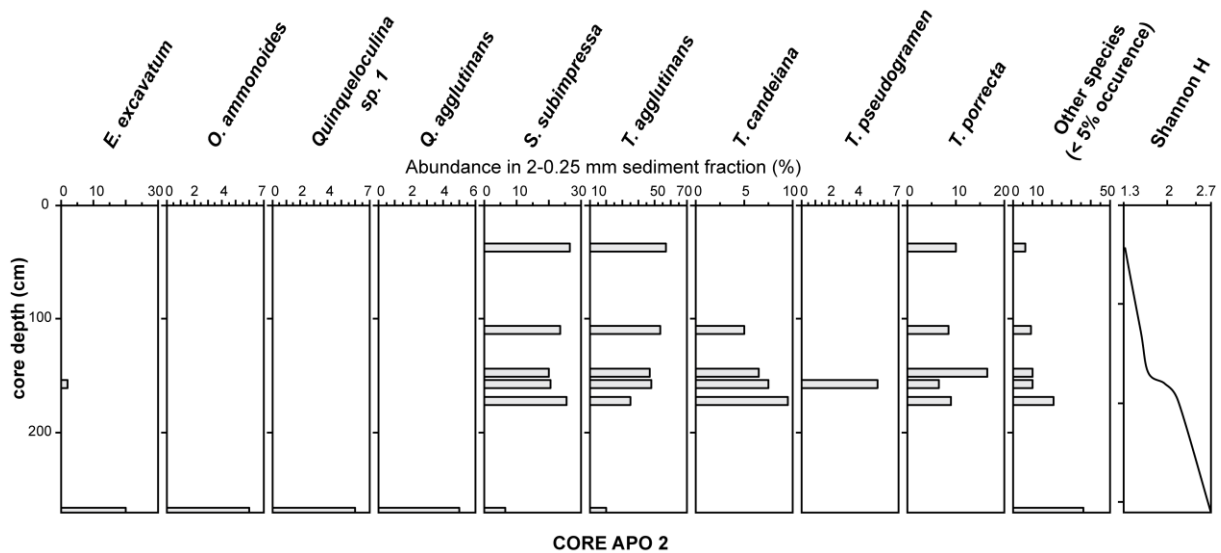


Fig. 4/8: Relative abundances of benthic foraminifera in the grain-size fraction 2-0.25 mm in **core APO 2**. Please note that each column has different scale

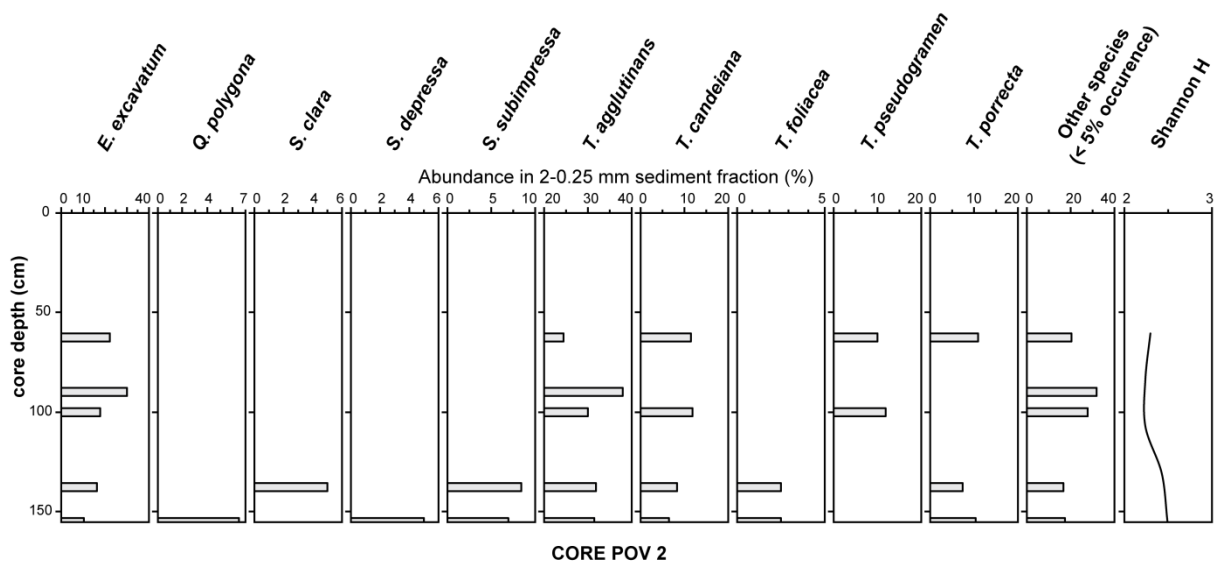


Fig. 4/9: Relative abundances of benthic foraminifera in the grain-size fraction 2-0.25 mm in **core POV 2**. Please note that each column has different scale

4.4.3 Multi-proxy data set of core APO 2

Because of the difficulty to convert qualitative XRF data to absolute concentrations without using quantitative geochemical analysis of bulk sediment (Löwemark et al., 2011; Weltje and Tjallingii, 2008); elemental intensities are reported in counts per second (cps). These data show relative variations of the elements instead of absolute concentrations and are influenced by matrix and dilution effects and changing properties of the sediment e.g., pore water, grain size, surface roughness (Gregory et al., 2015).

The highest Ti/Ca and Fe/Ca ratios occur at the corebase and decrease rapidly upcore without any appreciable peak (fig. 4/5). Although Fe can also be used as indicator for terrestrial sediment input, a compilation of Fe to other terrigenous indicators such as Ti is

useful, at least because of irons redox-sensitive behavior (Croudace and Rothwell, 2015; Haug et al., 2001). Ratios of Ti/Ca and Fe/Ca are generally used as proxy for variations in terrestrial sediment delivery (e.g., Gregory et al., 2015), probably induced by run-off and might assess changes in climatic conditions, such as the amount of precipitation and run-off (e.g., Haug et al., 2001).

Ca counts are lowest at the core base and are elevated during the interval of ca. 70-250 cm core depth (fig. 4/5). The lowest intensities of Ca occur at the corebase. Variations in Ca intensities can be used to illustrate variations in carbonate production (Croudace and Rothwell, 2015). Although calcium as CaCO_3 originates from skeletons of organisms (foraminifera, coccolithophorids, corals, algae, mollusks, etc.), lower Ca intensities may also correlate with carbonate dissolution and/or dilution by terrigenous material (Croudace and Rothwell, 2015) and might not necessarily be linked to lower carbonate production. In this study, XRF Ca intensities were thus used to indicate relative variations of carbonate availability.

XRF counts of Cl tend to increase from 430-270 cm core depth, and decrease between ca. 70-270 cm core depth (anti-correlation patterns with Ca counts). The use of Cl counts as indicator for salinity variability is not widely applied, however, variations in Cl intensity can be used as a proxy for relative variations in salinity (Kilian et al., 2013).

Total organic carbon (TOC) measured in core APO 2 (fig. 4/5) varies between 2-14.8%, with an average of 7.2%. Data show a generally decreasing trend upcore, except for an interval between 105-184 cm core depth where TOC values increase to an average of 11%. TOC values can be used as proxy for primary productivity (e.g., van Soelen et al., 2012).

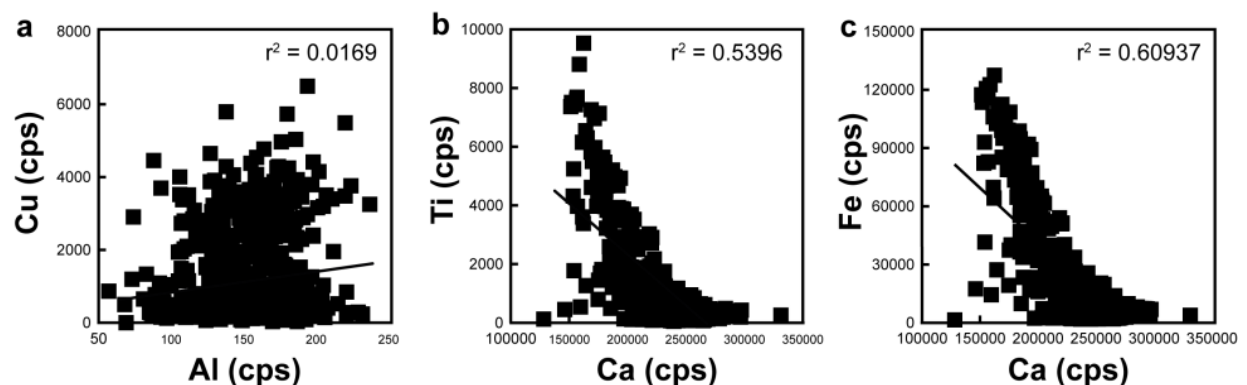


Fig. 4/10: Crossplots showing the correlation between elements a) Cu versus Al; b) Ti versus Ca; c) Fe versus Ca Intensities of Cu were normalized to Al as described by Böning et al. (2012). Lagoonal Cu/Al ratios exhibit a positive excursion during the mid-late Holocene and might be used as further indicator for terrestrial sediment delivery, based on the observation that the Cu/Al are also

high during times of elevated input of siliciclastic material in the early-Holocene (fig. 4/5). However, Cu generally tends to bind with organic matter (Böning et al., 2004; Sparrenbom et al., 2006) and Cu/Al ratios may also predict a marine source for the organic material, because Cu is also common in high amounts in marine plankton (Böning et al., 2004). Because of this issue, the interpretation of Cu/Al ratios should therefore be handled with care. Crossplots of element counts show correlations between Cu and Al with $r^2 = 0.016$ (fig. 4/10a); Ti and Ca with $r^2 = 0.539$ (fig. 4/10b) and Fe and Ca with $r^2 = 0.61$ (fig. 4/10c). For statistical analyses, uneven sample space of parameters Ca, Cu/Al, Ti/Ca, TOC of core APO 2 was interpolated to the insoluble residue and the 2-0.25 mm fraction curve using the software Analyseries (Paillard et al., 1996). Correlation analysis shows statistically significant correlations among the given parameters, which are shown in table 4/2.

A principle component analysis (PCA) was used to test the similarity between samples considering their sedimentary parameters. The early Holocene coarse-grained mixed carbonate-siliciclastic sediments at the corebase are separated from sediments of the transgression and from those of the mid-late Holocene (fig. 4/11). The PCA also shows that the latter sediments, which plot on the right hand side of the graph, can be separated into slumped and redeposited sediments of the mid-late Holocene and into carbonate-dominated sediments deposited during the past 1000 yrs (fig. 4/11).

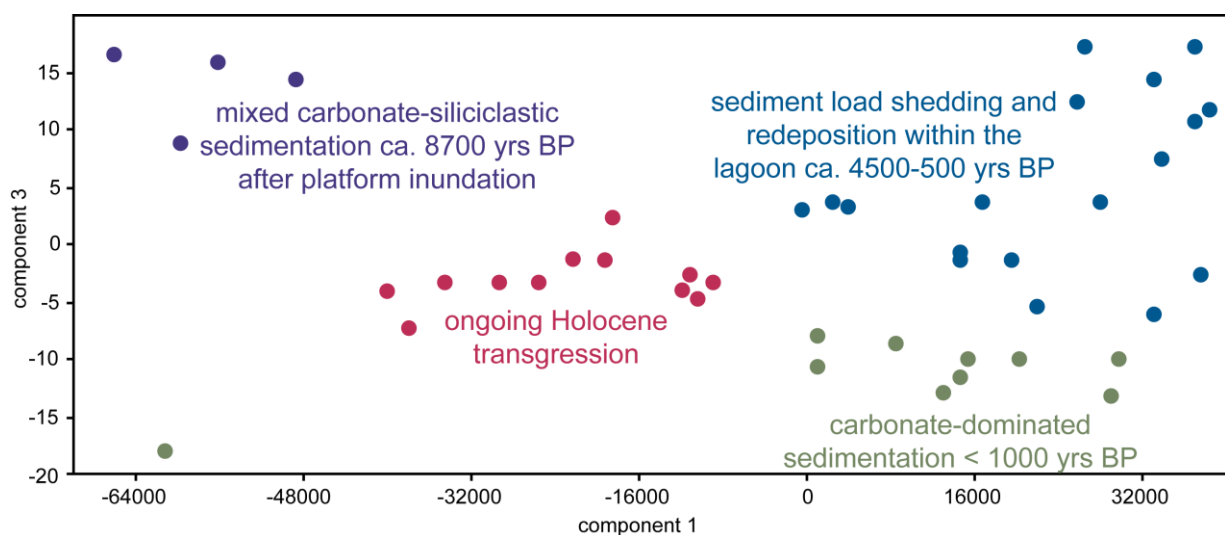


Fig. 4/11: Result of a principle component analysis (PCA) of sedimentological and geochemical data from core APO 2. Parameters used for PCA include grain-size, insoluble residue, total organic carbon and XRF data

4.4.4 Pelagic organisms

Planktonic foraminifera are generally rare in the 0.25-0.125 mm grain-size fraction. Pteropods are most abundant in the 0.25-0.125 mm grain-size fraction with 0.7% in 352.5 cm core depth, 0.6% in 302.5 cm core depth, 0.1% in 227.5 cm core depth and 0.3% in 32.5 cm core

depth (fig. 4/5). The highest amount of planktonic organism with 1.2% was reached in 147.5 cm core depth (fig. 4/5).

Table 4/2: Correlation matrix of core APO 2; ins. residue = insoluble residue. Please note that r-values are plotted in the lower left and p-values in the upper right corners. Statistically significant r-values ($p < 0.05$) are marked in bold

	2-0.25 mm (wt%)	< 2 μm (wt%)	Ins. residue (rel%)	TOC (wt%)	Cu/Al	Ca (cps)	Cl (cps)	Ti/Ca	Fe/Ca
2-0.25 mm (wt%)		0.143	0.747	0.542	0.016	0.099	0.001	0.777	0.454
< 2 μm (wt%)	-0.224		0.960	0.186	0.147	0.002	0.287	0.141	0.100
Ins. residue (rel%)	0.050	0.008		0.122	0.066	0.272	0.180	0.007	0.004
TOC (wt%)	0.095	0.203	0.236		0.000	0.357	0.797	0.025	0.011
Cu/Al	0.360	0.223	0.280	0.516		0.550	0.088	0.017	0.041
Ca (cps)	0.252	0.452	-0.169	-0.142	0.093		0.000	0.000	0.000
Cl (cps)	-0.499	-0.164	-0.206	-0.040	-0.260	-0.541		0.034	0.005
Ti/Ca	-0.044	-0.226	0.404	0.338	0.359	-0.715	0.321		0.000
Fe/Ca	-0.116	-0.251	0.430	0.379	0.310	-0.784	0.413	0.970	

4.4.5 Ages and sedimentation rates

The soils represent the oldest deposits within the lagoon and most likely formed during the late Pleistocene. Peat accumulated 9463 ± 33 yrs cal BP in core APO 2 in the eastern lagoon, and the chunks of peat in core CHA 1C are dated to $10,654 \pm 46$ yrs cal BP in the western lagoon (tab. 4/3). Lagoonal carbonate sedimentation started 8725 ± 135 to 7718 ± 73 yrs cal BP in the eastern lagoon; and 8125 ± 80 to 5428 ± 112 yrs cal BP in the western lagoon (tab. 4/3). Radiometric age data were used to generate age models for cores APO 2, APO 3, FAA 1B, POV 2 (fig. 4/12). The coarse-grained intervals have ages of 4490 ± 85 to 518 ± 38 yrs cal BP in APO 2 and 3290 ± 85 to 1698 ± 98 yrs cal BP in POV 2 (tab. 4/3). A coarse-grained layer at ca. 37.5 cm core depth in core APO 3 is dated to 65 ± 65 yrs cal BP (modern) (tab. 4/3). The rudstone-packstone transition in core TAI 1 has an age of 2595 ± 115 yrs cal BP (tab. 4/3). The base of the coarse-grained layer in core TAI 1 is dated to 650 ± 40 yrs cal BP (tab. 4/3). The coarse-grained layer at 102.5 cm core depth in FAA 6 was deposited 1750 ± 150 yrs BP (tab. 4/3).

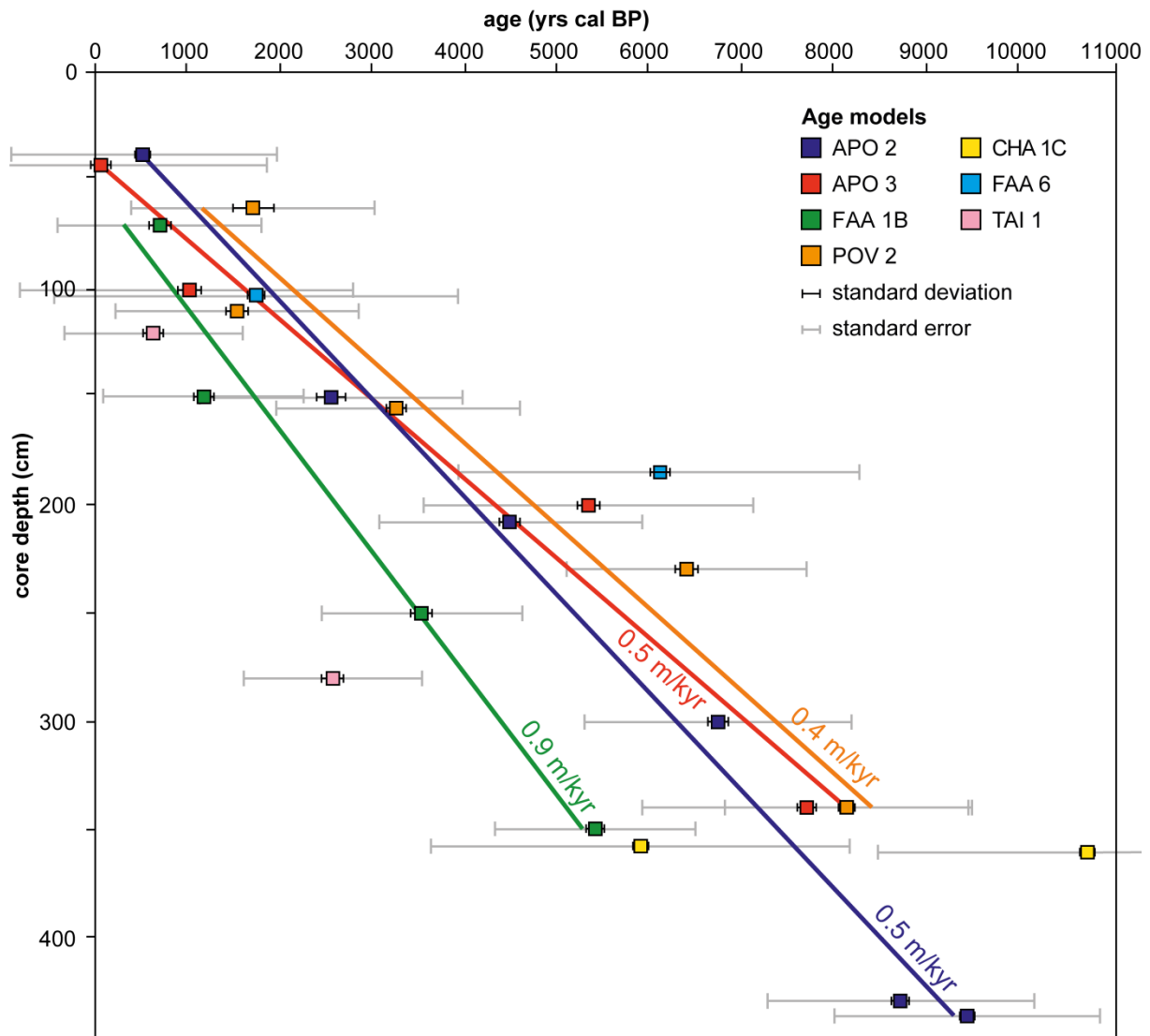


Fig. 4/12: Age models of cores APO 2, APO 3, FAA 1B and POV 2 including mean sedimentation rates based on (2-sigma) calibrated radiometric age data. Cores CHA 1C, FAA 6 and TAI 1 are excluded because only two age data are available for these cores

Calendar-calibrated radiocarbon ages and related sediment depth allow the calculation of sedimentation rates (tab. 4/3). From 9000-8000 yrs BP, carbonate sediments accumulated above peat very slowly at ca. 0.08 m/kyr (observed in core APO 2). From 8000-6500 yrs BP, sedimentation rates increased to 0.65 m/kyrs. Sedimentation rates vary between 0.24-0.78 m/kyrs from 6500-3000 yrs BP. From 3000-1000 kyrs BP, sedimentation rates average 0.31 m/kyrs. Maximum sedimentation rates of 0.55-1.74 m/kyrs were reached in subrecent sediments (1000-0 yrs BP).

Table 4/3: Accelerator mass spectrometry (AMS) ^{14}C ages of samples from seven cores reported by Beta Analytic Inc., Miami, Florida

Sample	Beta No.	Mean age (cal yrs BP)	Material	Sedimentation rate (m/kyr)
APO 2 37-38	416704	518 ± 38	mix of shell fragments	0.55
APO 2 149-151	404458	2568 ± 255	mix of shell fragments	0.30
APO 2 207-208	416705	4490 ± 85	mix of shell fragments	0.41
APO 2 299-301	404459	6740 ± 180	mix of shell fragments	0.65
APO 2 429-431	400239	8725 ± 135	mix of shell fragments	0.08
APO 2 436-437	400240	9463 ± 33	peat	
APO 3 42-43	416706	65 ± 65	mix of shell fragments	0.60
APO 3 99-101	404460	1023 ± 175	mix of shell fragments	0.28
APO 3 219-221	404461	5345 ± 170	mix of shell fragments	0.51
APO 3 339-341	393312	7718 ± 73	mix of shell fragments	
CHA 1 354.5-355.5	430910	6110 ± 100	mix of shell fragments	0.78
CHA 1 349.5-355.5	430909	10,654 ± 46	peat	
FAA 1B 69-71	404462	703 ± 115	mix of shell fragments	1.74
FAA 1B 149-151	404463	1163 ± 175	mix of shell fragments	0.42
FAA 1B 249-251	404464	3530 ± 180	mix of shell fragments	0.53
FAA 1B 349-351	393313	5428 ± 112	mix of shell fragments	
FAA 6 102-103	433866	1750 ± 150	mix of shell fragments	0.19
FAA 6 184.5-185.5	430911	6123 ± 98	mix of shell fragments	
POV 2 62-63	416707	1698 ± 98	mix of shell fragments	
POV 2 109-111	404465	1555 ± 140	mix of shell fragments	0.26
POV 2 154.5-155.5	416708	3290 ± 85	mix of shell fragments	0.24
POV 2 229-231	404466	6423 ± 155	mix of shell fragments	0.65
POV 2 339-341	400245	8125 ± 80	mix of shell fragments	
TAI 1 119.5-120.5	430912	650 ± 40	mix of shell fragments	0.81
TAI 1 277-278	430913	2595 ± 115	mix of shell fragments	

4.5 Discussion

4.5.1 Factors controlling lagoonal sediment transport

Hydrodynamic energy is one of the most important factors driving sediment entrainment under non-stormy conditions along back-reef areas (Harris et al., 2014a; Kench, 1998b; Kench and Brander, 2006). Back-reef lagoons represent the most distal areas from the wave-breaking zone of the reef crest and adjacent reef flat areas. A major part of the wave energy is dissipated on the reef crest during initial transformation processes and propagation across the reef flat (Harris et al., 2015). Wave energy rapidly slows down on the reef flat before reaching back-reef sand aprons. Less than 1% of fair weather waves are capable of sediment entrainment along the sand apron, so higher wave energy generated by storms and tsunamis

are necessary to cause geomorphological change and significant sediment transport in back-reef areas (Harris et al., 2015).

The effect of tsunamis

Tsunami waves are capable of mobilizing sediment of different grain-sizes including boulder, gravel or finer material depending on the source material available (e.g., Nandasena et al., 2013; Nott, 2003; Paris et al., 2010). So far, in carbonate settings, most of the studies are dealing with onshore tsunami deposits (e.g., May et al., 2016; Morton et al., 2007; Spiske and Jaffe, 2009). The potential of lagoon settings as site of tsunami deposition has been demonstrated by several studies. Jackson et al. (2014) found eight sandy tsunami layers (including the 2004 tsunami) in coastal lagoon cores from Karagan Lagoon, Sri Lanka, Indian Ocean. These coastal tsunami event layers contain offshore marine sediments as well as pelagic microfossils. In a mid-oceanic atoll lagoon of the Maldives, Indian Ocean, Klostermann et al. (2014) interpreted six event layers to be deposited by tsunamis based on grain-size variability and the occurrence of typical reefal organisms such as corals, coralline algae and foraminifera within deep lagoon sediments. Both study areas are rarely influenced by tropical storms, because of their very close position to the equator, which only leaves tsunamis as trigger for event deposition. Because of the central position in the South Pacific, the area of French Polynesia is strongly exposed to far-field tsunamis, and therefore tsunamis as trigger for sediment redeposition cannot entirely be ruled out (Sladen et al., 2007). However, sedimentary features unequivocally identifying tsunami deposits (e.g., single sand beds fining both upward and landward, with few layers, and rip-up clasts; forming wide, thin drapes), either deposited onshore or offshore, are largely lacking in general (e.g., Bahlburg and Spiske, 2012; and references therein).

The influence of tropical cyclones

A globally distributed data set from Holocene cyclone reconstructions from the Indian, Atlantic and Pacific Oceans for the past 5000 years suggests spatial and temporal variation of elevated tropical storm activity (Nott and Forsyth, 2012). Toomey et al. (2013) used the comprehensive data set compiled by Pirazzoli and Montaggioni (1988; and references within) for the correlation of dated reef blocks and coral conglomerate on reef flats of carbonate platforms in French Polynesia with peaks of coarse-grained sediments from the barrier-reef lagoon of Tahaa. According to Toomey et al. (2013), coarse-grained deposits represent overwash deposits that preferentially formed 5000-3800 and 2900-500 yrs BP when storm waves and storm surges frequently flushed the reef crest and moved coarser-grained reef-

derived material into the fine-grained low-energy back-reef setting. However, in this study, (carbonate-)sediment composition or input of terrestrial material from the volcanic hinterland was not considered, which may also accumulate within the lagoon. Based on grain-size variations, Toomey et al. (2013) concluded that the sediment fraction 2-0.25 mm represent a viable proxy of cyclone overwash events.

Due to the fact that the barrier-reef complex has a high-relief central volcanic island representing a further sediment source, we suggest that terrestrial sediment supply triggered by precipitation during storm landfall should be enhanced and leave a significant signal within the lagoonal sediments as well. In Bora Bora, however, proportions of siliciclastic material expressed by the Ti/Ca and Fe/Ca ratios within mixed carbonate-siliciclastic sediments did not correlate with peaks of coarse-grain fractions in the cores investigated (fig. 4/13). From a sedimentological point of view, peaks within the 2-0.25 mm sediment fraction still belong to the wackestone and mudstone facies and do not necessarily represent “high-energy layers” as postulated by Toomey et al. (2013; p. 186). Also, tropical storm pathways do not always cover entire lagoons so it is rather difficult to detect every storm that passed the region. So it is not surprising that the effects of storms and storm damage on coral reefs and carbonate platforms can be extremely patchy (Fabricius et al., 2008; Harmelin-Vivien, 1994).

Tropical storms passing a carbonate platform not only move sediment from the margin to the interior but they are also able to redeposit sediments within the lagoon. An indication for sediment redeposition could be the age reversals found in cores CHA 1C and POV 2 from the western lagoon (fig. 4/6a, c). Nevertheless, this could alternatively result from active bioturbation in the upper part of core POV 2 (fig. 4/6a) and in the lower part of core CHA 1C (fig. 4/6c). Time-averaging effects due to bioturbation can be a common feature in lagoonal environments (Tudhope and Scoffin, 1984). A more reliable evidence for event (re-) deposition might be given by a shell layer in core FAA 6 from the western lagoon (fig. 4/6f). This interval is characterized by a shift of the insoluble residue curve towards more carbonate content (fig. 4/6f). However, the shell layer accumulated within wackestones and shows no significant variation in grain-size.

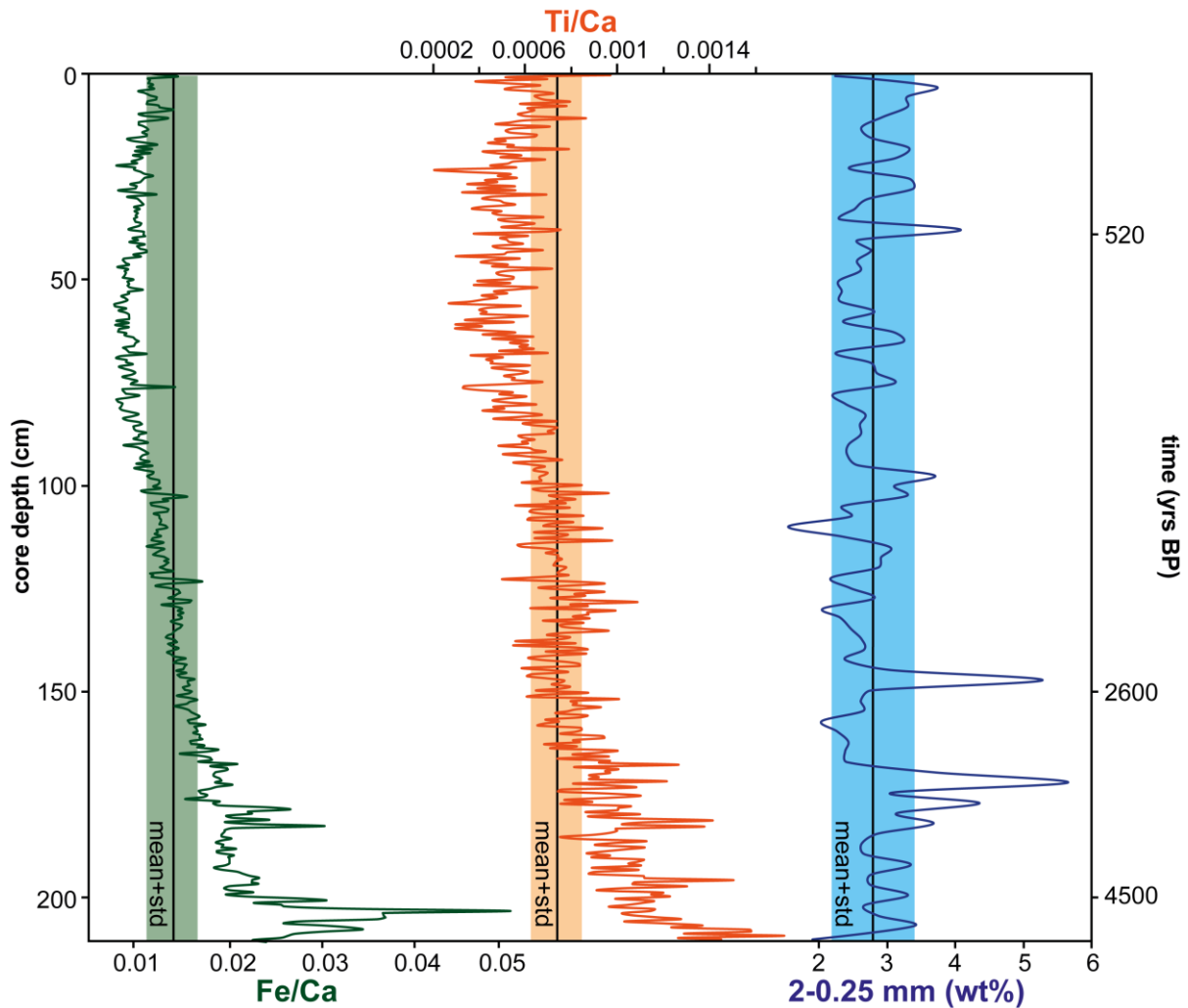


Fig. 4/13: Coarse-grained sediment fraction (2-0.25 mm), Ti/Ca ratios and Fe/Ca ratios of core APO 2 plotted against core depth the past 4500 yrs

Occurrence, distribution and taphonomy of foraminifera and coralline algae can be useful tools for the reconstruction of sediment transport and the identification of possible overwash deposits (e.g., Klostermann et al., 2014; Pilarczyk et al., 2014; Wizemann et al., 2015). Because of the difficulty to disentangle reef-derived (allochthonous) material from sediment produced *in situ* (autochthonous) in the lagoon, faunal composition of foraminifera were consulted to find further evidence for event (re-)deposition than only grain-size variability. The occurrence of reef-associated foraminifera within the lagoonal sediment fraction 2-0.25 mm is supposed to maintain event (re-)deposition of sediments from the reef flat into the lagoon, hypothetically swept in during storms. Typical tracers are e.g., *Calcarina* sp., *Amphistegina* spp. (Fujita et al., 2009; Klostermann et al., 2014) and *Homotrema rubra* (Pilarczyk et al., 2014). In the lagoonal sediments of Bora Bora, the most abundant foraminifera taxa are textularids. The western lagoon is characterized by *Textularia agglutinans* and *Elphidium excavatum*; in the eastern lagoon *Textularia agglutinans* and *Spiroloculina subimpressa* predominate. Various species of *Textularia* are typical for

lagoonal fauna (J. Parker, personal communication; Parker and Gischler, 2011; Storz et al., 2014; Venec-Peyre, 1991). Typical foraminifera living at the reef crest were nearly absent in the lagoonal sediments, only few specimens of *Sorites* sp. and *Amphistegina* spp. were identified. These taxa usually live at or close to the reef crest, whereas *Sorites* sp. can also occur in deeper lagoonal environments (Debenay, 2012). However, their abundance was still statistically insignificant. Bora Bora is supposed to represent a type of reef system, where foraminifera specimens are apparently rarely dispersed on the reef flat, beach and sand aprons for hitherto unknown reasons (Gischler, 2011). Nevertheless, Gischler et al. (2016) found *Homotrema rubra* and *Carpentaria* sp. commonly encrusting the coralgal barrier reef sections. The abundance of *Homotrema* fragments in lagoonal sediments of Wallis (Uvea), western Pacific, is reported to be very low and specimens to be small in size and poorly preserved (Pilarczyk et al., 2014). They likely represent fragments transported into the lagoon during fair weather conditions. Overwash deposits are expected to comprise high concentrations of *Homotrema* specimens, which are larger and better preserved than fragments derived from surrounding sediment (Pilarczyk et al., 2014; Pilarczyk and Reinhardt, 2012).

Intense rainfall events related to cyclone landfalls are able to enhance weathering and transport processes and increase the amount of terrestrial sediments in lagoonal environments (e.g., Peros et al., 2015). However, lagoonal Ti/Ca and Fe/Ca ratios do not support variations in run-off as a response to increased precipitation during storms during the past 5000 years (fig. 4/13). An explanation could be the absence of permanent watercourses draining the volcanic island and hence, limit siliciclastic input from the hinterland (Gischler, 2011). Fringing reefs surrounding the volcanic island (fig. 4/2a) might act as natural barriers and could hamper terrigenous input into the deep lagoon. The fringing reefs developed contemporaneously to the barrier reef (Gischler et al., 2016) and started growing at the same time as the beginning of lagoonal carbonate sedimentation ca. 8700 yrs BP. Measurements of carbonate contents show that fringing reef samples almost consists of 100% carbonate (Gischler et al., 2016), which would speak against this interpretation, however, surficial sediments from the coastal area show a light brownish-gray color typical for siliciclastic-rich sediments (fig. 4/3a) and do comprise ca. 20% of siliciclastic material (Gischler, 2011). The increase in Cu/Al ratios during the mid-late Holocene (fig. 4/5) could alternatively be explained by enhanced erosion of siliciclastic material and transport into the lagoon during times of elevated storm activity and rainfall events. However, this is unlikely, because the

Ca/Al do not show a strong correlation with the Ti/Ca and Fe/Ca ratios, the other proxies of terrestrial input.

Titanium is commonly used as an indicator for erosion, and was interpreted to reflect reduced precipitation and the onset of gradually drier climatic conditions during the mid-late Holocene (Haug et al., 2001). Likewise, in Bora Bora, the Ti/Ca ratio decreases upcore and suggests a reduction in run-off and precipitation. This also largely excludes storms as a trigger for enhanced coarser-grained sediment transport into the lagoon during the mid-late Holocene. In general, warmer and wetter climatic conditions fuel tropical storm generation (Emanuel, 1991). An alternative explanation is given by Gregory et al. (2015), who interpreted decreasing trends in Ti counts and Ti/Ca ratios in coastal lagoon cores from Cuba, Caribbean Sea, over the past 4000 yrs to represent changes in lagoonal geomorphology or dilution of Ti by marine overwash sediments. However, the gradual upcore decrease of the Ti/Ca ratio in the Bora Bora lagoon cores does not fit in this model.

Sea-level and climate

Toomey et al. (2013) assumed that higher sea level could be responsible for increased advection of silt- and clay-sized particles in the suspended sediments of the Tahaa lagoon. Accordingly, an increase in the clay-sized fraction ($< 2 \mu\text{m}$) in the Bora Bora lagoon cores might be associated with the mid-Holocene sea-level highstand, which forced enhanced hydrological activity and a relatively open hydrodynamic system. Flushing of oceanic seawater into the inner platform would have diluted lagoonal salinity due to the fact that salinity of the open ocean water is lower as compared to the salinity of the inner platform and is consistent with decreased Cl intensities in lagoon cores. Another consequence would be the presence or an increase of pelagic organism within lagoonal sediments, respectively (fig. 4/5). On the other hand, a decrease in Cl intensities in lagoonal environments can also be a consequence of lowered salinity by torrential rainfall (e.g., Fabricius et al., 2008; Madin and Connolly, 2006) as a direct effect of storm activity (Madin, 2011) or by more rain due to a wetter climate. On the one hand, hydrodynamic activity can stimulate primary productivity by stirring up deeper and nutrient-rich waters (Babin et al., 2004; van Soelen et al., 2012). An increase in wind-derived terrestrial material accumulating into the lagoon during the mid-late Holocene could on the other hand deliver nutrients needed for (enhanced) primary productivity and might be reflected in an increase of Cu/Al ratios. Altogether, tropical storms may play a role for sporadic sediment transport and they cannot be excluded as factor controlling sediment dynamics. However, the lagoonal records show that there must be a

more constant, overriding mechanism leading to these kinds of sedimentation patterns and geochemical signals, for example the climatic shift towards more sustained and higher hydrodynamic energy conditions and a higher sea level.

Holocene climate has been highly variable and multiple factors controlled these variations with orbital and, to a lesser extent, solar forcing playing the central role during the last 11,500 yrs (Mayewski et al., 2004). A change in tropical storm frequency is controlled by changes in climate (e.g., Walsh et al., 2016). Several studies have shown that the early-Holocene was warmer and wetter than the mid-late Holocene in the tropical western Atlantic Ocean (e.g., Haug et al., 2001). The occurrence of a Holocene Climate Optimum or Thermal Maximum in the tropical Pacific is not unambiguous. For example, oxygen isotope and Sr/Ca ratios of corals from the barrier reef offshore Tahiti (IODP Expedition 310) showed that temperatures averaged 24.3 °C around 9500 yrs BP, i.e., 3.2 °C cooler than today (DeLong et al., 2010). Gagan et al. (1998) postulated warmer sea surface temperatures (SSTs) 5300 yrs BP as compared to today in the Great Barrier Reef based on oxygen isotope and Sr/Ca ratios of corals. Comparison of fossil and modern coral Sr/Ca and Ba/Ca ratios from New Caledonia also reveal SSTs to be at least 1 °C higher around 6000 yrs BP than today (Montaggioni et al., 2006). Foraminiferal Mg/Ca data from the western equatorial Pacific show a lowering trend in SSTs during the past 10,000 yrs but oxygen isotopes indicate a decrease in salinity over the same time interval (Stott et al., 2004). A global climate data set compiled by Marcott et al. (2013) clearly suggests the existence of a Holocene Climate Optimum, which is followed by a cooling trend through the mid-late Holocene. However, Marcott et al. (2013) have included data from the eastern and western Pacific margins including Galapagos, but not from the south Pacific region.

The variability of climatic features such as the El Niño Southern Oscillation (ENSO) activity can be to a large part related to changes in insolation (Clement et al., 2000). For the Caribbean region, Donnelly and Woodruff (2007) claimed that hurricane frequency was influenced by variability in ENSO over the past 5000 yrs. Times with frequent and strong ENSO apparently corresponded to intervals with fewer intense cyclones, and vice versa. Holocene ENSO variability is controversially discussed, but a general trend towards an increase in frequency and amplitude during the past several thousand years has been favored by some authors (Conroy et al., 2008; Gagan et al., 2004). Cobb et al. (2013) found that ENSO has been highly variable during the past 7000 yrs with no systematic trend in its variability. A stronger ENSO system in the mid-late Holocene would result in a decrease in tropical storm activity following Donnelly and Woodruff (2007), which on the other hand

would largely exclude storms as a trigger for sediment redeposition in the mid-late Holocene.

An alternative mechanism influencing the stability of the hydrodynamic system towards constantly higher wave energy could be more permanent southeast trade winds and strengthening of the Walker circulation such as during the mid-Holocene in the eastern tropical Pacific (Koutavas et al., 2006; Salvattecchi et al., 2016, 2014). The mid-Holocene represents a time with ice volume and greenhouse gas concentrations similar to today, but due to the precession of the equinoxes, seasonal and latitudinal distribution of solar radiation were different to today and the early Holocene (Braconnot et al., 2012). Seasonality was enhanced (reduced) compared to today and reduced (enhanced) compared to the early Holocene in the northern (southern) hemisphere (Emile-Geay et al., 2016). This pattern of mid-Holocene climatic conditions is presumably linked to an attenuated ENSO and a northwards-displaced position of the intertropical convergence zone (Fleitmann et al., 2003; Haug et al., 2001; Mollier-Vogel et al., 2013). Still, other studies concluded that ENSO remained active during the mid-Holocene (Cobb et al., 2013; Karamperidou et al., 2015). It has to be kept in mind that knowledge of ENSO history is limited in general and especially in the central tropical Pacific, and its relation to climate variability is disputed and in parts controversial (Emile-Geay et al., 2015; Cobb et al., 2013; Conroy et al., 2010).

Environmental and morphological mechanisms driving long-term sedimentation in the lagoon

Geomorphological changes and variations in sea level can influence sedimentation patterns. Elongated reef islands (motus) can act as natural barriers for sediment transport from marginal reefs into inner lagoons (Gischler, 2011). An important trigger for reef island formation in the central Pacific Ocean was the sea-level fall following the mid-late Holocene highstand (Dickinson, 2009, 2003). According to Kench et al. (2014), the mid-late Holocene sea-level highstand was accompanied by the formation of motus starting ca. 4800-4000 yrs BP in the central Pacific Ocean.

In Bora Bora, motus are developed on the northeastern and eastern side of the volcanic island (fig. 4/3c) where they reduce sediment transport from the marginal reef area resulting in narrower and deeper sand aprons (Gischler, 2011). However, core APO 2 from the eastern lagoon shows an increase in coarser-grained sediments since 4500 yrs and elevated sedimentation rates during the past ca. 2500 yrs. Cores APO 3, POV 2 and TAI 1 show an increase in sedimentation rates after 1000-2000 yrs BP. A possible mechanism could be rapid sediment transport from back-reef areas and reef islands during storms resulting in poorly

sorted sediments (Kalbfleisch and Jones, 1998). However, the degree of sorting changes from very well-sorted and well-sorted sediments towards moderately well-sorted and moderately-sorted sediments during this period and speaks against the model. Nonetheless, it should be kept in mind that the mechanical breakdown of carbonate components (Sorby principle) limits the environmental significance of textural analyses including the degree of sorting (Scoffin, 1992) and shows the need of a broad and comparative data set.

The supply of carbonate sediment, which can be transported into the lagoon, depends on carbonate production at the reef margin and to a lesser extent on sand aprons (e.g., Kench, 2011). At present, sand aprons in Bora Bora are widest in the south and southeast (fig. 4/3d) probably due to the exposed position to hydrodynamic forces. On the eastern and northeastern side, sand aprons extent is restricted because extensive motus have developed during the last few thousand years, separating sand aprons from the reef margin. In general, lagoonal infill by sand-apron progradation is considered to be more important than lagoonal background sedimentation (e.g., Klostermann and Gischler, 2015; Purdy and Gischler, 2005). Beside the hydrodynamic regime, which controls the spatial evolution of sand apron geomorphology (Harris et al., 2014a, 2011), sand apron formation is driven to a large part by antecedent topography and platform size (Isaack and Gischler, 2015). The interplay of antecedent topography and sea-level rise determines variations in accommodation space and geomorphological changes and is therefore crucial for lagoonal sedimentation processes. During the mid-late Holocene, the depositional style of sand aprons has changed from aggradation to progradation because of reduced accommodation space (Purdy and Gischler, 2005), i.e., due to the stagnation and slight fall in sea level ca. 6000-1000 yrs BP in Bora Bora (Gischler et al., 2016; Rashid et al., 2014).

Recently, Harris et al. (2014b) postulated that rapid sand-apron accretion in the southern Great Barrier Reef occurred between 6000-3000 yrs BP; followed by decreased sedimentation rates from 3000 yrs to present and a cessation of sand-apron accretion and turn-off of carbonate production during the last 2000 yrs. Lagoonal sedimentation rates of Bora Bora slightly decreased during 6700-4500 yrs BP from 0.65 m/kyr to 0.51 m/kyrs on average and increased again after 3000 yrs BP in cores located between the volcanic island and the sand apron. The pattern of the coarse-grained sedimentation found in five cores indicates an interval of intense sediment dynamics during ca. 4500-500 kyrs BP. Based on the model of Harris et al. (2014b), we assume that intensified sediment dynamics in the mid-late Holocene could be an expression of sediment load shedding of sand aprons and slumping due to gravity processes initiated by higher shear stress at sand apron/lagoon edges. Sediment load shedding

is initiated by oversteepening of sand apron slopes. The maximum loading of sand aprons was reached during progradation when sea level stagnated and dropped down to modern level. Although gravity flows are supposed to result in sand lobes or sand ridges accumulating at the toe of the slope and thinning out lagoonwards, this process is also capable to disperse, suspend and redeposit coarser-grained sediments within the center of the lagoon. The central position of most of our sediment cores within the lagoon between the main volcanic island and sand aprons confirms this statement. The redeposition associated with sand-apron slumping can be detected and dated in cores within the eastern lagoon to ca. 4490 ± 85 yrs cal BP, in the western lagoon to ca. 3290 ± 85 yrs cal BP, and on the northern side to < 1000 yrs BP (fig. 4/6). It is assumed that the exposition to southeasterly trade winds and higher-than-present sea level amplified progradation and sediment redeposition. The cores CHA 1C and FAA 1B have on the one hand an exposed position close to the channel with an open ocean connection, but are on the other hand protected from the southeasterly trades. Therefore, these cores are less impacted by slumping-induced redeposition. Also, the very proximal position to the volcanic island of core FAA 6 attenuates the detection of lagoonal infill pattern by sand-apron slumping. The sedimentary pattern of this core is rather an expression of sediment shedding from adjacent fringing and patch reefs.

Our new model of sand apron load shedding into the lagoon is consistent with trends observed in sedimentary patterns of the coarse-grained sediment fraction (2-0.25 mm) of cores located nearby sand aprons such as APO 2, APO 3 (eastern lagoon), POV 2 (western lagoon) and TAI 1 (northern lagoon). The model provides an alternative mechanism driving coarse-grained sediment transport into back-reef lagoons including the role of sea-level change and lagoonward progradation of sand aprons during the mid-late Holocene. Higher and sustained hydrodynamic energy was presumably induced by stronger trade winds and a higher sea level during this time interval.

4.5.2 Holocene evolution of the mixed carbonate-siliciclastic system

Holocene development of the barrier-reef lagoon can be divided into different sedimentological substages (fig. 4/11): (1) Sediment dynamics ca. 8700 yrs BP was determined mainly by the supply of terrestrial material from the volcanic island and lagoonal carbonate production. (2) During ongoing Holocene transgression in the early-mid Holocene, sedimentation was largely characterized by lagoonal carbonate production and reef-derived material. Sand aprons formed because of lagoonward movement of coarse reef-derived material and allowed the fine material (mud) to accumulate within the lagoon diluting the

siliciclastic components to carbonate-dominated sediments. (3) Sediment load shedding of sand aprons into the lagoon during ongoing progradation led to increased sediment dynamics during the mid-late Holocene except for proximal areas and areas with open ocean connection on the western lagoon side. The strengthening of the hydrodynamic system as well as a higher-than-present sea level and subsequent fall to modern level forced sand-apron progradation. (4) When modern conditions were reached, lagoonal infill continued with fine-grained carbonate-dominated material produced both within the lagoon and on the reef crest and with only very minor terrestrial input.

Lowstand Systems Tract (LST)

The subaerial exposure of the barrier reef and lagoon during the Lowstand Systems Tract (LST) before ca. 10,650 yrs BP allowed the accumulation of dark brown to brown-reddish loamy soil on the karstified Pleistocene reef limestone within the lagoon (fig. 4/14a). Terrestrial material such as goethite is the result of extensive weathering of volcanoclastic rocks and lagoonward transport from the volcanic hinterland. Age data of the soil in Bora Bora is not available. In the Mayotte lagoon, for comparison, soils terminate ca. 12,000 yrs BP in the deep lagoon and ca. 9700 yrs in proximal platform areas (Zinke et al., 2005).

Transgressive Systems Tract (TST)

The rising Holocene sea inundated the carbonate platform ca. 10,650 yrs ago as seen in the oldest peat data. The barrier reef started growing shortly afterwards with average accretion rates of 6.15 m/kyrs during the Holocene (Gischler et al., 2016). The early Transgressive Systems Tract (TST) is characterized by mangroves flourishing in pre-lagoonal brackish swamps and peat deposited locally within the deepest parts of the lagoon (fig. 4/14b). Kuhn (1984) explained local differences in peat deposits in the lagoon of Bermuda, northwestern Atlantic, with Pleistocene antecedent topography. He found peat deposition to take place in

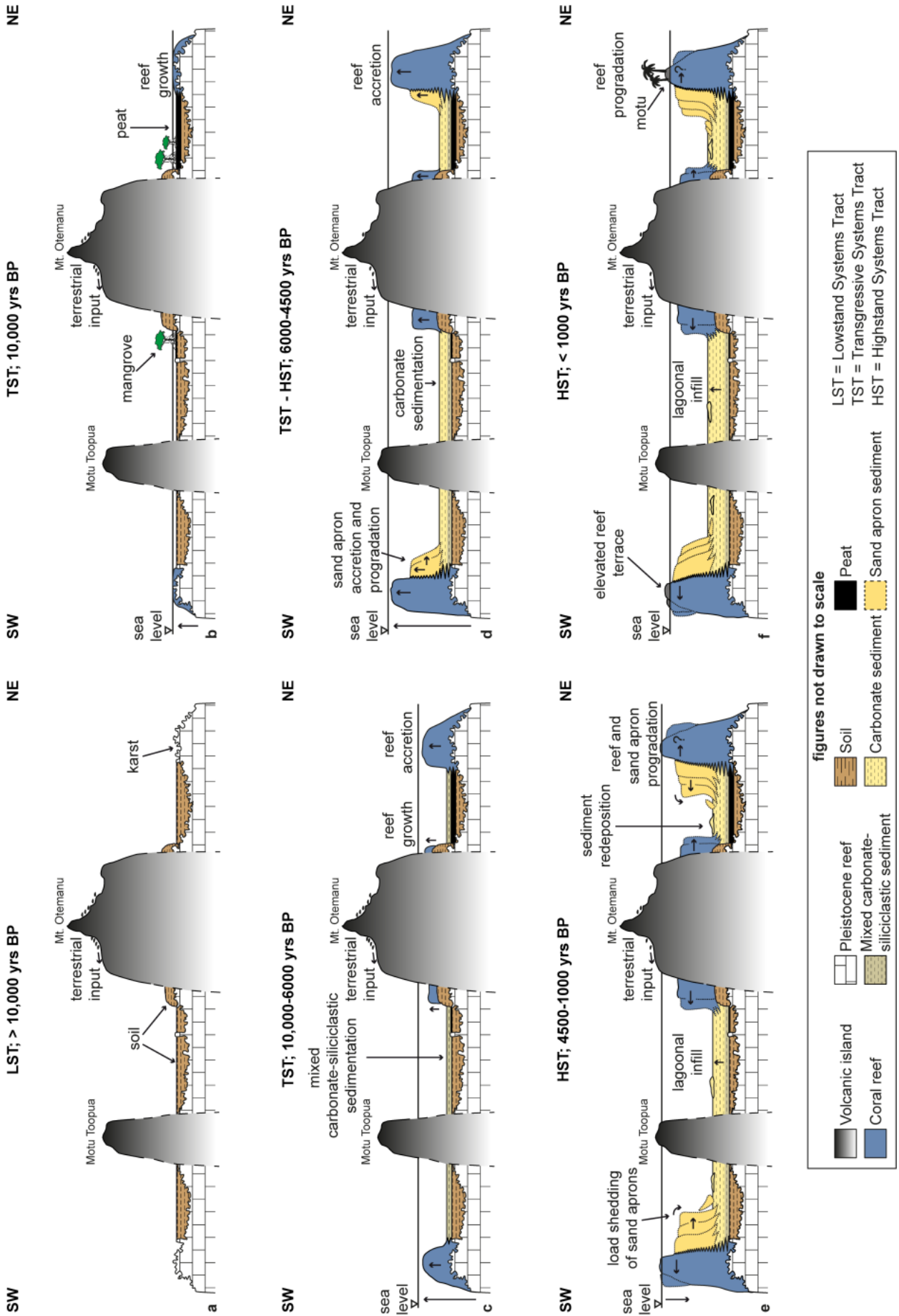


Fig. 4/14: Schematic transects (vertically exaggerated) showing the evolution of the barrier reef system through the Holocene: **a)** Sea-level lowstand > 10,000 yrs BP, subaerial exposure of the karstified Pleistocene reef, terrestrial input from the volcanic hinterland and soil formation within the inner platform, low carbonate production; **b)** Transgression of sea level and platform inundation ca. 10,000 kyrs BP, swamp development with mangroves depositing peat in the deepest parts of the lagoon, barrier-reef growth started; **c)** Sea-level rise continued, barrier-reef accretion proceeded, fringing-reef growth and mixing of carbonates and siliciclastics ca. 10,000-6000 yrs BP; **d)** Sea-level highstand was reached ca. 6000-4500 yrs BP, barrier and fringing reef accretion proceeded, high carbonate production and relative decrease in terrestrial sediment input, sand-apron formation and lagoonal progradation started; **e)** Stagnation and slight fall of sea level to modern level ca. 4500-1000 yrs BP, reef and sand apron progradation, sediment load shedding of sand aprons due to oversteepening of sand apron slopes is responsible for sediment redeposition within the lagoon, terrestrial sediment input declined, lagoonal infill is carbonate-dominated; **f)** Modern conditions were established < 1000 yrs BP, elevated reef terraces and motus are relicts of the former sea-level highstand, reef progradation proceeded, sand-apron accretion declined, lagoonal infill is carbonate-dominated. Please note that figures are not drawn to scale

topographic lows of the underlying bedrock but not on the topographic highs. The top of the peat deposits is dated to 9462 ± 32 yrs BP in the eastern lagoon of Bora Bora. Loose pieces of peat dated to $10,654 \pm 46$ yrs cal BP were found in between basal mixed carbonate-siliciclastic sediments, probably as the result of extensive bioturbation near the channel in the western lagoon. The basal peat age of Bora Bora is comparable to peat data from Mayotte lagoon dated to $10,775 \pm 270$ yrs BP (Zinke et al., 2005, 2003a) and from the Maldives dated to $10,320 \pm 100$ yrs BP (Klostermann and Gischler, 2015).

Persistent humid climate and sustained rainfall during the Holocene Thermal Maximum ca. 10,000-6000 yrs BP (e.g., Mayewski et al., 2004) led to enhanced erosion and weathering of the volcanic hinterland and allowed the input of large amounts of siliciclastics and to a lesser degree organic material into the lagoon (fig. 4/14c), indicated by Ti/Ca and Fe/Ca ratios (fig. 4/5). Dated peat and carbonate sediment from core APO 2 show that conditions conducive for carbonate-producing organisms were established ca. 700 yrs after the peat deposited in the inner platform. The lagoonal carbonate factory turned on and *in situ* carbonate production started. At this stage, only minor amounts of sediment input from the outer barrier reef was received by the central inner lagoon. Mixed carbonate-siliciclastic sediments accumulated (fig. 4/14d) slowly with 0.08 m/kyr above soil or local peat. Lagoonal carbonate sedimentation started 8725 ± 135 to 7718 ± 73 yrs cal BP in the eastern lagoon and 8125 ± 80 yrs cal BP to 5428 ± 112 in the western lagoon, respectively. It continued with sedimentation rates of 0.65 m/kyrs during 8000-6500 yrs BP, slightly elevated as compared to latter times. Contemporaneous to the initiation of lagoonal carbonate sedimentation, fringing reef growth started 8780 ± 50 yrs BP, and Holocene accretion rate average 5.65 m/kyr (Gischler et al., 2016). The fringing reefs comprise coralgall and microbial material and unconsolidated sediments at the base (Gischler et al., 2016), which had apparently created a

highly permeable framework allowing siliciclastics to be shed into the lagoon during the early Holocene transgression.

Highstand Systems Tract (HST)

In Bora Bora, sea level is reported to have reached its present position ca. 6000 yrs BP, and sea level was subsequently up to 180 cm above present level (Gischler et al., 2016; Rashid et al., 2014). Changes in climatic conditions towards drier tropical climate (Mayewski et al., 2004) following the Holocene Thermal Maximum presumably restricted terrestrial sediment delivery from the central volcanic island (fig. 4/14e). Both, barrier and fringing reef growth continued during the Highstand Systems Tract (HST) (fig. 4/14e).

Ongoing transgression also allowed enhanced entrainment of carbonate sediments from marginal reef areas and consequently, sand apron accretion started ca. 6000 yrs BP (fig. 4/14e). Forming sediment transport pathways, sand aprons play a crucial role infilling lagoon accommodation space due to lagoonward progradation in general (Isaack and Gischler, 2015; Kench, 1998a; Marshall and Davies, 1982; Purdy and Gischler, 2005). However, the spatial distribution of sand aprons restricted sediment transport to move preferentially fine material (mud) into the lagoon, while very coarse material was retained on sand aprons. At this time, the amount of carbonate material exceeded the amount of siliciclastic material within the lagoon. So therefore, the siliciclastic component within the sediment was diluted by carbonate material, which was indirectly facilitated by the lack of permanent river drainage from the central volcanic island into the lagoon.

When the sea level stagnated in the highstand position, reefs responded with lateral accretion (Gischler et al., 2016). In the Great Barrier Reef, Dechnik et al. (2016) showed that during sea level stillstand leeward (protected) reefs prograded seawards, while windward (exposed) reefs prograded lagoonwards. Coral cores and age data from Bora Bora show seaward progradation of leeward reefs (Gischler et al., 2016), the movement direction of the windward reefs still needs to be tested. Lagoonal infill continued and sedimentation rates in the Bora Bora lagoon varied from 0.24-0.78 m/kyrs (average 0.51 m/kyrs) from 6500-3000 yrs BP. For comparison, sedimentation rates in Mayotte, Indian Ocean diminished from 0.39 cm/kyrs to 0.29 cm/kyrs ca. 7000 yrs BP (Zinke et al., 2003a). In the Maldives, Indian Ocean, sedimentation rates averaged 0.55 cm/kyr from 6000-3000 yrs BP (Klostermann and Gischler, 2015). In Bora Bora, oversteepening of sand apron slopes led to sediment load shedding and redeposition of lagoonal sediments within the lagoon ca. 4500 yrs BP, during sea level stillstand (fig. 4/14e).

Modern conditions of sea level were reached after a slight fall of sea level ca. 1000 yrs BP (fig. 4/14f). Elevated reef terraces (feos) and extensive motus have remained as a relict of the sea-level highstand. Progradation of reefs as well as lagoonal infill with carbonate-dominated sediment continued. During the past 1000 yrs, lagoonal sedimentation rates varied between 0.26-1.74 m/kyrs.

Drawing comparison between Mayotte and Bora Bora shows differences in the sedimentary history of both oceanic barrier-reef complexes. This is because of the much larger central island size and the existence of permanent creeks draining Mayotte. Furthermore, the sand apron in Mayotte is smaller proportional to the platform size in Bora Bora, which extremely minors sediment input from the marginal reef into the proximal lagoon even during the sea-level highstand. In Bora Bora, mixed carbonate-siliciclastic sediments characterize the TST during the early Holocene. Sediments of the TST in Mayotte consist of a strongly siliciclastic-dominated or mixed siliciclastic-carbonate units (Zinke et al., 2003a, 2000). Sediments of the HST are carbonate-dominated in the lagoon of Bora Bora, while sediments from Mayotte mainly consists of siliciclastic-carbonate sediments (Zinke et al., 2003a, 2000). Sedimentation rates in Mayotte decrease throughout the Holocene while sedimentation rates in Bora Bora are variable: sedimentation rates increased during the early-Holocene, slightly decreased in the mid-Holocene and increased again during the past 3000 yrs.

4.5.3 Reef accretion, lagoonal sedimentation and sand-apron progradation – implications for infilling lagoonal accommodation space

It can be generally observed that carbonate platforms form the structure of a bucket with raised reef rims and deep lagoons as a result of the interplay between accommodation space, and sediment supply (Schlager, 1993, 1981). In Bora Bora, marginal reefs accreted with 6.03 m/kyr on average whereas lagoonal sedimentation rates average 0.53 m/kyr during the Holocene (fig. 4/15). This difference of an order of magnitude certainly amplified the development of the empty bucket morphology. Reef accretion rates have decreased during the Holocene due to the stagnation of sea level and reduction of accommodation space in the mid-late Holocene. Lagoonal sedimentation rates have slightly increased during the Holocene as a consequence of infilling of lagoonal accommodation space by in situ carbonate production and lateral progradation of sand aprons, respectively (fig. 4/15). In Bora Bora, reef accretion rates were calculated based on dated sections of barrier and fringing reefs (Gischler et al., 2016). Lagoonal sedimentation rates were also calculated only between dated core sections (figs. 4/5, 4/6, 4/15). Comparable relationships between lagoonal sedimentation and reefal

accretion may be found further afield in the Indian and Atlantic Oceans. Reef accretion rates of marginal and patch reefs average 7 m/kyr in an atoll of the Maldives, Indian Ocean (Gischler et al., 2008). Lagoonal sedimentation rates of the atoll lagoon average 0.92 m/kyr (Klostermann and Gischler, 2015). Holocene barrier and atoll reefs of Belize, western Atlantic Ocean, have accreted with an average of 3.03 m/kyr (Gischler, 2008; Gischler and Hudson, 2004, 1998), whereas sedimentation in reef lagoons average 1.18 m/kyr (Gischler, 2003). Possibly because of the presence of abundant lagoonal patch reefs and extensive *in situ* carbonate production, sedimentation rates in the Maldives and Belize reef lagoons are approximately twice as high as in Bora Bora. The fact that patch reefs are nearly absent in the lagoon of Bora Bora underlines the importance of the prograding sand apron for lagoonal infill.

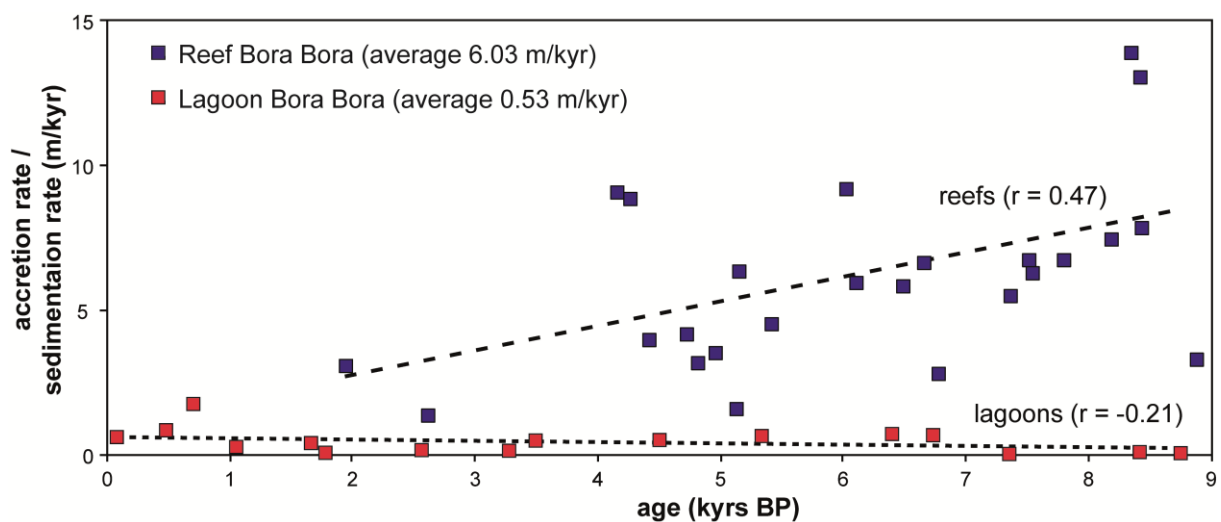


Fig. 4/15: Reef accretion rates versus lagoonal sedimentation rates of Holocene carbonate platforms of Bora Bora, southern Pacific Ocean (data from Gischler et al., 2016 and this study). While reef accretion rates have decreased during the Holocene due to stagnation of sea level and reduction of accommodation space, lagoonal sedimentation rates have increased during the Holocene as a consequence of infilling of lagoonal accommodation space by lagoonal carbonate production and lateral progradation of sand aprons. Please note that average reef accretion rates include marginal and fringing reef data

Klostermann and Gischler (2015) estimated lagoonal infill by sand aprons in a Maldivian atoll to be up to three times higher than lagoonal background sedimentation. Following the simple calculation method of Klostermann and Gischler (2015), lateral infill for Bora Bora via sand aprons can be estimated based on the fact that sand aprons prograded some 1.5 km on average since the Holocene sea level reached its present position ca. 6000 yrs BP. This equals a progradation of 250 m/kyr and is in the same range as sand apron progradation calculated by Klostermann and Gischler (2015) for a Maldives atoll. Hence, it would take 11,200 yrs to completely fill in accommodation space of the Bora Bora lagoon (2.8 km on average from the back-reef area towards the main volcanic island). With a mean lagoonal background sedimentation rate of 0.53 m/kyr, another 6 m of sediment would accumulate during this time

span. Based on lagoonal background sedimentation alone, it would take 45,300 yrs with a minimum lagoon depth of 24 m and 84,900 yrs with maximum lagoon depth of 45 m to completely fill in lagoonal accommodation space in Bora Bora. These simplified calculations ignore increasing water depth towards the lagoon center, decreasing water depth towards the central island, the irregular morphology of the lagoon floor in general, future sea-level changes, subsidence of 0.05-0.14 m/kyr (Gischler et al. 2016) and a slowdown or cessation of sand apron progradation with time. However, it gives an approximation of a possible duration of infilling of lagoonal accommodation space. In addition to the different modes of reef accretion versus lagoonal background sedimentation, the progradation of sand aprons is to a large part responsible in determining reef buckets either to be filled up with sediments or to remain in the empty bucket stage.

4.6 Conclusions

The coupled sedimentological, palaeontological, geochemical and geochronological data of seven sediment cores from the barrier reef lagoon of Bora Bora show the response of the sedimentary system with respect to geomorphological and palaeo-environmental (sea level and climate) change during the Holocene.

The evolution of the barrier-reef lagoon started with the accumulation of a loamy soil presumably during the late Pleistocene sea-level lowstand. Peat accumulated above the soil marking the Holocene flooding ca. 10650-9400 yrs BP. After a hiatus, mixed carbonate-siliciclastic sedimentation started ca. 8700-7700 yrs BP in the eastern lagoon and 8100-5400 yrs BP in the western lagoon. During this stage, sediment accumulation was dominated by lagoonal carbonate production and enhanced siliciclastic input from the volcanic hinterland, which decreased throughout the Holocene. Sand apron accretion started ca. 6000 yrs BP approximately when sea level reached modern level. Carbonate sediment produced at marginal reef areas started to be transported towards the lagoon, and hence fine material (mud) accumulated in the lagoon, very coarse grains were retained on the sand apron and enhanced rapid lagoonward progradation. The multi-proxy approach applied to core APO 2 from the eastern lagoon reflects an interval of enhanced primary productivity based on total organic carbon (TOC), Cu/Al ratios, Ca intensities and a decrease in Cl intensities during the mid-late Holocene. The upcore increase in coarse-grained sediments seems to indicate event deposition and can be correlated with coarse-grained deposits in the nearby Tahaa barrier reef lagoon, explained by higher cyclone activity. Cyclone landfall might have enhanced precipitation rates and run-off from the volcanic hinterland and resulted in lower

lagoonal salinity. Reefal sediment would have been transported into the lagoon. However, Ti/Ca and Fe/Ca ratios as proxies for terrestrial sediment input have decreased steadily during that time period and do not support enhanced run-off. Also, composition of foraminiferal faunas does not indicate reef-to-lagoon transport of coarser material. Alternatively, more permanent southeast trade winds and higher-than-present sea level during the mid-late Holocene could have favored higher hydrodynamic energy conditions and flushed higher amounts of open ocean water into the lagoon, enhanced primary productivity and the amount of pelagic organism and lowered lagoonal salinity. We assume that increased sediment dynamics ca. 4500-500 yrs BP, detected in most of the lagoon cores, display sediment load shedding of sand aprons into the lagoon and redeposition of lagoonal sediments due to oversteepening of sand apron slopes during ongoing progradation and sea-level fall to modern level. Modern conditions were reached ca. 1000 yrs BP and lagoonal infill is since dominated by fine-grained carbonate produced within the lagoon and on marginal reef areas, and only minor input of terrestrial material from the volcanic hinterland.

Even though temporarily occurring storms as mechanism driving sediment transport from reef to lagoon cannot entirely be excluded, it seems that in the long term tropical storms have played a more ancillary role in lagoonal sedimentation. Finally, this study shows different modes of sediment dynamics through time and highlights the importance of sand-apron formation and lagoonal infill by progradation during the Holocene, which exceeds lagoonal background sedimentation rates up to 6 times. Furthermore, our research underlines the need of an understanding of possible feedback mechanisms on sediment generation and entrainment to geomorphological and palaeo-environmental variations (e.g., sea level and climate) in barrier-reef systems.

Acknowledgements

The Deutsche Forschungsgemeinschaft (Gi 222/23-1) funded this research project and is gratefully acknowledged. We would like to thank Gabriela Meyer (Frankfurt) and Stefan Haber (Bad Karlshafen) for their hard work and enthusiasm during the expedition. Dominik Schmitt and Nico Neuwirth (Frankfurt) assisted during sample preparation. Furthermore we thank Doris Bergmann-Dörr und Dagmar Schneider (Frankfurt) for their efforts in the lab and introduction to the Laser Particle Size Analyzer, Reiner Petschick (Frankfurt) for running the x-ray diffractometer (XRD) and Claudia Franz (Frankfurt) for operating the scanning electron microscope (SEM). A.I. is grateful to Justin Parker (Perth) for helping with foraminifera identification and Jacek Raddatz (Frankfurt) for fruitful discussions considering the XRF

data. We thank S.A.R.L. Ti Ai Moana (Paea, Tahiti), Captain Yann Paureau and his first mate Sebastien Bertaut for logistical support. Gérard Bion supported us in many ways in Bora Bora. Research permits were kindly issued by the mayor of Bora Bora and the Ministère du Logement, des Affaires Foncières, de l'Économie Numérique et de l'Artisanat (Papeete). LPL Group (Hamburg), SDV (Papeete) and C.H. Robinson (Houston) transported equipment and samples. The constructive comments of Jody Webster, an anonymous reviewer and editor Brian Jones helped to improve this publication and are gratefully acknowledged.

References

- Babin, S.M., Carton, J.A., Dickey, T.D., Wiggert, J.D., 2004. Satellite evidence of hurricane-induced phytoplankton blooms in an oceanic desert. *J. Geophys. Res.* 109, C03043. doi:10.1029/2003JC001938
- Babinot, J.-F., Kouyoumontzakis, G., 1995. Associations d'ostracodes d'un environnement récifal envasé: le lagon de l'île de Mayotte (Archipel des Comores, Océan Indien occidental). *Geobios* 18, 17–38.
- Bahlburg, H., Spiske, M., 2012. Sedimentology of tsunami inflow and backflow deposits: key differences revealed in a modern example. *Sedimentology* 59, 1063–1086. doi:10.1111/j.1365-3091.2011.01295.x
- Bard, E., 1998. Geochemical and geophysical implications of the radiocarbon calibration. *Geochim. Cosmochim. Acta* 62, 2025–2038. doi:10.1016/S0016-7037(98)00130-6
- Berner, A., 1971. *Principles of Chemical Sedimentology*. New York, McGraw-Hill.
- Blais, S., Guille, G., Guillou, H., Chauvel, C., Maury, R.C., Caroff, M., 2000. Géologie, géochimie et géochronologie de l'île de Bora Bora (Société, Polynésie française). *Earth Planet. Sci.* 331, 579–585. doi:10.1016/S1251-8050(00)01456-7
- Blott, S.J., Pye, K., 2001. GRADISTAT: A grain size distribution and statistics package for the analyses unconsolidated sediments. *Earth Surf. Process. Landforms* 1248, 1237–1248. doi:10.1002/esp.261
- Böning, P., Brumsack, H.-J., Böttcher, M.E., Schnetger, B., Kriete, C., Kallmeyer, J., Borchers, S.L., 2004. Geochemistry of Peruvian near-surface sediments. *Geochim. Cosmochim. Acta* 68, 4429–4451. doi:10.1016/j.gca.2004.04.027
- Böning, P., Fröllje, H., Beck, M., Schnetger, B., Brumsack, H.-J., 2012. Underestimation of the authigenic fraction of Cu and Ni in organic-rich sediments. *Mar. Geol.* 323–325, 24–28. doi:10.1016/j.margeo.2012.07.004

- Braconnot, P., Harrison, S.P., Kageyama, M., Bartlein, P.J., Masson-Delmotte, V., Abe-Ouchi, A., Otto-Bliesner, B., Zhao, Y., 2012. Evaluation of climate models using palaeoclimatic data. *Nat. Clim. Chang.* 2, 417–424. doi:10.1038/nclimate1456
- Braithwaite, C.J.R., 2016. Coral-reef records of Quaternary changes in climate and sea-level. *Earth-Science Rev.* 156, 137–154. doi:10.1016/j.earscirev.2016.03.002
- Braithwaite, C.J.R., 1994. Quaternary oolites in the Indian Ocean. *Atoll Res. Bull.* 420, 1–6. doi:10.5479/si.00775630.420.1
- Burne, R. V., 1991. Carbonate sediment budgets and coastal management in South Pacific Island nations. *Work. Coast. Processes South Pacific Isl. Nations SOPAC Tech. Bull.* 7, 45–53.
- Cabioch, G., Camoin, G., Webb, G.E., Le Cornec, F., Garcia Molina, M., Pierre, C., Joachimski, M.M., 2006. Contribution of microbialites to the development of coral reefs during the last deglacial period: Case study from Vanuatu (South-West Pacific). *Sediment. Geol.* 185, 297–318. doi:10.1016/j.sedgeo.2005.12.019
- Cabioch, G., Taylor, F.W., Corre, T., Re, J., 1999. Occurrence and significance of microbialites in the uplifted Tasmaloum reef (SW Espiritu Santo, SW Pacific). *Sediment. Geol.* 126, 305–316. doi:10.1016/S0037-0738(99)00046-9
- Camoin, G., Cabioch, G., Eisenhauer, A., Braga, J.-C., Hamelin, B., Lericolais, G., 2006. Environmental significance of microbialites in reef environments during the last deglaciation. *Sediment. Geol.* 185, 277–295. doi:10.1016/j.sedgeo.2005.12.018
- Camoin, G.F., Gautret, P., Montaggioni, L.F., Cabioch, G., 1999. Nature and environmental significance of microbialites in Quaternary reefs: the Tahiti paradox. *Sediment. Geol.* 126, 271–304.
- Camoin, G.F., Webster, J.M., 2015. Coral reef response to Quaternary sea-level and environmental changes: State of the science. *Sedimentology* 62, 401–428. doi:10.1111/sed.12184
- Cheng, J., Collins, L.S., Homes, C., 2012. Four thousand years of habitat change in Florida Bay, as indicated by benthic foraminifera. *J. Foraminifer. Res.* 42, 3–17.
- Choi, K.S., Khim, B.K., Woo, K.S., 2003. Spherulitic siderites in the Holocene coastal deposits of Korea (eastern Yellow Sea): Elemental and isotopic composition and depositional environment. *Mar. Geol.* 202, 17–31. doi:10.1016/S0025-3227(03)00258-5
- Clement, A.C., Seager, R., Cane, M.A., 2000. Suppression of El Niño during the mid-Holocene by changes in the Earth's orbit. *Paleoceanography* 15, 731–737.

- Cobb, K.M., Westphal, N., Sayani, H.R., Watson, J.T., Di Lorenzo, E., Cheng, H., Edwards, R.L., Charles, C.D., 2013. Highly variable El Niño-Southern Oscillation throughout the Holocene. *Science* 339, 67–70. doi:10.1126/science.1228246
- Coleman, M.L., 1985. Geochemistry of diagenetic non-silicate minerals: kinetic considerations. *Philos. Trans. R. Soc. London* 315, 39–56.
- Coleman, M.L., Hedrick, D.B., Lovley, D.R., White, D.C., Pye, K., 1993. Reduction of Fe(III) in sediments by sulphate-reducing bacteria. *Nature* 361, 436–438. doi:10.1038/361436a0
- Conroy, J.L., Overpeck, J.T., Cole, J.E., 2010. El Niño/Southern Oscillation and changes in the zonal gradient of tropical Pacific sea surface temperature over the last 1.2 ka. *PAGES news* 18, 32–34.
- Conroy, J.L., Overpeck, J.T., Cole, J.E., Shanahan, T.M., Steinitz-Kannan, M., 2008. Holocene changes in eastern tropical Pacific climate inferred from a Galápagos lake sediment record. *Quat. Sci. Rev.* 27, 1166–1180. doi:10.1016/j.quascirev.2008.02.015
- Croudace, I.W., Rothwell, R.G., 2015. Micro-XRF studies of sediment cores: applications of a non-destructive tool for the environmental sciences (Developments in Paleoenvironmental Research). Springer Heidelberg. doi:10.1007/978-94-017-9849-5
- Curtis, C.D., Coleman, M.L., 1981. Controls on the precipitation of early diagenetic calcite, dolomite and siderite concretions in complex depositional sequences. *SEPM Spec. Publ.* 38, 23–33.
- Curtis, C.D., Coleman, M.L., Love, L.G., 1986. Pore water evolution during sediment burial from isotopic and mineral chemistry of calcite, dolomite and siderite concretions 2321–2334.
- Cushman, J.A., 1942. The foraminifera of the tropical Pacific collection of the “Albatross,” 1899-1900 Part 3—Heterohelicidae and Buliminidae. *Smithson. Inst. Bull.* 161.
- Cushman, J.A., 1933. The foraminifera of the tropical Pacific collection of the “Albatross,” 1899-1900 Part 2—Lagenidae to Alveolinellidae. *Smithson. Inst. Bull.* 161.
- Cushman, J.A., 1932. The foraminifera of the tropical Pacific collection of the “Albatross,” 1899-1900 Part 1—Astrohizidae to Trochamminidae. *Smithson. Inst. Bull.* 161.
- Cushman, J.A., Todd, R., Post, R.J., 1954. Recent foraminifera of the Marshall Islands. *Geol. Surv. Prof. Pap.* 260–H, 319–410.
- Daly, R.A., 1915. The Glacial-Control Theory of Coral Reefs. *Proc. Am. Acad. Arts Sci.* 51,

157–251.

- Debenay, J.-P., 2012. A guide to 1,000 foraminifera from the southwestern Pacific New Caledonia. IRD Editions Publications Scientifiques du Muséum.
- Debenay, J.-P., 2000. Foraminifera of paralic tropical environments. *Micropaleontology* 46, 153–160.
- Dechnik, B., Webster, J.M., Nothdurft, L., Webb, G.E., Zhao, J., Duce, S., Braga, J.C., Harris, D.L., Vila-Concejo, A., Puotinen, M., 2016. Influence of hydrodynamic energy on Holocene reef flat accretion, Great Barrier Reef. *Quat. Res.* 85, 44–53. doi:10.1016/j.yqres.2015.11.002
- Delong, K.L., Quinn, T.M., Shen, C.-C., Lin, K., 2010. A snapshot of climate variability at Tahiti at 9.5 ka using a fossil coral from IODP Expedition 310. *Geochemistry, Geophys. Geosystems* 11, 1–14. doi:10.1029/2009GC002758
- Dickinson, W.R., 2009. Pacific atoll living: how long already and until when. *GSA Today* 19, 4–10. doi:10.1130/GSATG35A.1
- Dickinson, W.R., 2003. Impact of mid-Holocene hydro-Isostatic highstand in regional sea level on habitability of islands in Pacific Oceania. *J. Coast. Res.* 19, 489–502.
- Donnelly, J.P., Woodruff, J.D., 2007. Intense hurricane activity over the past 5,000 years controlled by El Niño and the West African monsoon. *Nature* 447, 465–468. doi:10.1038/nature05834
- Dunham, R.J., 1962. Classification of carbonate rocks according to depositional texture, in: Ham, W.E. (Ed.), *Classification of Carbonate Rocks - A Symposium*. American Association of Petroleum Geologist Memoir, Vol. 1, American Association of Petroleum Geologist, Tulsa, pp. 108–121.
- Ehrlich, H.L., Newman, D.K., 2009. *Geomicrobiology*. CRC Press Taylor Francis Group. doi:10.1017/CBO9781107415324.004
- Emanuel, K.A., 1991. A scheme for representing cumulus convection in large-scale models. *J. Atmos. Sci.* doi:10.1175/1520-0469(1991)048<2313:ASFRCC>2.0.CO;2
- Embry, A., Klovan, E., 1972. Absolute water depths limits of late Devonian paleoecological zones. *Geol. Rundschau* 61, 672–686.
- Emile-Geay, J., Cobb, K.M., Carré, M., Braconnot, P., Leloup, J., Zhou, Y., Harrison, S.P., 2016. Links between tropical Pacific seasonal, interannual and orbital variability during the Holocene. *Nat. Geosci.* 9, 168–175. doi:10.1038/NGEO2608

- Fabricius, K.E., De'ath, G., Puotinen, M.L., Done, T., Cooper, T.F., Burgess, S.C., 2008. Disturbance gradients on inshore and offshore coral reefs caused by a severe tropical cyclone. *Limnol. Oceanogr.* 53, 690–704. doi:10.4319/lo.2008.53.2.0690
- Fajemila, O.T., Langer, M.R., Lipps, J.H., 2015. Spatial patterns in the distribution, diversity and abundance of benthic foraminifera around Moorea (Society Archipelago, French Polynesia). *PLoS One* 10, e0145752. doi:10.1371/journal.pone.0145752
- Fleitmann, D., Burns, S.J., Mudelsee, M., Neff, U., Kramers, J., Mangini, A., Matter, A., 2003. Holocene forcing of the Indian monsoon recorded in a stalagmite from southern Oman. *Science* 300, 1737–1739. doi:10.1126/science.1083130
- Friedman, G.M., 1959. Identification of carbonate minerals by staining methods. *J. Sediment. Petrol.* 29, 87–97.
- Frith, A.C., 1983. Circulation at One Tree Reef, Southern Great Barrier Reef. *BMR J. Aust. Geol. Geophys.* 8, 211–221.
- Fujita, K., Osawa, Y., Kayanne, H., Ide, Y., Yamano, H., 2009. Distribution and sediment production of large benthic foraminifers on reef flats of the Majuro Atoll, Marshall Islands. *Coral Reefs* 28, 29–45. doi:10.1007/s00338-008-0441-0
- Gabrié, C., Baldwin, J., Bonvallet, J., Chauvet, C., Vernaudon, Y., Payri, C., Galzin, R., 1994. Study of the coral reefs of Bora Bora (Society Archipelago, French Polynesia) for the development of a conservation and management plan. *Ocean Coast. Manag.* 25, 189–216.
- Gabrié, C., Salvat, B., 1985. General features of French Polynesian islands and their coral reefs, in: Delesalle, R., Galzin, R., Salvat, B. (Eds.), 5th International Coral Reef Congress, Tahiti, 27.05-01.06.1985 Vol. 1: French Polynesian Coral Reefs, Reef Knowledge and Field Guides. pp. 1–16.
- Gagan, M.K., Ayliffe, L.K., Hopley, D., Cali, J.A., Mortimer, G.E., Chappell, J., McCulloch, M.T., Head, M.J., 1998. Temperature and surface-ocean water balance of the mid-Holocene tropical western Pacific. *Science* 279, 1014–1018. doi:10.1126/science.279.5353.1014
- Gagan, M.K., Hendy, E.J., Haberle, S.G., Hantoro, W.S., 2004. Post-glacial evolution of the Indo-Pacific Warm Pool and El Niño-Southern oscillation. *Quat. Int.* 118–119, 127–143. doi:10.1016/S1040-6182(03)00134-4
- Gautier, D.L., 1982. Siderite concretions: Indicators of early diagenesis in the Gammon Shale (Cretaceous). *J. Sediment. Res.* 52, 859–871. doi:10.1306/212F8076-2B24-11D7-

- Ginsburg, R.N., 1956. Environmental relationships of grain size and constituent particles in some south Florida carbonate sediments. *Am. Assoc. Pet. Geol. Bull.* 40, 2384–2427.
- Gischler, E., 2011. Sedimentary facies of Bora Bora, Darwin's type barrier reef (Society Islands, South Pacific): the unexpected occurrence of non-skeletal grains. *J. Sediment. Res.* 81, 1–17. doi:10.2110/jsr.2011.4
- Gischler, E., 2010. Indo-Pacific and Atlantic spurs and grooves revisited: the possible effects of different Holocene sea-level history, exposure, and reef accretion rate in the shallow fore reef. *Facies* 56, 173–177. doi:10.1007/s10347-010-0218-0
- Gischler, E., 2008. Accretion patterns in Holocene tropical coral reefs: do massive coral reefs in deeper water with slowly growing corals accrete faster than shallower branched coral reefs with rapidly growing corals? *Int. J. Earth Sci.* 97, 851–859. doi:10.1007/s00531-007-0201-3
- Gischler, E., 2003. Holocene lagoonal development in the isolated carbonate platforms off Belize. *Sediment. Geol.* 159, 113–132. doi:10.1016/S0037-0738(03)00098-8
- Gischler, E., Hudson, J.H., 2004. Holocene development of the Belize Barrier Reef. *Sediment. Geol.* 164, 223–236. doi:10.1016/j.sedgeo.2003.10.006
- Gischler, E., Hudson, J.H., 1998. Holocene development of three isolated carbonate platforms, Belize, Central America. *Mar. Geol.* 144, 333–347.
- Gischler, E., Hudson, J.H., Humblet, M., Braga, J.C., Eisenhauer, A., Isaack, A., Anselmetti, F.S., Camoin, G.F., 2016. Late Quaternary barrier and fringing reef development of Bora Bora (Society Islands, south Pacific): first subsurface data from the Darwin-type barrier-reef system. *Sedimentology* 63, 1522–1549. doi:10.1111/sed.12272
- Gischler, E., Hudson, J.H., Pisera, A., 2008. Late Quaternary reef growth and sea level in the Maldives (Indian Ocean). *Mar. Geol.* 250, 104–113. doi:10.1016/j.margeo.2008.01.004
- Gregory, B.R.B., Peros, M., Reinhardt, E.G., Donnelly, J.P., 2015. Middle–late Holocene Caribbean aridity inferred from foraminifera and elemental data in sediment cores from two Cuban lagoons. *Palaeogeogr. Palaeoclimatol. Palaeoecol.* 426, 229–241. doi:10.1016/j.palaeo.2015.02.029
- Guilcher, A., Berthois, L., Doumenge, F., Michel, A., Saint-Requier, A., Arnold, R., 1969. Le récifs et lagons coralliens de Mopelia et de Bora Bora (Îles de la Société). *Mem. Orstom* 38, 38–103.

- Guillou, D., Maury, R.C., Blais, S., Cotten, J., Legendre, C., Guille, G., Caroff, M., 2005. Age progression along the Society hotspot chain (French Polynesia) based on new unspiked K-Ar ages. *Bull. la Société Géologique Fr.* 176, 135–150. doi:10.2113/176.2.135
- Gustafsson, Ö., Widerlund, A., Andersson, P.S., Ingri, J., Roos, P., Ledin, A., 2000. Colloid dynamics and transport of major elements through a boreal river — brackish bay mixing zone. *Mar. Chem.* 71, 1–21.
- Hallmann, N., Camoin, G., Eisenhauer, A., Vella, C., Samankassou, E., Fietzke, J., Milne, G.A., 2013. Sea-level changes over the past 6,000 years in the Society and Tuamotu Islands, French Polynesia, in: American Geophysical Union, Fall Meeting 2013.
- Hallock, P., 2011. Foraminifera, in: Hopley, D. (Ed.), *Encyclopedia of Modern Coral Reefs: Structure, Form and Process*. Springer Netherlands, Dordrecht, pp. 416–421. doi:10.1007/978-90-481-2639-2_80
- Hammer, Ø., Harper, D.A.T., Ryan, P.D., 2001. PAST: Paleontological Statistics software package for education and data analysis. *Palaeontol. Electron.* 4, 1–9.
- Harmelin-Vivien, M.L., 1994. The effects of storms and cyclones on coral reefs: a review. *J. Coast. Res.* 211–231.
- Harris, D.L., Vila-Concejo, A., Webster, J.M., 2014a. Geomorphology and sediment transport on a submerged back-reef sand apron: One Tree Reef, Great Barrier Reef. *Geomorphology* 222, 132–142. doi:10.1016/j.geomorph.2014.03.015
- Harris, D.L., Vila-Concejo, A., Webster, J.M., Power, H.E., 2015. Spatial variations in wave transformation and sediment entrainment on a coral reef sand apron. *Mar. Geol.* 363, 220–229. doi:10.1016/j.margeo.2015.02.010
- Harris, D.L., Webster, J.M., Carli, E.V. De, 2011. Geomorphology and morphodynamics of a sand apron, One Tree Reef, Southern Great Barrier Reef. *J. Coast. Res.* 760–764. doi:10.2112/SI65-086.1
- Harris, D.L., Webster, J.M., Vila-Concejo, A., Hua, Q., Yokoyama, Y., Reimer, P.J., 2014b. Late Holocene sea-level fall and turn-off of reef flat carbonate production: rethinking bucket fill and coral reef growth models. *Geology* 43, 175–178. doi:10.1130/G35977.1
- Haug, G.H., Hughen, K.A., Sigman, D.M., Peterson, L.C., Röhl, U., 2001. Southward migration of the Intertropical Convergence Zone through the Holocene. *Science* 293, 1304–1308. doi:10.1126/science.1059725
- Heindel, K., Birgel, D., Brunner, B., Thiel, V., Westphal, H., Gischler, E., Ziegenbalg, S.B.,

- Cabioch, G., Sjövall, P., Peckmann, J., 2012. Post-glacial microbialite formation in coral reefs of the Pacific, Atlantic, and Indian Oceans. *Chem. Geol.* 304–305, 117–130. doi:10.1016/j.chemgeo.2012.02.009
- Hogg, A.G., Hua, Q., Blackwell, P.G., Niu, M., Buck, C.E., Guilderson, T.P., Heaton, T.J., Palmer, J.G., Reimer, P.J., Reimer, R.W., Turney, C.S.M., Zimmerman, S.R.H., 2013. SHCAL13 southern hemisphere calibration, 0–50,000 years cal bp. *Radiocarbon* 55, 1889–1903.
- Hopley, D., 2011. Lagoons, in: Hopley, D. (Ed.), *Encyclopedia of Modern Coral Reefs: Structure, Form and Process*. Springer Netherlands, Dordrecht, pp. 617–618. doi:10.1007/978-90-481-2639-2_224
- Hubbard, D.K., 2016. Coral Reefs at the Crossroads – An Introduction, in: Hubbard, D.K., Rogers, C.S., Lipps, J.H., Stanley, G.D. (Eds.), *Coral Reefs of the World 6 Coral Reefs at the Crossroads*. Springer-Verlag, p. 314.
- ICPP, 2014. Summary for Policymakers, in: *Climate Change 2014: Impacts, Adaptation, and Vulnerability. Part A: Global and Sectoral Aspects. Contribution of Working Group II to the Fifth Assessment Report of the Intergovernmental Panel on Climate Change* (Field, C.B., V.R. Barros, D.J. Dokken, K.J. Cambridge University Press, Cambridge, United Kingdom and New York, NY, USA, pp. 1–32.
- Isaack, A., Gischler, E., 2015. The significance of sand aprons in Holocene atolls and carbonate platforms. *Carbonates and Evaporites*. doi:10.1007/s13146-015-0268-z
- Isaack, A., Gischler, E., Hudson, J.H., Anselmetti, F.S., Lohner, A., Vogel, H., Garbode, E., Camoin, G.F., 2016. A new model evaluating Holocene sediment dynamics: Insights from a mixed carbonate–siliciclastic lagoon (Bora Bora, Society Islands, French Polynesia, South Pacific). *Sediment. Geol.* 343, 99–118. doi:10.1016/j.sedgeo.2016.08.002
- Jackson, K.L., Eberli, G.P., Amelung, F., McFadden, M., Moore, L., Rankey, E.C., Jayasena, H.H., 2014. Holocene Indian Ocean tsunami history in Sri Lanka. *Geology* 42, 859–862. doi:10.1130/G35796.1
- Jones, R.W., 2014. *Foraminifera and their applications*. Cambridge University Press.
- Joshi, K.B., 2014. Microbes: Mini Iron Factories. *Indian J. Microbiol.* 54, 483–485.
- Kalbfleisch, W.B.C., Jones, B., 1998. Sedimentology of shallow, hurricane-affected lagoons: Grand Cayman, British West Indies. *J. Coast. Res.* 14, 140–161.
- Karamperidou, C., Nezio, P.N. Di, Timmermann, A., Jin, F., Cobb, K.M., 2015. The response

- of ENSO flavors to mid-Holocene climate: implications for proxy interpretation. *Paleoceanography* 527–547. doi:10.1002/2014PA002742
- Kench, P.S., 2011. Sediment dynamics, in: Hopley, D. (Ed.), *Encyclopedia of Modern Coral Reefs*. Springer Netherlands, pp. 994–1005.
- Kench, P.S., 1998a. Physical controls on development of lagoon sand deposits and lagoon infilling in an Indian Ocean Atoll. *J. Coast. Res.* 14, 1014–1024.
- Kench, P.S., 1998b. A currents of removal approach for interpreting carbonate sedimentary processes. *Mar. Geol.* 145, 197–223. doi:10.1016/S0025-3227(97)00101-1
- Kench, P.S., Brander, R.W., 2006. Response of reef island shorelines to seasonal climate oscillations: South Maalhosmadulu atoll, Maldives. *J. Geophys. Res.* 111, 2–12. doi:10.1029/2005JF000323
- Kench, P.S., Nichol, S.L., Smithers, S.G., McLean, R.F., Brander, R.W., 2008. Tsunami as agents of geomorphic change in mid-ocean reef islands. *Geomorphology* 95, 361–383. doi:10.1016/j.geomorph.2007.06.012
- Kench, P.S., Owen, S.D., Ford, M., 2014. Evidence for coral island formation during rising sea level in the central Pacific Ocean. *Geophys. Res. Lett.* 41, 820–827. doi:10.1002/2013GL059000
- Kendall, B., Anbar, A.D., Kappler, A., Konhauser, K.O., 2012. The Global Iron Cycle. *Fundam. Geobiol.* 65–92. doi:10.1002/9781118280874.ch6
- Kilian, R., Baeza, O., Breuer, S., Rios, F., Arz, H., Lamy, F., Wirtz, J., Baque, D., Korf, P., Kremer, K., Rios, C., Mutschke, E., Simon, M., De Pol-Holz, R., Arevalo, M., Worner, G., Schnieder, C., Casassa, G., 2013. Late glacial and Holocene paleogeographical and paleoecological evolution of the Seno Skyring and Otway fjord systems in the Magellan region. *An. Inst. Patagon.* 41, 5–26.
- Kim, S.T., Mucci, A., Taylor, B.E., 2007. Phosphoric acid fractionation factors for calcite and aragonite between 25 and 75°C: Revisited. *Chem. Geol.* 246, 135–146. doi:10.1016/j.chemgeo.2007.08.005
- Klostermann, L., Gischler, E., 2015. Holocene sedimentary evolution of a mid-ocean atoll lagoon, Maldives, Indian Ocean. *Int. J. Earth Sci.* 104, 289–307. doi:10.1007/s00531-014-1068-8
- Klostermann, L., Gischler, E., Storz, D., Hudson, J.H., 2014. Sedimentary record of late Holocene event beds in a mid-ocean atoll lagoon, Maldives, Indian Ocean: Potential for deposition by tsunamis. *Mar. Geol.* 348, 37–43. doi:10.1016/j.margeo.2013.11.014

- Konhauser, K., Riding, R., 2012. Bacterial Biomineralization, in: Knoll, A., Canfield, D., Konhauser, K. (Eds.), *Fundamentals of Geobiology*. John Wiley & Sons, Ltd, pp. 105–130. doi:10.1002/9781118280874.ch8
- Koutavas, A., DeMenocal, P.B., Olive, G.C., Lynch-Stieglitz, J., 2006. Mid-Holocene El Niño–Southern Oscillation (ENSO) attenuation revealed by individual foraminifera in eastern tropical Pacific sediments. *Geology* 34, 993–996. doi:10.1130/G22810A.1
- Krachler, R., Krachler, R.F., Kammer, F. von der, Süphandag, A., Jirsa, F., Ayromlou, S., Hofmann, T., Keppler, B.K., 2010. Relevance of peat-draining rivers for the riverine input of dissolved iron into the ocean. *Sci. Total Environ.* 408, 2402–2408. doi:10.1016/j.scitotenv.2010.02.018
- Krom, D., Berner, R.A., 1980. Adsorption of phosphate in anoxic marine sediments. *Limnol. Oceanogr.* 25, 797–806. doi:10.4319/lo.1980.25.5.0797
- Kuhn, G., 1984. *Sedimentations-Geschichte der Bermuda North Lagoon im Holozän*. Universität Göttingen, Deutschland.
- Ladd, H.S., 1949. The problem of coral reefs. *Sci. Mon.* 69, 297–305.
- Lambeck, K., Rouby, H., Purcell, A., Sun, Y., M., S., 2014. Sea level and global ice volumes from the Last Glacial Maximum to the Holocene. *PNAS* 111, 15296–15303.
- Lambeck, K., Woodroffe, C.D., Antonioli, F., Anzidei, M., Gehrels, W.R., Laborel, J., Wright, A.J., 2010. Paleoenvironmental records, geophysical modeling, and reconstruction of sea-level trends and variability on centennial and longer timescales, in: J. Church, P.L., Aarup, W.T., Wilson, W.S. (Eds.), *Understanding Sea- Level Rise and Variability*. Blackwell, Chichester, pp. 61–121.
- Lancelot, Y., Ewing, J.I., 1972. Correlation of natural gas zonation and carbonate diagenesis in Tertiary sediments from the northwest Atlantic. *Initial Reports Deep Sea Drill. Proj.* 11, 791–799.
- Langer, M.R., Lipps, J.H., 2003. Foraminiferal distribution and diversity, Madang Reef and Lagoon, Papua New Guinea. *Coral Reefs* 22, 143–154. doi:10.1007/s00338-003-0298-1
- Lebeau, O., Busigny, V., Chaduteau, C., Ader, M., 2014. Organic matter removal for the analysis of carbon and oxygen isotope compositions of siderite. *Chem. Geol.* 372, 54–61. doi:10.1016/j.chemgeo.2014.02.020
- Lim, D.I., Jung, H.S., Yang, S.Y., Yoo, H.S., 2004. Sequential growth of early diagenetic freshwater siderites in the Holocene coastal deposits, Korea. *Sediment. Geol.* 169, 107–120. doi:10.1016/j.sedgeo.2004.05.002

- Loeblich, A.R., Tappan, H., 1988. Foraminifera genera and their classification. Springer US, New York. doi:10.1007/978-1-4899-5760-3
- Lohner, A., 2015. Zwischen Barriereriff und Vulkaninsel: Meeresspiegelanstieg, Paläoböden und pleistozäne Sedimente in der Lagune von Bora Bora. Universität Bern, Schweiz.
- Löwemark, L., Chen, H.F., Yang, T.N., Kylander, M., Yu, E.F., Hsu, Y.W., Lee, T.Q., Song, S.R., Jarvis, S., 2011. Normalizing XRF-scanner data: a cautionary note on the interpretation of high-resolution records from organic-rich lakes. *J. Asian Earth Sci.* 40, 1250–1256. doi:10.1016/j.jseaes.2010.06.002
- Luther, G.W., 1991. Pyrite synthesis via polysulfide compounds. *Geochim. Cosmochim. Acta* 55, 2839–2849.
- MacNeil, F.S., 1954. The shape of atolls; an inheritance from subaerial erosion forms. *Am. J. Sci.* 252, 402–427.
- Madin, J., 2011. Climate change: Increasing storm activity, in: Hopley, D. (Ed.), *Encyclopedia of Modern Coral Reefs: Structure, Form and Process*. Springer Netherlands, Dordrecht, pp. 218–221. doi:10.1007/978-90-481-2639-2_57
- Madin, J.S., Connolly, S.R., 2006. Ecological consequences of major hydrodynamic disturbances on coral reefs. *Nature* 444, 477–80. doi:10.1038/nature05328
- Marcott, S.A., Shakun, J.D., Clark, P.U., Mix, A.C., 2013. A reconstruction of regional and global temperatures for the past 11,300 years. *Science* 339, 1198–1201.
- Marshall, J.F., Davies, P.J., 1982. Internal structure and Holocene evolution of One Tree Reef, Southern Great Barrier Reef. *Coral Reefs* 1, 21–28.
- Masse, J.P., Thomassin, B.A., Acquaviva, M., 1989. Bioclastic sedimentary environments of the coral reefs and lagoon around Mayotte Island (Comoro Archipelago, Mozambique Channel, SW Indian Ocean). *J. Coast. Res.* 5, 419–432.
- May, S.M., Falvard, S., Norpoth, M., Pint, A., Brill, D., Engel, M., Scheffers, A., Dierick, M., Paris, R., Squire, P., Brückner, H., 2016. A mid-Holocene candidate tsunami deposit from the NW Cape (Western Australia). *Sediment. Geol.* 332, 40–50. doi:10.1016/j.sedgeo.2015.11.010
- Mayewski, P.A., Rohling, E.E., Curt Stager, J., Karlén, W., Maasch, K.A., David Meeker, L., Meyerson, E.A., Gasse, F., van Kreveld, S., Holmgren, K., Lee-Thorp, J., Rosqvist, G., Rack, F., Staubwasser, M., Schneider, R.R., Steig, E.J., 2004. Holocene climate variability. *Quat. Res.* 62, 243–255. doi:10.1016/j.yqres.2004.07.001

- Middelton, A.P., Freestone, L.C., Leese, M.N., 1985. Textural analysis of ceramic thin sections: evaluation of grain sampling procedures. *Archaeometry* 27, 64–74.
- Milankovitch, M.M., 1941. Kanon der erdbestrahungen und seine anwendung auf das Eiszeitenproblem. *Serb. Acad. Beorg. Spec. Pub.* 132 p.
- Milliman, J.D., 1974. *Marine Carbonates*. Springer-Verlag, Berlin, Heidelberg, New York.
- Milliman, J.D., 1969. Four southwestern Caribbean atolls: Courtown Cays, Albuquerque Cays, Roncador Bank and Serrana Bank. *Atoll Res. Bull.* 1–41.
- Milne, G.A., Mitrovica, J.X., 2008. Searching for eustasy in deglacial sea-level histories. *Quatern. Sci. Rev.* 27, 2292–2302.
- Mitrovica, J.X., Milne, G.A., 2002. On the origin of late Holocene sea-level highstands within equatorial ocean basins. *Pergamon* 21, 2179–2190.
- Mitrovica, J.X., Peltier, W.R., 1991. On postglacial subsidence over the equatorial oceans. *J. Geophys. Res.* 96, 20,053–20,071.
- Mollier-Vogel, E., Leduc, G., Bösch, T., Martinez, P., Schneider, R.R., 2013. Rainfall response to orbital and millennial forcing in northern Peru over the last 18 ka. *Quat. Sci. Rev.* 76, 29–38. doi:10.1016/j.quascirev.2013.06.021
- Montaggioni, L.F., Le, F., Corrège, T., Cabioch, G., 2006. Coral barium/calcium record of mid-Holocene upwelling activity in New Caledonia, South-West Pacific. *Paleogeography, Paleoclimatology, Paleoecol.* 237, 436–455. doi:10.1016/j.palaeo.2005.12.018
- Mortimer, R.J.G., Galsworthy, A.M.J., Bottrell, S.H., Wilmot, L.E., Newton, R.J., 2011. Experimental evidence for rapid biotic and abiotic reduction of Fe(III) at low temperatures in salt marsh sediments: a possible mechanism for formation of modern sedimentary siderite concretions. *Sedimentology* 58, 1514–1529. doi:10.1111/j.1365-3091.2011.01224.x
- Morton, R.A., Gelfenbaum, G., Jaffe, B.E., 2007. Physical criteria for distinguishing sandy tsunami and storm deposits using modern examples. *Sediment. Geol.* 200, 184–207. doi:10.1016/j.sedgeo.2007.01.003
- Mozley, P.S., 1989. Relation between depositional environment and the elemental composition of early diagenetic siderite. *Geology* 17, 704–706. doi:10.1130/0091-7613(1989)017<0704
- Mozley, P.S., 1989. Complex compositional zonation in concretionary siderite: Implications

- for geochemical studies. *J. Sediment. Petrol.* 59, 815–818. doi:10.1306/212F907A-2B24-11D7-8648000102C1865D
- Mozley, P.S., Carothers, W.W., 1992. Elemental and isotopic composition of siderite in the Kuparuk Formation, Alaska; effect of microbial activity and water sediment interaction on early pore-water. *J. Sediment. Res.* 62, 681–692. doi:10.1306/D4267988-2B26-11D7-8648000102C1865D
- Mozley, P.S., Wersin, P., 1992. Isotopic composition of siderite as an indicator of depositional environment. *Geology* 20, 817–820.
- Müller, G., 1964. *Sediment-Petrologie Teil I: Methoden der Sediment-Untersuchung.* Schweizerbart, Stuttgart.
- Murray, J.W., 2006. *Ecology and applications of benthic foraminifera.* Cambridge University Press.
- Nandasena, N.A.K., Tanaka, N., Sasaki, Y., Osada, M., 2013. Boulder transport by the 2011 Great East Japan tsunami: comprehensive field observations and whether model predictions? *Mar. Geol.* 346, 292–309. doi:10.1016/j.margeo.2013.09.015
- Nott, J., Forsyth, A., 2012. Punctuated global tropical cyclone activity over the past 5,000 years. *Geophys. Res. Lett.* 39, 1–5. doi:10.1029/2012GL052236
- Nott, J.F., 2003. Intensity of prehistoric tropical cyclones. *J. Geophys. Res.* 108, 4212. doi:10.1029/2002JD002726
- Paillard, D., Labeyrie, L., Yiou, P., 1996. Macintosh program performs time-series analysis. *EOS Trans. AGU* 77, 377–380.
- Paris, R., Fournier, J., Poizot, E., Etienne, S., Morin, J., Lavigne, F., Wassmer, P., 2010. Boulder and fine sediment transport and deposition by the 2004 tsunami in Lhok Nga (western Banda Aceh, Sumatra, Indonesia): a coupled offshore-onshore model. *Mar. Geol.* 268, 43–54. doi:10.1016/j.margeo.2009.10.011
- Parker, J.H., 2009. Taxonomy of foraminifera from Ningaloo Reef, Western Australia. *Memoir of the Association of Australasian Paleontologists* 36.
- Parker, J.H., Gischler, E., 2011. Modern foraminiferal distribution and diversity in two atolls from the Maldives, Indian Ocean. *Mar. Micropaleontol.* 78, 30–49. doi:10.1016/j.marmicro.2010.09.007
- Peros, M., Gregory, B., Matos, F., Reinhardt, E., Desloges, J., 2015. Late-Holocene record of lagoon evolution, climate change, and hurricane activity from southeastern Cuba. *The*

Holocene 25, 1483–1497. doi:10.1177/0959683615585844

- Petschick, R., Kuhn, G., Gingele, F., 1996. Clay mineral distribution in surface sediments of the South Atlantic: sources, transport, and relation to oceanography. *Mar. Geol.* 130, 203–229.
- Pilarczyk, J.E., Goff, J., Mountjoy, J., Lamarche, G., Pelletier, B., Horton, B.P., 2014. Sediment transport trends from a tropical Pacific lagoon as indicated by *Homotrema rubra* taphonomy: Wallis Island, Polynesia. *Mar. Micropaleontol.* 109, 21–29. doi:10.1016/j.marmicro.2014.03.004
- Pilarczyk, J.E., Reinhardt, E.G., 2012. Testing foraminiferal taphonomy as a tsunami indicator in a shallow arid system lagoon: Sur, Sultanate of Oman. *Mar. Geol.* 295–298, 128–136. doi:10.1016/j.margeo.2011.12.002
- Pirazzoli, P.A., 1991. *World atlas of Holocene sea-level changes*. Elsevier Science.
- Pirazzoli, P.A., Brousse, R., Delibrias, G., Montaggioni, L.F., Sachet, M.H., Salvat, B., Sinoto, Y.H., 1985a. Leeward Islands (Maupiti, Tupai, Bora Bora, Huanine) Society Archipelago, in: Delesalle, R.G., Salvat, B. (Eds.), *5th International Coral Reef Congress, Tahiti, 27.05-01.06.1985 Vol. 1: French Polynesian Coral Reefs, Reef Knowledge and Field Guides*. pp. 17–72.
- Pirazzoli, P.A., Montaggioni, L.F., 1988. Holocene sea-level changes in French Polynesia. *Palaeogeogr. Palaeoclimatol. Palaeoecol.* 68, 153–175.
- Pirazzoli, P.A., Montaggioni, L.F., Delibrias, G., Faure, G., Salvat, B., 1985b. Late Holocene sea-level changes in the Society Islands and in the northwest Tuamotu atolls, in: Gabriele, C., J.L.T. (Ed.), *Proceedings of the Fifth International Coral Reef Congress, Tahiti*. pp. 131–136.
- Pirazzoli, P.A., Montaggioni, L.F., Salvat, B., Faure, G., 1988. Late Holocene sea-level indicators from twelve atolls in the central and eastern Tuamotus (Pacific Ocean). *Coral Reefs* 7, 57–68.
- Pirazzoli, P.A., Montaggioni, L.F., Vergnaud-Grazzini, C., Saliege, J.F., 1987. Late Holocene sea level and coral reef development in Vahitahi atoll, eastern Tuamotu Islands, Pacific Ocean. *Mar. Geol.* 76, 105–116.
- Postma, D., 1982. Pyrite and siderite formation in brackish and freshwater swamp sediments. *Am. J. Sci.* 282, 1151–1183.
- Purdy, E.G., 1974. Reef Configurations: Cause and Effect, in: Laporte, L.F. (Ed.), *Reefs in Time and Space*. pp. 9–76.

- Purdy, E.G., Gischler, E., 2005. The transient nature of the empty bucket model of reef sedimentation. *Sediment. Geol.* 175, 35–47. doi:10.1016/j.sedgeo.2005.01.007
- Purdy, E.G., Gischler, E., Lomando, A.J., 2003. The Belize margin revisited. 2. Origin of Holocene antecedent topography. *Int. J. Earth Sci.* 92, 552–572. doi:10.1007/s00531-003-0325-z
- Purdy, E.G., Winterer, E.L., 2006. Contradicting Barrier Reef relationships for Darwin's Evolution of reef types. *Int. J. Earth Sci.* 95, 143–167. doi:10.1007/s00531-005-0511-2
- Purdy, E.G., Winterer, E.L., 2001. Origin of atoll lagoons. *GSA Bull.* 113, 837–854.
- Purkis, S.J., Harris, P.M. (Mitch), 2016. The extent and patterns of sediment filling of accommodation space on Great Bahama Bank. *J. Sediment. Res.* 86, 294–310.
- Pye, K., Dickson, J.A.D., Schiavon, N., Coleman, M.L., Cox, M., 1990. Formation of siderite-Mg-calcite-iron sulphide concretions in intertidal marsh and sandflat sediments, north Norfolk, England. *Sedimentology* 37, 325–343.
- Rankey, E.C., Reeder, S.L., 2009. Holocene ooids of Aitutaki Atoll, Cook Islands, South Pacific. *Geology* 37, 971–974. doi:10.1130/G30332A.1
- Rankey, E.C., Reeder, S.L., Garza-Perez, J.R., 2011. Controls on links between geomorphical and surface sedimentological variability: Aitutaki and Maupiti Atolls, South Pacific Ocean. *J. Sediment. Res.* 81, 885–900. doi:10.2110/jsr.2011.73
- Rashid, R., Eisenhauer, A., Stocchi, P., Liebetrau, V., Fietzke, J., Rüggeberg, A., Dullo, W.C., 2014. Constraining mid to late Holocene relative sea-level change in the southern equatorial Pacific Ocean relative to the Society Islands, French Polynesia. *Geochemistry, Geophys. Geosystems* 15, 2601–2615. doi:10.1002/2014GC005272
- Reimer, P.J., Bard, E., Bayliss, A., Beck, J.W., Blackwell, P.G., Bronk Ramsey, C., Buck, C.E., Cheng, H., Edwards, R.L., Friedrich, M., Grootes, P.M., Guilderson, T.P., Haflidason, H., Hajdas, I., Hatté, C., Heaton, T.J., Hoffmann, D.L., Hogg, A.G., Hughen, K.A., Kaiser, K.F., Kromer, B., Manning, S.W., Niu, M., Reimer, R.W., Richards, D.A., Scott, E.M., Southon, J.R., Staff, R.A., Turney, C.S.M., van der Plicht, J., 2013. INTCAL13 and MARINE13 radiocarbon age calibration curves 0–50,000 years cal bp. *Radiocarbon* 55, 1869–1887.
- Roh, Y., Zhang, C.L., Vali, H., Lauf, R.J., Zhou, J., Phelps, T.J., 2003. Biogeochemical and environmental factors in Fe biomineralization: Magnetite and siderite formation. *Clays Clay Miner.* 51, 83–95. doi:10.1346/CCMN.2003.510110
- Röhl, U., Abrams, L.J., 2000. High-resolution, downhole, and nondestructive core

- measurements from site 999 and 1001 in the Caribbean Sea: application to the Late Paleocene Thermal Maximum. *Proceedings Ocean Drill. Program, Sci. Results* 165, 191–203. doi:10.2973/odp.proc.sr.165.009.2000
- Rosenbaum, J., Sheppard, S.M.F., 1986. An isotopic study of siderites, dolomites and ankerites at high temperatures. *Geochim. Cosmochim. Acta* 50, 1147–1150. doi:10.1016/0016-7037(86)90396-0
- Salvatteci, R., Gutiérrez, D., Field, D., Sifeddine, A., Ortlieb, L., Bouloubassi, I., Boussafir, M., Boucher, H., Cetin, F., 2014. The response of the Peruvian Upwelling Ecosystem to centennial-scale global change during the last two millennia. *Clim. Past* 10, 715–731. doi:10.5194/cp-10-715-2014
- Salvatteci, R., Gutierrez, D., Sifeddine, A., Ortlieb, L., Druffel, E., Boussafir, M., Schneider, R., 2016. Centennial to millennial-scale changes in oxygenation and productivity in the Eastern Tropical South Pacific during the last 25,000 years. *Quat. Sci. Rev.* 131, 102–117. doi:10.1016/j.quascirev.2015.10.044
- Sapota, T., Aldahan, A., Al-Aasm, I.S., 2006. Sedimentary facies and climate control on formation of vivianite and siderite microconcretions in sediments of Lake Baikal, Siberia. *J. Paleolimnol.* 36, 245–257. doi:10.1007/s10933-006-9005-x
- Schlager, W., 1993. Accommodation and supply - a dual control on stratigraphic sequences. *Sediment. Geol.* 86, 111–136.
- Schlager, W., 1981. The paradox of drowned reefs and carbonate platforms. *Geol. Soc. Am. Bull.* 92, 197–211.
- Schlager, W., Purkis, S.J., 2015. Reticulate reef patterns - antecedent karst versus self-organization. *Sedimentology* 62, 501–515. doi:10.1111/sed.12172
- Schlager, W., Purkis, S.J., 2013. Bucket structure in carbonate accumulations of the Maldives, Chagos and Laccadive archipelagos. *Int. J. Earth Sci.* 102, 2225–2238. doi:10.1007/s00531-013-0913-5
- Schoonen, M.A.A., Barnes, H.L., 1991. Reactions forming pyrite and marcasite from solution: II. Via FeS precursors below 100°C. *Geochim. Cosmochim. Acta* 55, 1505–1514.
- Scoffin, T.P., 1992. Taphonomy of coral reefs: a review. *Coral Reefs* 11, 57–77.
- Scoffin, T.P., Tudhope, A.W., 1988. Shallowing-upwards sequences in reef lagoon sediments: examples from the Holocene of the Great Barrier Reef of Australia and the Silurian of Much Wenlock, Shropshire, England. *Proc. 6th Int. Coral Reef Symp. Aust.* 3, 479–484.

- Searđ, C., Camoin, G., Yokoyama, Y., Matsuzaki, H., Durand, N., Bard, E., Sepulcre, S., Deschamps, P., 2011. Microbialite development patterns in the last deglacial reefs from Tahiti (French Polynesia; IODP Expedition #310): Implications on reef framework architecture. *Mar. Geol.* 279, 63–86. doi:10.1016/j.margeo.2010.10.013
- Sieger, R., Grobe, H., 2005. PanPlot - software to visualize profiles and core logs. doi:10.1594/PANGAEA.330147
- Sladen, A., Hébert, H., Schindelé, F., Reymond, D., 2007. Evaluation of far-field tsunami hazard in French Polynesia based on historical data and numerical simulations. *Nat. Hazard Earth Syst. Sci.* 7, 195–206. doi:10.5194/nhess-7-195-2007
- Sparrenbom, C., Bennike, O., Björck, S., Lambeck, K., 2006. Holocene relative sea-level changes in the Qaqortoq area, southern Greenland. *Boreas* 35, 171–187. doi:10.1080/03009480600578032
- Spiske, M., Jaffe, B.E., 2009. Sedimentology and hydrodynamic implications of a coarse-grained hurricane sequence in a carbonate reef setting. *Geology* 37, 839–842. doi:10.1130/G30173A.1
- Stoddart, D., 1969. Ecology and morphology of recent coral reefs. *Biol. Rev.* 44, 433–498.
- Storz, D., Gischler, E., Parker, J., Klostermann, L., 2014. Changes in diversity and assemblages of foraminifera through the Holocene in an atoll from the Maldives, Indian Ocean. *Mar. Micropaleontol.* 106, 40–54. doi:10.1016/j.marmicro.2013.12.001
- Stott, L., Cannariato, K., Thunell, R., Haug, G.H., Koutavas, A., 2004. Decline of surface temperature and salinity in the western tropical Pacific Ocean in the Holocene epoch. *Nature* 431, 56–59. doi:10.1038/nature02903
- Straub, K.L., 2011. Fe(II)-Oxidizing Prokaryotes, in: Reitner, J., Thiel, V. (Eds.), *Encyclopedia of Geobiology*. Springer Netherlands, Dordrecht, pp. 367–370. doi:10.1007/978-1-4020-9212-1_88
- Suess, E., 1979. Mineral phases formed in anoxic sediments by microbial decomposition of organic matter. *Geochim. Cosmochim. Acta* 43, 339–352.
- Talma, A.S., Vogel, J.C., 1993. A simplified approach to calibrating ¹⁴C dates. *Radiocarbon* 35, 317–322.
- Tasse, N., Hesse, R., 1984. Origin and significance of complex authigenic carbonates in Cretaceous black shales of the Western Alps. *J. Sediment. Res.* 54, 1012–1027. doi:10.1306/212F8553-2B24-11D7-8648000102C1865D

- Todd, R., 1965. The Foraminifera of the Tropical Pacific Collections of the “Albatross,” 1899-1900 Part 4—Rotaliform Families and Planctonic Families. *Smithson. Inst. Bull.* 161.
- Toomey, M., Ashton, A.D., Perron, J.T., 2013. Profiles of ocean island coral reefs controlled by sea-level history and carbonate accumulation rates. *Geology* 41, 731–734. doi:10.1130/G34109.1
- Toomey, M.R., Ashton, A.D., Raymo, M.E., Perron, J.T., 2016a. Late Cenozoic sea level and the rise of modern rimmed atolls. *Palaeogeogr. Palaeoclimatol. Palaeoecol.* 451, 73–83. doi:10.1016/j.palaeo.2016.03.018
- Toomey, M.R., Donnelly, J.P., Tierney, J.E., 2016b. South Pacific hydrologic and cyclone variability during the last 3000 years. *Paleoceanography* 31, 491–504. doi:10.1002/2015PA002870
- Toomey, M.R., Donnelly, J.P., Woodruff, J.D., 2013. Reconstructing mid-late Holocene cyclone variability in the Central Pacific using sedimentary records from Tahaa, French Polynesia. *Quat. Sci. Rev.* 77, 181–189. doi:10.1016/j.quascirev.2013.07.019
- Tudhope, A.W., Scoffin, T.P., 1984. The effects of *Callianassa* bioturbation on the preservation of carbonate grains in Davies Reef lagoon, Great Barrier Reef, Australia. *J. Sediment. Petrol.* 54, 1091–1096.
- Uto, K., Yamamoto, Y., Sudo, M., Uchiumi, S., Ishizuka, O., Kogiso, T., Tsunakawa, H., 2007. New K-Ar ages of the Society Islands, French Polynesia, and implications for the Society hotspot feature. *Earth Planets Sp.* 59, 879–885. doi:10.1186/BF03352750
- van der Plaas, L., Tobi, A.C., 1965. A chart for judging the reliability of point-counting results. *Am. J. Sci.* 263, 87–90.
- van Soelen, E., Brooks, G., Larson, R., Sinninghe Damste, J., Reichert, G., 2012. Mid- to late-Holocene coastal environmental changes in southwest Florida, USA. *The Holocene* 22, 929–938. doi:10.1177/0959683611434226
- Veizer, J., 1982. Chemical diagenesis of carbonates: Theory and application of trace element technique. *Stable Isot. Sediment. Geol.* 10, 1–99. doi:10.2110/scn.83.01.0000
- Vè nec-Peyré, M.-T., 1991. Distribution of living benthic foraminifera on the back-reef and outer slopes of a high island (Moorea, French Polynesia). *Coral Reefs* 105–113. doi:10.1016/B978-012374473-9.00090-4
- Walsh, K.J.E., McBride, J.L., Klotzbach, P.J., Balachandran, S., Camargo, S.J., Holland, G., Knutson, T.R., Kossin, J.P., Lee, T., Sobel, A., Sugi, M., 2016. Tropical cyclones and climate change. *Wiley Interdiscip. Rev. Clim. Chang.* 7, 65–89. doi:10.1002/wcc.371

- Weltje, G.J., Tjallingii, R., 2008. Calibration of XRF core scanners for quantitative geochemical logging of sediment cores: theory and application. *Earth Planet. Sci. Lett.* 274, 423–438. doi:10.1016/j.epsl.2008.07.054
- Wizemann, A., Mann, T., Klicpera, A., Westphal, H., 2015. Microstructural analyses of sedimentary *Halimeda* segments from the Spermonde Archipelago (SW Sulawesi, Indonesia): a new indicator for sediment transport in tropical reef islands? *Facies* 61, 4. doi:10.1007/s10347-015-0429-5
- Wolf, K.H., Easton, A.J., Warne, S., 1967. Techniques of examining and analyzing carbonate skeletons, minerals and rocks, in: Chilingar, G. V, Bissell, H.J., Fairbridge, R.W. (Eds.), *Developments in Sedimentology 9B - Carbonate Rocks - Physical and Chemical Aspects*. pp. 252–341.
- Woodroffe, C.D., Kennedy, D.M., Jones, B.G., Phipps, C.V.G., 2004. Geomorphology and late Quaternary development of Middleton and Elizabeth Reefs. *Coral Reefs* 23, 249–262. doi:10.1007/s00338-004-0374-1
- Woodroffe, C.D., Mclean, R.E., Wallensky, E., 1994. Geomorphology on the Cocos (Keeling) Islands. *Atoll Res. Bull.* 402, 1–33.
- Woodroffe, C.D., Webster, J.M., 2014. Coral reefs and sea-level change. *Mar. Geol.* 352, 248–267. doi:10.1016/j.margeo.2013.12.006
- Yamano, H., Kayanne, H., Matsuda, F., 2002. Lagoonal facies, ages, and sedimentation in three atolls in the Pacific. *Mar. Geol.* 185, 233–247.
- Yu, K.-F., Zhao, J.-X., Done, T., Chen, T.-G., 2009. Microatoll record for large century-scale sea-level fluctuations in the mid-Holocene. *Quat. Res.* 71, 354–360. doi:10.1016/j.yqres.2009.02.003
- Zinke, J., Reijmer, J.J.G., Taviani, M., Dullo, W.-C., Thomassin, B.A., 2005. Facies and faunal assemblage changes in response to the Holocene transgression in the lagoon of Mayotte (Comoro Archipelago, SW Indian Ocean). *Facies* 50, 391–408. doi:10.1007/s10347-004-0040-7
- Zinke, J., Reijmer, J.J.G., Thomassin, B.A., 2003a. Systems tracts sedimentology in the lagoon of Mayotte associated with the Holocene transgression. *Sediment. Geol.* 160, 57–79. doi:10.1016/S0037-0738(02)00336-6
- Zinke, J., Reijmer, J.J.G., Thomassin, B.A., Dullo, W.-C., Grootes, P.M., Erlenkeuser, H., 2003b. Postglacial flooding history of Mayotte lagoon (Comoro Archipelago, southwest Indian Ocean). *Mar. Geol.* 194, 181–196. doi:10.1016/S0025-3227(02)00705-3

- Zinke, J., Reijmer, J.J.G., Dullo, W.-C., Thomassin, B.A., 2000. Paleoenvironmental changes in the lagoon of Mayotte associated with the Holocene transgression. *Geolines* 11, 150–153.
- Zinke, J.Y., Reijmer, J.J.G., Thomassin, B.A., 2001. Seismic architecture and sediment distribution within the Holocene barrier reef lagoon complex of Mayotte (Comoro archipelago, SW Indian Ocean). *Paleogeography, Paleoclimatology, Paleoecol.* 175, 343–368. doi:10.1016/S0031-0182(01)00379-0

CHAPTER 5

FACIES VARIATIONS IN THE MIXED CARBONATE-SILICICLASTIC LAGOON OF BORA BORA, FRENCH POLYNESIA: THE INFLUENCE OF HOLOCENE SEA-LEVEL AND CLIMATE CHANGE IN THE SOUTH PACIFIC

Anja Isaack¹, Eberhard Gischler¹, J. Harold Hudson², Flavio S. Anselmetti³,
Stephan Buhre⁴, Gilbert F. Camoin⁵

¹Institut für Geowissenschaften, Goethe-Universität, Frankfurt/Main, Germany

²Reef Tech Inc., Miami, Florida, USA

³Institute of Geological Sciences and Oeschger Centre for Climate Change
Research, University of Bern, Bern, Switzerland

⁴Institut für Geowissenschaften, Johannes Gutenberg Universität, 55128 Mainz,
Germany

⁵Aix-Marseille Université, CNRS, IRD, CEREGE UM34, Aix-en-Provence &
Europôle Méditerranéen de l'Arbois, BP 80, Aix-en-Provence cedex 4, France

Keywords: sediment composition; microfacies; siderite; Holocene; barrier-reef
lagoon; Pacific

submitted to Marine Geology (Oktober 2016)

Abstract

Five mixed carbonate-siliciclastic sedimentary facies were identified using microfacies analyses and statistical testing of 70 sediment samples taken at high resolution from two vibrocores of the barrier-reef lagoon of Bora Bora. Facies and facies successions were interpreted in respect to Holocene sea-level and climate changes. The windward lagoon core site is characterized by siderite-rich marly wackestones and foraminifera-siderite wackestones, which have been deposited around 7700 yrs BP (years before present) during the early-mid Holocene transgression. At that time, extensive weathering and erosion of iron from the volcanic island due to wetter climate conditions were expressed in the formation of synsedimentary siderite in lagoonal sediments. The enrichment in $\delta^{18}\text{O}$ (+0.32 to +0.54‰) indicates marine to mixed marine-meteoric conditions during siderite precipitation. Siderite

formation results from microbial degradation of organic material, indicated by depleted $\delta^{13}\text{C}$ values (-13.61 to -14.48%), and iron reduction in the presence of dissolved bicarbonate, which led to reducing conditions in lagoonal sediments. The chemical composition of siderites changes upcore from relatively high Fe (91-95 mol%) and low Mn (5-6 mol%) concentrations at the core base to lower Fe (83-88 mol%) and higher Mn (11-16 mol%) concentrations in the upper core part. The substitutions of Mn, Ca and Mg at grain margins illustrate changes in pore-water chemistry, possibly water quality, towards more oxygenated conditions and reflect sea-level rise and elevated rainfall during the early-mid Holocene. Contemporaneously with reduced iron input accompanied with drier climate conditions during the mid-late Holocene, the amount of siderites decreases and approaches zero in the upper core section. In the leeward lagoon core site, mollusk-foraminifera marly packstones and mollusk-rich wackestones accumulated ~ 5400 - 3500 yrs BP during the mid-Holocene. Rotalid and miliolid foraminifera dominate during the early-mid Holocene and are supposed to tolerate environmental stress such as changes in water quality, nutrients and salinity. Siderite is again common in the lower core section, and the abundance also decreases upcore. From mid-Holocene to the present, textularid foraminifera are prevalent in both cores indicating normal marine lagoonal conditions. Since the mid-late Holocene sea-level highstand and fall to modern level, mudstones have dominated in the windward and leeward core sites. The abundance of coral fragments has increased during the past 1000 yrs in the windward lagoon, and is assumed to result from lagoonward progradation of fringing reefs in the mid-late Holocene. Motus on the windward side of Bora Bora have hampered sediment transport and lagoonward progradation of sand aprons towards the lagoon since the late Holocene. Therefore, the increased amount of peloids in the windward core site during the past 1000 yrs is assumed to reflect early submarine lithification within the lagoon favored by low sedimentation rate and sediment stability. In summary, our study shows that sea-level and climate changes appreciably influenced sediment import, composition and distribution in the Bora Bora lagoon during the Holocene. The sensitive reaction of the lagoonal environment to external geomorphological and climate changes demonstrates the need of further research considering the global climate change in the 21st century.

5.1 Introduction

In this paper, we emphasize how and when oceanic (Darwinian) barrier-reef lagoons have responded to sea-level and climate changes in terms of temporal and spatial facies distribution and sediment composition in the recent past. Sediment sources include the lagoon itself, the

marginal reef areas and the volcanic hinterland so that their palaeoenvironmental conditions can be detected within the sediments. Such investigations are important to extent our knowledge in order to evaluate how these systems will react to future sea-level and climate changes.

There is a limited number of studies, which focused on the spatial distribution and controlling factors of recent sedimentary facies in oceanic barrier-reef systems. These include Maupiti and Bora Bora, French Polynesia (Guilcher et al., 1969; Gischler, 2011; Rankey et al., 2011), Mayotte, Indian Ocean (Masse et al., 1989), and Aitutaki, Cook Islands (Rankey et al., 2011). Core studies investigating oceanic barrier-reef lagoon successions are rather rare. Based on seismic and core data from the lagoon of Mayotte, Zinke et al. (2000, 2001, 2003a, b) interpreted Holocene lagoonal successions and sedimentary facies in terms of sequence stratigraphy and delineated lowstand, transgressive and highstand deposits. Toomey et al. (2013) identified high-energy deposits induced by tropical cyclones over the past 5000 yrs using grain-size variability in sediment cores from the barrier-reef lagoon of Tahaa, French Polynesia. However, systematic analyses of sediment composition are lacking.

To detail temporal and spatial distributions of mixed carbonate-siliciclastic facies and to better understand factors and environmental conditions controlling lagoonal sedimentation throughout the Holocene, it is mandatory to examine sediment content and faunal changes in response to sea-level and climate changes. Zinke et al. (2005) provided a detailed record of Holocene facies and faunal assemblage changes in the barrier-reef lagoon of Mayotte. In addition to the faunal composition (e.g., mollusks, foraminifera), these authors grouped lithoclasts, ferralitic concretions, aggregates and plant remains as non-skeletal fraction; however, they did not distinguish their terrestrial and marine origins.

Authigenic iron minerals such as pyrite and siderite are common features of fine-grained organic-rich sediments (Postma, 1982). Siderite precipitation is normally restricted to reducing environments (Berner, 1971) and is therefore a useful tool for palaeoenvironmental reconstructions (e.g., Mozley and Wersin 1992). Its distribution includes a wide range of localities, from freshwater to brackish to the marine realm. Postma (1982) found siderites precipitated in swamp sediments in the Skjernå delta, Ringkøbing Fjord, Denmark. Lim et al. (2004) recorded siderites in Holocene coastal freshwater sediments of Namyang Bay, Korea. Authigenic siderite microconcretions were found in Miocene sediments of Lake Baikal, Siberia by Sapota et al. (2006). In intertidal salt marshes of Norfolk, UK, Pye et al. (1990) found siderite concretions in sediments in which sulphate-reducing bacteria are active. During

a Deep Sea Drilling Project in the North-West Atlantic Ocean, Tertiary siderite-bearing hemipelagic muds were recovered (Lancelot and Ewing, 1972).

To decipher environmental conditions during siderite formation and to test whether biotic or abiotic processes are involved, elemental composition and stable isotope analyses can be used (Gautier, 1982; Mozley, 1989a; Lebeau et al., 2014), under the assumption that the trace-element composition of carbonates is strongly influenced by the chemical composition of the water in which they precipitated (e.g., Veizer, 1982).

In order to generally enlarge the restricted knowledge of oceanic barrier-reef lagoon successions, this study is designed to detail sediment composition, facies variability and changes in response to sea-level and climate change during the Holocene in Bora Bora, Pacific Ocean. In addition, this study aims deciphering the conditions of formation of syndepositional siderite in this lagoon providing a tool to reconstruct palaeoenvironmental conditions during siderite precipitation in the early Holocene.

5.2 Study area

Bora Bora is located in the northwestern part of the Society archipelago in the southern Pacific Ocean (fig. 5/1). The Society archipelago, the Austral, Gambier, Tuamotu and Marquesas islands form the overseas territory of French Polynesia in the South Pacific Ocean. A plate movement of 11 cm/yr over the Society hotspot is suggested based on increasing ages of volcanic islands from southeast (Mehetia: 0.3 Ma) to northwest (Bellingshausen: 4.3 Ma; Blais et al., 2000; Guillou et al., 2005). Radiometric (K/Ar) dating of basalts revealed an age of 3.45-3.10 Ma BP for the volcanic islands of Bora Bora, which consist of alkali basalt, rare hawaiites, intrusive gabbros, and volcanic breccia (Blais et al., 2000). The Baie de Povai is supposed to outline the caldera.

The densely wooded volcanic island of Bora Bora covers an area of about 30 km². The highest point is Mount Otemanu, which rises 727 m above sea level. The complex coastline creates peninsulas and six extensive bays: Baie Faanui, Baie Tamoo, Baie Haamaire, Baie Aponapu, Baie Faapore and Baie de Povai (fig. 5/1). Disconnected fringing reefs encircle the volcanic island. The lagoon floor is quite irregular and up to 45 m deep (Baie Aponapu) (Guilcher et al., 1969; Gischler, 2011). The extensive barrier reef system of Bora Bora including wide sand aprons, covers an area of ~70 km². Pinnacle and patch reefs occur in the deeper parts of the sand apron, however, they lack within the deep lagoon. A wide (0.7-3.3 km) and shallow (0.3-4.3 m) sand apron extends towards the lagoon and reaches its maximum in the southern part of the lagoon. The sand apron displays its minimum width of

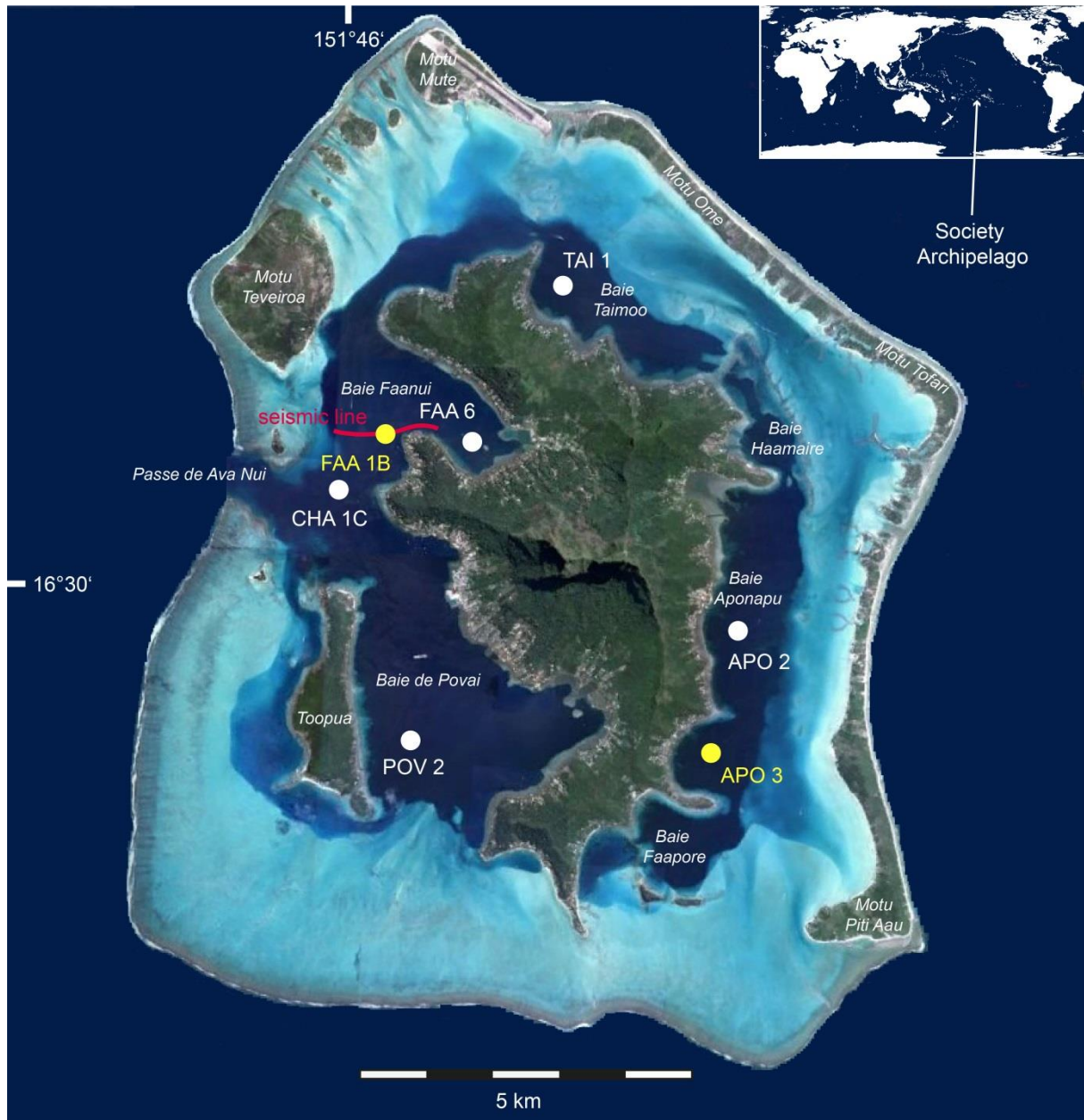


Fig. 5/1: Satellite image of Bora Bora (from Google Earth) showing vibrocore stations of Isaack et al (2016) and the seismic track line shown on figure 12. Cores analyzed in this study are marked yellow. Inset map depicts location of Society Archipelago in Pacific Ocean

0.7 km in the eastern side of the lagoon, probably due to the barrier effect of motus (elongated sand islands) on the windward side of the barrier reef, which prevent reefal sediments to be transported lagoonwards. The motus are interrupted by small passages, so-called hoas. The lack of motus on the southwestern and southern reef margin could be an expression of a southwestward tilt of the volcanic edifice (Blais et al., 2000), i.e., a deeper position of the antecedent topography (Gischler, 2011). The channel Passe de Ava Nui connects the lagoon with the open ocean in the western part of the platform and is up to 48 m deep. Ocean water enters the hoas in the east and leaves the lagoon in the west through the channel Ava Nui (Gabri  et al., 1994). On the ocean sides of the motus, coral rubble conglomerate, beachrock

and elevated fossil reef terraces occur (Pirazzoli et al. 1985, 1988; Pirazzoli and Montaggioni 1988; Rashid et al. 2014; Gischler et al. 2016). A well-developed spur and groove system can be found on the seaward side of the reef crest (Gabri  et al., 1994; Gischler, 2010).

Bora Bora has a tropical climate with a hot and rainy (austral summer) season from November to April and a dry and relatively cool season (austral winter) from May to October (Gabri  and Salvat, 1985). Prevailing trade winds blow from northeastern to southeastern directions (Pirazzoli et al., 1985a). Major storms Lisa, Reva, and Veena have passed the Society Islands during 1982-1983 (Pirazzoli et al., 1985a). Tropical cyclone Oli (category 4) hit the Society Islands in February 2010. Recently in January 2015, tropical cyclone Niko formed north of the Leeward Islands of French Polynesia and intensified while moving south. Annual average air temperatures in French Polynesia decrease from 27 to 21  C from north to south. Monthly air-temperature extremes in the Society Islands range from 24 to 28  C (Gabri  and Salvat, 1985). The spring tidal range is less than 30 cm in the Society Islands (Pirazzoli et al., 1985a). Precipitation measurements taken in Bora Bora from 1951 to 1961 show that annual precipitation rates average 2000 mm/yr (Guilcher et al., 1969). Lagoonal sea-surface temperatures ranged from 23.8 to 26.7  C in August 1963; during the same time period, salinity was slightly elevated above normal marine and ranged from 36.7 to 36.9‰ (Guilcher et al., 1969).

5.3 Methods

Based on shallow reflection seismic data, a total of thirteen vibrocore stations were selected in the deep barrier reef lagoon of Bora Bora during May 2014. The seismic survey was conducted using a GeoAcoustics 3.5 kHz 4-element pinger system mounted on an AIRE cataraft. The digitally recorded data were stored with GPS coordinates in SEG-Y format. Data was processed by applying a bandpass filter (2–6 kHz). An on-screen live navigation system was used to obtain a regular, closely-spaced survey grid with a survey speed of 5-6 km/h. Seismic data were analyzed in KingdomSuite software.

Coring was undertaken using a Rossfelder P3 vibrocorer connected with aluminum core tubes of 6 m in length and 7.5 cm in diameter. Following sediment recovery, cores were split and their tops were sealed with plastic caps. Cores were opened in the core lab of the Institute of Geoscience at the Goethe University, Frankfurt am Main and sediments were photographed and described. For detailed analyses of sediment texture, samples were taken every 2.5 cm, wet sieved through a 0.125 mm sieve and after drying through 2 mm sieve. Weight percentages of sediment fractions were calculated based on total dry weights of the samples.

Bulk samples for geochemical analyses (calciometer, XRD) were taken within an interval of 10 cm. Carbonate content of pulverized bulk sediment samples was measured using a Scheibler-type calciometer following the simple reaction of carbonate solution with hydrochloric acid (Müller, 1964). The percentages of the non-carbonate content (siliciclastic and organic material; from hereon insoluble residue) were calculated by the subtraction of percentages of the carbonate content from 100%.

In order to quantify carbonate phases and to determine qualitative mineralogy of the bulk sediment samples, x-ray powder diffraction (XRD) was performed (Milliman, 1974). Each sample was measured using a Panalytical X'Pert Pro diffractometer; mineral phases were identified using the software X'Pert HighScore Plus and MacDiff (Petschick et al., 1996). Results of XRD analyses are given with the weight-based reference intensity ratio (RIR) for each mineral phase.

One representative core from both the eastern (windward) lagoon (APO 3) and western (leeward) lagoon (FAA 1B, fig. 5/1) was selected for microfacies analysis. A total of 70 thin-sections were prepared with 10 cm sample interval with representative splits of the 2-0.125 mm fraction being embedded in epoxy resin. A total of 300 grains per thin section were point-counted after the method of Middelton et al. (1985), standard deviation was obtained from van der Plaas and Tobi (1965). Based on sedimentological, mineralogical and palaeontological analyses, sedimentary facies were defined using the classification of limestones by Dunham (1962). Component-supported and matrix-supported sediment textures were differentiated based on either more or less than 50% fines (< 0.125 mm fraction).

Carbon and oxygen isotope analyses of ten siderite samples were undertaken at the GeoZentrum Nordbayern at the University of Erlangen-Nürnberg. Siderite samples were powdered and reacted with 100% phosphoric acid at 70 °C for 48 hours using a Gasbench II connected to a ThermoFisher Delta V Plus mass spectrometer. All values are reported in per mil (‰) relative to V-PDB. Oxygen isotope values of siderite were corrected using the phosphoric acid fractionation factors given by Kim et al. (2007) and Rosenbaum and Sheppard (1986).

For the electron microprobe (EMP) analyses, two representative siderite samples were embedded in epoxy resin, polished well, cleaned and sputtered with carbon. Elemental composition and distribution were analyzed using the JEOL JXA 8200 located at the Institute of Geoscience of Mainz University, which is equipped with five wavelength-dispersive spectrometers (WDX). For the analyses a beam diameter of 5-10 µm, a 12 nA beam current and an acceleration potential of 15 kV were chosen. Peak counting times were 60 seconds

(Zn), 50 seconds (Mn, Mg, Ca) and 20 seconds (Fe). MnTiO_3 , FeCO_3 , $\text{CaMg}(\text{CO}_3)_2$ and ZnS were used as reference materials, whereas CO_2 was calculated by difference.

For scanning electron microscope (SEM) imaging, three siderite samples were coated with gold/palladium for ~4 minutes. SEM imaging was performed using a Jeol JSM 6490 LV scanning electron microscope at the Senckenberg Research Institute, Frankfurt am Main. Statistical assessments (cluster analysis, principle component analysis, correlation table) were made using the PAST software by Hammer et al. (2001). The Panplot software was used for graphical presentations (Sieger and Grobe, 2005).

To identify carbonate minerals in thin-sections, a sample from the base of core APO 3 was first stained with Alizarin red-S and afterwards stained with a combination of Alizarin red-S and NaOH (30%), following the recipes of Friedman (1959) and Wolf et al. (1967). Therefore, a solution of Alizarin red-S was mixed using 100 ml HCl (2%) and 0.2 g Alizarin red-S powder. Thin section was immersed for ca. 20 seconds in the Alizarin red-S solution and gently washed with demineralized water. For the solution of Alizarin red-S and NaOH (30%), equal volumes of Alizarin red-S and NaOH (30%) were mixed and boiled on a heating plate. Thin section was added and boiled for ca. 5 minutes and also gently washed with demineralized water afterwards.

5.4 Results

5.4.1 Microfacies

The carbonate content of the lagoon sediments consists of aragonite, high-magnesium calcite and low-magnesium calcite (tab. 5/1). To a less extent, lagoon sediments are composed of non-carbonate material (insoluble residue), which includes detrital siliciclastics and organic material (tab. 5/1). The siliciclastic component consists mainly of weathering products of basalt such as iron- and titanium-bearing hydroxides and oxides (goethite, anatase), silicates such as pyroxene (identified in thin section, see fig. 5/2e) and clay minerals such as smectite and halloysite, and pyrite (Isaack et al., 2016).

Staining with Alizarin red-S turned the colors of almost all components deeply red and gave evidence of a calcium carbonate (CaCO_3) origin. After staining with a mixture of Alizarin red-S and NaOH (30%), components made of high-magnesium calcite (e.g., foraminifera and coralline algae) turned dark pink to purple, while low-magnesium calcite and aragonite remained colorless. Siderite components stained black (fig. 5/2b, c). The siderite grains are dumbbell-shaped (figs. 5/3; 5/4a) or form aggregates (figs. 5/3; 5/4c, e). The siderite grains consist of platy rhombs (3-4 μm) and small octahedrons (< 1 μm), which

Table 5/1: Percentages of insoluble residue (siliciclastics and organic matter) and carbonate phases of core APO 3 and FAA 1B. Ara = aragonite; LMC = low-Mg calcite; HMC = high-Mg calcite; ins. res. = insoluble residue

cores core depth (cm)	APO 3				FAA 1B			
	Ara (wt%)	LMC (wt%)	HMC (wt%)	ins. res (%)	Ara (wt%)	LMC (wt%)	HMC (wt%)	ins. res (%)
0	91.7	0.7	7.6	13.2	94.4	0.8	4.8	17.1
10	92.1	0.7	7.2	10.0	94.4	0.8	4.8	17.1
20	91.8	0.8	7.4	9.7	94.7	0.7	4.6	14.1
30	91.7	0.9	7.4	8.2	94.8	0.7	4.5	11.7
40	91.7	0.8	7.5	8.6	94.5	0.7	4.8	10.5
50	91.4	0.7	7.9	16.8	94.2	0.8	5.0	8.2
60	91.5	0.8	7.7	14.1	94.1	0.8	5.0	13.2
70	91.5	0.8	7.7	8.6	93.7	0.9	5.4	20.7
80	90.2	1.9	7.9	12.0	94.1	0.7	5.2	7.7
90	90.7	0.9	8.5	9.9	94.1	0.9	5.0	10.6
100	90.6	0.9	8.5	20.4	93.4	0.8	5.8	7.1
110	89.6	2.3	8.1	11.9	93.6	0.8	5.6	8.2
120	91.6	0.7	7.6	13.8	93.6	0.7	5.7	29.2
130	91.7	0.7	7.6	5.3	93.5	0.8	5.7	10.2
140	91.7	0.7	7.6	8.0	93.8	0.8	5.4	27.2
150	91.1	0.9	8.0	11.5	93.7	0.7	5.5	24.9
160	91.3	0.9	7.7	13.3	93.6	0.9	5.5	10.2
170	91.6	0.9	7.5	13.8	93.7	0.8	5.4	12.6
180	91.4	0.9	7.7	11.8	93.7	0.9	5.4	12.8
190	91.1	1.0	7.9	15.4	93.7	0.7	5.6	10.5
200	89.6	1.2	9.2	15.4	94.1	0.8	5.0	7.3
210	89.3	1.3	9.4	19.8	92.7	1.9	5.4	12.1
220	89.5	1.3	9.2	14.5	93.2	1.0	5.8	9.9
230	89.4	1.3	9.4	9.6	93.7	1.0	5.3	11.9
240	88.8	1.2	10.0	10.5	93.2	1.1	5.7	13.3
250	89.2	1.1	9.7	14.3	93.1	1.2	5.7	11.0
260	88.9	1.4	9.7	27.4	91.8	1.9	6.3	12.6
270	89.2	1.3	9.5	23.3	91.9	1.5	6.6	21.6
280	87.4	1.6	11.0	12.0	91.0	2.2	6.8	14.8
290	87.7	1.3	11.0	11.6	91.1	1.9	7.0	22.6
300	87.6	1.2	11.2	12.6	90.6	1.9	7.5	16.2
310	86.1	1.9	12.0	16.6	85.1	5.0	9.8	18.5
320	86.6	1.5	11.9	16.8	83.8	7.0	9.2	15.8
330	85.0	1.7	13.3	20.4	77.1	12.7	10.2	18.4
340	83.3	4.1	12.6	34.7	84.9	6.2	8.9	29.3
350					83.6	7.7	8.7	34.2
mean	89.8	1.2	9.0	14.2	92.0	2.0	6.1	15.4
std	2.2	0.6	1.7	5.8	4.0	2.6	1.5	6.9

show a plate-shaped arrangement on the surface (fig. 5/4b, d, f). Partially fractured aggregated siderite grains show a lamellar or radial inner structure (figs. 5/3; 5/4e). Also in thin-sections, all siderite grains show radial structures from the center to the rim (fig. 5/2b, d). The center is darker as compared to the rim (fig. 5/2b, d) and some of the grains seem to contain opaque material (fig. 5/2d). Under crossed nicols, siderite grains show undulatory extinction. Siderite grains from the upper core samples are smaller and paler as compared to basal core samples (fig. 5/3a, c).

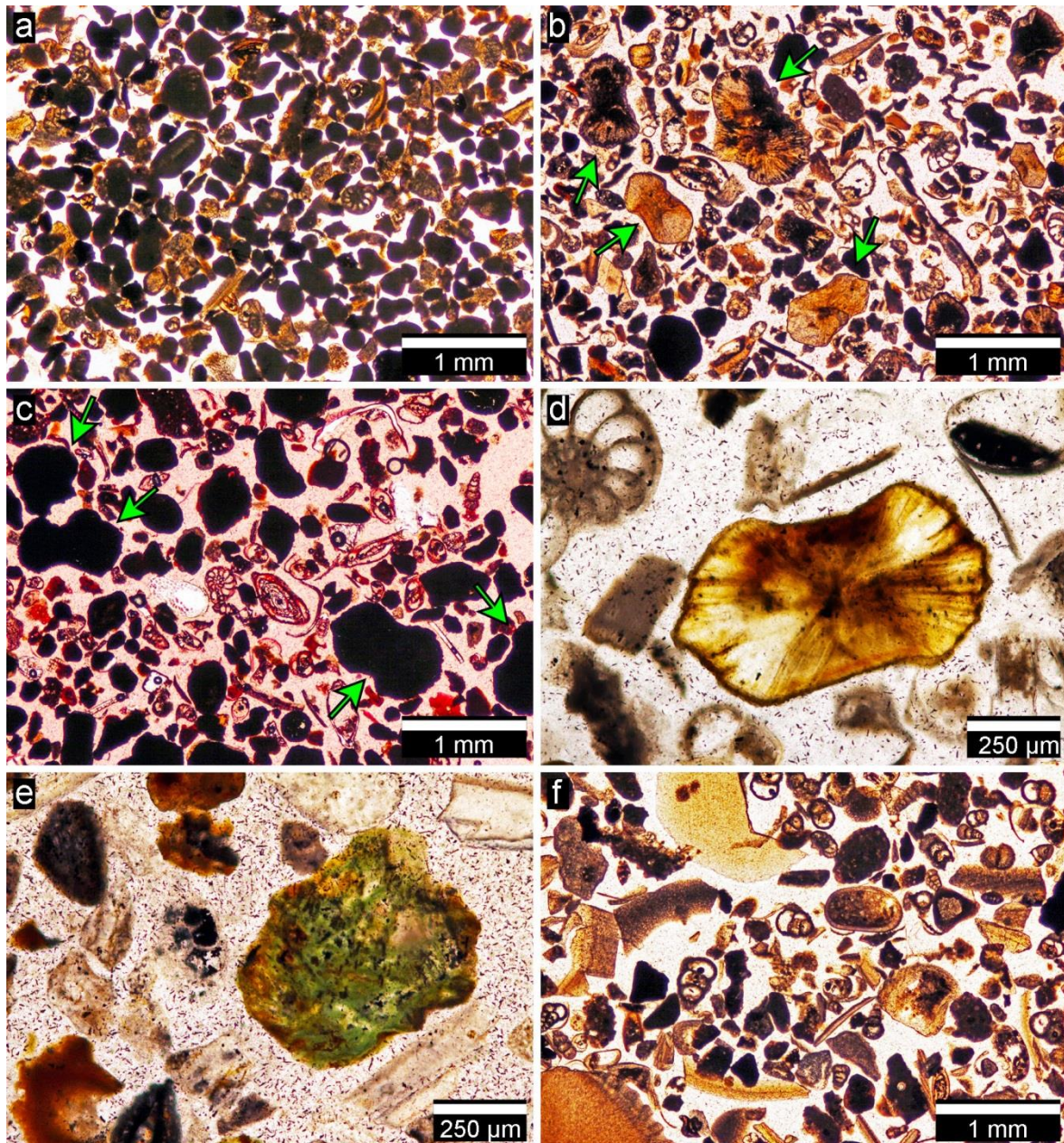


Fig. 5/2: Thin-section micrographs of sediments (2-0.125 mm fraction) showing a) peloid-rich sample from the mudstone facies, core APO 3 60 cm core depth; b) siderite grains (green arrows) differently shaped, siderite-rich wackestone, core APO 3 340 cm core depth; c) thin section stained with Alizarin red-S and NaOH (30%), note that siderites stained black (green arrows), while calcite stained pink to purple, siderite-rich wackestone facies, core APO 3 340 cm core depth; d) siderite grain showing radial structures from center to margin (see also fig. 4f), a dark rim and opaque phases within the center, foraminifera-siderite wackestone, core APO 3 320 cm core depth; e) siliciclastic grain (pyroxene), mollusk-rich wackestone, core FAA 1B 310 cm core depth; f) mollusk and foraminifera (largely miliolids) rich sample from the mudstone facies, core FAA 1B 70 cm core depth

The sediment fraction < 0.125 mm (from here on referred as mud) comprises the bulk of the lagoonal sediments. In this study, the composition of mud is not further investigated. The 2-0.125 mm sediment fraction is mostly composed of mollusk-shell fragments, benthic foraminifera, coralline algae fragments, non-skeletal grains such as peloids and aggregate grains, siderite grains, siliciclastics (olivine, pyroxene) and organic material.

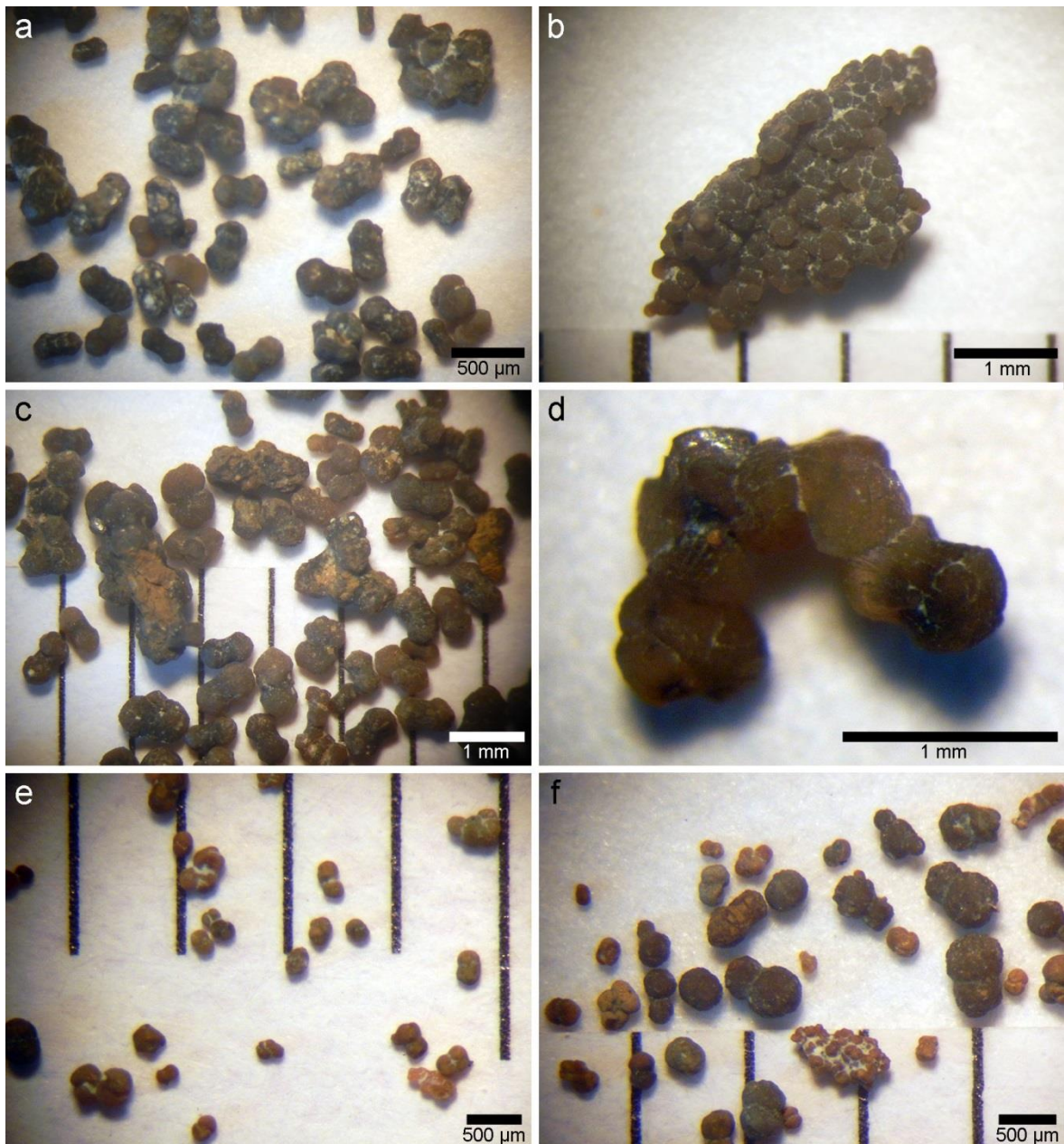


Fig. 5/3: Binocular microscope photographs of siderite grains from the 2-0.125 mm sediment fraction showing **a**) dark brown siderite grains, dumbbell-shaped, often aggregated, APO 3, 300 cm core depth (windward lagoon); **b**) nodular siderite aggregate, APO 3, 320 cm core depth (windward lagoon); **c**) dark brown siderite grains, often aggregated, larger as compared to (a), APO 3 340 cm core depth (windward lagoon); **d**) several dumbbell-shaped siderite grains, aggregated, APO 3 330 cm core depth (windward lagoon); **e**) pale brown dumbbell-shaped siderite grains and siderite aggregates; please note that siderites are smaller and lighter in the upper core section as compared to those of core APO 3, FAA 1B, 310 cm core depth (leeward lagoon); **f**) dark and pale brown siderite grains and siderite aggregates FAA 1B, 350 cm core depth (leeward lagoon)

The > 2 mm sediment fraction consists mainly of fragments of mollusk shells, serpulids tubes and crustacean carapaces.

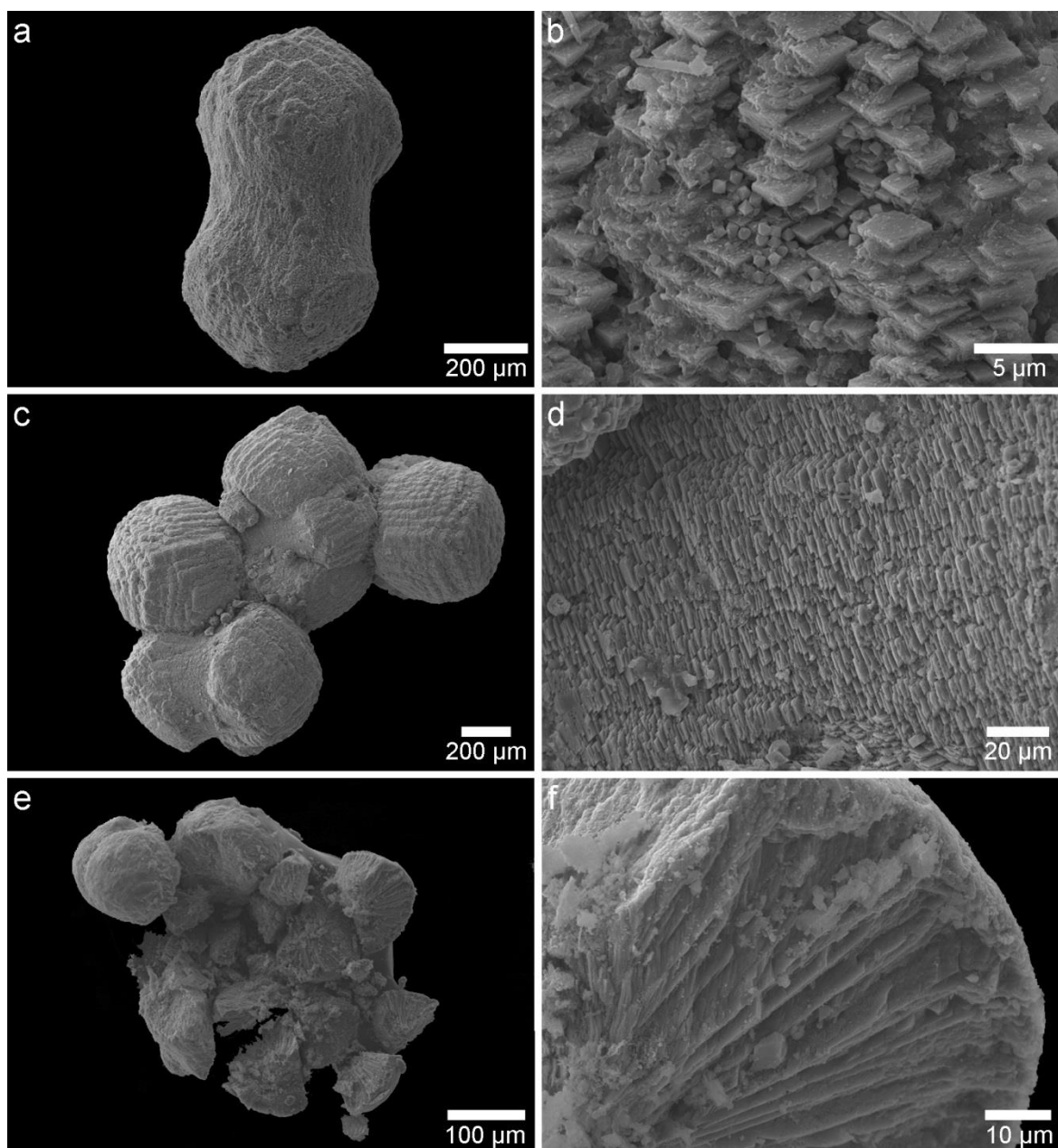


Fig. 5/4: Scanning electron microscopy (SEM) photographs showing different shapes of siderites: a) dumbbell-shaped siderite (single grain); b) close-up view shows microcrystalline structure: platy rhombs and octahedrons forming the grain surface of the dumbbell-shaped siderite; c) siderite aggregate; d) close-up view of c exhibits platy rhombs plate-shaped arranged; e) partially fractured siderite aggregate; f) close-up view of e: lamellar and fibrous inner structure of the siderite

Based on microfacies analyses, abundance trends of sediment components in both cores, APO 3 from the windward (fig. 5/5) and FAA 1B from the leeward (fig. 5/6) side, can be observed. Foraminifera are very abundant in all lagoon sediments, and the three major groups (miliolids, rotalids, textularids) show similar abundance trends in both cores. Miliolids and rotalids are very abundant at the base of the cores and their abundances decrease upcore (figs. 5/5; 5/6). The occurrence of textularids increases upcore (figs. 5/5; 5/6). In core FAA 1B from the western lagoon, mollusks are abundant at the corebase and their abundance decreases upcore (fig. 5/6). Corals and coralline algae are generally rare, but are common at the

corebase and decrease upcore (fig. 5/6). The abundance of ostracods increases upcore. The amounts of terrestrial material (siliciclastics such as olivine and pyroxene, and organic material; figs. 5/2e, 5/6) as well as siderite are very high at the corebase and decrease steadily upcore. In core APO 3 from the eastern lagoon, peloids become very abundant upcore (figs. 5/2a, 5/5). The frequency of coral fragments also increases upcore (fig. 5/5). At the corebase, siliciclastics, organic material and siderite are very abundant and decrease upcore (fig. 5/5).

Statistical assessment includes correlation analysis (tab. 5/2), principal component analysis (fig. 5/7) and cluster analysis (fig. 5/8). Point-counting on thin-sections and subsequent statistical testing delineated five sedimentary facies based on cluster analysis of textural and compositional data from both lagoon cores (figs. 5/5; 5/6; 5/7; 5/8; tab. 5/3), which are described below.

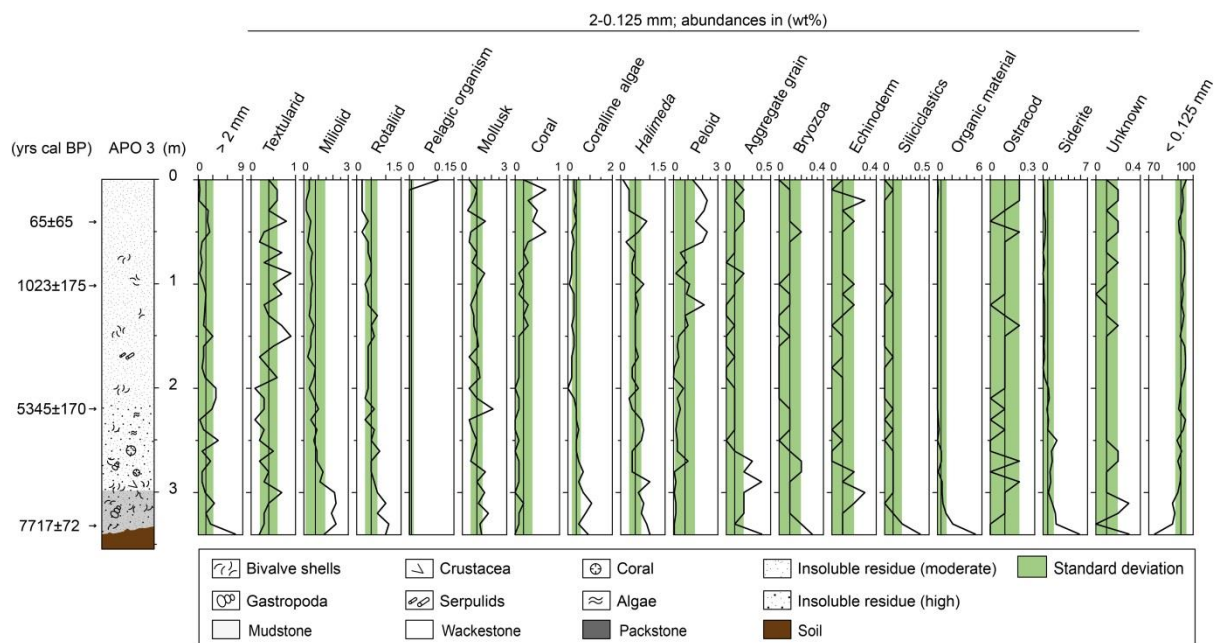


Fig. 5/5: Corelog with age data, abundance and distribution of sediment components in core APO 3

(1) Siderite-rich marly wackestone

The facies is most common at the base of core APO 3 from the windward lagoon. It is made of up to 5.7% of siderite grains, which are dumbbell-shaped (figs. 5/3; 5/4a) or form siderite aggregates (figs. 5/3; 5/4c, e) up to 1.8 mm in size. Siderite grains are present at the base of both cores. Siderite content and size reach the highest values in sediments from the eastern lagoon. Foraminifera are common with 2.6%, miliolids make up 1.4%, rotalids 1% abundance. The amount of mud is 74.4%, the > 2 mm fraction reaches 7.5%. The average content of insoluble residue from bulk sample measurements averages 34.7%. Aragonite represents 76.6%, high-magnesium calcite 17% and low-magnesium calcite 6.5%.

(2) Foraminifer-siderite wackestone

This facies occurs in core APO 3 from the windward lagoon. Major components of this facies are foraminifera with 3.4% and siderite grains with 1.6% abundance on average. Miliolid foraminifera reach with 2.1% abundance. Coralline algae and *Halimeda* are common with an average frequency of 0.8%. The fines content makes up to 87.6%. The content of aragonite yields a value of 79.6%, high-magnesium calcite 17.9% and low-magnesium calcite 2.5%. The average content of insoluble residue from bulk samples measurements is 16.6%.

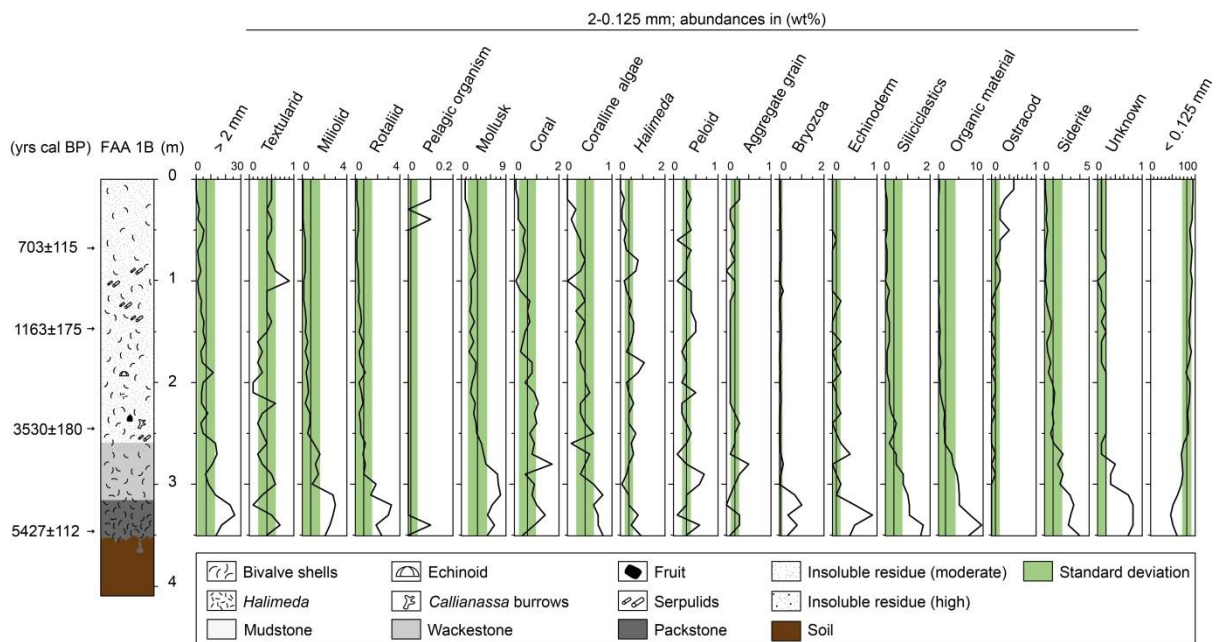


Fig. 5/6: Corelog with ages, abundance and distribution of sediment components in core FAA 1B

(3) Mollusk-foraminifer marly packstone

This facies prevails in core FAA 1B from the leeward lagoon and consists of 18.7% of components > 2 mm on average. The major common components are mollusks with 6.3% and foraminifera with 5.5% abundance on average. Rotalids and miliolids are the dominant foraminifera groups with 3% and 2.8% abundance on average. The average amount of aragonite measures 77.3%, high-magnesium calcite 12.4%, low-magnesium calcite 10.3%. The amount of insoluble residue from bulk samples measurements averages 23.2%. Mean amount of mud in this facies is 53.7%.

Table 5/2: Result of a correlation analysis of sediment compositions of cores APO 3 and FAA 1B. Note that r values are plotted in the lower left and p values in the upper right corners. R values are statistically significant when $p < 0.05$ and are marked in bold. LMC = low-Mg calcite; HMC = high-Mg calcite

	> 2 mm (wt%)	Textilard (wt%)	Miliolid (wt%)	Rotalid (wt%)	Pelagic organism (wt%)	Mollusk (wt%)	Coral (wt%)	Coralline algae (wt%)	<i>Halméda</i> (wt%)	Peloid (wt%)	Aggregate grain (wt%)	Bryozoa (wt%)	Echinoderm (wt%)	Siliciclastics (wt%)	Organic material (wt%)	Ostracod (wt%)	Siderite (wt%)	Unknown (wt%)	> 0.125 mm (wt%)	Aragonite (wt%)	LMC (wt%)	HMC (wt%)	Isoluble residue (%)
> 2 mm (wt%)		0.15	0.00	0.00	0.87	0.00	0.00	0.00	0.15	0.04	0.12	0.00	0.00	0.00	0.00	0.00	0.00	0.00	0.00	0.00	0.00	0.95	0.00
Textil. (wt%)	-0.17		0.35	0.55	0.21	0.96	0.29	0.13	0.22	0.59	0.73	0.49	0.90	0.67	0.77	0.10	0.01	0.63	0.35	0.40	0.46	0.53	0.23
Miliolid (wt%)	0.67	-0.11		0.00	0.62	0.00	0.04	0.00	0.01	0.02	0.09	0.00	0.00	0.00	0.00	0.00	0.00	0.00	0.00	0.00	0.00	0.00	0.00
Rotalid (wt%)	0.84	-0.07	0.80		0.76	0.00	0.00	0.00	0.06	0.05	0.38	0.00	0.00	0.00	0.00	0.00	0.00	0.00	0.00	0.00	0.00	0.01	0.00
Pelagic organism (wt%)	-0.02	0.15	-0.06	-0.04		0.97	0.57	0.11	0.00	0.89	0.09	0.56	0.98	0.28	0.25	0.00	0.55	0.49	0.94	0.33	0.91	0.12	0.45
Mollusk (wt%)	0.78	-0.01	0.59	0.70	0.00		0.00	0.00	0.96	0.02	0.04	0.00	0.00	0.00	0.00	0.00	0.00	0.00	0.00	0.04	0.00	0.27	0.01
Coralline algae (wt%)	0.68	-0.13	0.24	0.44	-0.07	0.67		0.19	1.00	0.97	0.02	0.01	0.00	0.00	0.00	0.01	0.05	0.00	0.00	0.80	0.00	0.00	0.57
Coral (wt%)	0.41	-0.18	0.74	0.56	-0.19	0.38	0.16		0.00	0.12	0.05	0.00	0.00	0.00	0.00	0.00	0.00	0.00	0.00	0.00	0.00	0.00	0.00
<i>Halméda</i> (wt%)	0.17	-0.15	0.33	0.22	-0.37	-0.01	0.00	0.43		0.23	0.91	0.35	0.02	0.40	0.13	0.00	0.00	0.25	0.09	0.00	0.07	0.00	0.08
Peloid (wt%)	-0.25	0.07	-0.28	-0.23	0.02	-0.27	0.00	-0.19	-0.14		0.37	0.80	0.95	0.12	0.13	0.22	0.02	0.257	0.08	0.38	0.14	0.93	0.31
Aggregate grains (wt%)	0.19	0.04	0.20	0.11	0.20	0.25	0.28	0.24	0.01	-0.11		0.32	0.68	0.03	0.00	0.33	0.01	0.08	0.02	0.12	0.10	0.33	0.13
Bryozoa (wt%)	0.68	-0.08	0.73	0.75	0.07	0.57	0.33	0.51	0.11	-0.03	0.12		0.00	0.00	0.00	0.02	0.00	0.00	0.00	0.00	0.00	0.03	0.00
Echinoderm (wt%)	0.74	0.02	0.64	0.74	0.00	0.46	0.37	0.44	0.28	-0.01	0.05	0.54		0.00	0.00	0.00	0.00	0.00	0.00	0.00	0.00	0.01	0.03
Siliciclastics (wt%)	0.81	-0.05	0.70	0.83	0.13	0.85	0.53	0.51	0.10	-0.19	0.27	0.74	0.61		0.00	0.00	0.00	0.00	0.00	0.00	0.00	0.05	0.00
Organic material (wt%)	0.81	-0.04	0.76	0.83	0.14	0.79	0.48	0.57	0.18	-0.18	0.37	0.73	0.65	0.95		0.00	0.00	0.00	0.00	0.00	0.00	0.06	0.00
Ostracod (wt%)	-0.39	0.20	-0.40	-0.43	0.41	-0.35	-0.29	-0.46	-0.42	0.15	0.12	-0.28	-0.34	-0.36	-0.37		0.00	0.01	0.00	0.00	0.00	0.02	0.01
Siderite (wt%)	0.65	-0.29	0.77	0.73	-0.07	0.54	0.23	0.71	0.37	-0.28	0.32	0.63	0.48	0.71	0.81	-0.44		0.00	0.00	0.00	0.00	0.00	0.00
Unknown (wt%)	0.80	-0.06	0.72	0.84	0.08	0.72	0.54	0.56	0.14	-0.07	0.21	0.82	0.64	0.88	0.86	-0.32	0.68		0.00	0.00	0.18	0.00	0.00
< 0.125 mm (wt%)	-0.96	0.11	-0.78	-0.90	-0.01	-0.86	-0.64	-0.55	-0.20	0.21	-0.27	-0.76	-0.73	-0.92	-0.93	0.42	-0.77	-0.89		0.00	0.00	0.26	0.00
Aragonite (wt%)	-0.45	0.10	-0.86	-0.70	0.12	-0.24	0.03	-0.71	-0.42	0.11	-0.19	-0.61	-0.61	-0.48	-0.61	0.38	-0.74	-0.59	0.57		0.00	0.00	0.00
LMC (wt%)	0.81	-0.09	0.79	0.89	0.01	0.60	0.39	0.55	0.22	-0.18	0.20	0.79	0.75	0.80	0.83	-0.35	0.75	0.87	-0.86	-0.76		0.01	0.00
HMC (wt%)	0.01	-0.08	0.62	0.30	-0.19	-0.13	-0.36	0.60	0.43	-0.01	0.18	0.20	0.29	0.06	0.22	-0.27	0.48	0.16	-0.14	-0.85	0.31		0.02
isoluble residue (%)	0.36	-0.15	0.43	0.38	0.09	0.30	0.07	0.41	0.21	-0.12	0.18	0.36	0.26	0.50	0.56	-0.29	0.63	0.40	-0.46	-0.42	0.42		0.02

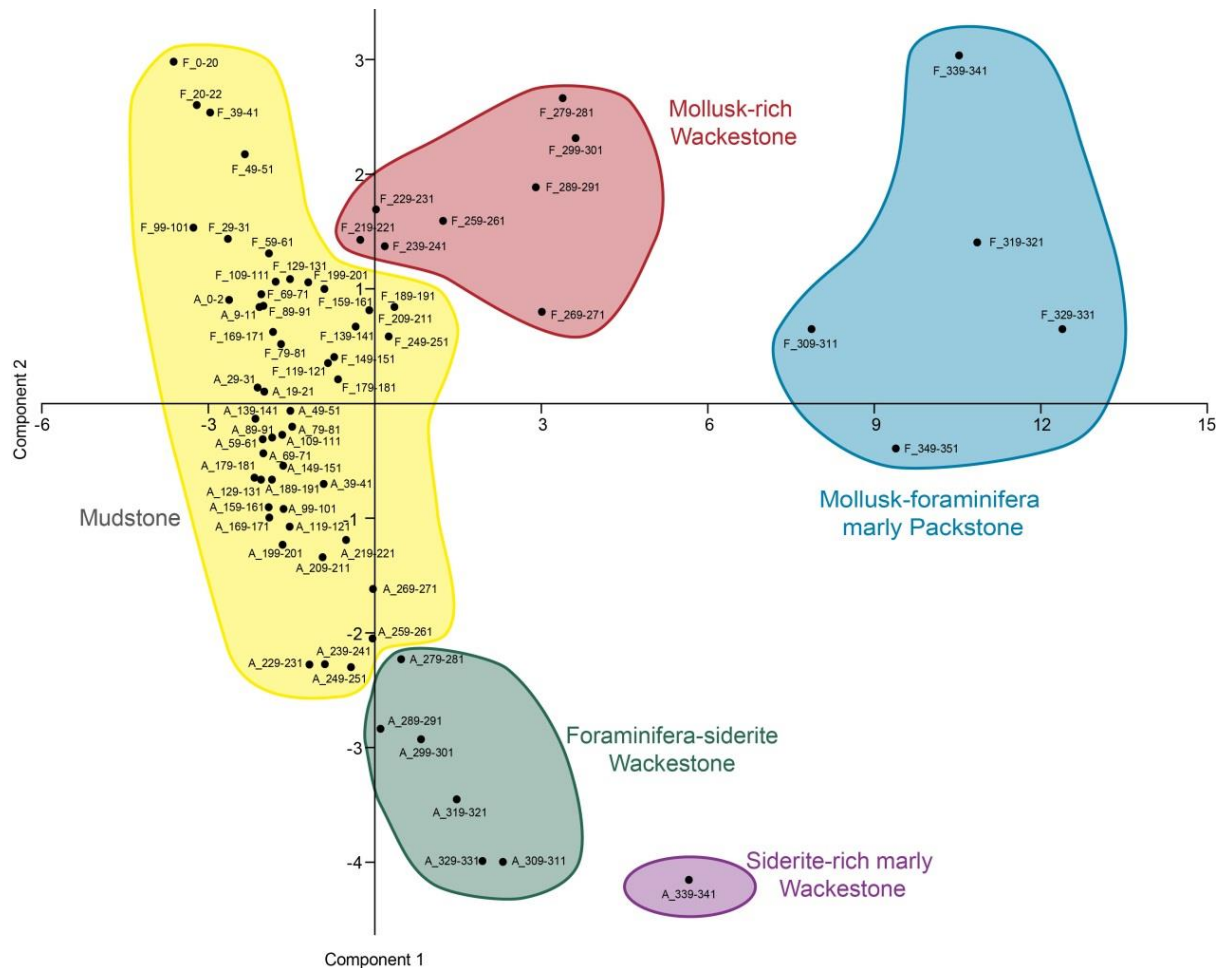


Fig. 5/7: Result of principle component analysis (PCA) based on abundances of sediment components, grain size and carbonate mineralogy of cores APO 3 and FAA 1B. Please note that labels with “A_” refer to samples of core APO 3 and labels “F_” refer to samples of core FAA 1B

(4) Mollusk-rich wackestone

This facies also occurs in core FAA 1B from the leeward lagoon and is composed of mollusk shell fragments (6% abundance). Foraminifera are very common in this facies with 2.7% abundance on average, whereas rotalids reach 1.9%. Mean proportions of mud are of 72.3%. Aragonite content is 87.3%, high-magnesium calcite 9.6%, and low-magnesium calcite 3.1%. Content of insoluble residue from bulk samples measurements averages 17.6%.

(5) Mudstone

This facies is characterized by 91.6% mud on average. The mudstone facies occurs in the windward and leeward lagoon cores, and there are only a few differences in composition. In core APO 3 from the windward lagoon, the amount of foraminifera averages 1.4% (including 0.6% miliolids), the mean values of peloid abundance is 1%. Mean aragonite content is 85.6%, high-magnesium calcite 12.5% and low-magnesium calcite 1.8%. Insoluble residue from bulk samples measurements measures 14.1%. In core FAA 1B from the leeward lagoon,

mollusks are most common with 1.9% abundance. Foraminifera are abundant components with 1.2% (including 0.5% textularids, 0.4% rotalids and 0.3% miliolids). Aragonite content averages 91.1%, high-magnesium calcite 7.6% and low-magnesium calcite 1.3%. In the western lagoon, this facies contains 24.6% of insoluble residue on average.

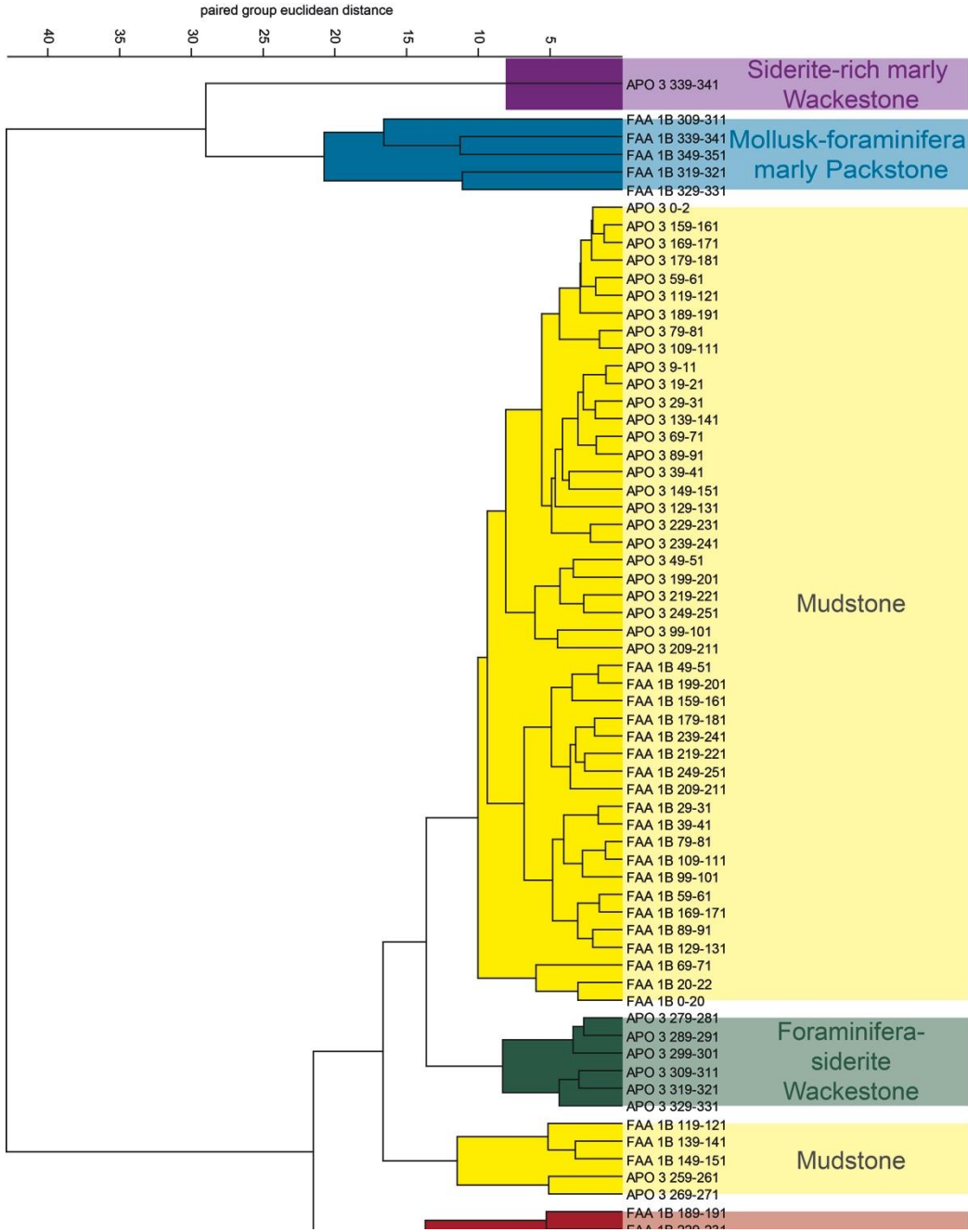


Fig. 5/8: Dendrogram of cluster analysis of data from cores APO 3 and FAA 1B. Clustering was based on the abundances of sediment components, grain size and carbonate mineralogy of each vibrocore

Table 5/3: Sediment composition, texture and geochemistry of facies of cores APO 3 and FAA 1B. Pelagic org. = pelagic organism; organic mat. = organic material; ara = aragonite; LMC = low-Mg calcite; HMC = high-Mg calcite

sample	> 2 mm (wt%)	Textilart (wt%)	Milhoit (wt%)	Rohid (wt%)	Pelagic org. (wt%)	Mollusk (wt%)	Coral (wt%)	Coralline algae (wt%)	Halimeda (wt%)	Peloids (wt%)	Aggregate grain (wt%)	Brzoza (wt%)	Echinoderm (wt%)	Siliclastics (wt%)	Organic mat. (wt%)	Ostracod (wt%)	Siderite (wt%)	Unknown (wt%)	< 0.125 mm (wt%)	Ara (wt%)	LMC (wt%)	HMC (wt%)	Insoluble (%)	
Siderite-rich marly Wackestone																								
A 339-341	7.5	0.2	1.4	1.0	0.0	1.3	0.0	0.9	1.0	0.1	0.4	0.3	0.1	0.4	5.1	0.0	5.7	0.3	74.4	76.6	6.5	17.0	34.7	
Mollusk-Foraminifera marly Packestone																								
F 309-311	13.3	0.3	2.8	1.4	0.0	8.0	0.8	0.8	0.4	0.3	0.1	0.7	0.1	1.0	4.8	0.0	2.9	0.7	61.7	79.2	8.0	12.8	18.5	
F 339-341	17.5	0.7	2.5	1.9	0.1	6.7	0.9	0.7	0.5	0.6	0.3	0.8	0.5	1.7	9.8	0.0	2.7	0.8	51.0	80.3	8.1	11.5	29.3	
F 349-351	13.8	0.4	2.1	2.4	0.0	5.3	0.4	0.8	0.9	0.3	0.1	0.4	0.5	1.6	6.9	0.0	3.9	0.7	59.5	78.9	9.5	11.6	34.2	
F 319-321	22.9	0.1	3.0	3.3	0.0	6.3	1.0	0.6	0.4	0.3	0.0	1.0	0.5	1.1	4.8	0.0	3.3	0.8	50.7	77.4	11.0	11.6	15.8	
F 329-331	26.2	0.5	2.8	3.0	0.0	5.4	1.4	0.7	0.8	0.1	0.3	0.4	0.9	1.1	7.1	0.0	3.0	0.8	45.5	70.5	15.0	14.4	18.4	
mean	18.7	0.4	2.7	2.4	0.0	6.3	0.9	0.7	0.6	0.3	0.2	0.6	0.5	1.3	6.7	0.0	3.2	0.8	53.7	77.3	10.3	12.4	23.2	
std	5.7	0.2	0.3	0.8	0.0	1.1	0.4	0.1	0.2	0.2	0.1	0.3	0.3	0.3	2.0	0.0	0.5	0.1	6.7	3.9	2.9	1.3	8.0	
Mudstone																								
A 0-2	0.2	0.4	0.4	0.2	0.1	0.5	0.2	0.3	0.1	1.3	0.1	0.0	0.1	0.0	0.0	0.2	0.1	0.1	95.7	87.7	1.3	10.9	13.2	
A 159-161	1.1	0.5	0.5	0.4	0.0	1.1	0.1	0.3	0.5	0.3	0.0	0.0	0.1	0.0	0.0	0.1	0.2	0.1	94.4	87.0	1.6	11.4	13.3	
A 169-171	1.2	0.2	0.3	0.4	0.0	0.5	0.1	0.2	0.6	0.4	0.1	0.0	0.1	0.1	0.1	0.1	0.3	0.1	95.2	87.2	1.5	11.3	13.8	
A 179-181	0.8	0.4	0.8	0.4	0.0	1.1	0.1	0.2	0.4	0.1	0.0	0.0	0.0	0.0	0.1	0.1	0.1	0.1	95.1	87.5	1.5	11.0	11.8	
A 59-61	0.8	0.2	0.3	0.4	0.0	0.5	0.3	0.3	0.2	2.0	0.1	0.1	0.1	0.0	0.1	0.1	0.3	0.1	94.2	87.3	1.4	11.2	14.1	
A 119-121	1.4	0.3	0.5	0.4	0.0	0.6	0.3	0.3	0.6	2.1	0.0	0.1	0.2	0.0	0.1	0.0	0.3	0.1	92.6	87.3	1.3	11.4	13.8	
A 189-191	1.4	0.6	0.7	0.4	0.0	1.2	0.1	0.2	0.4	0.0	0.0	0.0	0.1	0.1	0.0	0.1	0.3	0.1	94.3	87.0	1.6	11.4	15.4	
A 79-81	0.9	0.3	0.5	0.5	0.0	0.7	0.3	0.2	0.4	0.9	0.0	0.1	0.1	0.0	0.1	0.1	0.3	0.2	94.5	86.5	4.1	9.4	12.0	
A 109-111	1.6	0.7	0.5	0.4	0.0	0.9	0.1	0.3	0.5	0.9	0.1	0.1	0.1	0.1	0.1	0.1	0.2	0.0	93.4	86.8	4.3	8.9	11.9	
A 9-11	0.4	0.6	0.4	0.2	0.0	1.0	0.7	0.3	0.3	1.9	0.2	0.1	0.0	0.1	0.2	0.2	0.2	0.2	93.1	88.3	1.3	10.3	10.0	
A 19-21	0.2	0.6	0.2	0.2	0.0	0.8	0.3	0.4	0.3	2.3	0.1	0.1	0.3	0.0	0.1	0.2	0.2	0.2	93.3	87.9	1.3	10.9	9.7	
A 29-31	2.1	0.4	0.2	0.2	0.0	0.4	0.5	0.3	0.3	2.1	0.2	0.1	0.1	0.0	0.1	0.1	0.2	0.1	92.8	87.6	1.4	11.0	8.2	
A 139-141	1.1	0.7	0.7	0.5	0.0	0.8	0.3	0.2	0.5	1.0	0.1	0.0	0.0	0.0	0.1	0.1	0.2	0.3	93.2	87.3	1.3	11.4	8.0	
A 69-71	0.6	0.7	0.6	0.4	0.0	1.0	0.2	0.2	0.5	0.5	0.1	0.1	0.1	0.0	0.0	0.1	0.1	0.1	94.7	87.3	1.4	11.4	8.6	
A 89-91	0.4	0.9	0.5	0.5	0.0	1.5	0.1	0.2	0.4	0.2	0.2	0.1	0.1	0.0	0.0	0.1	0.1	0.1	94.6	86.5	1.5	12.0	9.9	
A 39-41	2.0	0.8	0.5	0.4	0.0	1.6	0.4	0.4	0.9	1.5	0.2	0.1	0.2	0.0	0.0	0.0	0.4	0.2	90.5	87.5	1.6	10.9	8.6	
A 149-151	3.1	0.9	0.5	0.6	0.0	1.0	0.1	0.3	0.5	0.4	0.0	0.1	0.1	0.0	0.1	0.1	0.3	0.1	91.7	87.1	1.5	11.4	11.5	
A 129-131	1.3	0.4	0.4	0.7	0.0	0.8	0.2	0.3	0.5	0.8	0.0	0.0	0.1	0.0	0.1	0.1	0.3	0.1	94.0	87.5	1.3	11.2	5.3	
A 229-231	0.4	0.1	0.5	0.3	0.0	0.5	0.0	0.4	0.7	0.3	0.1	0.1	0.1	0.0	0.2	0.0	0.9	0.1	95.2	84.8	2.1	13.1	9.6	
A 239-241	1.1	0.3	0.9	0.6	0.0	0.7	0.0	0.5	0.8	0.2	0.1	0.1	0.0	0.1	0.3	0.1	0.8	0.1	93.5	84.6	1.9	13.4	10.5	
A 49-51	2.4	0.3	0.4	0.2	0.0	0.6	0.7	0.2	0.6	2.3	0.1	0.2	0.1	0.0	0.1	0.2	0.4	0.2	91.2	87.3	1.3	11.4	16.8	
A 199-201	3.6	0.1	0.4	0.4	0.0	0.5	0.0	0.0	0.6	0.7	0.1	0.0	0.1	0.0	0.1	0.1	0.9	0.1	92.2	85.8	1.8	12.4	15.4	
A 219-221	2.9	0.3	1.0	0.6	0.0	2.1	0.1	0.4	0.5	0.1	0.1	0.1	0.1	0.0	0.1	0.1	0.7	0.1	90.5	84.5	2.5	13.0	14.5	
A 249-251	4.1	0.2	0.7	0.5	0.0	1.0	0.1	0.4	0.7	0.3	0.0	0.0	0.1	0.0	0.1	0.0	2.2	0.1	89.6	84.8	1.7	13.5	14.3	
A 99-101	1.2	0.5	0.6	0.3	0.0	1.1	0.2	0.1	0.8	1.1	0.1	0.0	0.2	0.0	0.1	0.1	0.2	0.1	93.2	87.4	1.5	11.1	20.4	
A 209-211	3.7	0.3	0.7	0.3	0.0	1.0	0.1	0.3	0.3	0.3	0.1	0.0	0.1	0.0	0.1	0.0	1.0	0.1	91.6	85.0	2.0	12.9	19.8	
F 49-51	5.3	0.5	0.2	0.3	0.0	2.1	0.5	0.2	0.3	0.4	0.2	0.1	0.0	0.1	0.1	0.4	0.4	0.1	88.6	91.9	1.3	6.9	8.2	
F 199-201	5.0	0.1	0.5	0.4	0.0	2.3	0.5	0.4	0.3	0.2	0.1	0.0	0.0	0.2	0.5	0.1	0.9	0.2	88.1	91.3	1.3	7.4	7.3	
F 159-161	6.7	0.2	0.5	0.7	0.0	2.5	0.4	0.2	0.5	0.3	0.1	0.1	0.2	0.2	0.3	0.1	0.3	0.1	87.0	91.0	1.3	7.7	10.2	
F 179-181	4.2	0.2	0.6	0.5	0.0	3.0	0.8	0.3	1.1	0.3	0.1	0.0	0.1	0.1	0.6	0.1	0.7	0.1	87.0	90.8	1.5	7.7	12.8	
F 239-241	3.6	0.2	0.7	0.5	0.0	3.1	1.0	0.4	0.4	0.3	0.3	0.0	0.0	0.5	1.3	0.0	1.1	0.2	86.1	90.1	1.8	8.1	13.3	
F 219-221	4.0	0.6	0.3	0.7	0.0	2.8	1.1	0.3	0.6	0.2	0.1	0.1	0.1	0.2	0.9	0.0	1.1	0.2	86.7	90.7	1.6	7.7	9.9	
F 249-251	5.0	0.3	0.5	0.5	0.0	3.2	0.7	0.6	0.7	0.4	0.2	0.0	0.1	0.4	1.5	0.0	0.7	0.2	85.1	90.0	1.9	8.0	11.0	
F 209-211	3.8	0.1	0.6	0.6	0.0	2.0	0.9	0.5	0.4	0.5	0.1	0.1	0.1	0.1	0.2	0.5	0.1	1.2	0.2	88.1	89.1	3.3	7.6	12.1
F 29-31	2.2	0.4	0.1	0.3	0.0	1.5	0.2	0.2	0.1	0.3	0.1	0.1	0.0	0.1	0.1	0.1	0.2	0.3	93.8	92.0	1.1	6.9	11.7	

Continue on next page

sample	> 2 mm (wt%)	Texturite (wt%)	Miloid (wt%)	Rohid (wt%)	Pelagic org. (wt%)	Mollusk (wt%)	Coral (wt%)	Coralline algae (wt%)	Halimeda (wt%)	Peloids (wt%)	Aggregate grain (wt%)	Bryozoa (wt%)	Echinoderm (wt%)	Siliclastics (wt%)	Organic mat. (wt%)	Ostracod (wt%)	Siderite (wt%)	Unknown (wt%)	< 0.125 mm (wt%)	Arca (wt%)	LMC (wt%)	HMC (wt%)	soluble residue (%)
Mudstone (continuation)																							
F 39-41	1.3	0.5	0.1	0.3	0.1	1.9	0.2	0.1	0.1	0.3	0.1	0.0	0.0	0.1	0.1	0.2	0.2	0.1	94.2	91.9	1.3	6.9	10.5
F 79-81	1.8	0.5	0.3	0.2	0.0	2.4	0.4	0.4	0.8	0.3	0.2	0.1	0.0	0.1	0.1	0.1	0.1	0.2	92.1	91.5	1.2	7.3	7.7
F 109-111	2.0	0.4	0.2	0.4	0.0	2.1	0.3	0.3	0.3	0.4	0.2	0.2	0.0	0.2	0.3	0.1	0.3	0.1	92.3	91.0	1.3	7.7	8.2
F 99-101	1.3	0.9	0.2	0.3	0.0	1.9	0.1	0.0	0.2	0.1	0.2	0.0	0.0	0.0	0.0	0.2	0.1	0.0	94.5	91.1	1.3	7.6	7.1
F 59-61	4.4	0.4	0.3	0.2	0.0	1.8	0.4	0.3	0.2	0.1	0.2	0.1	0.1	0.0	0.1	0.2	0.2	0.1	90.9	91.1	1.3	7.6	13.2
F 169-171	3.4	0.3	0.3	0.4	0.0	1.7	0.3	0.3	0.3	0.2	0.1	0.0	0.0	0.1	0.2	0.0	0.4	0.1	91.8	91.2	1.4	7.4	12.6
F 89-91	3.3	0.6	0.3	0.3	0.0	2.8	0.3	0.3	0.7	0.3	0.0	0.0	0.1	0.1	0.1	0.2	0.2	0.2	90.2	91.6	1.3	7.1	10.6
F 129-131	3.6	0.4	0.3	0.5	0.0	1.8	0.6	0.2	0.4	0.4	0.1	0.0	0.1	0.1	0.3	0.1	0.5	0.2	90.6	90.5	1.4	8.1	10.2
F 69-71	1.1	0.4	0.3	0.2	0.0	1.9	0.5	0.3	0.3	0.4	0.1	0.1	0.0	0.1	0.1	0.2	0.1	0.1	93.9	90.7	1.4	7.8	20.7
F 20-22	0.6	0.5	0.1	0.2	0.1	0.9	0.2	0.0	0.2	0.4	0.3	0.0	0.0	0.1	0.1	0.3	0.2	0.1	95.9	92.0	1.2	6.8	14.1
F 0-20	0.4	0.5	0.1	0.2	0.1	0.8	0.1	0.0	0.0	0.3	0.3	0.0	0.0	0.0	0.2	0.5	0.1	0.1	96.2	91.8	1.3	6.9	17.1
mean	2.2	0.4	0.4	0.4	0.0	1.4	0.3	0.3	0.4	0.7	0.1	0.1	0.1	0.1	0.2	0.1	0.4	0.1	92.1	88.6	1.6	9.7	11.9
std	1.6	0.2	0.2	0.2	0.0	0.8	0.3	0.1	0.2	0.6	0.1	0.0	0.1	0.1	0.3	0.1	0.4	0.0	2.8	2.4	0.7	2.2	3.5
Foraminifera-Siderite Wackestone																							
A 279-281	0.9	0.4	1.3	0.5	0.0	1.6	0.1	0.7	0.4	0.1	0.2	0.2	0.2	0.1	0.2	0.0	1.1	0.1	91.9	82.2	3.3	14.5	12.0
A 289-291	0.9	0.3	1.1	0.6	0.0	1.0	0.1	0.5	1.0	0.2	0.4	0.1	0.1	0.1	0.7	0.2	1.3	0.1	91.5	81.4	2.2	16.4	11.6
A 299-301	1.4	0.7	2.1	0.7	0.0	1.5	0.0	0.7	0.6	0.1	0.2	0.1	0.3	0.1	0.7	0.1	0.9	0.1	89.7	80.8	2.1	17.1	12.6
A 309-311	3.3	0.4	2.2	1.0	0.0	1.1	0.2	1.1	0.8	0.2	0.2	0.1	0.2	0.0	0.8	0.1	1.5	0.3	86.5	78.7	3.0	18.3	16.6
A 319-321	1.6	0.3	1.9	0.7	0.0	1.8	0.1	0.8	0.7	0.2	0.2	0.1	0.1	0.1	1.2	0.1	2.0	0.2	88.0	80.0	2.3	17.7	16.8
A 329-331	2.5	0.3	2.2	1.1	0.0	1.2	0.1	0.5	0.9	0.1	0.1	0.2	0.1	0.2	2.1	0.0	2.1	0.0	86.3	78.9	2.8	18.4	20.4
mean	1.8	0.4	1.8	0.8	0.0	1.4	0.1	0.7	0.9	0.7	0.2	0.2	0.1	0.2	0.1	0.9	1.5	0.1	89.0	80.3	2.6	17.1	15.0
std	1.0	0.2	0.5	0.2	0.0	0.3	0.1	0.2	0.2	0.0	0.1	0.1	0.1	0.1	0.7	0.1	0.5	0.1	2.4	1.4	0.5	1.5	3.5
Mudstone																							
F 119-121	3.7	0.4	0.2	0.3	0.0	2.1	0.7	0.4	0.5	0.4	0.1	0.0	0.2	0.1	0.1	0.0	0.2	0.1	90.4	90.5	1.2	8.3	29.2
F 139-141	5.6	0.5	0.4	0.6	0.0	2.7	0.7	0.4	0.6	0.5	0.1	0.1	0.0	0.2	0.3	0.0	0.8	0.1	86.3	91.1	1.5	7.4	27.2
F 149-151	5.1	0.4	0.3	0.4	0.0	1.8	0.5	0.3	0.6	0.5	0.1	0.1	0.0	0.2	0.4	0.0	0.7	0.2	88.2	90.9	1.2	7.9	24.9
A 269-271	2.5	0.2	0.9	0.5	0.0	0.6	0.1	0.5	0.4	1.0	0.3	0.2	0.0	0.1	0.6	0.2	1.5	0.2	90.0	83.5	2.4	14.1	23.3
A 279-281	0.9	0.4	1.3	0.5	0.0	1.6	0.1	0.7	0.4	0.1	0.2	0.2	0.2	0.1	0.2	0.0	1.1	0.1	91.9	82.2	3.3	14.5	12.0
mean	3.5	0.4	0.6	0.5	0.0	1.8	0.4	0.5	0.5	0.5	0.2	0.1	0.1	0.1	0.3	0.1	0.9	0.2	89.4	87.7	1.9	10.4	23.3
std	1.9	0.1	0.5	0.1	0.0	0.8	0.3	0.1	0.1	0.3	0.1	0.1	0.1	0.1	0.2	0.1	0.5	0.0	2.2	4.4	0.9	3.5	6.7
Mollusk-rich Wackestone																							
F 189-191	11.8	0.3	0.4	0.9	0.0	2.8	0.8	0.4	0.8	0.3	0.1	0.1	0.2	0.1	0.3	0.0	0.5	0.2	79.9	90.7	1.1	8.2	10.5
F 229-231	8.1	0.3	0.7	0.4	0.0	2.6	0.9	0.3	0.4	0.2	0.2	0.0	0.2	0.3	1.4	0.1	0.9	0.2	83.0	90.7	1.6	7.8	11.9
F 259-261	13.3	0.4	1.1	0.9	0.0	4.1	0.9	0.1	0.5	0.3	0.2	0.0	0.2	0.2	1.4	0.0	1.1	0.1	75.0	87.7	3.4	8.8	12.6
F 279-281	11.3	0.3	1.2	0.9	0.0	5.1	1.7	0.4	0.4	0.3	0.5	0.2	0.0	0.5	3.3	0.0	1.5	0.4	71.9	86.7	3.9	9.4	14.8
F 299-301	8.3	0.6	0.9	1.9	0.0	7.5	0.9	0.6	0.1	0.6	0.2	0.0	0.2	0.8	4.5	0.0	1.8	0.3	70.6	86.9	2.8	10.3	16.2
F 269-271	14.0	0.2	1.6	0.7	0.0	4.6	0.8	0.5	0.6	0.1	0.1	0.1	0.4	0.5	3.1	0.1	2.1	0.1	70.5	88.1	2.4	9.5	21.6
F 289-291	6.5	0.5	1.5	0.8	0.0	7.4	0.5	0.3	0.3	0.7	0.3	0.1	0.1	0.8	4.3	0.1	2.1	0.3	73.4	87.3	3.0	9.8	22.6
mean	10.5	0.4	1.1	0.9	0.0	4.9	0.9	0.4	0.5	0.3	0.2	0.1	0.2	0.5	2.6	0.0	1.4	0.2	74.9	88.3	2.6	9.1	15.7
std	2.9	0.1	0.4	0.5	0.0	2.0	0.4	0.2	0.2	0.2	0.1	0.1	0.1	0.3	1.6	0.0	0.6	0.1	4.8	1.7	1.0	0.9	4.7

5.4.2 Stable Isotope analyses of siderite

The isotopic composition of siderites is summarized in table 4 and illustrated in figure 5/9. Analyses of oxygen and carbon stable isotope ratios in siderites from core APO 3 (windward) indicate $\delta^{18}\text{O}$ values ranging from +0.32 to +0.54‰ and $\delta^{13}\text{C}$ values ranging from -13.61 to -14.48‰ (fig. 5/9b). Siderite samples from core FAA 1B (leeward) indicate isotope values of $\delta^{18}\text{O}$ ranging from +0.1 to -0.35‰ and those of $\delta^{13}\text{C}$ ranging from -16.31 to -17.06‰ (fig. 5/9d).

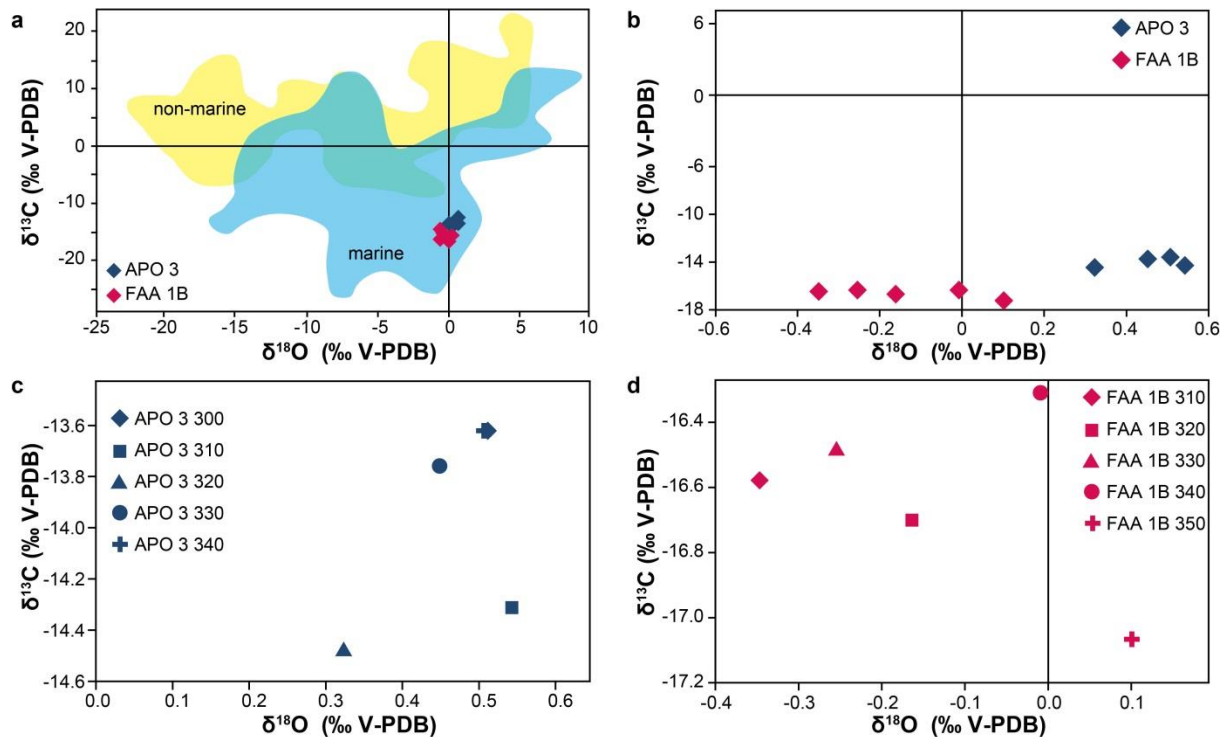


Fig. 5/9: Oxygen versus carbon isotopes ratios of **a)** samples from cores APO 3 and FAA 1B plotted in marine versus non-marine fields (modified after Mozley and Wersin, 1992); **b)** detailed sample plots of cores APO 3 and FAA 1B **c)** samples from different core depths of core APO 3; **d)** samples from different core depths of core FAA 1B

Table 5/4: Isotopic composition of lagoonal siderites, $\delta^{13}\text{C}$ and $\delta^{18}\text{O}$ in ‰ V-PDB

sample	$\delta^{18}\text{O}_{\text{Sid}}$ (‰)	$\delta^{13}\text{C}_{\text{Cal}}$ (‰)
APO 3 290-301	0.51	-13.61
APO 3 309-311	0.54	-14.30
APO 3 319-321	0.32	-14.48
APO 3 329-331	0.45	-13.77
APO 3 339-341	0.51	-13.61
FAA 1B 309-311	-0.35	-16.58
FAA 1B 319-321	-0.16	-16.71
FAA 1B 329-331	-0.25	-16.48
FAA 1B 339-341	-0.01	-16.31
FAA 1B 349-351	0.10	-17.06

5.4.3 Electron Microprobe analyses of siderite

The EMP data were recalculated to obtain molar percentages of stoichiometrically ideal carbonate minerals. Selective measurements of Fe, Ca, Mn and Mg of two siderite samples from different core depths show significant variations in the composition of analyzed elements. The siderite aggregate from 330 cm core depth is relatively impure in its composition with variations in Fe content of 82.76-88.28 mol%, a Mn content of 11.31-16.22 mol%, a Ca content of 0.4-0.98 mol% and a Mg content of 0.01-0.12 mol% (fig. 5/10a; tab. 5/5). The dumbbell-shaped siderite grain from 340 cm core depth has a relatively pure composition with variations in Fe content of 90.98-94.38 mol%, Mn content of 4.66-6.38 mol%, Ca content of 0.36-1.24 mol% and Mg content of 0.11-0.43 mol% (fig. 5/11a; tab. 5/5). Element mapping of siderite samples shows that the grain center contains high Fe concentrations, while higher Mn, Ca and Mg concentrations prevail towards the grain margins (figs. 5/10c, d, f; 5/11c, d, f). The radial structures are enriched in Ca and Mn (fig. 5/11c, f).

Table 5/5: Elemental composition of two siderite samples from core APO 3. Please note that analyzed points are marked in figs. 10a; 11a

sample		siderite aggregate, 330 cm core depth (see fig. 10a)							
Analyzed points		76	77	78	79	80	81	82	83
atomic fraction	CaO	0.21	0.19	0.18	0.18	0.41	0.38	0.47	0.37
	MgO	0.04	0.03	0.00	0.00	0.02	0.01	0.01	0.02
	MnO	7.50	7.37	6.66	6.78	9.58	9.35	9.84	8.46
	FeO	52.29	52.20	52.62	52.60	50.49	50.96	50.85	51.24
	CO ₂	36.89	36.74	36.51	36.57	37.21	37.32	37.63	36.95
	Total	96.94	96.53	95.98	96.14	97.71	98.02	98.80	97.03
mol %	CaCO ₃	0.45	0.42	0.40	0.40	0.87	0.81	0.98	0.79
	MgCO ₃	0.12	0.10	0.00	0.01	0.05	0.03	0.04	0.07
	MnCO ₃	12.62	12.45	11.31	11.50	15.97	15.53	16.22	14.20
	FeCO ₃	86.81	87.03	88.28	88.10	83.11	83.64	82.76	84.95
	Total	100.00	100.00	100.00	100.00	100.00	100.00	100.00	100.00

sample		dumbbell-shaped siderite, 340 cm core depth (see fig. 11a)							
Analyzed points		84	85	86	87	88	89	90	91
atomic fraction	CaO	1.10	1.27	1.24	0.86	0.36	0.40	0.70	0.62
	MgO	0.07	0.05	0.04	0.05	0.06	0.14	0.12	0.10
	MnO	3.82	3.70	3.72	3.27	2.72	2.74	3.16	2.85
	FeO	55.21	55.15	53.96	56.41	55.91	54.79	52.60	53.80
	CO ₂	37.13	37.13	36.37	37.31	36.29	35.73	34.86	35.33
	Total	97.33	97.29	95.32	97.89	95.34	93.80	91.45	92.70
mol %	CaCO ₃	2.33	2.68	2.67	1.80	0.78	0.88	1.58	1.38
	MgCO ₃	0.22	0.16	0.11	0.15	0.19	0.43	0.37	0.32
	MnCO ₃	6.38	6.18	6.35	5.44	4.66	4.76	5.62	5.01
	FeCO ₃	91.07	90.98	90.87	92.61	94.38	93.93	92.42	93.29
	Total	100.00	100.00	100.00	100.00	100.00	100.00	100.00	100.00

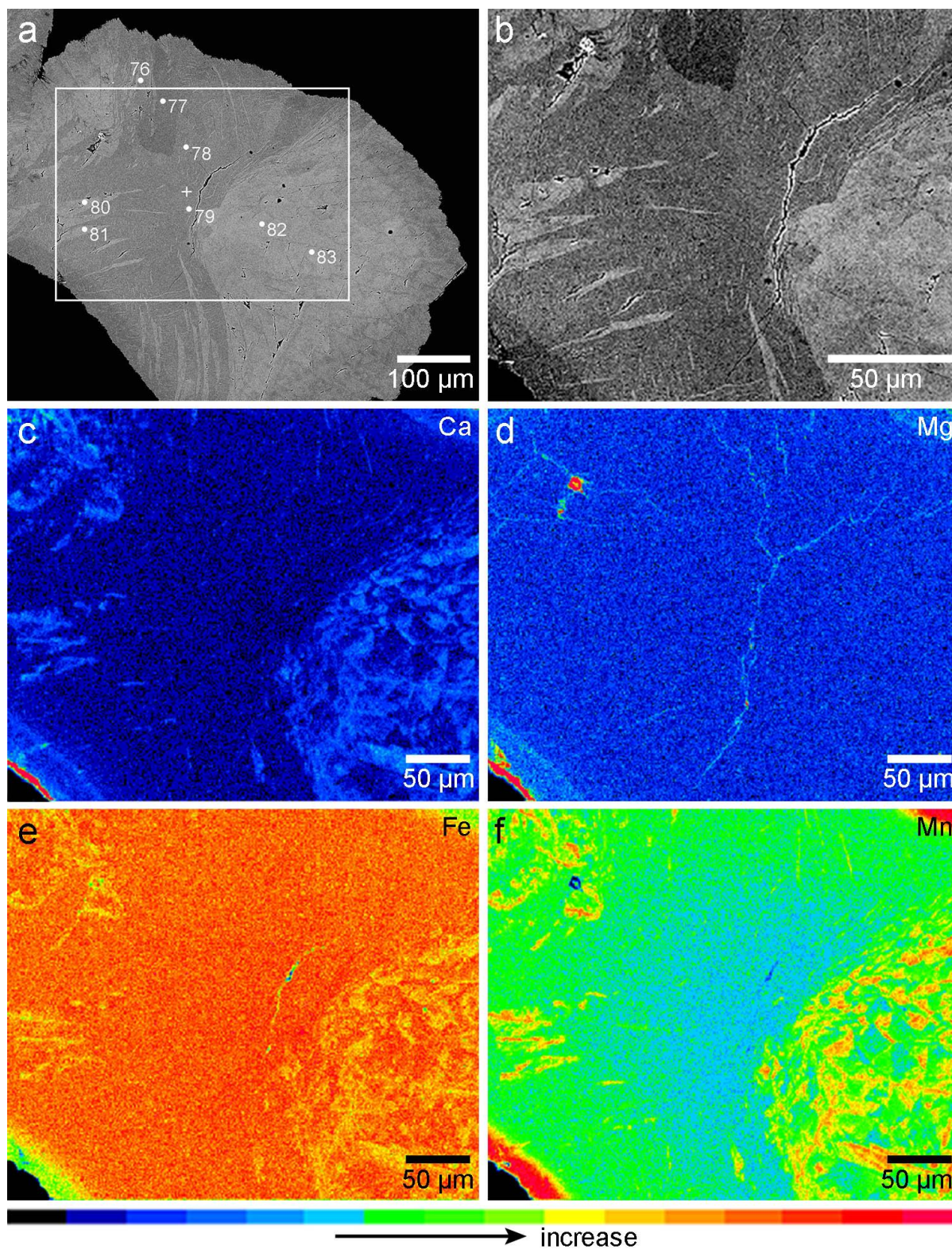


Fig. 5/10: Siderite aggregate from core APO 3 showing a) backscattered electron image with overview of analyzed area (element map) and marked points of EMP analyses; b) backscattered electron image with compositional contrast; c) element map with variations in Ca content; d) element map with variations in Mg content; e) element map with variations in Fe content; f) element map with variations in Mn content

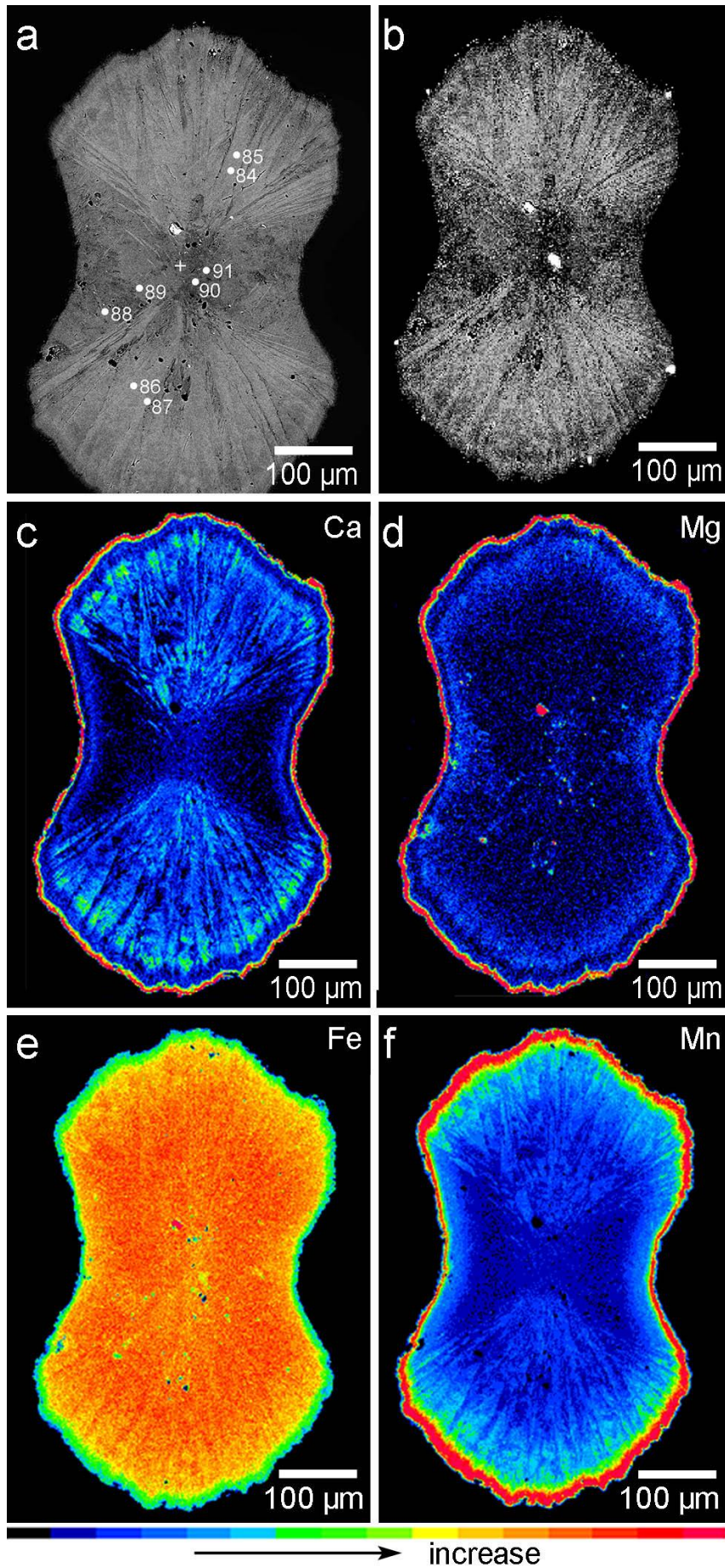


Fig. 5/11: Dumbbell-shaped siderite grain from core APO 3 showing **a)** backscattered electron image with marked points of EMP analyses; **b)** backscattered electron image with compositional contrast; **c)** element map with variations in Ca content; **d)** element map with variations in Mg content; **e)** element map with variations in Fe content; **f)** element map with variations in Mn content

5.5. Discussion

5.5.1 Lagoon facies in response to Holocene sea-level and climate variations

The rising Holocene sea flooded the barrier reef lagoon of Bora Bora ca. 10,650-9400 yrs BP (Isaack et al., 2016). The barrier reef started to accrete before 10,030 yrs BP (Gischler et al., 2016). After a hiatus in lagoonal sedimentation, mixed carbonate-siliciclastic sedimentation started ca. 8700-7700 yrs BP in the windward lagoon, and 8100-5400 yrs BP in the leeward lagoon (Isaack et al., 2016).

Based on quantitative microfacies analyses and statistical testing of texture and composition data obtained from the two sediment cores retrieved from the Bora Bora lagoon, the mixed carbonate-siliciclastic sediments can be divided into five facies. In the windward lagoon core site, siderite-rich marly wackestones and foraminifer-siderite wackestones accumulated during the early-mid Holocene around 7700 yrs BP on top of the Pleistocene soil (fig. 5/5). Subsequent sedimentation in the mid-late Holocene is characterized by mudstones (fig. 5/5). Above the Pleistocene soil in the leeward lagoon core site, sedimentation started with mollusk-foraminifer marly packstones and mollusk-rich wackestones deposited around 5400 yrs BP (fig. 5/6). The irregular morphology of the antecedent topography and elevation of the underlying karst causes shifts in the beginning of sedimentation within the lagoon; hence, deep depressions were first infilled during the early Holocene predating deposition on topographically elevated regions (fig. 5/12). Core FAA 1B is located nearshore, close to the main volcanic island in relatively shallow water depth on the leeward side, which delayed sedimentation in this area (fig. 5/12). Mudstones accumulated since ca. 3500 yrs BP in the leeward core section (fig. 5/6).

Occurrence and composition of the fossil fauna often indicate specific environmental conditions and can be useful with regard to the characterization and reconstruction of palaeoenvironments. In thin sections carried out on Bora Bora lagoonal vibrocores, pteropods and planktic foraminifera are present at core tops and in surface sediments (Gischler, 2011). Their abundances are very low, but suggest increased pelagic influence on late Holocene sedimentation (figs. 5/5, 5/6). In Mayotte, pelagic organisms (pteropods and planktonic foraminifera) are associated with the early Holocene transgression and became most dominant in times of maximum flooding (transgressive systems tract to highstand systems tract transition; Zinke et al., 2005). In the Bora Bora lagoon cores, planktonic foraminifera and pteropods also occur at the corebases, however, in proportions that were statistically negligible. Ostracods become abundant in the uppermost core sections in the Bora Bora

leeward lagoon (fig. 5/2f), but their taxonomy and paleoecology were not detailed. Ostracod assemblages of the Mayotte lagoon are assumed to indicate normal marine conditions in sheltered lagoon areas (Babinot and Kouyoumountzakakis, 1995; Zinke et al., 2005).

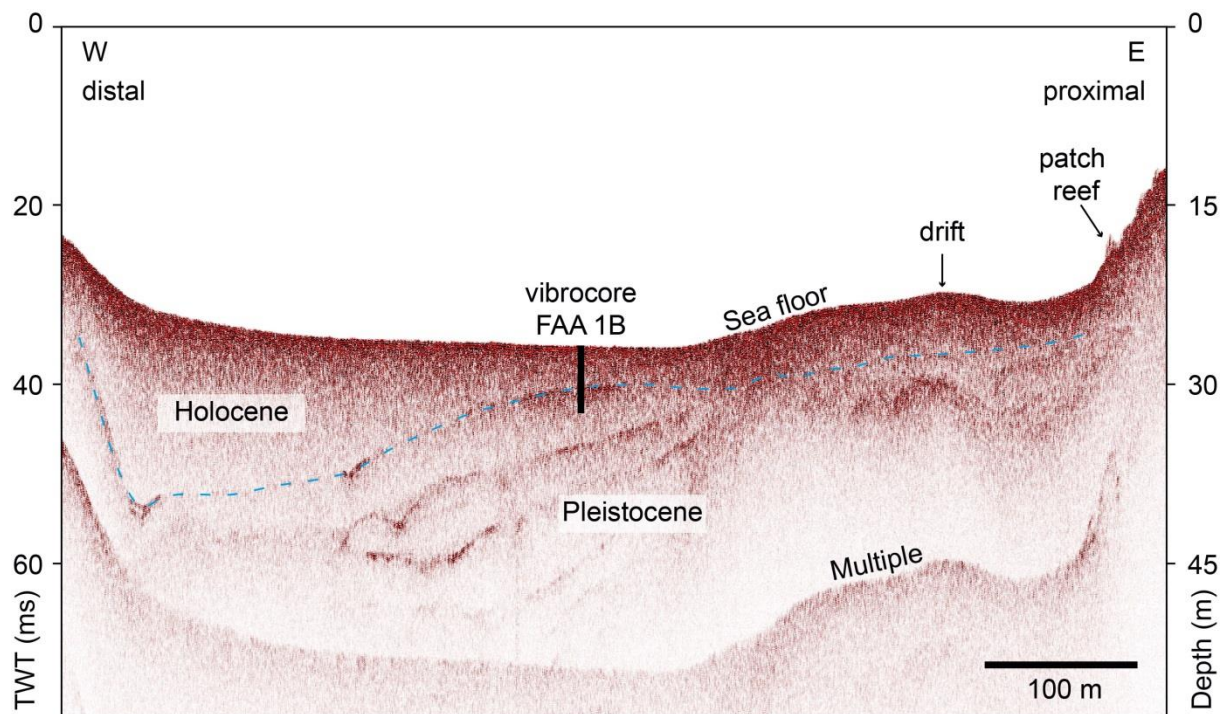


Fig. 5/12: Seismic profile along the deep lagoon, showing several morphological features of the lagoon, the Holocene/Pleistocene boundary and the position of vibrocore FAA 1B (initially 6 m long) on a Pleistocene topographic high. Please note the deep depression of the antecedent topography on the distal side, which has been infilled since the very beginning of sea-level transgression

Siliciclastics and organic material are very abundant in the early Holocene and indicate extensive erosion, weathering and transport of volcanic rocks and associated trace elements from the main central island during that time (figs. 5/2e; 5/5; 5/6; tab. 5/1). Siderites occurred during the early-mid Holocene, decreased in abundance upcore and vanished in the mid-late Holocene. Their occurrence correlates with the abundance of iron in the windward lagoon during the early Holocene (Isaack et al., 2016). Zinke et al. (2005) described ferrallitic concretions to occur in the “terrigenous mud to sandy mud with a mollusk assemblage” facies, which accumulated 9800-9500 yrs BP and in the “carbonate sand to gravel with a mollusk-foraminiferan-coral assemblage” facies around 6300 yrs BP and in the upper 15 cm of the Mayotte lagoonal core. However, the authors neither mentioned the origin of the concretions (terrestrial vs marine) nor described the habitus and the geochemical composition of these concretions. Because of the geomorphological similarity of Mayotte and Bora Bora – a central volcanic island (as main source for trace elements such as iron) surrounded by a deep lagoon – we assume that the ferrallitic concretions of Mayotte are similar to the siderite grains in Bora Bora. They probably indicate the same sedimentological and environmental

signals during times of formation such as wetter climate enhancing weathering and run-off from the volcanic island. However, Mayotte is more than ten times larger than Bora Bora and has numerous rivers effectively draining the central volcanic island. Therefore, weathered material should be transported into the lagoon even during times when climatic conditions became cooler and drier, as supposed for the mid-late Holocene (e.g., Mayewski et al., 2004; Marcott et al., 2013).

The mollusk-dominated facies at the base of the leeward lagoonal core indicates predominantly in situ carbonate production with adequate circulation and optimal conditions for suspension feeders during the mid-Holocene. Mollusk shells are also abundant in sediments during the early Holocene transgression and mid Holocene highstand of the Mayotte lagoon (Zinke et al., 2005). Gischler (2003) found that mollusk shell beds characterize basal lagoon sediments of the three Belizean atolls, Caribbean Sea. Also, early-mid Holocene sediments of Rasdhoo Atoll, Maldives often comprise a mollusk-rich sediment facies (Klostermann and Gischler, 2015).

Benthic foraminifera generally comprise one of the most common organisms in lagoonal sediments of modern carbonate platforms (e.g., Yamano et al., 2002). In Bora Bora, rotalids and miliolids are very abundant in early-mid Holocene sediments and decrease upcore (figs. 5/5; 5/6). Rotalid foraminifera include most of the stress-tolerant generalists (e.g., *Ammonia* sp.), which tolerate changes in water quality, nutrients, salinity, temperature and organic matter, and predominate in restricted environments such as hypersaline lagoons, estuaries or coastal areas (Debenay, 2000; Hallock, 2011; Langer and Lipps, 2003; Murray, 2006; Cheng et al., 2012). In shallow marine back-reef lagoon areas, they typically co-occur with miliolid taxa, which also tolerate hypersaline or restricted conditions (Jones, 2014). In Moorea, in the eastern part of the Society archipelago, surficial sediments of the inner bay inlets are characterized by rotalid foraminifera typifying low-oxygen and/or nutrient-rich habitats which are influenced by coastal processes such as fresh-water runoff and mangrove growth (Fajemila et al., 2015). Textularid foraminifera characterize back-reef lagoon sediments deposited under normal marine conditions (J. Parker, personal communication; Cushman et al., 1954; Parker and Gischler, 2011; Storz et al., 2014; Venec-Peyre, 1991) and their abundances increase upcore in Bora Bora lagoonal sediments.

The apparent lack of non-skeletal grains such as ooids, peloids, and aggregate grains in modern sediments of carbonate platforms from the Indo-Pacific region as compared to their abundance in carbonate platforms from the western Atlantic was discussed as the so-called “oolite problem” by Milliman (1969, 1974). However, a number of studies have recently

shown that non-skeletal grains also occur in Indo-Pacific carbonate platforms (e.g., Braithwaite, 1994; Rankey and Reeder, 2009; Gischler, 2011). These types of grains, mostly cemented peloids, are thought to form in shallow back-reef areas such as sand aprons, i.e. behind sand islands where sedimentation rates are low and sediment stability is high allowing early cementation, e.g., in Bora Bora, Pacific Ocean (Gischler, 2011) and in the Caribbean region, Atlantic Ocean (Milliman 1969, 1974). In addition to these conditions, Rankey and Reeder (2009) and Rankey et al. (2011) noted the importance of elevated pH and total alkalinity for the formation of non-skeletal grains in surficial sediments of the almost-atolls of Aitutaki (Cook Islands) and Maupiti (Society Islands) in the Pacific Ocean.

In the Bora Bora vibrocore retrieved from the windward lagoon, the amount of peloids has increased during the past 1000 yrs, which, on one hand, could indicate early submarine cementation within the lagoon, favored by sediment stability, reduced sedimentation rate and the factor time. On the other hand, the increase in peloids could indicate sediment transport from the adjacent sand apron into the lagoon. The abundance of coral fragments also increased during this time and indicates sediment transport. Patch reefs as potential shallow water sediment sources are lacking in the deep lagoon. However, coral fragments could also be imported from the fringing reefs, which prograded lagoonwards when sea level stabilized at its present position (Gischler et al., 2016).

Overfilling of accommodation space might be expressed in the formation of small reef islets behind the reef crest (e.g., Purkis and Harris, 2016), which results in restriction of sediment transport from the reef margins via sand aprons towards the lagoon (e.g., Gischler, 2011). In the Pacific region, the formation of large, elongated islets (motus) is attributed to the mid-late Holocene sea-level fall (e.g., Dickinson, 2003, 2009). Restricted sediment transport from reef margins towards back-reef areas flanked by motus, as on the windward side of Bora Bora, could potentially result in the shutdown of sand apron accretion since the late Holocene. As a result, the reduction of sediments imported from back-reef areas would also regulate sediment stability allowing early lithification processes to occur within the deep lagoon.

5.5.2 Nature and palaeoenvironmental significance of siderites

The occurrence of siderite grains at the base of the lagoon cores was an unexpected discovery and the formation of siderite in lagoonal sediments of tropical reefs and carbonate platforms is reported here for the first time. In Bora Bora, siderite grains can be found in unconsolidated mixed carbonate-siliciclastic sediments deposited during the early-mid Holocene (figs. 5/5;

5/6) but do not occur in sediments of mid-late Holocene age. Although siderites occur in both the windward and leeward lagoon, they are more abundant in the windward core location. The size of the siderites varies from 0.3 to 1.8 mm. Apparently, siderite grains are often aggregated (figs. 5/3; 5/4a, c) and can easily separated grain-by-grain. The last observation coincides with observations on siderites from early Holocene freshwater and tidal deposits of the west coast of Korea (Choi et al., 2003; Lim et al., 2004), and favors the assumption that siderite formed during the sediment deposition.

Siderite formation - processes and conditions

Biominalisation processes of iron-oxidizing and iron-reducing bacteria creating a variety of iron oxides (magnetite), carbonates (siderite) and sulphides (greigite) has played an important role in the geological record (e.g. the formation of Precambrian banded iron formations; Joshi, 2014). In the earth crust, iron is the fourth most common element and Fe(III)-bearing minerals are the dominant electron acceptors for bacteria in most anoxic ecosystems (Straub, 2011). In general, iron is very abundant in rocks, but scarce in natural waters. Oxidative weathering processes produces Fe(III), which is immediately immobilized generating iron-oxide residues leaving river waters with relatively low dissolved iron concentration, often as colloidal or suspended iron load (Kendall et al., 2012). The mixing between freshwater and seawater, e.g., in estuaries, leads to the removal of colloidal iron from solution and the high ionic strength of seawater neutralizes surface charges on colloidal particles allowing them to coagulate and precipitate (Gustafsson et al., 2000; Krachler et al., 2010). Because of different chemical bonding affinities of Fe(II) and Fe(III), the behavior of iron is largely controlled by redox conditions (Kendall et al., 2012). Diagenetic siderite formation depends on the availability of Fe²⁺ ions in pore waters and is restricted to suboxic to anoxic environments (Berner 1971) and thereby indicates reducing conditions within the sediment (Mozley and Wersin, 1992).

Siderite is a sensitive indicator of the chemical environment and the precipitation requires neutral pH conditions (Roh et al., 2003). Iron can be removed from solution under low Eh conditions by the abundance of dissolved sulphide (HS⁻ and H₂S) (Kendall et al., 2012), which reacts to insoluble iron sulphide (pyrite) (Luther, 1991; Schoonen and Barnes, 1991). When Fe(II) is in excess of HS⁻, a further process leading to the removal of iron from solution in the presence of bicarbonate and phosphate is the formation of siderite (FeCO₃) and vivianite (hydrated iron phosphate mineral), respectively (Krom and Berner, 1980; Coleman, 1985). Apparently, the formation of siderite tolerates various salinity conditions including freshwater (e.g., Lim et al., 2004), brackish waters (e.g., Pye et al., 1990) and marine

environments (e.g., deep sea, Lancelot and Ewing, 1972). Furthermore, the precipitation of siderite increases with increasing bicarbonate concentration (Roh et al., 2003).

Geochemical composition of siderites and implications on siderite formation in Bora

Bora

The relationship between siderite and the chemistry of pore-water from which it precipitated can be a useful tool to clarify palaeoenvironmental conditions (Mozley, 1989a; Mozley and Wersin, 1992). For example, the chemical zonation within siderite grains in cores from Baffin Bay, Texas, has been attributed to variations of pore-water chemistry during precipitation, probably caused by sea-level changes (Mozley and Carothers, 1992). Siderites from freshwater environments are relatively pure in chemistry (Fe > 90 mol%), while siderites with an impure chemical composition and Ca, Mg and Mn substitution (up to 15 mol%) are considered as being marine in origin (Mozley, 1989b). Choi et al. (2003) postulated extensive Mn, Ca and Mg substitution coupled with the enrichment of $\delta^{18}\text{O}$ in siderites to reflect marine conditions during times of siderite formation in Holocene sediments from the Yellow Sea, Korea. Curtis et al. (1986) assumed that Mn-rich siderites concretions in fossil coastal deposits precipitated close to the sediment/water interface, a zone where Mn and Fe are mobilized from oxides and hydroxides in the sediment under reducing conditions. The enrichment in Mn at siderite grain margins requires changes in the oxidation state, however, authigenic siderite with Mn coatings can also be interpreted as Fe-depletion during the very late stages of siderite precipitation (Tasse and Hesse, 1984).

The siderites from the Bora Bora lagoon reveal significant variations in their elemental composition. The analyzed siderite sample from 340 cm core depth shows a relatively pure chemical composition with Fe-concentrations varying between 90.87-93.93 mol% and minor concentrations of Mn (< 6.38 mol%), Ca (< 2.68 mol%) and Mg (< 0.42 mol%) (tab. 5). The siderite sample from 330 cm core depth shows an impure chemical composition with Fe concentrations ranging between 82.76-88.28 mol% and Mn concentrations between 11.31-16.22 mol% (tab. 5). In the same sample, Ca and Mg concentrations are < 1 mol% and < 0.1 mol%, respectively (tab. 5).

The isotopic composition of siderites can also elucidate environmental conditions and precipitation processes during times of formation. A dataset compiled by Mozley and Wersin (1992) allows distinguishing between non-marine versus marine siderites as siderite precipitation in a non-marine environment can be identified by positive $\delta^{13}\text{C}$ values (< 8‰) and negative $\delta^{18}\text{O}$ values (< -13‰), while siderites precipitated under marine conditions are

very depleted in carbon-isotope composition (see also fig. 5/9a). In Bora Bora, the siderites have $\delta^{13}\text{C}$ values with -15.29‰ on average and $\delta^{18}\text{O}$ with $+0.17\text{‰}$ on average (fig. 5/9a, b), which indicates formation under marine conditions during the early Holocene. Pye et al. (1990) reported $\delta^{18}\text{O}$ values ranging between -6.4 to $+0.8\text{‰}$ in siderite from salt marsh sediments from Norfolk, UK and postulated that these values indicate carbonate precipitation in pore waters filled with seawater and seawater diluted with meteoric water, respectively.

Microbial processes such as sulphate reduction and methanogenesis play a significant role in the formation of (early) diagenetic siderite minerals within unconsolidated sediments (e.g., Curtis et al., 1986). Coleman et al. (1993) used lipid biomarker (polar lipid fatty acid) analysis of siderite concretions and host sediments from Norfolk, UK to demonstrate that sulphate-reducing bacteria dominate the microbial community. Iron precipitation (immobilization) is often driven by microbial iron oxidation, and microbial iron reduction may lead to iron solubilization (mobilization; Ehrlich and Newman, 2009). In modern sediments, siderite formation can be associated with bacterial respiration of organic matter coupled with dissimilatory iron reduction (Suess, 1979; Pye et al., 1990; Roh et al., 2003; Ehrlich and Newman, 2009). Carbon derived from microbial decomposition of organic matter is generally indicated by a depletion of $\delta^{13}\text{C}$ values (Curtis and Coleman, 1981; Pye et al., 1990; Mozley and Carothers, 1992; Mozley and Wersin, 1992; Choi et al., 2003). This depletion can either result from iron reduction (Mozley and Carothers, 1992) or sulphate reduction (Coleman, 1985). The latter occurs when the rate of bacterial iron reduction exceeds the rate of sulfate reduction performed by sulphate-reducing bacteria (Pye et al., 1990; Mortimer et al., 2011; Konhauser and Riding, 2012) and produces siderite rather than pyrite in recent sediments (Coleman et al., 1993).

Indirect evidence for the existence of sulfate-reducing bacteria in Holocene reefal deposits is given by the presence of microbialites in Quaternary coral reefs and modern carbonate platforms in the wider study area and in general (Camoin et al., 1999; Cabioch et al., 2006; Gischler, 2008; Gischler et al., 2008; Gischler et al., 2016). Heindel et al. (2012) showed that sulfate-reducing bacteria took active part in the formation of microbialites within the last deglacial reef sequence from Tahiti. Microbialites develop in anoxic micro-environments up to 6 m below the living coral surface (Seard et al., 2011; Heindel et al., 2012) and are also present in fringing reef sections (G. Camoin, unpublished). Microbialite formation in French Polynesia is considered to reflect changes in water quality, especially an increase in nutrients (Camoin et al., 2006). Terrestrial input of nutrients derived from weathering of volcanic rocks appears to be a natural fertilizer, but is not necessarily required for microbialite growth

(Heindel et al., 2012). During the mid-Holocene when sea level stabilized as the deglaciation terminated, microbialites seemed to have disappeared in coral reefs (Cabioch et al., 1999; Camoin et al., 1999; Cabioch et al., 2006). Likewise, in the lagoonal sediments of Bora Bora, the occurrence of siderites is highest in the early and early-mid Holocene and vanishes in the mid-Holocene, respectively.

The disposability of iron in the mixed carbonate-siliciclastic sediments of Bora Bora can be explained by extensive weathering of the volcanic hinterland. Early Holocene climatic conditions were more humid, which presumably favored weathering and erosion of the volcanic rocks and transport of weathered material into the lagoon (Isaack et al., 2016). Pleistocene soils are enriched in goethite (Isaack et al., 2016), and alternatively, iron potentially might have been mobilized by pore waters circulating and dissolving iron in underlying soils, and subsequent capillary rising of iron-rich fluids to the overlying sediments.

In summary, we assume that differences in the chemical compositions of the lagoonal siderites reflect the interaction of sea-level variations and changes in rainfall and run-off in the early Holocene. After platform inundation and slowly rising sea level around 10,650-9400 yrs BP (Isaack et al., 2016), siderites apparently precipitated under marine and mixed marine-meteoric conditions when Fe (imported from the volcanic island), and organic material (as supplier for organic carbon) were available in the presence of dissolved bicarbonate and within lagoonal sediments. As a consequence of microbial activity due to the respiration of organic material and iron reduction, environmental conditions within the lagoon became suboxic. Lagoonal bottom waters became more oxygenized as sea-level rise continued, illustrated by the fact that the chemical content of siderites became enriched in Mn upcore, and by the occurrence of Mn-rich crusts coating the siderite grains. Because of decreasing iron input during the early-mid Holocene and increasing bicarbonate uptake by marine organisms for shell formation, siderite occurrence and size have decreased during the Holocene.

5.6 Conclusions

Temporal and spatial distributions of five mixed carbonate-siliciclastic facies are an expression of Holocene sea-level and climate variations in the barrier reef lagoon of Bora Bora, South Pacific. Siderite-rich and foraminifera-siderite wackestones accumulated during the early-mid Holocene in the windward lagoon core site. The early-mid Holocene foraminifera fauna is dominated by rotalid and miliolid taxa and their abundances decrease

during the Holocene. These groups are typically known to cope with environment stress such as changes in water quality, nutrient input and oxygen level.

Iron input from the volcanic island due to wetter climate conditions is expressed in the formation of siderite within early-mid Holocene lagoonal sediments. The precipitation of siderite is assumed to be the result of microbial decomposition of organic matter indicated by a depletion of $\delta^{13}\text{C}$ (-13.61 to -14.48%) and iron reduction in the presence of bicarbonate. The enrichment of $\delta^{18}\text{O}$ ($+0.32$ to $+0.54\%$) indicates marine to mixed marine-meteoric conditions during its formation. The chemical composition of siderites varies, with high Fe (> 90 mol%) and low Mn (< 6 mol%) concentrations at the base of the lagoon core, and lower Fe (< 90 mol%) and higher Mn (up to 16 mol%) concentrations upcore. The substitutions of Mn, Ca and Mg especially at grain margins are the result of changes in the oxidation state and are assumed to reflect changes in pore-water chemistry due to sea-level rise and climate changes (rainfall). As far as climate conditions became drier during the mid-late Holocene, iron input became reduced and siderite precipitation decreased and vanished.

In the leeward lagoon core site, mollusk-foraminifera marly packstones and mollusk-rich wackestones accumulated ca. 5400-3500 yrs BP during the mid-Holocene. Textularid foraminifera have prevailed since the mid-Holocene and represent a fauna typically associated with normal marine back-reef lagoons. In the windward and leeward lagoon core sites, sedimentation is characterized by mudstones since the sea-level highstand and fall to modern level in the mid-late Holocene. The increase of coral fragments in the windward lagoon during the past 1000 yrs probably results from lagoonward progradation of fringing reefs during the mid-late Holocene. As a further consequence of the sea-level fall, motus formed due to overfilling of accommodation space behind reef crests on the windward side and restricted sediment transport from the outer reef areas towards the lagoon and lagoonward progradation of sand aprons. Therefore, the increase in peloids since the late Holocene might be an expression of early submarine lithification due to sediment stability and time rather than the expression of sediment transport.

Acknowledgements

We are grateful to the Deutsche Forschungsgemeinschaft (Gi 222/23-1), who funded this project. The help of Gabriela Meyer (Frankfurt am Main) and Stefan Haber (Bad Karlshafen) during field work is gratefully acknowledged. We thank Dominik Schmitt and Nico Neuwirth (Goethe Universität, Frankfurt am Main) who helped during sample preparation; Silviu Martha (Goethe Universität, Frankfurt am Main) assisted during recalculations of trace-

element concentrations. Thanks to Nils Prawitz (Goethe Universität, Frankfurt am Main) for help during thin-section preparation and Claudia Franz (Senckenberg Forschungsinstitute und Naturmuseen, Frankfurt am Main) for operating the scanning electron microscopy. Many thanks also to Michael Joachimski (GeoZentrum Erlangen-Nürnberg) for carbon and oxygen isotopes analyses, and Nora Groschopf (Johannes Gutenberg Universität Mainz) for her support during the electron microprobe work. We thank S.A.R.L. Ti Ai Moana (Paea, Tahiti), Captain Yann Paureau and his first mate Sebastien Bertaut for logistical support. Gérard Bion supported us in many ways in Bora Bora. The mayor of Bora Bora and the Ministère du Logement, des Affaires Foncières, de l'Économie Numérique et de l'Artisanat (Papeete) kindly issued research permits. LPL Group (Hamburg), SDV (Papeete) and C.H. Robinson (Houston) transported equipment and samples.

References

- Babinot, J.-F., Kouyoumontzakis, G., 1995. Associations d'ostracodes d'un environnement récifal envasé: le lagon de l'île de Mayotte (Archipel des Comores, Océan Indien occidental). *Geobios* 18, 17–38.
- Berner, A., 1971. *Principles of Chemical Sedimentology*. New York, McGraw-Hill.
- Blais, S., Guille, G., Guillou, H., Chauvel, C., Maury, R.C., Caroff, M., 2000. Géologie, géochimie et géochronologie de l'île de Bora Bora (Société, Polynésie française). *Earth Planet. Sci.* 331, 579–585. doi:10.1016/S1251-8050(00)01456-7
- Braithwaite, C.J.R., 1994. Quaternary oolites in the Indian Ocean. *Atoll Res. Bull.* 420, 1–6. doi:10.5479/si.00775630.420.1
- Cabioch, G., Camoin, G., Webb, G.E., Le Cornec, F., Garcia Molina, M., Pierre, C., Joachimski, M.M., 2006. Contribution of microbialites to the development of coral reefs during the last deglacial period: Case study from Vanuatu (South-West Pacific). *Sediment. Geol.* 185, 297–318. doi:10.1016/j.sedgeo.2005.12.019
- Cabioch, G., Taylor, F.W., Corre, T., Re, J., 1999. Occurrence and significance of microbialites in the uplifted Tasmaloum reef (SW Espiritu Santo, SW Pacific). *Sediment. Geol.* 126, 305–316. doi:10.1016/S0037-0738(99)00046-9
- Camoin, G., Cabioch, G., Eisenhauer, A., Braga, J.-C., Hamelin, B., Lericolais, G., 2006. Environmental significance of microbialites in reef environments during the last deglaciation. *Sediment. Geol.* 185, 277–295. doi:10.1016/j.sedgeo.2005.12.018
- Camoin, G.F., Gautret, P., Montaggioni, L.F., Cabioch, G., 1999. Nature and environmental

- significance of microbialites in Quaternary reefs: the Tahiti paradox. *Sediment. Geol.* 126, 271–304.
- Cheng, J., Collins, L.S., Homes, C., 2012. Four thousand years of habitat change in Florida Bay, as indicated by benthic foraminifera. *J. Foraminifer. Res.* 42, 3–17.
- Choi, K.S., Khim, B.K., Woo, K.S., 2003. Spherulitic siderites in the Holocene coastal deposits of Korea (eastern Yellow Sea): Elemental and isotopic composition and depositional environment. *Mar. Geol.* 202, 17–31. doi:10.1016/S0025-3227(03)00258-5
- Coleman, M.L., 1985. Geochemistry of diagenetic non-silicate minerals: kinetic considerations. *Philos. Trans. R. Soc. London* 315, 39–56.
- Coleman, M.L., Hedrick, D.B., Lovley, D.R., White, D.C., Pye, K., 1993. Reduction of Fe(III) in sediments by sulphate-reducing bacteria. *Nature* 361, 436–438. doi:10.1038/361436a0
- Curtis, C.D., Coleman, M.L., 1981. Controls on the precipitation of early diagenetic calcite, dolomite and siderite concretions in complex depositional sequences. *SEPM Spec. Publ.* 38, 23–33.
- Curtis, C.D., Coleman, M.L., Love, L.G., 1986. Pore water evolution during sediment burial from isotopic and mineral chemistry of calcite, dolomite and siderite concretions 2321–2334.
- Cushman, J.A., Todd, R., Post, R.J., 1954. Recent foraminifera of the Marshall Islands. *Geol. Surv. Prof. Pap.* 260-H, 319–410.
- Debenay, J.-P., 2000. Foraminifera of paralic tropical environments. *Micropaleontology* 46, 153–160.
- Dickinson, W.R., 2003. Impact of mid-Holocene hydro-isostatic highstand in regional sea level on habitability of islands in Pacific Oceania. *J. Coast. Res.* 19, 489–502.
- Dickinson, W.R., 2009. Pacific atoll living: how long already and until when. *GSA Today* 19, 4–10. doi:10.1130/GSATG35A.1
- Dunham, R.J., 1962. Classification of carbonate rocks according to depositional texture, in: Ham, W.E. (Ed.), *Classification of Carbonate Rocks - A Symposium*. American Association of Petroleum Geologist Memoir, Vol. 1, American Association of Petroleum Geologist, Tulsa, pp. 108–121.
- Ehrlich, H.L., Newman, D.K., 2009. *Geomicrobiology*. CRC Press Taylor Francis Group. doi:10.1017/CBO9781107415324.004

- Fajemila, O.T., Langer, M.R., Lipps, J.H., 2015. Spatial patterns in the distribution, diversity and abundance of benthic foraminifera around Moorea (Society Archipelago, French Polynesia). *PLoS One* 10, e0145752. doi:10.1371/journal.pone.0145752
- Friedman, G.M., 1959. Identification of carbonate minerals by staining methods. *J. Sediment. Petrol.* 29, 87–97.
- Gabrié, C., Baldwin, J., Bonvallot, J., Chauvet, C., Vernaudeau, Y., Payri, C., Galzin, R., 1994. Study of the coral reefs of Bora Bora (Society Archipelago, French Polynesia) for the development of a conservation and management plan. *Ocean Coast. Manag.* 25, 189–216.
- Gabrié, C., Salvat, B., 1985. General features of French Polynesian islands and their coral reefs, in: Delesalle, R., Galzin, R., Salvat, B. (Eds.), 5th International Coral Reef Congress, Tahiti, 27.05-01.06.1985 Vol. 1: French Polynesian Coral Reefs, Reef Knowledge and Field Guides. pp. 1–16.
- Gautier, D.L., 1982. Siderite concretions: Indicators of early diagenesis in the Gammon Shale (Cretaceous). *J. Sediment. Res.* 52, 859–871. doi:10.1306/212F8076-2B24-11D7-8648000102C1865D
- Gischler, E., 2003. Holocene lagoonal development in the isolated carbonate platforms off Belize. *Sediment. Geol.* 159, 113–132. doi:10.1016/S0037-0738(03)00098-8
- Gischler, E., 2008. Accretion patterns in Holocene tropical coral reefs: do massive coral reefs in deeper water with slowly growing corals accrete faster than shallower branched coral reefs with rapidly growing corals? *Int. J. Earth Sci.* 97, 851–859. doi:10.1007/s00531-007-0201-3
- Gischler, E., 2010. Indo-Pacific and Atlantic spurs and grooves revisited: the possible effects of different Holocene sea-level history, exposure, and reef accretion rate in the shallow fore reef. *Facies* 56, 173–177. doi:10.1007/s10347-010-0218-0
- Gischler, E., 2011. Sedimentary facies of Bora Bora, Darwin's type barrier reef (Society Islands, South Pacific): the unexpected occurrence of non-skeletal grains. *J. Sediment. Res.* 81, 1–17. doi:10.2110/jsr.2011.4
- Gischler, E., Hudson, J.H., Humblet, M., Braga, J.C., Eisenhauer, A., Isaack, A., Anselmetti, F.S., Camoin, G.F., 2016. Late Quaternary barrier and fringing reef development of Bora Bora (Society Islands, south Pacific): first subsurface data from the Darwin-type barrier-reef system. *Sedimentology* 63, 1522–1549. doi:10.1111/sed.12272
- Guilcher, A., Berthois, L., Doumenge, F., Michel, A., Saint-Requier, A., Arnold, R., 1969. Le

- récifs et lagons coralliens de Mopelia et de Bora Bora (Îles de la Société). Mem. Orstom 38, 38–103.
- Guillou, D., Maury, R.C., Blais, S., Cotten, J., Legendre, C., Guille, G., Caroff, M., 2005. Age progression along the Society hotspot chain (French Polynesia) based on new unspiked K-Ar ages. Bull. la Société Géologique Fr. 176, 135–150. doi:10.2113/176.2.135
- Gustafsson, Ö., Widerlund, A., Andersson, P.S., Ingri, J., Roos, P., Ledin, A., 2000. Colloid dynamics and transport of major elements through a boreal river — brackish bay mixing zone. Mar. Chem. 71, 1–21.
- Hallock, P., 2011. Foraminifera, in: Hopley, D. (Ed.), Encyclopedia of Modern Coral Reefs: Structure, Form and Process. Springer Netherlands, Dordrecht, pp. 416–421. doi:10.1007/978-90-481-2639-2_80
- Hammer, Ø., Harper, D.A.T., Ryan, P.D., 2001. PAST: Paleontological Statistics software package for education and data analysis. Palaeontol. Electron. 4, 1–9.
- Heindel, K., Birgel, D., Brunner, B., Thiel, V., Westphal, H., Gischler, E., Ziegenbalg, S.B., Cabioch, G., Sjövall, P., Peckmann, J., 2012. Post-glacial microbialite formation in coral reefs of the Pacific, Atlantic, and Indian Oceans. Chem. Geol. 304-305, 117–130. doi:10.1016/j.chemgeo.2012.02.009
- Isaack, A., Gischler, E., Hudson, J.H., Anselmetti, F.S., Lohner, A., Vogel, H., Garbode, E., Camoin, G.F., 2016. A new model evaluating Holocene sediment dynamics: Insights from a mixed carbonate–siliciclastic lagoon (Bora Bora, Society Islands, French Polynesia, South Pacific). Sediment. Geol. 343, 99–118. doi:10.1016/j.sedgeo.2016.08.002
- Jones, R.W., 2014. Foraminifera and their applications. Cambridge University Press.
- Joshi, K.B., 2014. Microbes: Mini Iron Factories. Indian J. Microbiol. 54, 483–485.
- Kendall, B., Anbar, A.D., Kappler, A., Konhauser, K.O., 2012. The Global Iron Cycle. Fundam. Geobiol. 65–92. doi:10.1002/9781118280874.ch6
- Kim, S.T., Mucci, A., Taylor, B.E., 2007. Phosphoric acid fractionation factors for calcite and aragonite between 25 and 75°C: Revisited. Chem. Geol. 246, 135–146. doi:10.1016/j.chemgeo.2007.08.005
- Klostermann, L., Gischler, E., 2015. Holocene sedimentary evolution of a mid-ocean atoll lagoon, Maldives, Indian Ocean. Int. J. Earth Sci. 104, 289–307. doi:10.1007/s00531-014-1068-8
- Konhauser, K., Riding, R., 2012. Bacterial Biomineralization, in: Knoll, A., Canfield, D.,

- Konhauser, K. (Eds.), *Fundamentals of Geobiology*. John Wiley & Sons, Ltd, pp. 105–130. doi:10.1002/9781118280874.ch8
- Krachler, R., Krachler, R.F., Kammer, F. von der, Süphandag, A., Jirsa, F., Ayromlou, S., Hofmann, T., Keppler, B.K., 2010. Relevance of peat-draining rivers for the riverine input of dissolved iron into the ocean. *Sci. Total Environ.* 408, 2402–2408. doi:10.1016/j.scitotenv.2010.02.018
- Krom, D., Berner, R.A., 1980. Adsorption of phosphate in anoxic marine sediments. *Limnol. Oceanogr.* 25, 797–806. doi:10.4319/lo.1980.25.5.0797
- Lancelot, Y., Ewing, J.I., 1972. Correlation of natural gas zonation and carbonate diagenesis in Tertiary sediments from the northwest Atlantic. *Initial Reports Deep Sea Drill. Proj.* 11, 791–799.
- Langer, M.R., Lipps, J.H., 2003. Foraminiferal distribution and diversity, Madang Reef and Lagoon, Papua New Guinea. *Coral Reefs* 22, 143–154. doi:10.1007/s00338-003-0298-1
- Lebeau, O., Busigny, V., Chaduteau, C., Ader, M., 2014. Organic matter removal for the analysis of carbon and oxygen isotope compositions of siderite. *Chem. Geol.* 372, 54–61. doi:10.1016/j.chemgeo.2014.02.020
- Lim, D.I., Jung, H.S., Yang, S.Y., Yoo, H.S., 2004. Sequential growth of early diagenetic freshwater siderites in the Holocene coastal deposits, Korea. *Sediment. Geol.* 169, 107–120. doi:10.1016/j.sedgeo.2004.05.002
- Luther, G.W., 1991. Pyrite synthesis via polysulfide compounds. *Geochim. Cosmochim. Acta* 55, 2839–2849.
- Marcott, S.A., Shakun, J.D., Clark, P.U., Mix, A.C., 2013. A reconstruction of regional and global temperatures for the past 11,300 years. *Science* 339, 1198–1201.
- Masse, J.P., Thomassin, B.A., Acquaviva, M., 1989. Bioclastic sedimentary environments of the coral reefs and lagoon around Mayotte Island (Comoro Archipelago, Mozambique Channel, SW Indian Ocean). *J. Coast. Res.* 5, 419–432.
- Mayewski, P.A., Rohling, E.E., Curt Stager, J., Karlén, W., Maasch, K.A., David Meeker, L., Meyerson, E.A., Gasse, F., van Kreveld, S., Holmgren, K., Lee-Thorp, J., Rosqvist, G., Rack, F., Staubwasser, M., Schneider, R.R., Steig, E.J., 2004. Holocene climate variability. *Quat. Res.* 62, 243–255. doi:10.1016/j.yqres.2004.07.001
- Middelton, A.P., Freestone, L.C., Leese, M.N., 1985. Textural analysis of ceramic thin sections: evaluation of grain sampling procedures. *Archaeometry* 27, 64–74.

- Milliman, J.D., 1969. Four southwestern Caribbean atolls: Courtown Cays, Albuquerque Cays, Roncador Bank and Serrana Bank. *Atoll Res. Bull.* 1–41.
- Milliman, J.D., 1974. *Marine Carbonates*. Springer-Verlag, Berlin, Heidelberg, New York.
- Montaggioni, L.F., Le, F., Corrège, T., Cabioch, G., 2006. Coral barium/calcium record of mid-Holocene upwelling activity in New Caledonia, South-West Pacific. *Paleogeography, Paleoclimatology, Paleoecol.* 237, 436–455. doi:10.1016/j.palaeo.2005.12.018
- Mortimer, R.J.G., Galsworthy, A.M.J., Bottrell, S.H., Wilmot, L.E., Newton, R.J., 2011. Experimental evidence for rapid biotic and abiotic reduction of Fe(III) at low temperatures in salt marsh sediments: a possible mechanism for formation of modern sedimentary siderite concretions. *Sedimentology* 58, 1514–1529. doi:10.1111/j.1365-3091.2011.01224.x
- Mozley, P.S., 1989. Relation between depositional environment and the elemental composition of early diagenetic siderite. *Geology* 17, 704–706. doi:10.1130/0091-7613(1989)017<0704
- Mozley, P.S., 1989. Complex compositional zonation in concretionary siderite: Implications for geochemical studies. *J. Sediment. Petrol.* 59, 815–818. doi:10.1306/212F907A-2B24-11D7-8648000102C1865D
- Mozley, P.S., Carothers, W.W., 1992. Elemental and isotopic composition of siderite in the Kuparuk Formation, Alaska; effect of microbial activity and water sediment interaction on early pore-water. *J. Sediment. Res.* 62, 681–692. doi:10.1306/D4267988-2B26-11D7-8648000102C1865D
- Mozley, P.S., Wersin, P., 1992. Isotopic composition of siderite as an indicator of depositional environment. *Geology* 20, 817–820.
- Murray, J.W., 2006. *Ecology and applications of benthic foraminifera*. Cambridge University Press.
- Parker, J.H., Gischler, E., 2011. Modern foraminiferal distribution and diversity in two atolls from the Maldives, Indian Ocean. *Mar. Micropaleontol.* 78, 30–49. doi:10.1016/j.marmicro.2010.09.007
- Petschick, R., Kuhn, G., Gingele, F., 1996. Clay mineral distribution in surface sediments of the South Atlantic: sources, transport, and relation to oceanography. *Mar. Geol.* 130, 203–229.
- Pirazzoli, P.A., Brousse, R., Delibrias, G., Montaggioni, L.F., Sachet, M.H., Salvat, B., Sinoto, Y.H., 1985. *Leeward Islands (Maupiti, Tupai, Bora Bora, Huanine) Society*

- Archipelago, in: Delesalle, R.G., Salvat, B. (Eds.), 5th International Coral Reef Congress, Tahiti, 27.05-01.06.1985 Vol. 1: French Polynesian Coral Reefs, Reef Knowledge and Field Guides. pp. 17–72.
- Pirazzoli, P.A., Montaggioni, L.F., 1988. Holocene sea-level changes in French Polynesia. *Palaeogeogr. Palaeoclimatol. Palaeoecol.* 68, 153–175.
- Pirazzoli, P.A., Montaggioni, L.F., Salvat, B., Faure, G., 1988. Late Holocene sea-level indicators from twelve atolls in the central and eastern Tuamotus (Pacific Ocean). *Coral Reefs* 7, 57–68.
- Postma, D., 1982. Pyrite and siderite formation in brakish and freshwater swamp sediments. *Am. J. Sci.* 282, 1151–1183.
- Purkis, S.J., Harris, P.M. (Mitch), 2016. The extent and patterns of sediment filling of accommodation space on Great Bahama Bank. *J. Sediment. Res.* 86, 294–310.
- Pye, K., Dickson, J.A.D., Schiavon, N., Coleman, M.L., Cox, M., 1990. Formation of siderite-Mg-calcite-iron sulphide concretions in intertidal marsh and sandflat sediments, north Norfolk, England. *Sedimentology* 37, 325–343.
- Rankey, E.C., Reeder, S.L., 2009. Holocene ooids of Aitutaki Atoll, Cook Islands, South Pacific. *Geology* 37, 971–974. doi:10.1130/G30332A.1
- Rankey, E.C., Reeder, S.L., Garza-Perez, J.R., 2011. Controls on links between geomorphical and surface sedimentological variability: Aitutaki and Maupiti Atolls, South Pacific Ocean. *J. Sediment. Res.* 81, 885–900. doi:10.2110/jsr.2011.73
- Rashid, R., Eisenhauer, A., Stocchi, P., Liebetrau, V., Fietzke, J., Rüggeberg, A., Dullo, W.C., 2014. Constraining mid to late Holocene relative sea-level change in the southern equatorial Pacific Ocean relative to the Society Islands, French Polynesia. *Geochemistry, Geophys. Geosystems* 15, 2601–2615. doi:10.1002/2014GC005272
- Roh, Y., Zhang, C.L., Vali, H., Lauf, R.J., Zhou, J., Phelps, T.J., 2003. Biogeochemical and environmental factors in Fe biomineralization: Magnetite and siderite formation. *Clays Clay Miner.* 51, 83–95. doi:10.1346/CCMN.2003.510110
- Rosenbaum, J., Sheppard, S.M.F., 1986. An isotopic study of siderites, dolomites and ankerites at high temperatures. *Geochim. Cosmochim. Acta* 50, 1147–1150. doi:10.1016/0016-7037(86)90396-0
- Sapota, T., Aldahan, A., Al-Aasm, I.S., 2006. Sedimentary facies and climate control on formation of vivianite and siderite microconcretions in sediments of Lake Baikal, Siberia. *J. Paleolimnol.* 36, 245–257. doi:10.1007/s10933-006-9005-x

- Schoonen, M.A.A., Barnes, H.L., 1991. Reactions forming pyrite and marcasite from solution: II. Via FeS precursors below 100°C. *Geochim. Cosmochim. Acta* 55, 1505–1514.
- Searđ, C., Camoin, G., Yokoyama, Y., Matsuzaki, H., Durand, N., Bard, E., Sepulcre, S., Deschamps, P., 2011. Microbialite development patterns in the last deglacial reefs from Tahiti (French Polynesia; IODP Expedition #310): Implications on reef framework architecture. *Mar. Geol.* 279, 63–86. doi:10.1016/j.margeo.2010.10.013
- Sieger, R., Grobe, H., 2005. PanPlot - software to visualize profiles and core logs. doi:10.1594/PANGAEA.330147
- Storz, D., Gischler, E., Parker, J., Klostermann, L., 2014. Changes in diversity and assemblages of foraminifera through the Holocene in an atoll from the Maldives, Indian Ocean. *Mar. Micropaleontol.* 106, 40–54. doi:10.1016/j.marmicro.2013.12.001
- Straub, K.L., 2011. Fe(II)-Oxidizing Prokaryotes, in: Reitner, J., Thiel, V. (Eds.), *Encyclopedia of Geobiology*. Springer Netherlands, Dordrecht, pp. 367–370. doi:10.1007/978-1-4020-9212-1_88
- Suess, E., 1979. Mineral phases formed in anoxic sediments by microbial decomposition of organic matter. *Geochim. Cosmochim. Acta* 43, 339–352.
- Tasse, N., Hesse, R., 1984. Origin and significance of complex authigenic carbonates in Cretaceous black shales of the Western Alps. *J. Sediment. Res.* 54, 1012–1027. doi:10.1306/212F8553-2B24-11D7-8648000102C1865D
- Toomey, M.R., Donnelly, J.P., Woodruff, J.D., 2013. Reconstructing mid-late Holocene cyclone variability in the Central Pacific using sedimentary records from Tahaa, French Polynesia. *Quat. Sci. Rev.* 77, 181–189. doi:10.1016/j.quascirev.2013.07.019
- van der Plaas, L., Tobi, A.C., 1965. A chart for judging the reliability of point-counting results. *Am. J. Sci.* 263, 87–90.
- Veizer, J., 1982. Chemical diagenesis of carbonates: Theory and application of trace element technique. *Stable Isot. Sediment. Geol.* 10, 1–99. doi:10.2110/scn.83.01.0000
- Vè nec-Peyré, M.-T., 1991. Distribution of living benthic foraminifera on the back-reef and outer slopes of a high island (Moorea, French Polynesia). *Coral Reefs* 105–113. doi:10.1016/B978-012374473-9.00090-4
- Wolf, K.H., Easton, A.J., Warne, S., 1967. Techniques of examining and analyzing carbonate skeletons, minerals and rocks, in: Chilingar, G. V, Bissell, H.J., Fairbridge, R.W. (Eds.), *Developments in Sedimentology 9B - Carbonate Rocks - Physical and Chemical Aspects*. pp. 252–341.

- Yamano, H., Kayanne, H., Matsuda, F., 2002. Lagoonal facies, ages, and sedimentation in three atolls in the Pacific. *Mar. Geol.* 185, 233–247.
- Zinke, J., Reijmer, J.J.G., Taviani, M., Dullo, W.-C., Thomassin, B.A., 2005. Facies and faunal assemblage changes in response to the Holocene transgression in the lagoon of Mayotte (Comoro Archipelago, SW Indian Ocean). *Facies* 50, 391–408. doi:10.1007/s10347-004-0040-7
- Zinke, J., Reijmer, J.J.G., Thomassin, B.A., 2003a. Systems tracts sedimentology in the lagoon of Mayotte associated with the Holocene transgression. *Sediment. Geol.* 160, 57–79. doi:10.1016/S0037-0738(02)00336-6
- Zinke, J., Reijmer, J.J.G., Thomassin, B.A., Dullo, W.-C., Grootes, P.M., Erlenkeuser, H., 2003b. Postglacial flooding history of Mayotte lagoon (Comoro Archipelago, southwest Indian Ocean). *Mar. Geol.* 194, 181–196. doi:10.1016/S0025-3227(02)00705-3
- Zinke, J., Reijmer, J.J.G., Dullo, W.-C., Thomassin, B.A., 2000. Paleoenvironmental changes in the lagoon of Mayotte associated with the Holocene transgression. *Geolines* 11, 150–153.
- Zinke, J.Y., Reijmer, J.J.G., Thomassin, B.A., 2001. Seismic architecture and sediment distribution within the Holocene barrier reef lagoon complex of Mayotte (Comoro archipelago, SW Indian Ocean). *Paleogeography, Paleoclimatology, Paleoecol.* 175, 343–368. doi:10.1016/S0031-0182(01)00379-0

CHAPTER 6

SUMMARY AND OUTLOOK

To evaluate the influence of geomorphological and environmental factors on reef, sand apron and lagoon development through the Holocene, a multi-proxy data set was compiled.

Based on remote sensing and morphological data from 122 atolls and carbonate platforms in the Pacific, Indian and Atlantic Oceans, proportions of sand aprons were quantified and correlated to maximum lagoon depth, total platform area and marginal reef thickness, when available. The current model describes antecedent topography, i.e., the elevation of the underlying Pleistocene karst as a fundamental factor controlling Holocene sand apron development and extension. This is supported by the covariance of sand apron proportions and maximum lagoon depth (as a proxy for antecedent topography). Sand apron proportions increase with decreasing lagoon depths and also increase with decreasing platform area, underlining the importance of platform size. The interaction of antecedent topography and Holocene sea-level rise determines variations in accommodation space and is responsible for the lateral expansion of sand aprons. In general, sand apron formation started when marginal reefs reached modern sea level. It is assumed that regional variability in the course of Holocene sea-level let sand apron formation start earlier in the Indo-Pacific region (transgressive-regressive) than in the Western Atlantic Ocean (transgressive). However, subsurface data of reefs sand aprons to prove this assumption are largely lacking. In the Indo-Pacific region, the mid-late Holocene sea-level highstand and fall restricted vertical accretion of sand aprons due to the constriction of accommodation space, thereby constraining the lateral extent of sand aprons. Carbonate production and sediment generation on marginal reef areas (and to a lesser extent on sand aprons) supplies sediment to be transported into atoll lagoons by sand aprons. The sedimentation rates of sand aprons exceeds lagoonal background sedimentation up to three times and are therefore suited to infill lagoonal accommodation space and create "filled buckets" in small and medium-sized sized carbonate platforms.

Detailed insights into the late Quaternary reef growth and lagoonal evolution of the barrier-reef system of Bora Bora, French Polynesia, South Pacific arises from coupled high-resolution sedimentological, palaeontological, geochronological and geochemical data. These are based on six rotary drill cores taken from barrier and fringing reefs and seven vibrocores taken from the deep lagoon.

Holocene reef architecture is an expression of the interplay of sea-level rise (and fall), antecedent topography and subsidence, all of which created (reduced) accommodation space.

Barrier-reef growth started 10,030 yrs BP with an average accretion rate of 6.15 m/kyr. The Holocene barrier reef consists of more than 30 m thick coralgall and microbial successions, which are characterized by an upcore transition of a massive, to columnar agaricid-rich, to an *Acropora-Pocillopora* assemblage and a robust-branching *Acropora* assemblage including thick *Porolithon onkodes* crusts, vermetids and *Homotrema*. The Holocene barrier reef is located on a Pleistocene barrier reef dated to ca. 117,000 yrs BP (marine isotope stage 5e). The fringing reef started to grow 8780 yrs BP on Pleistocene soil and accreted with 5.65 m/kyrs on average. The fringing reef consists of an *Acropora-Montipora* assemblage with an upcore transition to an *Acropora-Pocillopora*-faviid assemblage with thick crusts of *P. onkodes*, vermetids, and *Homotrema*. Coralgall palaeo-bathymetry data indicates shallowing upcore trends during the Holocene in both barrier and fringing reef sections. In the course of Holocene sea-level variations, barrier and fringing reefs prograded seawards and lagoonwards, respectively. The subsidence rate of Bora Bora is calculated based on an absolute Pleistocene age-depth datum, and on coralgall palaeo-bathymetry and range from a minimum of 0.05 m/kyr to a maximum of 0.14 m/kyr.

The lagoonal succession started with a loamy Pleistocene soil representing the sea-level lowstand in the late Pleistocene. Peat was deposited above the soil, marking the flooding of the rising Holocene sea ca. 10,650-9400 yrs BP. After a hiatus, mixed carbonate-siliciclastic sedimentation started 8700-7700 yrs BP in the eastern lagoon (windward) and 8100-5400 yrs BP in the western lagoon (leeward). During that time, sediment deposition was dominated by lagoonal carbonate production and siliciclastic input from the volcanic hinterland. When sea level reached the modern level of ca. 6000 yrs BP, sand apron formation and vertical accretion started. Sediments produced on the marginal reef were transported lagoonward and hence, fine material was deposited into the lagoon, while coarser grains were retained on the sand apron, forcing their lagoonward progradation. The multi-proxy approach applied to vibrocore APO 2 from the windward lagoon shows an interval of enhanced primary productivity based on total organic carbon (TOC), Cu/Al ratios, Ca intensities and a decrease in Cl intensities during the mid-late Holocene. Enhanced sediment dynamics indicated by an upcore increase in coarse-grained sediments seems to indicate event deposition and might be correlated with coarse-grained deposits found in the barrier-reef lagoon in nearby Tahaa, explained by higher cyclone activity. Cyclone landfall might have caused extensive rainfall events and enhanced run-off from the volcanic hinterland and might have furthermore resulted in lower lagoonal salinity. Reefal sediment would have been transported into the lagoon. However, Ti/Ca and Fe/Ca ratios as proxies for terrestrial sediment input have

decreased steadily during the Holocene and do not support enhanced run-off. Also, foraminifera assemblages do not indicate a reef-to-lagoon transport of coarser material. Alternatively, sustained southeast trade winds and a higher-than-present sea level during the mid-late Holocene could have favored higher hydrodynamic energy conditions and flushed higher amounts of open ocean waters into the lagoon, enhanced primary productivity and the amount of pelagic organism and lowered lagoonal salinity. The increased sediment dynamics between 4500-500 yrs BP are assumed to display sediment-load shedding of sand aprons into the lagoon due to the oversteepening of sand apron slopes during ongoing progradation and sea-level fall to the present level. Since modern conditions were reached ca. 1000 yrs BP, lagoonal infill is characterized by fine-grained carbonate produced within the lagoon and on marginal reef areas, and comprises only minor amounts of terrestrial material imported from the volcanic hinterland. Tropical storms as a driving mechanism of sediment transport from reef to lagoon cannot entirely be excluded; however, it seems that they have played a more ancillary role in lagoonal sedimentation in the long term. Lagoonal infill by sand apron progradation exceeds lagoonal background sedimentation rates up to six times and underlines the importance of sand-apron formation during the Holocene.

Microfacies analyses of two vibrocores, one from the windward and one from the leeward lagoon, reveal temporal and spatial distributions of five mixed carbonate-siliciclastic facies in the barrier-reef lagoon of Bora Bora. During the early-mid Holocene, marly siderite-rich and foraminifera-siderite wackestones accumulated in the windward lagoon core site. Rotalid and miliolid taxa dominate the early-mid Holocene foraminifera fauna and are supposed to tolerate environmental stress such as changes in water quality, nutrients, salinity and oxygen level. The formation of siderite within early-mid Holocene lagoonal sediments is an expression of enhanced iron input from the volcanic island due to wetter climate. Siderite precipitation probably results from microbial decomposition of organic matter indicated by a depletion of $\delta^{13}\text{C}$ (-13.61 to -14.48‰) and iron reduction in the presence of bicarbonate. Marine to mixed marine-meteoric conditions during siderite formation are indicated by the enrichment of $\delta^{18}\text{O}$ ($+0.32$ to $+0.54\text{‰}$). The chemical composition of siderites changes upcore from relatively high Fe (91-95 mol%) and low Mn (5-6 mol%) concentrations at the core base, to lower Fe (83-88 mol%) and higher Mn (11-16 mol%) concentrations in the upper core part. The substitutions of Mn, Ca and Mg, especially at grain margins, illustrate changes in the oxidation state towards more oxygenated conditions and reflect changes in pore-water chemistry due to sea-level rise and climate changes (rainfall) during the early-mid Holocene. When climate conditions became drier, iron input and associated siderite precipitation

declined and vanished during the mid-late Holocene. Mollusk-foraminifera marly packstones and mollusk-rich wackestones accumulated ca. 5400-3500 yrs BP during the mid-Holocene in the leeward lagoon core site. Since the mid-Holocene, textularid foraminifera are prevalent in both lagoons and represent a fauna typically associated with normal marine back-reef lagoons. Since the sea-level highstand and fall to modern level in the mid-late Holocene, sedimentation is characterized by mudstones in both the windward and the leeward lagoon. The amount of coral fragments increased during the past 1000 yrs in the windward lagoon, and has probably resulted from the lagoonward progradation of fringing reefs during the mid-late Holocene. Motus formed due to the overfilling of accommodation space behind reef crests on the windward side and has hampered sediment transport and lagoonward progradation of sand aprons since the late Holocene. Therefore, the increase in peloids since the late Holocene is assumed to reflect early submarine lithification due to sediment stability and time, rather than the expression of sediment transport.

The Holocene development of reefs and lagoons, facies successions, sediment import, composition and distribution were interpreted in respect to Holocene sea-level and climate variations. Climate change is an overriding mechanism guiding Quaternary eustatic sea-level fluctuations, variations of the hydrodynamic energy system and at least terrestrial sediment input into a marine system. The combination of sea-level rise, subsidence and antecedent topography plays a crucial role in that these factors created accommodation space for the reefs to grow and the sediments to be generated, transported (via sand aprons) and deposited.

Several interesting results originated from this thesis and may be used as starting points for further research:

- The antecedent topography model of reef development (Purdy, 1974) was applied to the Holocene development of sand aprons, however, subsurface data of sand aprons are still lacking (Isaack and Gischler, 2015). A future project considering the Holocene formation and development of sand aprons is planned and will help to solve questions regarding the timing and behavior of sand aprons with respect to lagoonal infill processes (empty vs. filled bucket).
- Contrary to traditional interpretations of marginal reefs prograding seawards in the course of the Holocene, Dechnik et al. (2016) postulated a lagoonward movement direction for the windward marginal reefs in the Southern Great Barrier Reef. To validate this assumption in Bora Bora, a second field trip will be taken in May 2017.

- Additional identification and quantification of benthic foraminifera species from the Bora Bora lagoon could give more precise indications of their palaeo-ecology and the variations of their palaeo-environment during very short time spans in the Holocene.
- Further geochemical investigations of syngedimentary siderite within the Bora Bora lagoon, e.g., chemical composition, will help to decipher the timing of palaeo-environmental changes, e.g., variations in the oxygenation state. Lipid biomarker analyses could be used to prove the assumption of microbial activity during formation processes of siderite within the lagoon and might link the siderite formations process to the occurrence of microbialites in the coral reef sections.
- A climate challenge during the past 3000 yrs BP caused hydrologic and cyclone variability in nearby Tahaa, French Polynesia (Toomey et al., 2016b). Further investigations, e.g., xrf core scanning of lagoonal vibrocores (e.g., core TAI 1) might reveal information regarding environmental changes e.g., possible storm deposition.
- The combination of oxygen and carbon isotope, along with the Sr/Ca analyses and Gamma-densitometer measurements of a coral skeleton (42 cm long) from the early Holocene is currently in progress. These analyses are going to be used for the reconstruction of palaeo-climate and the calculation of calcification rates during the early Holocene.
- The interpretation of the seismic survey is still in progress and will probably reveal insights into palaeo-geomorphology and the role of antecedent topography and the late Pleistocene sea-level lowstand for the formation of the back-reef lagoon of Bora Bora.

References

- Dechnik, B., Webster, J.M., Nothdurft, L., Webb, G.E., Zhao, J., Duce, S., Braga, J.C., Harris, D.L., Vila-Concejo, A., Puotinen, M., 2016. Influence of hydrodynamic energy on Holocene reef flat accretion, Great Barrier Reef. *Quat. Res.* 85, 44–53. doi:10.1016/j.yqres.2015.11.002
- Isaack, A., Gischler, E., 2015. The significance of sand aprons in Holocene atolls and carbonate platforms. *Carbonates and Evaporites*. doi:10.1007/s13146-015-0268-z
- Purdy, E.G., 1974. Reef configurations: cause and effect, in: Laporte, L.F. (Ed.), *Reefs in Time and Space*. pp. 9–76.
- Toomey, M.R., Donnelly, J.P., Tierney, J.E., 2016. South Pacific hydrologic and cyclone variability during the last 3000 years. *Paleoceanography* 31, 491–504. doi:10.1002/2015PA002870

ZUSAMMENFASSUNG

Um den Einfluss geomorphologischer und Umweltfaktoren auf die Entwicklung von Riffen, Sand Aprons und Lagunen im Holozän zu bewerten wurde ein Multi-Proxy-Ansatz erstellt.

Per Fernerkundung wurden die flächenanteiligen Proportionen von Sand Aprons in 122 Atollen und Karbonatplattformen im Pazifik, Indischen Ozean und Atlantik quantifiziert. Diese Ergebnisse wurden mit maximaler Lagumentiefe, Plattformgröße und, wenn vorhanden, Riffmächtigkeit korreliert. Das vorliegende Model beschreibt die Topographie der Riffbasis, d.h. die Höhenlage des zugrunde liegenden Pleistozänen Karstes, als einen wichtigen Faktor, der die Entwicklung und Ausbreitung von Sand Aprons im Holozän steuert. Diese Annahme wird durch die Kovarianz von Sand Apron Proportionen und maximaler Lagumentiefe (Proxy für die Topographie der Riffbasis) forciert. Die Sand Apron Proportionen nehmen mit abnehmender Lagumentiefe und abnehmender Plattformgröße zu. Das Zusammenspiel der Topographie der Riffbasis und der Anstieg des Holozänen Meeresspiegels bestimmt die Variationen des Ablagerungsraumes, und ist für die laterale Ausdehnung der Sand Aprons verantwortlich. Im Allgemeinen begann die Bildung der Sand Aprons als die am Rand gelegenen Riffe das Niveau des relativen Meeresspiegels erreichten. Vermutlich führten regionale Unterschiede des Kurses des Holozänen Meeresspiegels dazu, dass die Bildung der Sand Aprons im Indo-Pazifik (transgressiv-regressiv) früher als im Atlantik (transgressiv) begann. Daten aus dem geologischen Untergrundes der Sand Aprons, die diese Annahme bestätigen könnten, fehlen allerdings. In der Indo-Pazifischen Region schränkt der Meeresspiegel-Hochstand und Fall im mittleren bis späten Holozän die vertikale Akkretion und laterale Ausdehnung der Sand Aprons durch die Minimierung des Ablagerungsraumes ein. Karbonatproduktion und Sedimentbildung findet an den Riffrändern (und in einem kleineren Ausmaß auf den Sand Aprons) statt und liefern Sediment, dass über die Sand Aprons in die Atoll-Lagunen transportiert wird. Die Sedimentationsraten der Sand Aprons sind bis zu dreimal höher als die lagunäre Hintergrundsedimentation und eignen sich aus diesem Grund für die Auffüllung des lagunären Ablagerungsraumes und erzeugen „Filled Buckets“ in kleinen und mittelgroßen Karbonatplattformen.

Untersuchungen an sechs Rotationsbohrkernen aus den Barriere- und Saumriffen sowie an sieben Vibrationsbohrkernen aus der tiefen Lagune von Bora Bora, Französisch Polynesien, Südpazifik, gewähren detaillierte Einblicke in das spät-Quartäre Riffwachstum und die lagunäre Entwicklung des Barriereriff-Systems.

Das Zusammenspiel von Meeresspiegelanstieg (und Fall), Topographie der Riffbasis und Subsidenz (in geringerem Ausmaß) bildet (bzw. reduziert) den Ablagerungsraum und ist für die Holozäne Riffarchitektur verantwortlich. Das Barriereriff-Wachstum begann 10030 a v.h. (Jahre vor heute) mit durchschnittlichen Akkretionsraten von 6.15 m/ka. Das Holozäne Barriereriff besteht aus mehr als 30 m mächtigen Abfolgen von Korallen/Algen und Mikrobialiten. Diese Abfolgen sind durch den Übergang einer massiv-säulenförmigen agaricid-reichen *Acropora-Pocillopora* Vergesellschaftung zu einer robust-verzweigten *Acropora* Vergesellschaftung geprägt, welche mächtige Krusten von *Porolithon onkodes*, Vermetiden und *Homotrema* enthalten. Das Holozäne Barriereriff sitzt auf einem Pleistozänen Barriereriff, welches auf ein Alter von 117000 a v.h. (Marines Isotopenstadium 5e) datiert wurde. Das Saumriff begann 8780 a v.h. auf Pleistozänem Boden und mit durchschnittlichen Akkretionsraten von 5.65 m/ka zu wachsen. Das Saumriff besteht aus einer *Acropora-Montipora* Vergesellschaftung, die in eine *Acropora-Pocillopora*-faviide Vergesellschaftung mit *P. onkodes* Krusten, Vermetiden und *Homotrema* übergehen. Paläobathymetrie Daten von Korallen und Algen aus Barriereriff- und Saumriffkernen weisen auf einen Shallowing-Upward Trend während des Holozäns hin. Im Zuge der Meeresspiegelschwankungen im Holozän progradieren die Barriereriffe seewärts und die Saumriffe lagunenwärts. Die Subsidenzrate in Bora Bora schwankt zwischen einem Minimum von 0.05 m/ka bis zu einem Maximum von 0.14 m/ka und basiert auf absoluten Pleistozänen Alter/Tiefen Angaben.

Die lagunäre Abfolge beginnt mit einem lehmigen Pleistozänem Boden, der den Meeresspiegel-Tiefstand im späten Pleistozän repräsentiert. Die Ablagerung von Torf markiert die Flutung des ansteigenden Meeresspiegels ca. 1065-9400 a v.h. Nach einer Sedimentationslücke setzt die gemischt karbonat-siliziklastische Sedimentation in der östlichen Lagune (luv) ca. 8700-7700 a v.h und in der westlichen Lagune (lee) ca. 8100-5400 a v.h. ein. Während dieser Zeit sind die Sedimente von der lagunären Karbonatproduktion und vom siliziklastischen Eintrag des vulkanischen Hinterlandes geprägt. Die Bildung und vertikale Akkretion der Sand Aprons begann ca. 6000 a v.h. als der Meeresspiegel sein heutiges Niveau erreichte. Sedimente wurden an den Riffändern produziert und lagunenwärts transportiert. Somit wurde überwiegend feines Material innerhalb der Lagune abgelagert, während grobkörniges Material auf den Sand Aprons liegen blieb und deren lagunenwärts gerichtete Progradation forcierte. Der Multi-Proxy-Ansatz wurde beim Kern APO 2 (windseitige Lagune) angewendet und zeigt basierend auf TOC-Gehalten (gesamter organischer Kohlenstoff), Cu/Al Verhältnissen und Ca Intensitäten ein

Interval erhöhter Primärproduktivität, sowie eine Abnahme der Cl Intensitäten während des mittleren bis späten Holozäns. Erhöhte Sedimentdynamik wird durch eine Zunahme von grobkörnigen Sedimentlagen im oberen Teil des Kerns angezeigt und weist möglicherweise auf Ereignissedimentation hin. Die grobkörnigen Sedimentlagen konnten mit Eventlagen aus der Barriereriff-Lagune des benachbarten Karbonatplattform Tahaa korreliert werden. Die vorhandenen Eventlagen werden mit einer Zunahme der Zyklonaktivität erklärt. Wenn Zyklonen an Land auftreffen, können Starkregenereignisse hervorgerufen werden, die den Run-off (Ablauf) vom vulkanischen Hinterland erhöhen und den lagunären Salzgehalt senken. Die Konsequenz daraus ist ein erhöhter Eintrag von grobkörnigem Sediment vom Riffrand in die Lagune. Als Proxys für terrestrischen Eintrag wurden Ti/Ca und Fe/Ca Verhältnisse verwendet; diese nehmen jedoch während des Holozäns stetig ab und zeigen insofern keinen erhöhten Run-off an. Auch die Zusammensetzung der Foraminiferen-Fauna zeigt keinen Transport des grobkörnigen Materials vom Riffrand in die Lagune an. Eine alternative Erklärung schließt die Südost-Passatwinde und einen höheren Meeresspiegelstand während des mittleren bis späten Holozäns ein. Eine starke und anhaltende Windaktivität würde das hydrodynamischen Energieniveau erhöhen und permanent offenozeanisches Wasser in die Lagune spülen. Somit würde die Primärproduktivität und die Menge an pelagischen Organismen erhöht, und weiterhin der Salzgehalt der Lagune verringert werden. Es wird angenommen, dass eine extreme Steillage der Sand-Apron Hänge während der lagunewärts gerichteten Progradation und Meeresspiegel fall zu Hangrutschungen (in die Lagune) führt. Dieser Vorgang wird durch die erhöhte Sedimentdynamik (grobkörnige Sedimentlagen in der Lagune) zwischen 4500-500 a v.h. widergespiegelt. Die heutigen Verhältnisse (Bedingungen) wurden etwa 1000 a v.h. erreicht. Die Auffüllung des lagunären Ablagerungsraumes ist seitdem durch feinkörnige Karbonatsedimente charakterisiert, die sowohl in der Lagune als auch am Randriff gebildet werden. Die Lagune erhält nur noch wenig terrestrisches Material vom vulkanischen Hinterland. Tropische Stürme können als treibender Faktor für Sedimenttransport nicht völlig ausgeschlossen werden. Allerdings scheint es als ob tropische Stürme dabei eine eher untergeordnete Rolle spielen. Die Auffüllung des lagunären Ablagerungsraumes durch die Progradation der Sand Aprons ist in Bora Bora bis zu sechsmal höher als die lagunäre Hintergrundsedimentation und unterstreicht die wichtige Bedeutung der Bildung der Sand Aprons während des Holozäns.

Mikrofazielle Untersuchungen zweier Vibrationsbohrkerne, jeweils von der lee- und luvseitigen Lagune, enthüllen die zeitliche und räumliche Verteilung gemischt karbonatisch-siliziklastischer Sedimentfazies in der Barriereriff-Lagune von Bora Bora. Mergelige Siderit-

reiche und Foraminiferen-Siderit Wackestones wurden während des frühen bis mittleren Holozäns in der luvseitigen Kernlokation der Lagune abgelagert. Rotalide und Miliolide Foraminiferen sind die dominanten Taxa während dieser Zeit. Es wird angenommen, dass diese Formen Umweltstress, wie etwa Schwankungen/Änderungen der Wasserqualität, Nährstoffgehalt, Salinität oder Sauerstoffgehalt tolerieren. Die Bildung von Sideriten in den Lagunensedimenten des frühen bis mittleren Holozäns ist die Konsequenz erhöhter Eisengehalte, die während Zeiten feuchteren Klimas von der Vulkaninsel eingetragen werden. Die Sideritausfällung resultiert aus mikrobieller Zersetzung des organischen Materials und ist durch eine Abreicherung des $\delta^{13}\text{C}$ (-13.61 to -14.48‰) und Eisenreduzierung in Gegenwart von Hydrogenkarbonat gekennzeichnet. Marin bis gemischt marin-meteorische Bedingungen während der Sideritbildung sind durch eine Anreicherung von $\delta^{18}\text{O}$ ($+0.32$ to $+0.54\text{‰}$) charakterisiert. Die chemische Zusammensetzung der Siderite verändert sich kernaufwärts, von relativ hohen Eisengehalten (91-95 mol%) und niedrigen Mangangehalten (5-6 mol%) im unteren Kernbereich bis hin zu niedrigeren Eisengehalten (83-88 mol%) und höheren Mangangehalten (11-16 mol%) im oberen Kernbereich. Die Substitutionen von Mangan, Calcium und Magnesium an den Rändern einzelner Sideritkörner veranschaulicht Veränderungen des Oxidationszustandes hin zu sauerstoffreicheren Bedingungen und spiegelt Änderungen in der Chemie des Poreswassers wider, die durch den Meeresspiegelanstieg und Klimawandel (Niederschlag) während des frühen bis späten Holozäns stattfanden. Als das Klima trockener wurde verringerten sich der Eiseneintrag und die Ausfällung von Sideriten. Die Siderite verschwanden schließlich im mittleren bis späten Holozän. Im Zeitraum von 5400-3500 a v.h. wurden mergelige Mollusken-Foraminiferen Packstones und Molluskenreiche Wackestones in der leeseitigen Kernlokation der Lagune abgelagert. Textularide Foraminiferen sind seit dem mittleren Holozän in der gesamten Lagune verbreitet und repräsentieren eine für normal-marine RückriffLAGUNEN typische Foraminiferen-Vergesellschaftung. Die Sedimentation ist seit dem Meeresspiegel-Hochstand und Absinken auf sein heutiges Niveau während des mittleren bis späten Holozäns in der gesamten Lagune durch Mudstones charakterisiert. Die Menge an Korallenfragmenten hat sich seit den letzten 1000 a v.h. erhöht und resultiert vermutlich aus der lagunenwärts gerichteten Progradation der Saumriffe während des mittleren bis späten Holozäns. Motus (kleine, langgestreckte Sandinseln) bildeten sich aufgrund von Überfüllung des Ablagerungsraumes hinter der Riffkante auf der Luvseite und hindern die lagunenwärts gerichtete Progradation der Sand Aprons seit dem späten Holozän. Deshalb wird angenommen, dass die Zunahme von Peloiden

seit dem späten Holozän eher eine frühe submarine Lithifikation statt Sedimenttransport vom nahe gelegenen Sand Apron repräsentiert.

Die Holozäne Entwicklung von Riffen, Faziesabfolgen, Sedimenteintrag, Zusammensetzung und Verteilung wurden hinsichtlich Holozäner Meeresspiegel- und Klimaschwankungen interpretiert. Klimawandel ist ein übergeordneter Mechanismus, der Quartäre eustatische Meeresspiegelschwankungen, Änderungen des hydrodynamischen Energiesystems und letztendlich den Eintrag von terrestrischem Sediment in das marine System steuert. Die Kombination von Umwelt- und geomorphologischen Faktoren wie Meeresspiegel, Subsidenz und Topographie der Riffbasis ist von großer Bedeutung, denn diese Faktoren sind für die Bildung des Ablagerungsraums zuständig, welcher essentiell wichtig für das Riffwachstum, Sedimentbildung und Transport via Sand Aprons ist.

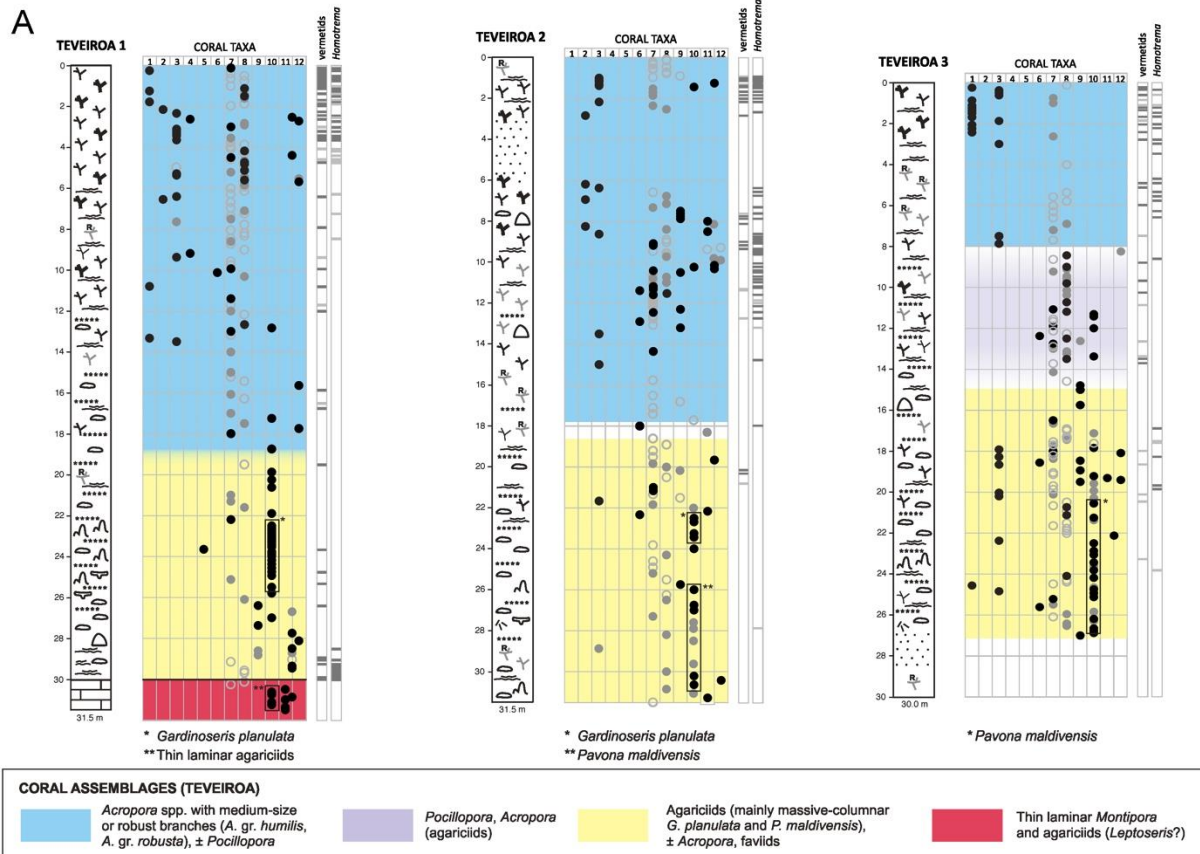
LIST OF NOTATIONS AND ABBREVIATIONS

%	Percent	MgCO ₃	Magnesium carbonate
°C	Degree Celcius	MgO	Magnesium oxide
µm	Micrometer	MIS	Marine Isotope Stage
‰	Per mill	Mn	Manganese
a v.h.	Jahre vor heute	MnCO ₃	Manganese carbonate
Al	Aluminium	MnO	manganese oxide
AMS	Accelerated Mass Spectroscopy	ms	Millisecond
APO	Aponapu	MSCL	Multi-Sensor Core Logger
Ba	Barium	MSL	Mean Sea Level
BB	Bora Bora	n	Number
BP	Before present	N	North
C	Carbon	NaOH	Sodium hydroxide
Ca	Calcium	NIST-SRM 3159 (Th)	National Institute of Standards and Technology Standard Reference Material for Thorium
ca.	Circa	NIST-SRM 3164 (U)	National Institute of Standards and Technology Standard Reference Material for Uranium
CaCO ₃	Calcium carbonate	O	Oxigen
cal.	Calibrated	p	Pages
CaO	Calcium oxide	PC	Principal component
CHA	Channel	PCA	Principal Component Analysis
Cl	Clorine	pg	Picogram
cm	Centimeter	POV	Povai
CO ₂	Carbon dioxide	ppm	Parts per million
cps	Counts per second	rel.	Relative
CRM 145	Certified Reference Material (uranium standard solution)	RSL-ICE-5G+VM2	ice sheet chronology and the viscosity profile (refers to Rashid et al., 2014)
Cu	Copper	RSL-RSES-ANU+VKL	ice sheet model and Mantle profile (refers to Rashid et al., 2014)
dpm	Defects per million	S	Sulfur
E	East	S	South
e.g.	<i>exempli gratia</i>	SEM	Scanning Electron Microscopy
EMP	Electron microprobe	sid	Siderite
ENSO	El Niño Southern Oscillation	sp.	Species
FAA	Faanui	spp.	Species pluralis
Fe	Iron	Sr	Strontium
FeO	Iron oxide	SST	Sea Surface Temperature
g	Gram	std	Standard
GIA	Glacial Isostatic Adjustments	TAI	Taimoo
GPS	Global Positioning System	TEV	Teveiroa
HCl	Hydrochloric acid	Th	Thorium
HS	Hydrogen sulphide	Ti	Titanium
HST	Highstand systems tract	TOC	Total Organic Carbon
HU-1	Harwell uraninite (standard)	TST	Transgressive systems tract
i.e.	<i>id est</i>	TWT	two-way time
Inc.	Incorporation	U	uranium
IODP	International Ocean Discovery Program	V-PDB	Vienna Pee-Dee Belemite
ITCZ	InterTropical Convergence Zone	W	West
ka/kyrs	Kiloyears	WDX	Wavelength-dispersive spectrometer
K-Ar	Potassium-argon	wt%	Weight percent
kHz	Kilohertz	XRD	X-Ray Diffractometer
km	Kilometer	XRF	X-Ray Fluorescence
kV	Kilovolt	yrs	Years
LST	Lowstand systems tract	Zn	Zinc
m	Meter	δ ¹³ C	Delta ¹³ C
Ma	Million years	δ ¹⁸ O	Delta ¹⁸ O
MC-ICP-MS	Multi-Ion-Counting Inductively Coupled Plasma Mass Spectroscopy		
Mg	magnesium		

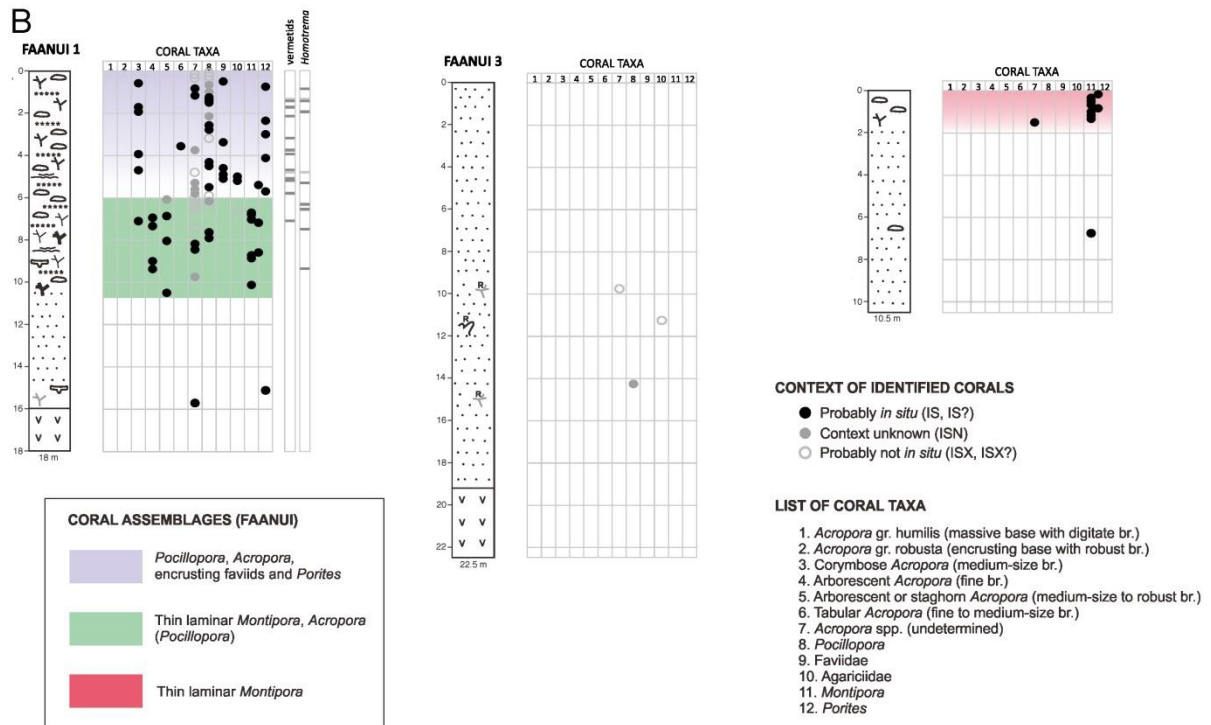
SUPPLEMENTAL MATERIAL

Chapter 3

Supplement Figures



Suppl. Fig. 3/1: **a)** Data on coral distribution, and the occurrence of high-energy indicators *Homotrema* and vermetids. Barrier reef cores; **b)** Data on coral distribution, and the occurrence of high-energy indicators *Homotrema* (encrusting foraminifer) and vermetids (worm gastropods). Fringing reef cores. Legend for core logs in figs. 3/4 and 3/5



Suppl. Fig. 3/2: a) Data on distribution of coralline algae and thickness of coralline algal crusts. Barrier reef cores; b) Data on distribution of coralline algae and thickness of coralline algal crusts. Fringing reef core FAA1. Legend for core logs in fig. 4 and 5

Chapter 4

Supplement Tables

Suppl. table 4/1: Contents of siliciclastic and organic material (insoluble residue) of bulk samples from lagoonal vibrocores

Siliciclastic & organic content (%)							
core depth (cm)	APO 2	APO 3	CHA 1C	FAA 1B	FAA 6	POV 2	TAI 1
9.7	13.2	13.5	17.1	17.2	4.1	3.5	
11.3	10.0		14.1	13.6	3.8		
8.7	9.7		11.7	12.7	3.1		
12.8	8.2		10.5	13.4	4.6		
6.8	8.6		8.2	11.1	3.6		
12.6	16.8	12.9	13.2	14.7	3.3		
12.9	14.1		20.7	13.5	2.3		
9.1	8.6		7.7	7.2	1.3		
17.6	12.0		10.6	8.1	3.4		
8.2	9.9		7.1	15.9	3.3	16.3	
12.2	20.4	15.4	8.2	16.9	7.7		
31.2	11.9		29.2	14.6	8.2		
12.2	13.8		10.2	12.0	9.6		
7.4	5.3		27.2	13.6	5.9		
9.2	8.0		24.9	18.3	5.2		
24.3	11.5	8.9	10.2	20.5	6.0		
10.9	13.3		12.6	15.6	5.7		
14.8	13.8		12.8	20.3	6.9		
11.2	11.8		10.5	18.5	5.4	8.0	
14.6	15.4		7.3		5.2		
16.1	15.4	7.2	12.1		7.0		
28.9	19.8		9.9		9.8		
23.7	14.5		11.9		11.9		
14.3	9.6		13.3		10.8		
7.3	10.5		11.0		8.8		
11.3	14.3	14.9	12.6		7.3		
6.9	27.4		21.6		7.8		
5.1	23.3		14.8		7.2	6.1	
8.3	12.0		22.6		8.3	16.7	
6.4	11.6		16.2		8.5	6.3	
6.1	12.6	12.9	18.5		9.6	5.4	
6.7	16.6		15.8		10.7	13.0	
8.9	16.8		18.4		9.9	20.7	
6.1	20.4		29.3		10.7	11.1	
7.7	34.7		34.2		12.1	9.8	
16.9		16.2					
13.8							
13.8							
19.4							
16.2							
30.5							
18.4							
22.3							
28.9							
13.7	14.2	12.7	15.3	14.6	6.8	10.6	
7.0	5.8	3.1	7.0	3.6	2.9	5.5	

Suppl. table 4/2: Carbonate phases of bulk samples from lagoonal vibrocores according to XRD measurements. Ara = aragonite; LMC = low magnesium calcite; HMC = high magnesium calcite

cores	APO 2			APO 3			CHA 1C			FAA 1B			FAA 6			POV 2			TAI 1		
	Ara (wt%)	LMC (wt%)	HMC (wt%)	Ara (wt%)	LMC (wt%)	HMC (wt%)	Ara (wt%)	LMC (wt%)	HMC (wt%)	Ara (wt%)	LMC (wt%)	HMC (wt%)	Ara (wt%)	LMC (wt%)	HMC (wt%)	Ara (wt%)	LMC (wt%)	HMC (wt%)	Ara (wt%)	LMC (wt%)	HMC (wt%)
0	92.2	0.7	7.1	91.7	0.7	7.6	92.7	0.7	6.6	94.4	0.8	4.8	92.4	1.2	6.4	89.9	1.1	9.0			
10	91.8	0.9	7.3	92.1	0.7	7.2				94.7	0.7	4.6	94.0	1.0	5.0	91.1	0.9	8.0			
20	92.0	0.6	7.3	91.8	0.8	7.4				94.8	0.7	4.5	94.2	1.0	4.8	89.9	0.9	9.1			
30	91.8	0.8	7.4	91.7	0.9	7.4				94.5	0.7	4.8	94.1	1.0	4.9	90.3	0.9	8.7			
40	91.0	0.8	8.2	91.7	0.8	7.5				94.2	0.8	5.0	93.9	1.2	4.9	90.7	0.9	8.4			
50	90.8	0.8	8.4	91.4	0.7	7.9	92.1	0.7	7.2	94.1	0.8	5.0	93.2	1.3	5.5	90.4	1.0	8.7			
60	91.3	0.9	7.8	91.5	0.8	7.7				93.7	0.9	5.4	93.9	1.0	5.1	90.5	0.9	8.6			
70	91.3	0.8	7.9	91.5	0.8	7.7				94.1	0.7	5.2	94.0	1.1	5.0	90.3	0.9	8.7			
80	90.9	0.9	8.2	90.2	1.9	7.9				94.1	0.9	5.0	94.4	0.9	4.8	91.0	1.0	8.0			
90	91.3	0.9	7.9	90.7	0.9	8.5				93.4	0.8	5.8	94.1	1.1	4.7	90.6	0.9	8.5	94.2	1.1	4.8
100	90.5	0.8	8.7	90.6	0.9	8.5	92.1	0.8	7.2	93.6	0.8	5.6	94.6	1.0	4.4	90.7	1.0	8.3			
110	90.1	1.0	8.9	89.6	2.3	8.1				93.6	0.7	5.7	94.5	1.0	4.6	91.0	0.9	8.1			
120	90.3	1.0	8.7	91.6	0.7	7.6				93.5	0.8	5.7	94.0	1.0	4.9	89.9	1.0	9.1			
130	90.8	0.9	8.3	91.7	0.7	7.6				93.8	0.8	5.4	94.5	1.1	4.5	90.0	1.2	8.8			
140	91.1	0.9	8.0	91.7	0.7	7.6				93.7	0.7	5.5	94.5	1.0	4.5	89.1	1.7	9.2			
150	91.6	1.0	7.4	91.1	0.9	8.0	92.0	0.8	7.2	93.6	0.9	5.5	94.4	0.9	4.7	90.0	1.1	8.9			
160	91.4	1.0	7.6	91.3	0.9	7.7				93.7	0.8	5.4	94.7	1.0	4.3	90.2	1.1	8.8			
170	91.0	1.2	7.8	91.6	0.9	7.5				93.7	0.9	5.4	94.9	1.1	4.0	90.2	1.2	8.6			
180	90.8	1.2	8.0	91.4	0.9	7.7				93.7	0.7	5.6	94.6	1.0	4.4	90.2	1.1	8.7	94.3	0.9	4.8
190	90.9	1.1	8.1	91.1	1.0	7.9				94.1	0.8	5.0	93.4	1.3	5.3	89.8	1.2	9.0			
200	90.6	1.2	8.2	89.6	1.2	9.2	91.8	0.8	7.4	92.7	1.9	5.4				89.7	1.3	9.0			
210	90.6	1.1	8.3	89.3	1.3	9.4				93.2	1.0	5.8				89.5	1.4	9.1			
220	89.6	1.4	9.0	89.5	1.3	9.2				93.7	1.0	5.3				89.6	1.4	9.1			
230	89.6	1.4	8.9	89.4	1.3	9.4				93.2	1.1	5.7				88.2	2.7	9.1			

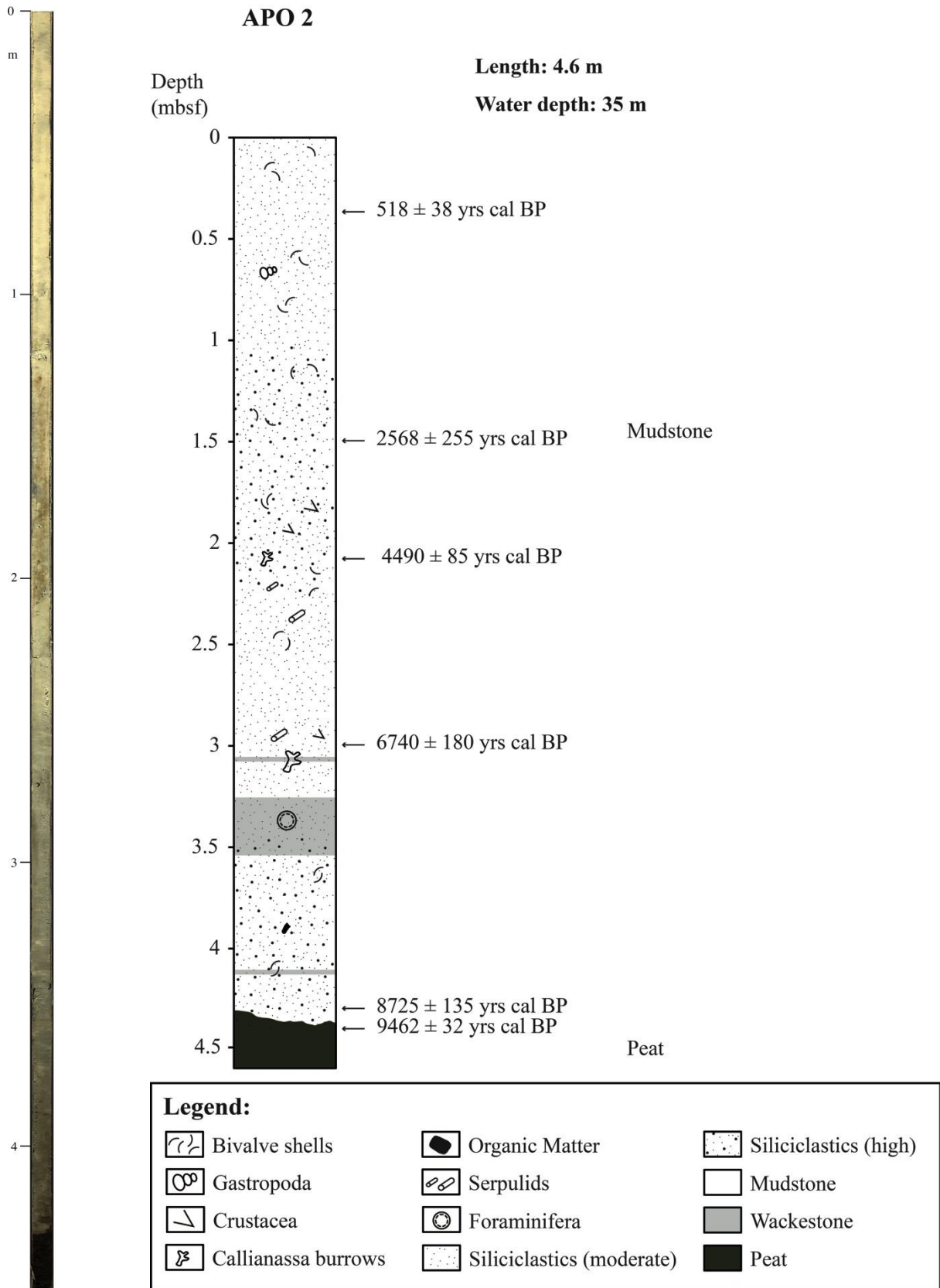
Continue on next page

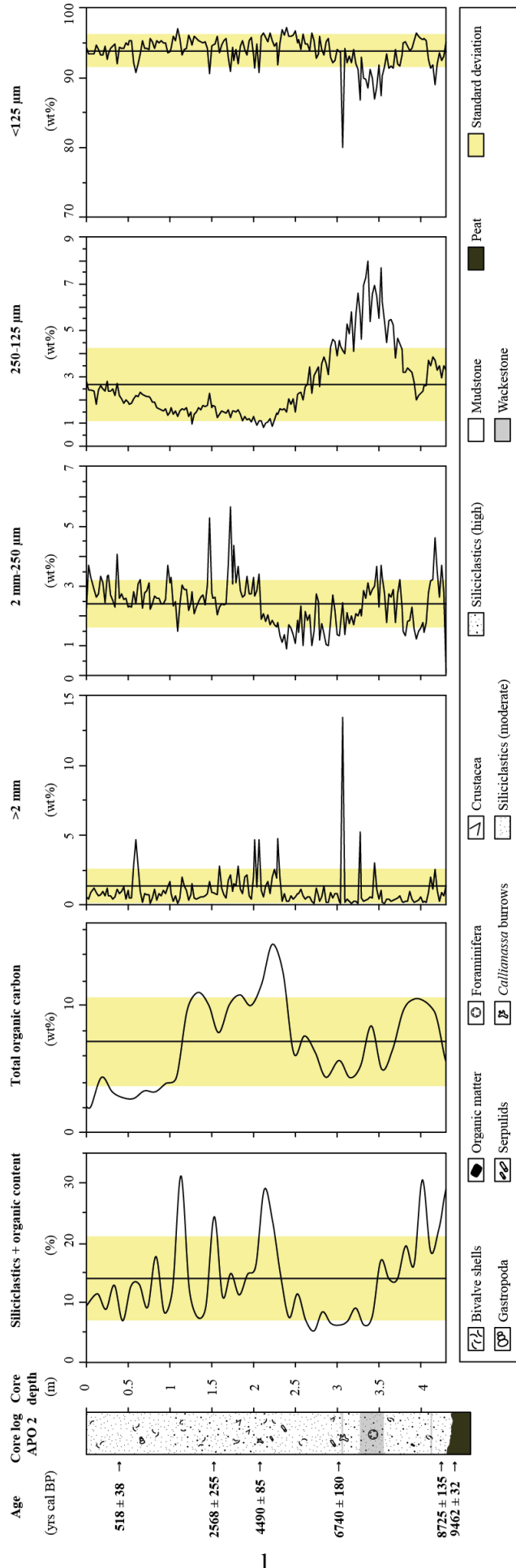
cores	APO 2			APO 3			CHA 1C			FAA 1B			FAA 6			POV 2			TAI 1					
	Ara (wt%)	LMC (wt%)	HMC (wt%)	Ara (wt%)	LMC (wt%)	HMC (wt%)	Ara (wt%)	LMC (wt%)	HMC (wt%)	Ara (wt%)	LMC (wt%)	HMC (wt%)	Ara (wt%)	LMC (wt%)	HMC (wt%)	Ara (wt%)	LMC (wt%)	HMC (wt%)	Ara (wt%)	LMC (wt%)	HMC (wt%)			
core depth (cm)																								
240	89.4	1.4	9.3	88.8	1.2	10.0				93.1	1.2	5.7				88.7	1.6	9.6						
250	89.6	1.4	8.9	89.2	1.1	9.7	92.3	0.9	6.7	91.8	1.9	6.3				88.6	1.5	9.9						
260	90.1	1.3	8.6	88.9	1.4	9.7				91.9	1.5	6.6				88.2	1.6	10.2						
270	89.6	1.5	8.9	89.2	1.3	9.5				91.0	2.2	6.8				87.7	1.7	10.6	94.0	1.2				
280	89.0	1.5	9.6	87.4	1.6	11.0				91.1	1.9	7.0				88.1	1.5	10.4	94.2	1.1	4.8			
290	89.3	1.5	9.3	87.7	1.3	11.0				90.6	1.9	7.5				87.7	1.6	10.7	93.4	1.2	4.7			
300	88.3	1.5	10.2	87.6	1.2	11.2	91.2	1.3	7.5	85.1	5.0	9.8				87.3	1.5	11.2	93.6	1.1	5.4			
310	87.6	1.8	10.6	86.1	1.9	12.0				83.8	7.0	9.2				86.2	1.8	12.0	93.4	1.1	5.3			
320	87.3	1.6	11.1	86.6	1.5	11.9				77.1	12.7	10.2				86.3	1.7	12.0	92.6	1.1	5.5			
330	87.1	1.6	11.3	85.0	1.7	13.3				84.9	6.2	8.9				85.0	2.1	12.9	92.4	1.0	6.3			
340	85.5	1.8	12.7	83.3	4.1	12.6				83.6	7.7	8.7				86.6	2.0	11.4	90.5	1.2	6.6			
350	85.4	1.6	12.9				88.3	1.9	9.8															
360	84.0	1.7	14.3																					
370	84.9	1.6	13.6																					
380	84.7	1.5	13.8																					
390	85.4	1.8	12.8																					
400	85.2	1.7	13.2																					
410	87.1	1.7	11.3																					
420	87.3	1.9	10.8																					
430	86.1	3.1	10.7																					
mean	89.2	1.3	9.5	89.8	1.2	9.0	91.6	1.0	7.5	91.9	2.0	6.1	94.1	1.1	4.8	89.2	1.3	9.4	93.3	1.1				
std	2.4	0.5	2.0	2.2	0.6	1.7	1.4	0.4	1.0	4.0	2.6	1.5	0.6	0.1	0.5	1.6	0.4	1.2	1.2	0.1		1.2	0.1	5.6
																								1.1

APPENDIX

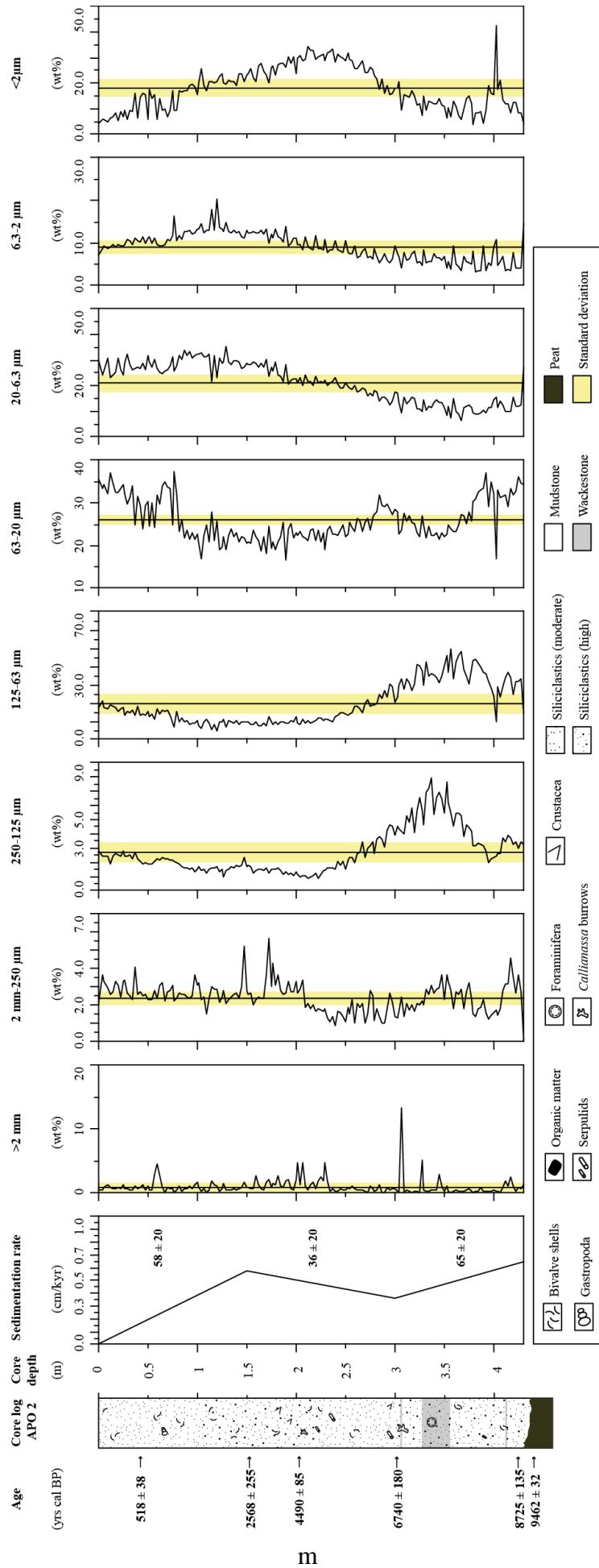
Additional figures and data of lagoonal vibrocores from Bora Bora, South Pacific

Core APO 2



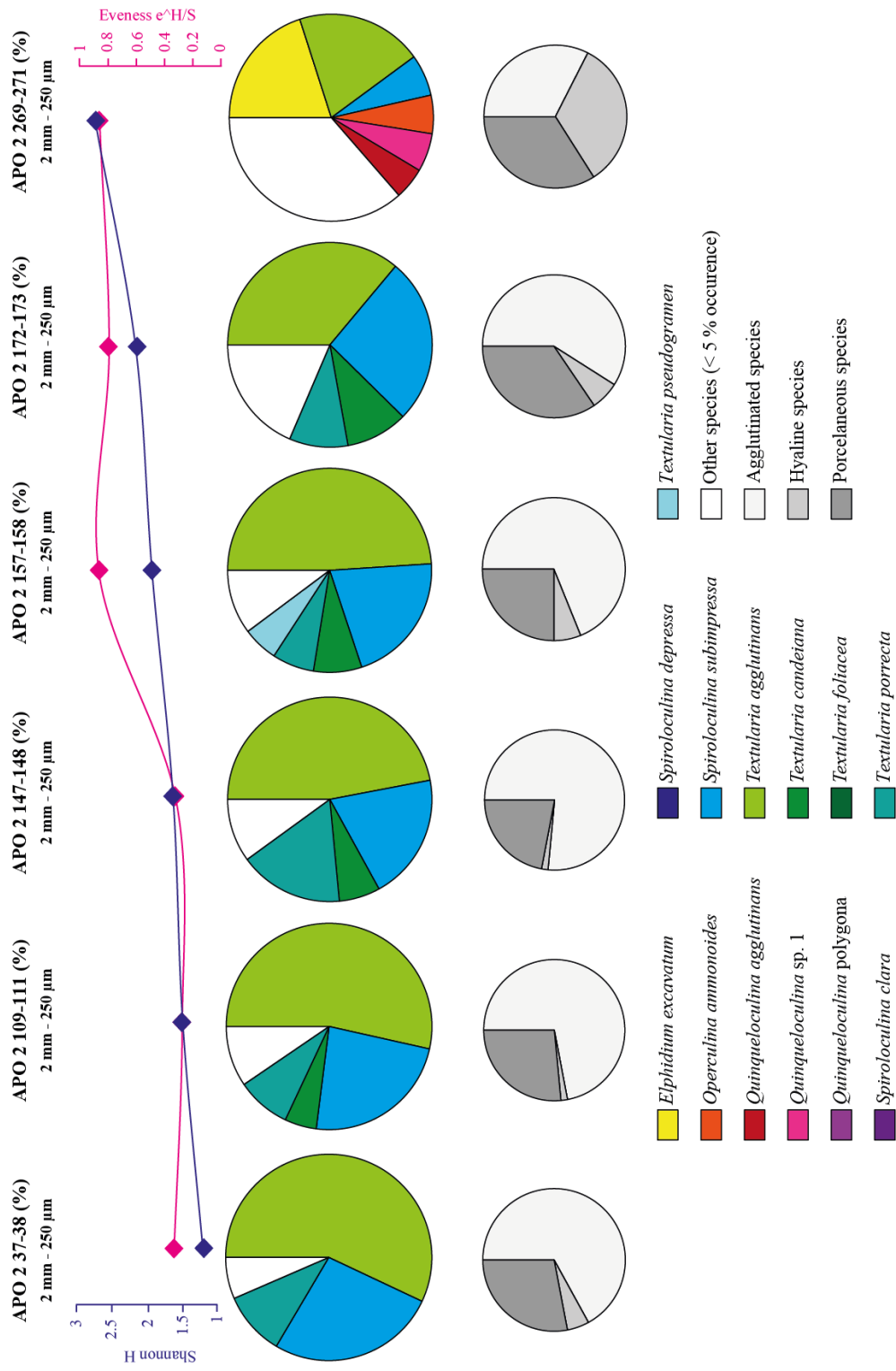


Core APO 2: Corelog, texture, siliciclastics and total organic carbon (TOC)



Core APO 2: Corelog and high-resolution grain-size analyses

potentially redeposited background sediment potentially redeposited background sediment potentially redeposited background sediment



n

Core APO 2: Foraminifera assemblages and diversity indices

Core APO 2: Grain-size analyses

core depth (cm)	>2 mm (wt%)	2-0.25 mm (wt%)	0.25-0.125 mm (wt%)	<0.125 mm (wt%)
3.0	0.44	3.70	2.44	93.42
6.5	0.88	3.30	2.46	93.37
12.5	0.89	2.62	1.84	94.65
15.0	0.69	2.75	2.43	94.13
17.5	0.72	3.32	2.64	93.32
22.5	0.68	2.44	2.40	94.48
25.0	1.26	3.32	2.80	92.62
27.5	0.71	3.38	2.40	93.52
32.5	0.42	2.52	2.48	94.59
35.0	0.58	2.32	2.21	94.90
37.5	1.11	4.08	2.74	92.07
42.5	1.01	2.76	2.07	94.16
45.0	1.32	2.56	1.86	94.26
47.5	0.42	2.61	2.02	94.95
52.5	0.50	2.33	1.84	95.33
55.0	0.52	2.31	1.89	95.28
57.5	2.89	2.81	2.07	92.23
62.5	2.78	3.09	2.16	91.97
65.0	0.95	3.22	2.35	93.48
67.5	0.18	2.25	2.25	95.32
72.5	0.75	2.85	2.14	94.27
75.0	0.76	3.10	2.14	94.00
77.5	0.10	2.23	2.10	95.58
82.5	1.11	2.68	1.91	94.30
85.0	0.34	2.60	1.66	95.40
87.5	0.79	2.61	1.65	94.95
92.5	1.06	2.41	1.54	94.99
95.0	0.81	2.57	1.62	95.00
97.5	1.34	3.70	1.37	93.59
102.5	0.86	3.28	1.68	94.18
105.0	0.31	2.34	1.39	95.96
107.5	0.70	2.47	1.55	95.28
112.5	0.48	2.37	1.52	95.64
115.0	2.03	3.04	1.62	93.32
117.5	1.39	2.91	1.58	94.12
122.5	0.32	2.18	1.29	96.21
125.0	0.78	2.46	1.47	95.29
127.5	1.52	2.81	0.95	94.73
132.2	0.45	2.31	1.51	95.73
135.0	0.53	2.47	1.66	95.34
137.5	0.63	2.63	1.58	95.17
142.5	0.70	2.38	1.72	95.20

continue on next page

core depth (cm)	>2 mm (wt%)	2-0.25 mm (wt%)	0.25-0.125 mm (wt%)	<0.125 mm (wt%)
145.0	0.86	3.05	1.79	94.30
147.5	1.73	5.28	2.31	90.68
152.5	0.94	2.61	1.78	94.67
155.0	0.79	2.65	1.72	94.85
157.5	0.76	2.04	1.24	95.96
162.5	1.26	2.43	1.53	94.78
165.0	0.77	2.38	1.50	95.35
167.5	0.50	2.41	1.44	95.65
172.5	2.17	5.65	1.27	90.91
175.0	0.98	3.06	1.53	94.43
177.5	1.55	4.35	1.55	92.55
182.5	2.79	3.68	1.57	91.96
185.0	1.18	2.85	1.41	94.56
187.5	0.84	2.62	1.12	95.42
192.5	2.21	3.35	1.14	93.31
195.0	0.69	2.76	1.22	95.33
197.5	0.44	2.76	1.07	95.74
202.5	4.72	2.66	1.17	91.44
205.0	1.29	2.87	0.92	94.92
207.5	4.70	3.40	1.09	90.81
212.5	0.56	2.08	0.84	96.51
215.0	1.42	1.84	1.00	95.74
217.5	1.70	2.03	1.07	95.20
222.5	1.98	1.85	0.86	95.32
225.0	2.58	1.72	1.17	94.53
227.5	1.95	1.65	1.43	94.97
232.5	1.97	1.33	1.65	95.05
235.0	0.30	1.13	1.58	96.99
237.5	0.79	1.37	1.63	96.21
242.5	0.25	1.71	2.07	95.96
245.0	0.66	1.59	1.83	95.93
247.5	0.46	1.37	2.07	96.11
252.5	0.86	1.86	2.23	95.05
255.0	0.81	1.46	2.31	95.43
257.5	1.17	2.35	2.35	94.13
262.5	0.46	2.14	2.56	94.84
265.0	0.58	1.85	2.68	94.89
267.5	0.61	2.05	3.45	93.89
272.5	0.08	1.50	3.04	95.38
275.0	1.21	2.76	3.23	92.81
277.5	0.68	2.48	3.42	93.42
282.5	0.61	1.75	3.59	94.05
285.0	1.39	1.43	3.84	93.34
287.5	0.20	1.04	3.57	95.18

Continue on next page

core depth (cm)	>2 mm (wt%)	2-0.25 mm (wt%)	0.25-0.125 mm (wt%)	<0.125 mm (wt%)
292.5	0.88	1.84	4.28	93.00
295.0	0.55	2.69	4.64	92.12
297.5	0.80	2.18	4.51	92.50
302.5	0.26	1.35	4.57	93.83
305.0	0.15	1.70	4.35	93.80
307.5	13.45	2.45	4.14	79.97
312.5	0.45	2.12	5.30	92.13
315.0	0.26	1.75	4.86	93.14
317.5	0.08	2.00	5.79	92.14
322.5	0.29	2.08	5.65	91.98
325.0	0.14	2.00	6.61	91.25
327.5	5.26	2.22	5.68	86.84
332.5	0.29	2.86	6.93	89.92
335.0	0.32	2.60	7.25	89.83
337.5	0.42	3.12	7.98	88.48
342.5	0.49	2.88	6.58	90.05
345.0	3.04	2.99	6.96	87.02
347.5	1.11	3.67	6.45	88.77
352.5	1.06	3.71	7.71	87.52
355.0	0.23	3.29	6.22	90.27
357.5	0.15	2.79	5.43	91.63
362.5	0.46	2.74	5.42	91.38
365.0	0.24	2.62	5.49	91.65
367.5	0.39	2.88	5.25	91.47
372.5	0.53	2.76	4.68	92.02
375.0	0.67	3.22	4.45	91.66
377.5	0.27	2.30	4.20	93.23
382.5	0.28	1.36	3.18	95.18
385.0	0.28	1.81	3.39	94.53
387.5	0.95	1.86	3.27	93.92
392.5	0.23	1.58	2.79	95.40
395.0	0.24	1.25	2.02	96.49
397.5	0.32	1.48	2.22	95.98
402.5	0.23	1.78	2.41	95.57
405.0	0.28	1.45	2.62	95.66
407.5	0.20	1.79	2.61	95.39
412.5	2.01	3.18	3.48	91.33
415.0	1.13	3.21	3.87	91.79
417.5	2.58	4.61	3.70	89.10
422.5	0.28	2.65	3.47	93.61
425.0	0.91	3.69	2.97	92.43
427.5	0.64	2.78	3.46	93.12

Core APO 2: Cu/Al ratios (correlated to TOC-scale) and total organic carbon (TOC)

core depth (cm)	Cu/Al	TOC
0	0.71801835	2.06
5	3.70342295	2.06
15	3.775821	4.37
25	3.21699765	3.23
35	1.65310377	2.76
45	1.70937334	2.7
55	1.58509406	3.3
65	1.8766048	3.22
75	1.36022362	3.88
85	1.58229002	4.41
95	3.77350649	9.68
105	2.28637558	11.05
115	3.27228698	10.05
124.3	2.89298874	7.88
134.3	18.097241	10.09
144.3	21.0257167	10.85
154.3	21.4298761	10.02
164.3	20.5367171	11.7
174.3	18.7276874	14.84
184.3	18.3782846	12.62
194.3	17.1343038	6.27
204.3	23.1192669	7.62
214.3	5.21459014	6.33
224.3	2.33585311	4.37
236.6	2.68453294	5.69
246.6	3.46905107	4.35
256.6	5.3795999	5.26
266.6	5.10632707	8.41
276.6	7.69382974	4.98
286.6	3.52286635	6.58
296.6	3.31345878	9.64
306.6	2.47994685	10.52
316.6	2.74522623	10.34
326.6	2.79475241	9.5
336.6	2.430241	10.58
356.7	1.83045483	10.58
366.7	2.4794978	6.37
376.7	4.43584989	12.58
386.7	10.0430119	9.08
396.7	10.424431	9.48
406.7	16.4739318	11.4
416.7	17.2702982	9.59
426.7	14.9203493	10.71

Core APO 2: Data from XRF core scanning

core depth (cm)	Ca (cps)	Cl (cps)	Ti/Ca	Fe/Ca
0.309	128202	1500	0.0009672	0.0117939
0.809	275026	2352	0.00052	0.0148095
1.309	226215	2438	0.000694	0.0113697
1.809	221102	2788	0.000389	0.0116055
2.309	212851	2971	0.0005121	0.0115057
2.809	196928	2649	0.0006652	0.011979
3.309	217494	2507	0.0005471	0.011536
3.809	231764	2613	0.0005135	0.0120726
4.309	243450	2530	0.0006531	0.0103266
4.809	243688	2524	0.0007222	0.0110715
5.309	233480	2600	0.0006425	0.0113757
5.809	233686	2580	0.0006547	0.0124055
6.309	231764	2494	0.000686	0.0124005
6.809	237336	2249	0.0007921	0.011351
7.309	242531	2463	0.0005772	0.0111903
7.809	240063	2520	0.000779	0.0126175
8.309	244997	2424	0.0006123	0.0127104
8.809	236050	2541	0.0006397	0.0142978
9.309	230738	2703	0.0006111	0.0127547
9.809	230624	2474	0.000568	0.0103805
10.309	226104	2553	0.0006059	0.0109905
10.809	232793	2482	0.0008634	0.0136516
11.309	236077	2515	0.0006057	0.0126272
11.809	242537	2439	0.000536	0.0103654
12.309	246938	2454	0.0004779	0.0102738
12.809	236637	2585	0.0007057	0.0108859
13.309	234741	2636	0.0005495	0.0112933
13.809	236914	2601	0.000515	0.0113965
14.309	231247	2603	0.0005362	0.0107634
14.809	229403	2644	0.0006495	0.0112858
15.309	241460	2374	0.0006378	0.0113145
15.809	235034	2636	0.0004723	0.0091008
16.309	231160	2744	0.0005148	0.0095345
16.809	223324	2926	0.0004388	0.0111676
17.309	203620	3133	0.00055	0.0124398
17.809	228911	2658	0.0005242	0.0101437
18.309	223133	2715	0.0007888	0.0118718
18.809	227778	2736	0.0004215	0.0099395
19.309	236164	2648	0.0004742	0.0116699
19.809	241886	2640	0.0005829	0.0097277
20.309	238817	2674	0.0004941	0.0107739
20.809	240619	2646	0.0006857	0.0103899
21.309	237894	2600	0.0005507	0.0095589
21.809	247775	2571	0.0005247	0.0101221
22.309	245178	2553	0.0004487	0.007827
22.809	245411	2519	0.0005542	0.009967
23.309	239480	2663	0.000213	0.009792
23.809	243074	2583	0.0003291	0.0105441
24.309	242295	2662	0.0005324	0.0110072
24.809	241111	2669	0.0004811	0.011982
25.309	243341	2602	0.000563	0.0110092
25.809	240938	2605	0.0004275	0.0107663
26.309	243035	2695	0.0004773	0.0105705

Continue on next page

core depth (cm)	Ca (cps)	Cl (cps)	Ti/Ca	Fe/Ca
26.809	243241	2753	0.0003494	0.0094145
27.309	243156	2613	0.0005552	0.0101416
27.809	239511	2904	0.0003925	0.0099995
28.309	242419	2848	0.0005569	0.0080315
28.809	244157	2730	0.0003277	0.0101083
29.309	240503	2732	0.0006902	0.0123658
29.809	228876	2883	0.0004588	0.0091097
30.309	239446	2768	0.0004135	0.0102152
30.809	247752	2642	0.0004884	0.0104742
31.309	244244	2675	0.0005077	0.0106615
31.809	238506	2710	0.0005534	0.0109641
32.309	244888	2606	0.0004124	0.0098412
32.809	243161	2681	0.0003701	0.0104663
33.309	254945	2326	0.0004942	0.0098963
33.809	250953	2564	0.0004583	0.0102649
34.309	243590	2581	0.0004926	0.0100374
34.809	245976	2480	0.0006789	0.0101595
35.309	250603	2339	0.0004868	0.0098762
35.809	252676	2317	0.0005145	0.0100643
36.309	256685	2324	0.0006389	0.010659
36.809	247781	2324	0.0005771	0.010586
37.309	250630	2498	0.0005027	0.0096956
37.809	242477	2685	0.0007506	0.0092545
38.309	242668	2602	0.0006964	0.0109491
38.809	233423	2712	0.000377	0.0108815
39.309	232727	2621	0.0006102	0.0110516
39.809	240827	2609	0.0004941	0.009675
40.309	245724	2503	0.0005209	0.0102758
40.809	247010	2543	0.0005303	0.0093195
41.309	249625	2366	0.0005889	0.0110205
41.809	243244	2596	0.0004604	0.0101791
42.309	243750	2587	0.0004841	0.0104903
42.809	245498	2401	0.0006762	0.0112547
43.309	254128	2371	0.0005234	0.0111794
43.809	257228	2208	0.0005054	0.0097657
44.309	257441	2186	0.0002991	0.0105849
44.809	260027	2118	0.000573	0.0086491
45.309	263075	2191	0.0004485	0.0085565
45.809	261989	2223	0.0004084	0.008863
46.309	259562	2192	0.000524	0.0092386
46.809	263994	2401	0.0004621	0.0079434
47.309	265396	2297	0.0007159	0.0091373
47.809	265861	2346	0.0005304	0.0087715
48.309	264699	2272	0.000476	0.0089422
48.809	264409	2274	0.0004879	0.0086797
49.309	264099	2340	0.000549	0.008493
49.809	262265	2387	0.0005453	0.0097573
50.309	265399	2269	0.0003919	0.0090807
50.809	267374	2247	0.0005348	0.0092642
51.309	264480	2298	0.0003781	0.0090555
51.809	263501	2380	0.0006452	0.0092713
52.309	265254	2295	0.0005693	0.0108274
52.809	268808	2292	0.000465	0.0091366
53.309	270706	2245	0.0005209	0.0091945
53.809	262338	2501	0.0004117	0.0083976

Continue on next page

core depth (cm)	Ca (cps)	Cl (cps)	Ti/Ca	Fe/Ca
54.309	258881	2542	0.000479	0.0088264
54.809	258049	2474	0.0004185	0.0091262
55.309	265633	2347	0.0003614	0.0085042
55.809	264778	2442	0.0002757	0.0075837
56.309	261811	2392	0.0005768	0.0077002
56.809	264645	2343	0.0004421	0.0089403
57.309	264587	2369	0.0004006	0.0080805
57.809	258974	2443	0.0004325	0.0088542
58.309	251842	2548	0.000409	0.0092598
58.809	251915	2678	0.0006113	0.0092531
59.309	251485	2647	0.0004652	0.0093167
59.809	244217	2684	0.0003399	0.0078291
60.309	245544	2676	0.0005498	0.0092326
60.809	243578	2915	0.0002997	0.007706
61.309	240040	2849	0.0004124	0.0092318
61.809	236876	2899	0.0002955	0.0081351
62.309	237255	2784	0.0004173	0.0080293
62.809	238831	2782	0.0005569	0.0089729
63.309	237842	2851	0.0004162	0.008657
63.809	248740	2716	0.0006352	0.0097491
64.309	242801	2675	0.0004572	0.0099876
64.809	252155	2772	0.0006107	0.0103349
65.309	243606	2669	0.0005336	0.010008
65.809	250272	2569	0.0006113	0.0097414
66.309	243611	2764	0.0005747	0.0085875
66.809	248837	2579	0.000635	0.0089215
67.309	239978	2781	0.0004875	0.0092759
67.809	254110	2457	0.0006965	0.011255
68.309	253156	2584	0.0003674	0.0083901
68.809	258909	2468	0.0005021	0.0077981
69.309	259179	2377	0.0004321	0.0090169
69.809	261600	2395	0.0004587	0.0088532
70.309	256840	2472	0.0004516	0.0096831
70.809	249964	2549	0.0006201	0.0081612
71.309	250882	2537	0.0004584	0.0086296
71.809	244364	2682	0.0005156	0.0095186
72.309	250657	2593	0.0006104	0.0099698
72.809	242250	2626	0.000582	0.0095439
73.309	249757	2469	0.0005085	0.0085163
73.809	247350	2397	0.0005539	0.0093309
74.309	242949	2554	0.0005433	0.0101956
74.809	245923	2657	0.000675	0.0095802
75.309	240210	2573	0.000537	0.0095417
75.809	255523	2376	0.0003366	0.014484
76.309	251427	2402	0.0003301	0.0085154
76.809	252937	2406	0.0004033	0.0086148
77.309	249717	2401	0.0005446	0.0089381
77.809	255875	2185	0.0004885	0.0104309
78.309	249672	2393	0.0006048	0.0093603
78.809	252172	2278	0.0005235	0.007824
79.309	246555	2475	0.0004583	0.0080874
79.809	249123	2327	0.0005258	0.0085339
80.309	248749	2436	0.0006472	0.0084543
80.809	249088	2314	0.0004657	0.0081256
81.309	247841	2300	0.0005084	0.0083723

Continue on next page

core depth (cm)	Ca (cps)	Cl (cps)	Ti/Ca	Fe/Ca
81.809	254788	2408	0.000416	0.0094196
82.309	258485	2260	0.0005996	0.010341
82.809	264787	2116	0.0006722	0.0097135
83.309	268952	2075	0.0005689	0.0086038
83.809	267855	2097	0.0004667	0.0090422
84.309	267613	2195	0.0007324	0.0104778
84.809	265094	2264	0.0005922	0.0107396
85.309	261866	2174	0.0006339	0.0097607
85.809	244555	2407	0.000736	0.0097851
86.309	257249	2350	0.000723	0.010002
86.809	245194	2370	0.0006974	0.0112075
87.309	271646	2075	0.0007215	0.0103775
87.809	269181	2095	0.0005721	0.0104056
88.309	268414	2132	0.0005849	0.0097759
88.809	268612	2116	0.0006403	0.0108893
89.309	264622	2242	0.0005857	0.0113369
89.809	254135	2390	0.0006099	0.0086647
90.309	262542	2133	0.0004837	0.0100898
90.809	263893	2205	0.0006139	0.0106634
91.309	270497	2034	0.0006359	0.0109983
91.809	270385	2107	0.0006842	0.0114429
92.309	275359	1985	0.0005048	0.0107859
92.809	269483	2138	0.0005937	0.0104793
93.309	275816	1988	0.0006925	0.0105288
93.809	271453	2109	0.0007552	0.0115784
94.309	262050	2152	0.0005533	0.0100935
94.809	261800	2134	0.000615	0.0119099
95.309	261418	2255	0.0006847	0.0098846
95.809	263260	2193	0.0006457	0.0107992
96.309	262034	2259	0.0006373	0.0120442
96.809	263155	2168	0.0006954	0.0119017
97.309	262294	2165	0.0006863	0.0113232
97.809	264100	2064	0.0006626	0.0116357
98.309	262466	2255	0.0006629	0.0126874
98.809	252558	2252	0.0006692	0.012706
99.309	257796	2173	0.0005896	0.0125797
99.809	257918	2131	0.0008414	0.0119999
100.309	260161	2198	0.0007342	0.0128036
100.809	262240	2156	0.000633	0.0106505
101.309	256241	2199	0.0006751	0.0112823
101.809	255807	2160	0.0009617	0.0142334
102.309	246197	2254	0.0007068	0.0158247
102.809	242366	2334	0.0007427	0.013133
103.309	244781	2261	0.0008171	0.0136734
103.809	256153	2063	0.0007066	0.0116961
104.309	252725	2099	0.0007716	0.0117875
104.809	244217	2275	0.0005569	0.0130048
105.309	258705	2106	0.0007924	0.0137415
105.809	252338	2116	0.0006341	0.0136602
106.309	258563	2042	0.0006188	0.0120822
106.809	264128	2079	0.0006777	0.012687
107.309	254711	2155	0.0008519	0.0127282
107.809	262437	2015	0.0006211	0.0128183
108.309	253784	2228	0.0006108	0.0129717
108.809	249196	2281	0.0008066	0.0127891

Continue on next page

core depth (cm)	Ca (cps)	Cl (cps)	Ti/Ca	Fe/Ca
109.309	264301	2092	0.0007037	0.0134241
109.809	258273	2151	0.0006814	0.0136561
110.309	247685	2231	0.0009326	0.0123746
110.809	248106	2327	0.00079	0.0125954
111.309	241337	2267	0.0006381	0.0122526
111.809	242939	2548	0.0007821	0.0128798
112.309	255715	1978	0.0007547	0.0119313
112.809	256428	2019	0.0006474	0.0118591
113.309	224173	2302	0.0009769	0.0131595
113.809	255872	2030	0.0006996	0.0123148
114.309	272702	2080	0.0005684	0.0112834
114.809	262127	2140	0.0005837	0.0132035
115.309	265097	2092	0.0007016	0.0127689
115.809	262307	2227	0.0007396	0.0123329
116.309	268525	2201	0.0006889	0.0119803
116.809	267359	2264	0.0007406	0.0132518
117.309	267359	2264	0.0007406	0.0132518
117.809	267359	2264	0.0007406	0.0132518
118.309	267359	2264	0.0007406	0.0132518
118.809	267359	2264	0.0007406	0.0132518
119.309	267359	2264	0.0007406	0.0132518
119.809	267359	2264	0.0007406	0.0132518
121.254	231096	2365	0.001904	0.0142495
121.754	331238	1846	0.0007849	0.0116502
122.254	272846	1733	0.0006377	0.0119958
122.754	278472	1599	0.0005027	0.0118863
123.254	258018	1904	0.0007945	0.0158594
123.754	244589	1989	0.0009444	0.0175028
124.254	279733	2032	0.0007936	0.0136344
124.754	296682	1833	0.0006573	0.0122555
125.254	295022	1889	0.0007796	0.0137685
125.754	285157	2063	0.0009433	0.014855
126.254	264957	2441	0.0008152	0.0151157
126.754	257746	2561	0.0008574	0.0147044
127.254	272278	2306	0.0007088	0.014342
127.754	276579	2120	0.0008424	0.0137863
128.254	275128	2117	0.0010868	0.0163306
128.754	265928	2271	0.000801	0.0161322
129.254	258181	2334	0.0008676	0.0129793
129.754	269564	2137	0.0006232	0.0144901
130.254	268256	2210	0.0009841	0.0152727
130.754	276032	2128	0.0008695	0.0147918
131.254	279202	2096	0.0008739	0.0154082
131.754	274012	2088	0.0008065	0.0148351
132.254	263700	2203	0.000876	0.0152181
132.754	270440	2187	0.0006767	0.0151457
133.254	273552	2234	0.0008518	0.0140229
133.754	271456	2230	0.0007515	0.0144959
134.254	271689	2211	0.0007619	0.0152822
134.754	270349	2213	0.0008545	0.0150657
135.254	272954	2268	0.0009599	0.0147387
135.754	267339	2156	0.0007593	0.0143675
136.254	267989	2070	0.0006941	0.0141573
136.754	273273	2150	0.0007941	0.0136128
137.254	274342	2227	0.0007509	0.013403

Continue on next page

core depth (cm)	Ca (cps)	Cl (cps)	Ti/Ca	Fe/Ca
137.754	261914	2370	0.0005574	0.0144208
138.254	262727	2182	0.0008183	0.0147568
138.754	261277	2226	0.0005473	0.0136905
139.254	266219	2125	0.0008114	0.0140185
139.754	269133	2160	0.0008695	0.01487
140.254	268569	2087	0.0006888	0.0143501
140.754	269423	2128	0.0008648	0.0135772
141.254	262632	2281	0.0007082	0.014012
141.754	264142	2302	0.0006133	0.0142461
142.254	267001	2236	0.0006629	0.0156704
142.754	266381	2235	0.0007733	0.0146895
143.254	268265	2326	0.000835	0.0143925
143.754	274128	2225	0.0008354	0.0157809
144.254	269248	2213	0.0005868	0.0156213
144.754	265696	2180	0.0007038	0.0154387
145.254	261304	2267	0.0007845	0.0146305
145.754	261474	2337	0.000631	0.0157492
146.254	264969	2224	0.0006076	0.0147527
146.754	269319	2230	0.0006906	0.0150268
147.254	257860	2405	0.0007679	0.0166641
147.754	255206	2184	0.0007563	0.0158852
148.254	253151	2449	0.000715	0.0160339
148.754	255738	2326	0.0007938	0.0162197
149.254	261574	2215	0.0007531	0.015357
149.754	249751	2636	0.0006486	0.0155675
150.254	257706	2404	0.0008731	0.0163675
150.754	247867	2572	0.0006737	0.0160489
151.254	273672	2276	0.0006139	0.0146782
151.754	282905	2150	0.0010039	0.0160018
152.254	257716	2445	0.0007993	0.0169877
152.754	247655	2522	0.0008237	0.0161273
153.254	268672	2187	0.0008077	0.015759
153.754	273678	2190	0.0009281	0.0144586
154.254	266538	2468	0.0008254	0.0153637
154.754	256395	2450	0.0007839	0.0160534
155.254	260697	2458	0.0007327	0.016337
155.754	268165	2258	0.0008689	0.0168068
156.254	269699	2339	0.0008343	0.0172489
156.754	277153	2204	0.0006892	0.0168319
157.254	277384	2203	0.0007463	0.0159094
157.754	273020	2410	0.0006813	0.016171
158.254	277562	2323	0.0006557	0.0179203
158.754	284604	2073	0.0008398	0.0166617
159.254	278177	2298	0.0008448	0.0167771
159.754	279634	2202	0.0008154	0.0170687
160.254	280861	2221	0.0007548	0.0165384
160.754	271413	2332	0.0009358	0.0173131
161.254	279105	2147	0.0009423	0.0172516
161.754	278235	2189	0.0008087	0.0175391
162.254	280306	2020	0.0008348	0.0161752
162.754	281704	2091	0.0006816	0.0162227
163.254	276787	2205	0.0008237	0.0177899
163.754	262895	2291	0.0007113	0.0170334
164.254	253854	2321	0.0009927	0.0193694
164.754	254172	2373	0.0009285	0.0181491

Continue on next page

core depth (cm)	Ca (cps)	Cl (cps)	Ti/Ca	Fe/Ca
165.254	267033	2234	0.0008051	0.0150131
165.754	266090	2118	0.0009621	0.017231
166.254	274401	2017	0.0007398	0.0184693
166.754	251554	2333	0.000966	0.0187117
167.254	255599	2051	0.0009233	0.0171832
167.754	227032	2527	0.0012641	0.0215168
168.254	246982	2124	0.0008179	0.0184831
168.754	233005	2432	0.001	0.0203601
169.254	248195	2347	0.0009468	0.0205202
169.754	240136	2326	0.0009661	0.0190517
170.254	249579	2121	0.0008775	0.0188678
170.754	230811	2449	0.0009185	0.0189072
171.254	229467	2408	0.0008803	0.0195322
171.754	238925	2464	0.0012138	0.0197259
172.254	238338	2389	0.000814	0.0190486
172.754	261611	2121	0.0009671	0.0209701
173.254	271738	2036	0.0010746	0.0192686
173.754	270441	1921	0.000758	0.0184144
174.254	269153	2010	0.0007431	0.0171538
174.754	270613	2081	0.0009682	0.0173754
175.254	258887	2156	0.0011009	0.0181237
175.754	262887	2210	0.0009662	0.0176692
176.254	259718	2025	0.0007701	0.0156477
176.754	263803	2164	0.0008908	0.0194691
177.254	268740	1914	0.0007554	0.0187877
177.754	280057	1962	0.0010534	0.0193782
178.254	279233	1928	0.0010027	0.0252513
178.754	283797	1965	0.0010007	0.0274915
179.254	287564	1812	0.0008624	0.0227532
179.754	279669	2197	0.0010977	0.0231702
180.254	281967	1919	0.0008724	0.0202861
180.754	282510	1852	0.0010513	0.0209975
181.254	276720	2046	0.001413	0.0251554
181.754	274690	2101	0.0011031	0.0201354
182.254	280923	1874	0.0010252	0.0231772
182.754	256394	2266	0.0013768	0.031397
183.254	251822	2091	0.0009928	0.0210188
183.754	260416	2349	0.0009984	0.0200871
184.254	270835	2189	0.0009674	0.0201156
184.754	274497	2034	0.0008925	0.0198108
185.254	265029	2122	0.0007509	0.0196469
185.754	261205	2194	0.0008346	0.0208572
186.254	267145	2112	0.001123	0.0196859
186.754	276357	2039	0.000977	0.0191021
187.254	276929	2019	0.0009064	0.0199546
187.754	271139	2154	0.0011138	0.0197463
188.254	269804	2025	0.0010378	0.0213822
188.754	270840	2004	0.0009452	0.0192032
189.254	275924	1948	0.0008662	0.019143
189.754	276896	2063	0.0009679	0.0210982
190.254	272955	2025	0.0008903	0.0204942
190.754	275970	1940	0.0011124	0.0206073
191.254	269589	2111	0.0010905	0.020687
191.754	274105	2051	0.001047	0.0206381
192.254	278016	1882	0.0010971	0.020114

Continue on next page

core depth (cm)	Ca (cps)	Cl (cps)	Ti/Ca	Fe/Ca
192.754	277982	1923	0.0008885	0.0188861
193.254	280228	1942	0.001092	0.0196447
193.754	282879	1863	0.0009014	0.0214438
194.254	268727	2137	0.0008782	0.0221489
194.754	249708	2309	0.0011133	0.0229148
195.254	207444	2145	0.0011184	0.0240017
195.754	226199	2107	0.0015031	0.0232052
196.254	247312	2714	0.0010756	0.0231408
196.754	265541	2142	0.0010657	0.0238344
197.254	271292	2244	0.0013012	0.0206899
197.754	271024	2058	0.0010073	0.0200277
198.254	275929	2101	0.0009133	0.0207517
198.754	283081	1894	0.001194	0.0233325
199.254	282803	2091	0.0011457	0.0202261
199.754	274666	2094	0.0012233	0.0225292
200.254	250311	2541	0.0009908	0.0288801
200.754	247058	2323	0.0011536	0.0314582
201.254	253671	1773	0.0011117	0.0235147
201.754	253417	1976	0.0010457	0.026486
202.254	266327	2233	0.000965	0.0268354
202.754	277610	2167	0.0011599	0.0354454
203.254	266125	2463	0.0011423	0.0524528
203.754	262492	2296	0.001021	0.0379973
204.254	266409	2214	0.0010585	0.0381556
204.754	257680	2431	0.0011681	0.0383809
205.254	265698	2443	0.0012721	0.0373055
205.754	277732	2287	0.0010298	0.0286931
206.254	255612	2101	0.001205	0.0267671
206.754	214081	1857	0.0013686	0.0312218
207.254	214181	2031	0.0012373	0.0343868
207.754	204019	1782	0.0015734	0.0356388
208.254	246494	2420	0.0015781	0.0311161
208.754	275308	2316	0.0012895	0.0281067
209.254	283769	2123	0.0017232	0.027251
209.754	276382	2118	0.00127	0.02642
210.254	297418	1920	0.0014491	0.0232837
210.754	292686	2124	0.0013632	0.0247877
211.254	289020	2099	0.0014186	0.0255034
211.754	294278	2093	0.0012777	0.0242356
212.254	291381	2115	0.001335	0.0251389
212.754	285644	2159	0.0012918	0.0286125
213.254	283292	2254	0.0015108	0.0272581
213.754	280402	2246	0.0013695	0.0261232
214.254	268737	2539	0.0013768	0.025378
214.754	275188	2303	0.0013227	0.0255171
215.254	270537	2400	0.001327	0.030835
215.754	271219	2469	0.0015817	0.0313842
216.254	271826	2379	0.0015709	0.029541
216.754	270426	2383	0.0017565	0.0301044
217.254	271049	2320	0.0013946	0.0295703
217.754	263150	2399	0.0015314	0.0306403
218.254	263332	2543	0.0016633	0.0332584
218.754	256183	2607	0.0014326	0.0306031
219.254	251185	2649	0.0016522	0.0330274
219.754	261669	2514	0.0017121	0.0328468

Continue on next page

core depth (cm)	Ca (cps)	Cl (cps)	Ti/Ca	Fe/Ca
220.254	260028	2485	0.0016806	0.0337425
220.754	261965	2374	0.0017598	0.0318974
221.254	263632	2330	0.0017221	0.0325188
221.754	259935	2397	0.0019774	0.0354512
222.254	260882	2474	0.0014183	0.0297376
222.754	259034	2557	0.0015326	0.0324591
223.254	251327	2578	0.0017069	0.0347834
223.754	263707	2133	0.0020477	0.0424183
224.254	260644	2231	0.0021639	0.0367283
224.754	255999	2302	0.001957	0.0414806
225.254	258053	2377	0.0015772	0.0343147
225.754	257649	2209	0.0018824	0.0335767
226.254	257249	2164	0.0017221	0.0379282
226.754	249786	2415	0.0017535	0.0377003
227.254	252565	2315	0.0018015	0.0341496
227.754	244095	2285	0.0019828	0.0379279
228.254	252090	2158	0.0017692	0.0356619
228.754	252922	2169	0.0019255	0.0381896
229.254	272155	2597	0.0015212	0.030806
229.754	272155	2597	0.0015212	0.030806
230.931	272155	2597	0.0015212	0.030806
231.431	246108	2797	0.0019097	0.0385237
231.931	242920	2685	0.001906	0.0380207
232.431	239424	2518	0.0023389	0.0451542
232.931	237840	2674	0.0021569	0.0518332
233.431	231400	2464	0.0021737	0.048777
233.931	224370	2550	0.0022463	0.0519544
234.431	232405	2497	0.0024483	0.0513887
234.931	185477	1899	0.002658	0.0534891
235.431	220952	2552	0.0024349	0.0547857
235.931	234003	2597	0.0027948	0.0521104
236.431	246947	2552	0.0025188	0.0469898
236.931	259897	2338	0.0024587	0.0410778
237.431	259023	2410	0.0020886	0.038761
237.931	256246	2515	0.0022556	0.0477822
238.431	261162	2339	0.0023587	0.042353
238.931	259760	2460	0.0023406	0.0454843
239.431	262612	2345	0.002319	0.0484098
239.931	256741	2612	0.0020176	0.0443443
240.431	260238	2557	0.0019405	0.0425649
240.931	224882	2814	0.001961	0.0450681
241.431	223796	2704	0.0021091	0.0464888
241.931	239724	2558	0.0019731	0.0397666
242.431	258377	2360	0.0022061	0.0398913
242.931	247884	2485	0.0019082	0.043597
243.431	261708	2478	0.0022812	0.0465137
243.931	266185	2341	0.0023292	0.0493942
244.431	262335	2485	0.0024701	0.0469972
244.931	244323	2483	0.0022061	0.0477524
245.431	245909	2724	0.0020333	0.0440976
245.931	245665	2451	0.0024749	0.0433639
246.431	221285	2568	0.0021194	0.0420498
246.931	252887	2313	0.0024359	0.0477328
247.431	246182	2416	0.0022951	0.046161
247.931	216859	2762	0.0024163	0.0562439

Continue on next page

core depth (cm)	Ca (cps)	Cl (cps)	Ti/Ca	Fe/Ca
248.431	235985	2685	0.0026273	0.0530203
248.931	231761	2628	0.0027701	0.0558679
249.431	226168	2696	0.0021931	0.05629
249.931	229424	2776	0.0026327	0.0568903
250.431	238999	2810	0.0027657	0.0614605
250.931	218850	2623	0.0029701	0.0581586
251.431	215010	2908	0.0029301	0.0553509
251.931	224976	2795	0.0022891	0.0537924
252.431	238839	2635	0.0028011	0.0597683
252.931	238691	2638	0.0029033	0.055796
253.431	233576	2658	0.0025773	0.058268
253.931	239704	2531	0.0028952	0.0612339
254.431	241584	2448	0.0029472	0.0626656
254.931	245573	2534	0.0029075	0.0653451
255.431	240624	2662	0.002959	0.0612574
255.931	236041	2661	0.0030334	0.0721104
256.431	224158	2850	0.0030157	0.0721009
256.931	239766	2635	0.002173	0.0446268
257.431	246006	2685	0.0022967	0.0430437
257.931	244347	2634	0.0032372	0.0621002
258.431	250238	2693	0.0026015	0.0544202
258.931	242073	2790	0.0031685	0.0653563
259.431	245569	2709	0.0031234	0.0682904
259.931	237423	2771	0.003559	0.0756498
260.431	242181	2823	0.0030927	0.0772439
260.931	223923	3073	0.0036352	0.0834439
261.431	231686	2884	0.0036213	0.0845843
261.931	242487	2811	0.0032662	0.0693645
262.431	238989	2989	0.0027198	0.0550653
262.931	236142	2975	0.0031379	0.0669766
263.431	225193	3171	0.0031839	0.0736213
263.931	232733	3016	0.0036351	0.0804613
264.431	252090	2828	0.0026697	0.0530326
264.931	244304	2819	0.0031887	0.0658851
265.431	243222	2902	0.0034824	0.06971
265.931	232082	2911	0.0031024	0.077925
266.431	243749	2898	0.0032205	0.0732229
266.931	233822	3108	0.0033102	0.0751255
267.431	225792	3275	0.0030426	0.0705782
267.931	242083	3010	0.0032757	0.0672084
268.431	239196	3015	0.0033529	0.0715397
268.931	218180	3198	0.0032634	0.0815473
269.431	223830	3135	0.0031006	0.0743734
269.931	199883	3367	0.003452	0.080357
270.431	159692	3572	0.0033815	0.0904429
270.931	215858	3007	0.0033819	0.0787647
271.431	192841	3507	0.0035729	0.0873206
271.931	214771	3207	0.0032779	0.0765699
272.431	223602	2955	0.0032111	0.0730718
272.931	203693	3179	0.0038244	0.0823396
273.431	222153	2909	0.0034301	0.0792472
273.931	228304	2647	0.0034997	0.0782378
274.431	146216	3485	0.003105	0.1196928
274.931	208801	3272	0.0031753	0.0979401
275.431	230244	3308	0.0032314	0.081153

Continue on next page

core depth (cm)	Ca (cps)	Cl (cps)	Ti/Ca	Fe/Ca
275.931	218075	3339	0.0035859	0.0917849
276.431	203196	3313	0.0039814	0.1042146
276.931	225380	3073	0.0039533	0.0854335
277.431	241860	2715	0.0035847	0.0793848
277.931	235955	2847	0.003471	0.080562
278.431	235435	2863	0.0035254	0.0859303
278.931	242563	2786	0.0043865	0.0872227
279.431	244094	2740	0.0037076	0.0768311
279.931	255664	2608	0.0033129	0.0722706
280.431	254073	2557	0.0037391	0.0806225
280.931	249889	2703	0.0034175	0.0695349
281.431	241443	2763	0.0034791	0.0786977
281.931	248569	2767	0.0037213	0.0820456
282.431	256928	2551	0.0033044	0.076897
282.931	247527	2734	0.0034622	0.0734142
283.431	232460	3113	0.0037125	0.0817861
283.931	239167	2747	0.0033993	0.0795469
284.431	227487	2965	0.0032749	0.0796485
284.931	212775	3228	0.0034497	0.0895406
285.431	205884	3145	0.0034437	0.0871267
285.931	226393	2832	0.0036441	0.091138
286.431	197088	3022	0.0039373	0.0950032
286.931	233334	2781	0.0034886	0.0773484
287.431	236656	2781	0.0030804	0.0781261
287.931	215372	3089	0.003812	0.0859629
288.431	220141	3045	0.0036795	0.0740435
288.931	208576	3118	0.0035383	0.0878625
289.431	225050	2964	0.0035592	0.083577
289.931	238013	2728	0.0036427	0.0796385
290.431	239042	2724	0.0032045	0.0804294
290.931	224634	2877	0.0035524	0.0833178
291.431	231682	2792	0.0034746	0.0830578
291.931	236352	2767	0.0037529	0.0795551
292.431	228505	2744	0.0035273	0.0847509
292.931	239795	2823	0.0034279	0.0833253
293.431	228759	2872	0.0039736	0.1002103
293.931	212800	2933	0.0037359	0.0962829
294.431	210139	2959	0.003669	0.0934382
294.931	210859	3056	0.0036043	0.0978948
295.431	222035	2996	0.0038643	0.0892157
295.931	227521	2835	0.0040304	0.0938331
296.431	218991	2901	0.0039591	0.0883552
296.931	208687	2970	0.0038239	0.0967861
297.431	219468	2958	0.0033855	0.0846274
297.931	204128	3195	0.0042228	0.106056
298.431	174756	3355	0.0045606	0.1104569
298.931	213572	3038	0.0037411	0.0952466
299.431	209668	3021	0.0038823	0.0932379
299.931	212630	2878	0.0040023	0.0898086
300.431	229198	2704	0.003774	0.0792066
300.931	219909	2762	0.0038925	0.1056073
301.431	209651	3045	0.004269	0.0983205
301.931	208736	2876	0.0040434	0.099954
302.431	209811	2889	0.004118	0.0949092
302.931	213787	2868	0.0039993	0.092971

Continue on next page

core depth (cm)	Ca (cps)	Cl (cps)	Ti/Ca	Fe/Ca
303.431	221467	2902	0.0038606	0.0916751
303.931	230744	2815	0.0036577	0.0826977
304.431	231651	2679	0.0036995	0.0890305
304.931	230586	2585	0.0038684	0.0843026
305.431	231746	2590	0.0036031	0.0829097
305.931	220699	2827	0.0034074	0.0849936
306.431	216556	2895	0.0041329	0.0870768
306.931	212785	2859	0.0040322	0.0951195
307.431	221070	2715	0.0036866	0.0884019
307.931	225610	2825	0.0038163	0.0899428
308.431	223529	2806	0.0040666	0.1038255
308.931	216315	2753	0.0070684	0.1248827
309.431	215523	2866	0.004445	0.1028336
309.931	225981	2795	0.0040446	0.0964417
310.431	235106	2570	0.0036707	0.0873478
310.931	233188	2655	0.003971	0.0948977
311.431	236212	2592	0.0033064	0.0850211
311.931	228177	2694	0.0044001	0.0950534
312.431	219310	2916	0.0045917	0.1088094
312.931	217503	2920	0.004593	0.1047756
313.431	211578	3081	0.0041403	0.1097657
313.931	211775	3007	0.0042592	0.1041199
314.431	231365	2833	0.0043351	0.1019688
314.931	227276	3014	0.0042723	0.0958042
315.431	198991	2908	0.0044726	0.1032057
315.931	194566	3105	0.0048878	0.1200107
316.431	198266	2975	0.0044687	0.1070985
316.931	210697	3049	0.004058	0.1012449
317.431	198126	2931	0.0040479	0.098291
317.931	229618	2774	0.0036103	0.0884469
318.431	206990	2944	0.003691	0.0960385
318.931	226697	2746	0.003798	0.0945226
319.431	206121	3161	0.0045556	0.1023768
319.931	208042	2160	0.0046193	0.0938609
320.431	212164	2863	0.0043316	0.110523
320.931	200832	2919	0.0042224	0.1083592
321.431	217618	2918	0.0037727	0.1012922
321.931	218110	3041	0.0041218	0.1043877
322.431	193993	3147	0.0040105	0.109205
322.931	217781	2936	0.0038387	0.1043525
323.431	227087	2704	0.0044344	0.115524
323.931	227732	2819	0.0046853	0.1051367
324.431	224156	2891	0.0044567	0.1052526
324.931	228111	2937	0.004454	0.1035461
325.431	229457	2865	0.0045194	0.0995393
325.931	230790	2798	0.0043546	0.099714
326.431	222425	2941	0.0037766	0.1048443
326.931	219900	2925	0.0042019	0.1019281
327.431	229728	2846	0.0042354	0.0974413
327.931	224864	2769	0.0042114	0.104899
328.431	226302	2783	0.0044807	0.1020937
328.931	212302	2861	0.004324	0.1103569
329.431	216094	2906	0.0043407	0.1082955
329.931	221862	2987	0.0043766	0.104538
330.431	230769	2620	0.004485	0.1014174

Continue on next page

core depth (cm)	Ca (cps)	Cl (cps)	Ti/Ca	Fe/Ca
330.931	233318	2684	0.0040288	0.0985436
331.431	240214	2600	0.0038133	0.0915642
331.931	232581	2675	0.003646	0.0971575
332.431	231593	2791	0.0038386	0.0964407
332.931	224367	2732	0.0043634	0.1179853
333.431	216678	2904	0.0049105	0.1148894
333.931	216329	2926	0.0048167	0.1150008
334.431	228148	2713	0.0046768	0.1184144
334.931	222378	2699	0.0050365	0.1146291
335.431	219095	2786	0.0047559	0.1194779
335.931	230207	2639	0.0055428	0.1186628
336.431	242948	2541	0.0048488	0.1059074
336.931	224750	2701	0.0045072	0.1171346
337.431	222554	2695	0.0048752	0.1259155
337.931	228967	2715	0.0051055	0.1225679
338.431	219697	2822	0.0057443	0.1386182
338.931	218647	2705	0.006156	0.1375596
339.431	222505	2591	0.0053572	0.1338981
339.931	221701	2508	0.005963	0.1416953
340.431	220054	2658	0.0058031	0.1387069
340.931	231047	2696	0.0053539	0.1382533
341.431	222770	2568	0.0048346	0.1144274
341.931	227398	2794	0.0049517	0.1187741
342.431	229297	2557	0.0046446	0.1145588
342.931	222950	2801	0.0052702	0.1401615
343.431	219033	2716	0.0059215	0.1430743
343.931	229445	2586	0.0056048	0.1196191
344.431	221764	2704	0.0057494	0.1338089
344.931	214788	2589	0.0052051	0.1352357
345.431	224245	2479	0.0059578	0.1394814
345.931	225572	2497	0.0048809	0.120436
346.431	232377	2303	0.005306	0.1111255
346.931	232068	2316	0.0054424	0.1149275
347.431	187257	2042	0.006419	0.1249406
347.931	187257	2042	0.006419	0.1249406
348.431	187257	2042	0.006419	0.1249406
348.931	187257	2042	0.006419	0.1249406
349.431	187257	2042	0.006419	0.1249406
349.931	187257	2042	0.006419	0.1249406
350.431	187257	2042	0.006419	0.1249406
350.931	187257	2042	0.006419	0.1249406
352.116	187257	2042	0.006419	0.1249406
352.616	187257	2042	0.006419	0.1249406
353.116	187257	2042	0.006419	0.1249406
353.616	187257	2042	0.006419	0.1249406
354.116	164539	2663	0.0076942	0.165833
354.616	219295	2677	0.0067671	0.1638569
355.116	203460	3140	0.0061929	0.1675219
355.616	217675	2465	0.0065189	0.1573033
356.116	214348	2040	0.0059809	0.1398427
356.616	212585	2746	0.006054	0.1507632
357.116	206252	2593	0.0058327	0.1492882
357.616	199614	3010	0.0064074	0.1605949
358.116	207022	2563	0.006125	0.1484577
358.616	206879	2546	0.0060808	0.1421411

Continue on next page

core depth (cm)	Ca (cps)	Cl (cps)	Ti/Ca	Fe/Ca
359.116	223700	2684	0.006017	0.1360215
359.616	198931	2918	0.0067611	0.1737839
360.116	186927	2847	0.0066764	0.1803485
360.616	191420	2935	0.0068279	0.1791297
361.116	196835	2953	0.0065486	0.1749943
361.616	195713	2976	0.007603	0.1746997
362.116	197973	2962	0.0077435	0.1780849
362.616	192172	3053	0.0072331	0.1812699
363.116	199980	2622	0.0079658	0.1675568
363.616	187614	3020	0.0072223	0.189117
364.116	184420	3136	0.0083613	0.1979991
364.616	188557	2914	0.0091802	0.2061976
365.116	182481	2840	0.0087845	0.2065147
365.616	182967	2900	0.0094553	0.2145414
366.116	177936	3130	0.0102115	0.2197925
366.616	176714	3147	0.0095635	0.2268864
367.116	175203	3118	0.0082818	0.2137406
367.616	190433	2786	0.0090583	0.1984162
368.116	201079	2751	0.007783	0.1691773
368.616	199483	2739	0.0082513	0.1874345
369.116	200422	2634	0.0093553	0.198591
369.616	195873	2667	0.0108387	0.2197189
370.116	200831	2727	0.0097794	0.2109137
370.616	195557	2664	0.0114391	0.2251313
371.116	193658	2724	0.0117165	0.231284
371.616	187771	2810	0.0124886	0.2461509
372.116	191348	2871	0.0113354	0.2303238
372.616	188873	2863	0.0101656	0.2173206
373.116	209844	2671	0.0088304	0.1906178
373.616	214929	2544	0.0087703	0.1808039
374.116	214402	2555	0.0086893	0.1744573
374.616	205707	2633	0.0091538	0.1914082
375.116	208005	2757	0.008394	0.1750727
375.616	202900	2716	0.009379	0.195101
376.116	200190	2731	0.0098157	0.1994056
376.616	213102	2667	0.0077756	0.1653199
377.116	205457	2442	0.0142658	0.2459347
377.616	205344	2567	0.0129587	0.2436399
378.116	203920	2617	0.0125834	0.2451255
378.616	190171	2687	0.0153967	0.2970958
379.116	184833	2885	0.0125465	0.2541105
379.616	194904	2796	0.010477	0.2200006
380.116	199614	2937	0.0091727	0.1887994
380.616	200759	2715	0.0100917	0.1971717
381.116	210074	2723	0.0083018	0.1729295
381.616	226858	2560	0.0057305	0.1184441
382.116	231597	2433	0.0075649	0.1455848
382.616	222929	2431	0.009752	0.1807436
383.116	218949	2508	0.0088103	0.1779044
383.616	217560	2498	0.0086505	0.1740347
384.116	222414	2633	0.0085201	0.168636
384.616	220950	2377	0.0092148	0.1794388
385.116	208981	2657	0.0119485	0.2320259
385.616	220394	2419	0.0123461	0.2311497
386.116	211717	2378	0.0130174	0.2348323

Continue on next page

core depth (cm)	Ca (cps)	Cl (cps)	Ti/Ca	Fe/Ca
386.616	220800	2282	0.0131612	0.2327083
387.116	218547	2251	0.0138597	0.2474067
387.616	210718	2394	0.0134018	0.244374
388.116	205721	2651	0.0122059	0.2432955
388.616	209616	2497	0.0131049	0.2416132
389.116	207602	2590	0.0124517	0.2415825
389.616	201213	2654	0.0145865	0.2609772
390.116	202224	2518	0.0145581	0.2756745
390.616	203743	2516	0.0161183	0.3043638
391.116	205554	2409	0.0171342	0.2993131
391.616	201431	2594	0.0159012	0.2903227
392.116	203193	2496	0.0181896	0.3104684
392.616	191393	2487	0.0191961	0.3385808
393.116	196567	2582	0.0196981	0.3513916
393.616	187231	2529	0.0204774	0.4198717
394.116	199007	2369	0.0176325	0.3493244
394.616	202930	2389	0.0174888	0.3214261
395.116	194862	2532	0.0178177	0.3243783
395.616	198920	2559	0.017585	0.3190579
396.116	182341	2630	0.0210265	0.3935319
396.616	182518	2650	0.0211102	0.3763684
397.116	161411	2918	0.0223343	0.4317797
397.616	162106	2757	0.0208814	0.3963086
398.116	176939	2512	0.0246865	0.4454699
398.616	179777	2638	0.0221163	0.4088565
399.116	184758	2690	0.0203401	0.3906732
399.616	180754	2653	0.0241876	0.4270777
400.116	157110	3199	0.0252753	0.5278404
400.616	153389	3141	0.0281572	0.5356381
401.116	153859	2866	0.0340832	0.604287
401.616	168703	2651	0.0344807	0.5873458
402.116	172006	2703	0.0347197	0.5755613
402.616	188206	2587	0.02603	0.4521854
403.116	187008	2464	0.0278491	0.4724343
403.616	181863	2653	0.0281806	0.4788
404.116	180251	2729	0.0273341	0.491093
404.616	168884	2452	0.0430059	0.6658772
405.116	151407	2779	0.0486701	0.7754199
405.616	155441	2585	0.0478059	0.7762431
406.116	156441	2530	0.0486318	0.7532936
406.616	171492	2548	0.0405792	0.6311023
407.116	180384	2556	0.0303408	0.5196193
407.616	169084	2929	0.0272941	0.5041577
408.116	161291	2741	0.0381298	0.6572654
408.616	156813	2442	0.0490265	0.7385867
409.116	158656	2279	0.0555226	0.7727284
409.616	162374	2072	0.0586855	0.7848794
410.116	151934	2678	0.0494359	0.7471139
410.616	164087	2687	0.0398935	0.624888
411.116	165378	2611	0.0381187	0.6667453
411.616	169823	2698	0.0323867	0.559353
412.116	172012	2724	0.033986	0.5862614
412.616	175749	2451	0.0406147	0.6172496
413.116	178823	2808	0.0315508	0.5466746
413.616	174498	2986	0.0241092	0.4621658

Continue on next page

core depth (cm)	Ca (cps)	Cl (cps)	Ti/Ca	Fe/Ca
414.116	189060	2613	0.0263356	0.4838411
414.616	193892	2548	0.0254265	0.4603542
415.116	184028	2690	0.0265014	0.485975
415.616	180871	2730	0.026577	0.4587247
416.116	181338	2847	0.0248817	0.4503248
416.616	182995	2775	0.025498	0.4395421
417.116	179172	2790	0.0270522	0.4836247
417.616	181103	2853	0.0240029	0.4461936
418.116	176515	2837	0.026621	0.4998329
418.616	183817	2888	0.0282509	0.5369308
419.116	184713	2832	0.0271123	0.5128659
419.616	181878	3056	0.0177207	0.355513
420.116	180549	2944	0.0219442	0.4160256
420.616	191823	2648	0.0243662	0.4791031
421.116	187289	2709	0.0265739	0.4910112
421.616	194791	2825	0.0199701	0.3964865
422.116	204202	2861	0.0122477	0.260972
422.616	206208	2930	0.0133894	0.2525314
423.116	184624	3097	0.0112282	0.2527407
423.616	154121	3154	0.0115169	0.2696518
424.116	196377	2737	0.012807	0.2621081
424.616	205940	2762	0.0131737	0.2503399
425.116	193417	2796	0.0148126	0.2863761
425.616	184469	2825	0.0140837	0.29953
426.116	184747	2854	0.0176999	0.3361354
426.616	173540	2902	0.0228996	0.4546733
427.116	178968	2789	0.0229035	0.4498905
427.616	175636	2980	0.0239074	0.4700346
428.116	177694	2814	0.0231465	0.4769548
428.616	189437	2730	0.0205398	0.3832673
429.116	192068	2697	0.0204719	0.3945998
429.616	174134	2676	0.0290868	0.562004
430.116	174331	2813	0.0297652	0.5689808
430.616	174887	3051	0.0276007	0.531143
431.116	181111	2776	0.0246037	0.4737095
431.616	182331	2695	0.0274994	0.5166483
432.116	179651	2741	0.0281045	0.5417448
432.616	183644	2857	0.0224238	0.4489393
433.116	181211	2781	0.0215274	0.4075525
433.616	181258	2700	0.0179358	0.3504232
434.116	173414	2863	0.0294671	0.5486235
434.616	143324	2695	0.0560827	1.1038905
435.116	144488	2658	0.0514506	1.0068518
435.616	150915	2769	0.0511281	0.9792996
436.116	142089	2344	0.0654942	1.2039144
436.616	157239	2534	0.0460128	0.8890097
437.116	189071	2727	0.0235097	0.447525
437.616	168676	2972	0.0251488	0.5074166
438.116	191968	2864	0.018003	0.358914
438.616	199701	2785	0.0161141	0.3104141
439.116	188509	2803	0.020381	0.3931324
439.616	173406	2701	0.0282459	0.5321904
440.116	144882	2725	0.0395701	0.8005894
440.616	19320	2772	0.3232919	8.4804865
441.116	5205	2844	1.2985591	36.656484

Continue on next page

core depth (cm)	Ca (cps)	Cl (cps)	Ti/Ca	Fe/Ca
441.616	9743	3104	0.7776865	21.338705
442.116	22260	3303	0.3653639	9.2467206
442.616	9289	3220	0.8027775	20.569275
443.116	11239	3313	1.0388825	21.817333
443.616	32140	3061	0.3528936	7.456285
444.116	23205	2784	0.3953889	9.311226
444.616	2623	2749	3.8734274	86.344262
445.116	14038	2414	0.646887	14.936886
445.616	12147	1829	0.5902692	13.483741
446.116	1983	2050	3.9082199	91.106404
446.616	14267	2841	0.7100301	15.87804
447.116	7438	2779	1.2586717	29.999462
447.616	8577	3007	1.2401772	28.454471
448.116	2167	2426	4.5505307	105.36041
448.616	4183	2546	2.1781018	50.93115
449.116	6790	2262	1.1768778	29.413402
449.616	2523	2418	3.5592549	96.32065
450.116	4596	2259	1.9852045	52.003046
450.616	3926	2535	2.7587876	66.749618
451.116	6482	2490	1.8012959	42.152114
451.616	11067	2886	0.9995482	24.580284
452.116	14223	2522	0.6515503	15.335513
452.616	7612	2311	1.0932738	26.503284
453.116	13608	2552	0.6638007	16.735303
453.616	10568	2516	0.8045988	20.597748
454.116	4431	2575	1.7296321	42.052358
454.616	2865	2435	2.9588133	72.084468
455.116	2409	2045	2.9946036	80.825654
455.616	4332	2047	1.7636196	47.750462
456.116	6680	2444	1.1497006	31.220359
456.616	3299	1666	1.5522886	41.519248
457.116	5099	1732	1.1439498	30.638949
457.616	1739	1329	2.4525589	66.124784

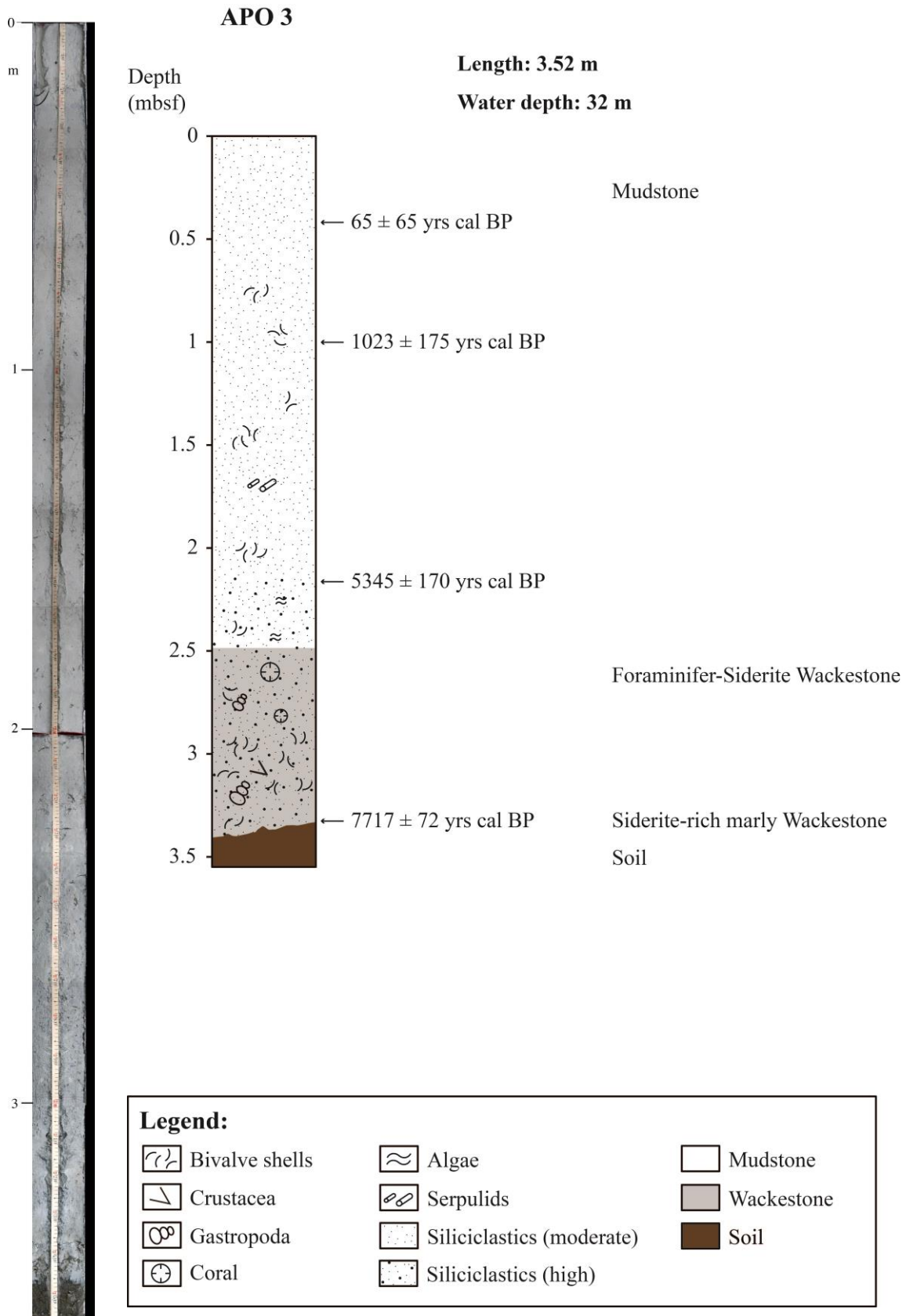
Core APO 2: List of foraminifera species

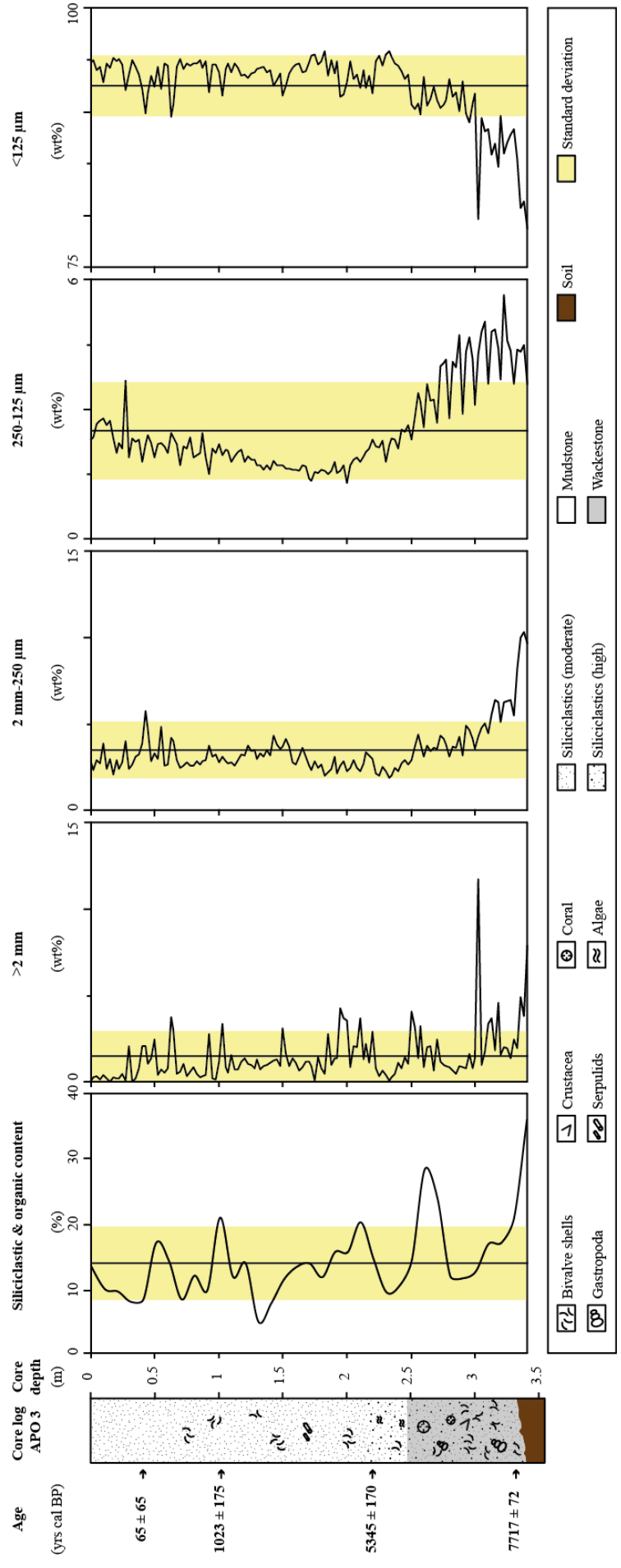
Foraminifera	*APO 2 37-38	APO 2 109-111	*APO 2 147-148	APO 2 157-158	*APO 2 172-173	APO 2 269-271
<i>Adelosina</i> sp. 1						1
<i>Ammonia</i> sp. 1					5	
<i>Amphistegina lessonii</i>						5
<i>Clavulina pacifica</i>						5
<i>Clavulina subangularis</i>					2	
<i>Elphidium excavatum</i>				4		40
<i>Elphidium</i> sp. 1					2	
<i>Fijiella simplex</i>						6
<i>Operculina ammonoides</i>					6	12
<i>Operculina</i> sp. 1						4
<i>Parasorites orbitolitoides</i>						3
<i>Peneroplis planatus</i>						1
<i>Pyrgo oblonga</i>						1
<i>Quinqueloculina agglutinans</i>						10
<i>Quinqueloculina debenayi</i>						3
<i>Quinqueloculina parkeri</i>						1
<i>Quinqueloculina polygona</i>						1
<i>Quinqueloculina</i> sp. 1					5	12
<i>Quinqueloculina</i> sp. 2					1	
<i>Quinqueloculina subpolygona</i>					3	9
<i>Spiroloculina angulata</i>						4
<i>Spiroloculina clara</i>						2
<i>Spiroloculina depressa</i>					2	
<i>Spiroloculina eximia</i>					2	
<i>Spiroloculina subimprensa</i>	53	47	40	41	51	13
<i>Textularia agglutinans</i>	114	107	94	96	70	40
<i>Textularia candeiana</i>		10	13	15	19	8
<i>Textularia pseudogramen</i>				11	4	7
<i>Textularia porrecta</i>	20	17	33	13	18	3
<i>Textularia</i> sp. 1					5	
<i>Textularia</i> sp. 2						2
<i>Triloculina oblonga</i>						6
<i>Triloculina</i> sp. 1					2	
<i>Triloculina</i> sp. 2					3	
<i>Triloculina</i> sp. 3						1
Other species (<5 % occurrence)	13	19	20	20		
sum	200	200	200	200	200	200

*** peak layer**

Agglutinated species	134	144	153	135	118	65
Hyaline species	10	3	3	16	13	67
Porcelaneous species	56	53	44	49	69	67
sum	200	200	200	200	200	200

Core APO 3:





Core APO 3: Corelog, texture and siliciclastics

Core APO 3: Grain-size analyses

core depth (cm)	>2 mm (wt%)	2-0.25 mm (wt%)	0.25-0.125 mm (wt%)	<0.125 mm (wt%)
2.5	0.27	2.36	2.36	95.02
5.0	0.33	2.94	2.67	94.06
7.5	0.14	2.75	2.75	94.37
12.5	0.24	2.41	2.65	94.71
15.0	0.00	2.98	2.73	94.29
17.5	0.31	2.10	2.34	95.25
22.5	0.20	2.44	2.24	95.12
25.0	0.48	2.79	2.10	94.63
27.5	0.12	4.05	3.68	92.15
32.5	0.04	2.65	2.34	94.97
35.0	0.25	3.11	2.25	94.38
37.5	0.80	3.23	2.31	93.66
42.5	2.11	5.77	2.21	89.91
45.0	1.07	4.73	2.40	91.80
47.5	1.41	2.86	2.24	93.49
52.5	0.42	2.97	2.21	94.40
55.0	0.76	4.83	2.23	92.19
57.5	0.53	2.60	2.15	94.72
62.5	3.76	4.23	2.46	89.55
65.0	3.03	4.09	0.24	92.63
67.5	0.47	2.94	2.21	94.37
72.5	1.09	2.61	2.14	94.15
75.0	0.37	2.82	2.09	94.72
77.5	0.58	2.61	2.35	94.47
82.5	0.46	2.87	1.95	94.72
85.0	0.27	2.68	2.00	95.04
87.5	0.35	2.88	2.47	94.30
92.5	2.81	3.76	1.51	91.91
95.0	2.40	3.04	2.05	92.51
97.5	1.59	3.23	1.96	93.22
102.5	3.40	3.11	1.94	91.55
105.0	0.88	2.87	2.07	94.18
107.5	0.57	2.73	2.04	94.66
112.5	0.76	2.63	1.91	94.71
115.0	0.75	2.94	2.01	94.29
117.5	1.18	3.26	2.08	93.48
122.5	1.06	3.77	1.91	93.26
125.0	1.01	3.45	1.85	93.69
127.5	0.80	3.50	1.83	93.87
132.2	0.76	3.30	1.71	94.23
135.0	0.96	3.10	1.62	94.33
137.5	0.99	3.48	1.71	93.82
142.5	1.26	4.37	1.81	92.56

continue on next page

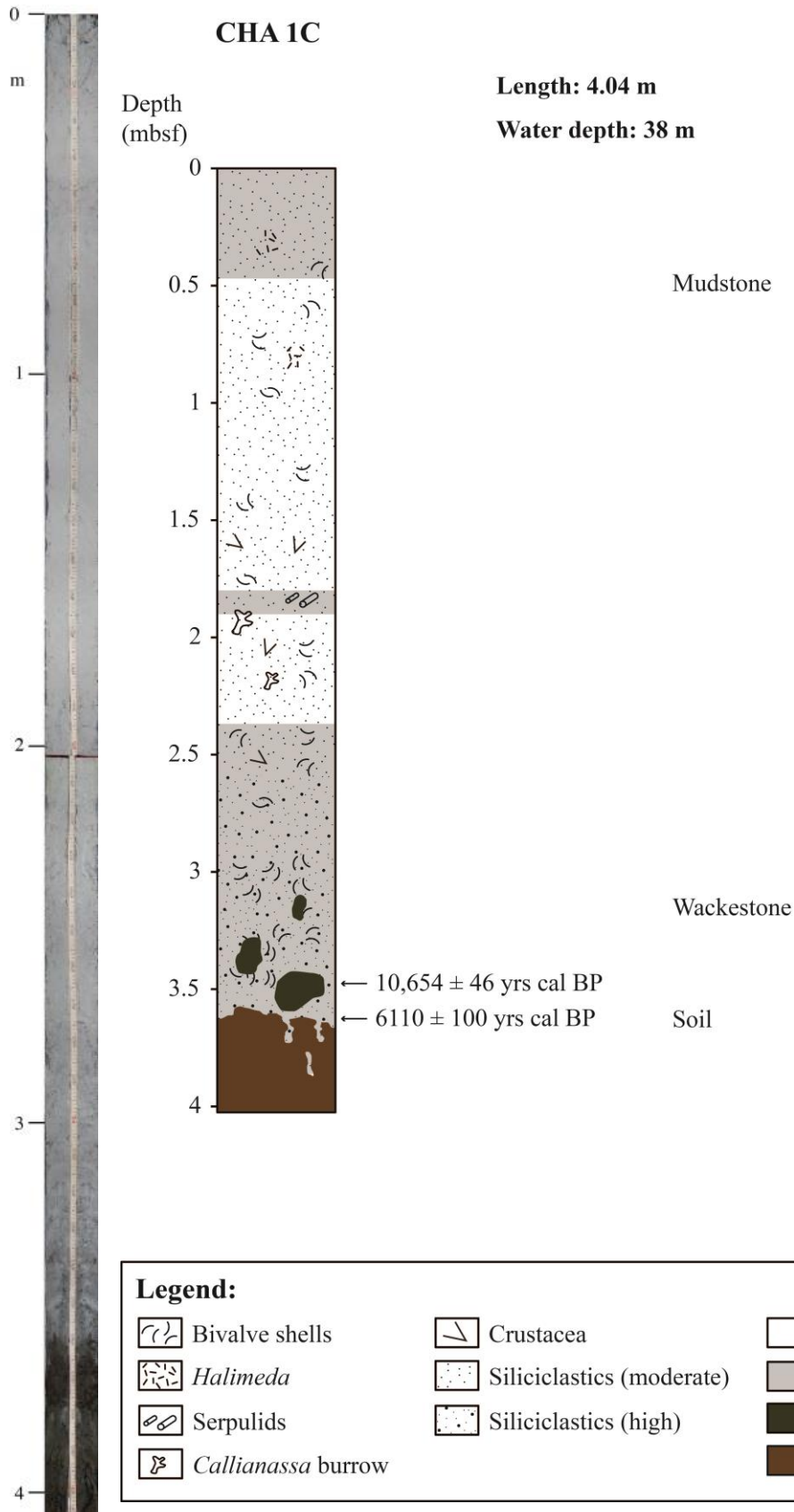
mm

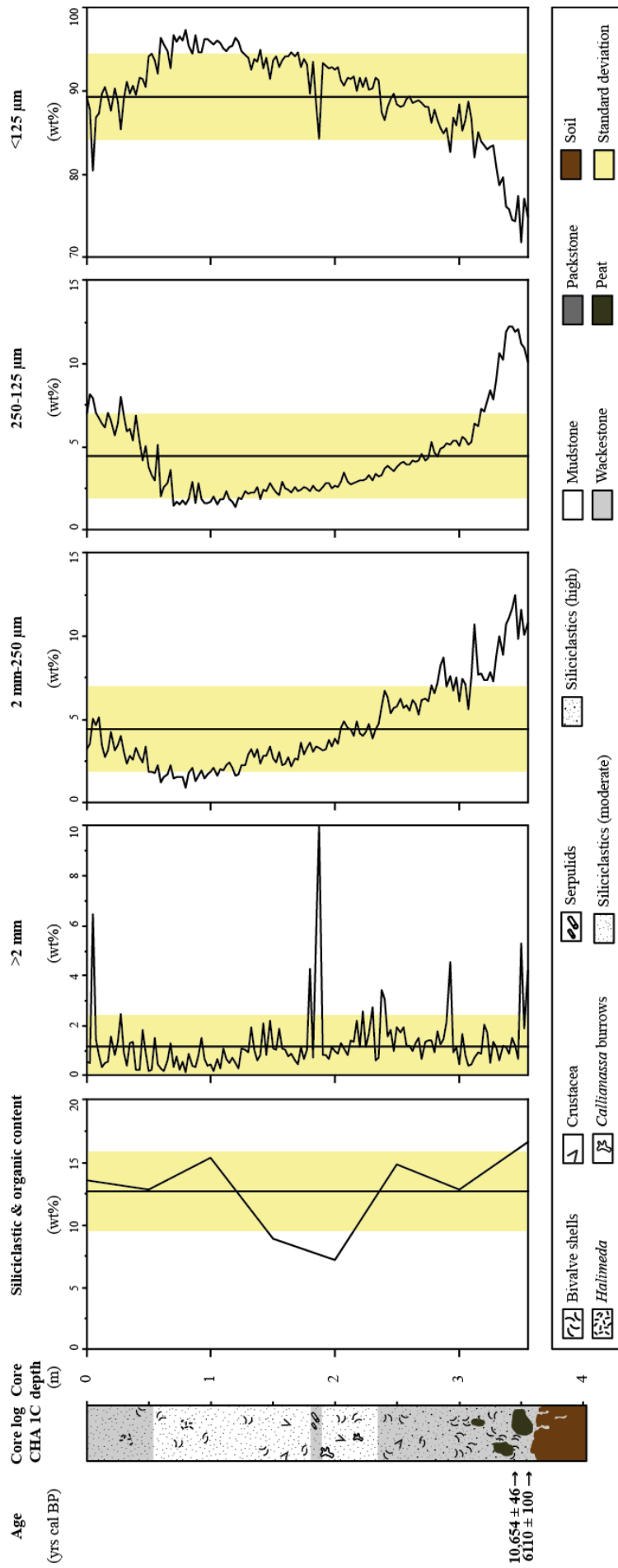
core depth (cm)	>2 mm (wt%)	2-0.25 mm (wt%)	0.25-0.125 mm (wt%)	<0.125 mm (wt%)
145.0	1.35	3.85	1.71	93.09
147.5	0.93	3.58	1.72	93.77
152.5	1.64	4.17	1.64	92.55
155.0	0.95	3.69	1.63	93.73
157.5	1.37	2.79	1.60	94.23
162.5	0.68	3.11	1.58	94.64
165.0	0.90	3.61	1.70	93.79
167.5	1.21	3.12	1.68	93.99
172.5	0.92	2.32	1.36	95.41
175.0	0.11	2.84	1.55	95.50
177.5	1.48	2.45	1.52	94.55
182.5	0.47	2.06	1.59	95.87
185.0	2.77	2.19	1.50	93.54
187.5	1.02	2.41	1.58	94.99
192.5	1.41	2.18	1.54	94.88
195.0	4.30	2.60	1.59	91.50
197.5	3.68	2.89	1.71	91.72
202.5	0.90	2.50	1.70	94.90
205.0	2.09	2.90	1.84	93.17
207.5	2.01	2.51	1.88	93.60
212.5	1.29	2.75	1.93	94.03
215.0	2.22	3.38	2.02	92.38
217.5	1.15	3.21	2.10	93.54
222.5	0.83	2.18	2.14	94.85
225.0	0.36	2.02	2.12	95.49
227.5	0.67	2.56	2.28	94.50
232.5	0.07	1.87	2.18	95.88
235.0	0.31	2.04	2.32	95.34
237.5	0.49	2.47	2.31	94.73
242.5	0.79	2.75	2.53	93.94
245.0	1.42	2.96	2.49	93.14
247.5	1.07	2.69	2.64	93.60
252.5	3.20	3.71	2.81	90.28
255.0	1.38	4.44	3.39	90.79
257.5	3.23	3.88	3.19	89.70
262.5	2.02	3.74	3.59	90.65
265.0	2.09	3.44	3.21	91.26
267.5	0.69	3.65	3.24	92.43
272.5	1.18	4.35	4.01	90.45
275.0	1.01	4.16	4.09	90.74
277.5	0.92	3.82	4.15	91.11
282.5	0.68	3.73	4.11	91.48
285.0	0.51	3.64	3.99	91.86
287.5	0.92	4.25	4.73	90.09

continue on next page

core depth (cm)	>2 mm (wt%)	2-0.25 mm (wt%)	0.25-0.125 mm (wt%)	<0.125 mm (wt%)
292.5	0.79	4.95	4.35	89.90
295.0	1.61	4.67	4.67	89.05
297.5	0.81	4.17	4.17	90.84
302.5	11.75	4.29	4.29	79.68
305.0	0.98	4.81	4.81	89.40
307.5	1.75	5.04	5.04	88.17
312.5	3.69	5.58	4.79	85.94
315.0	1.81	6.41	4.85	86.94
317.5	4.61	6.26	4.42	84.72
322.5	2.03	6.27	5.65	86.05
325.0	1.98	6.33	4.60	87.09
327.5	1.40	6.39	4.36	87.84
332.5	1.96	8.19	4.38	85.47
335.0	4.90	9.99	4.35	80.76
337.5	3.85	10.31	4.49	81.36

Core CHA 1C





Core CHA 1C: Corelog, texture and siliciclastics

Core CHA 1C: Grain-size analyses

core depth (cm)	>2 mm (wt%)	2-0.25 mm (wt%)	0.25-0.125 mm (wt%)	<0.125 mm (wt%)
0.0	0.56	3.21	6.99	89.24
2.5	0.48	3.55	8.15	87.82
5.0	6.47	5.04	7.97	80.51
7.5	1.45	4.68	7.03	86.84
10.0	0.85	5.16	6.75	87.24
12.5	0.37	3.46	6.43	89.74
15.0	0.50	2.76	6.16	90.58
17.5	0.55	3.18	7.10	89.17
20.0	1.56	4.28	6.57	87.60
22.5	0.80	3.15	5.67	90.38
25.0	1.34	3.44	6.42	88.80
27.5	2.46	4.06	8.02	85.46
30.0	0.91	3.09	6.91	89.09
32.5	0.42	2.39	5.97	91.22
35.0	1.28	2.86	6.14	89.72
37.5	1.36	2.59	5.41	90.64
40.0	0.26	3.33	6.93	89.48
42.5	0.25	2.77	5.32	91.66
45.0	1.86	2.45	4.21	91.49
47.5	0.94	3.43	5.05	90.57
50.0	0.21	1.88	3.79	94.11
52.5	0.26	1.85	3.33	94.55
55.0	1.51	1.81	2.96	93.72
57.5	0.44	2.31	5.16	92.08
60.0	0.27	1.24	2.02	96.46
62.5	0.16	1.53	2.62	95.69
65.0	0.59	1.74	2.84	94.82
67.5	1.32	2.31	3.63	92.75
70.0	0.33	1.48	1.45	96.74
72.5	0.79	1.52	1.68	96.01
75.0	0.25	1.53	1.58	96.63
77.5	0.54	1.52	1.83	96.11
80.0	0.13	0.94	1.54	97.39
82.5	0.88	1.81	1.91	95.41
85.0	0.42	2.10	2.91	94.56
87.5	0.35	1.32	1.60	96.73
90.0	0.85	1.67	2.85	94.63
92.5	1.51	1.94	1.84	94.70
95.0	0.67	1.45	1.64	96.24
97.5	0.41	1.72	1.66	96.22
100.0	0.45	1.89	1.70	95.96
102.5	0.21	2.13	2.01	95.65
105.0	0.65	1.67	1.56	96.12

continue on next page

core depth (cm)	>2 mm (wt%)	2-0.25 mm (wt%)	0.25-0.125 mm (wt%)	<0.125 mm (wt%)
107.5	0.28	2.07	1.85	95.81
110.0	1.09	1.96	1.87	95.08
112.5	0.65	2.24	2.36	94.74
115.0	0.51	2.42	1.86	95.22
117.5	0.70	2.09	1.72	95.49
120.0	0.52	1.65	1.41	96.42
122.5	0.31	1.74	1.94	96.00
125.0	1.08	2.28	1.87	94.77
127.5	1.03	2.26	2.34	94.37
130.0	0.92	2.93	2.17	93.98
132.2	1.96	3.21	2.29	92.53
135.0	1.05	2.78	2.31	93.85
137.5	0.63	3.27	2.61	93.48
140.0	0.80	2.35	1.88	94.98
142.5	2.10	2.80	2.42	92.69
145.0	0.83	2.86	2.35	93.96
147.5	2.20	3.43	2.84	91.53
150.0	1.09	2.68	2.54	93.69
152.5	1.06	2.45	2.28	94.20
155.0	1.91	3.04	2.11	92.94
157.5	1.07	2.31	2.91	93.71
160.0	1.03	2.38	2.50	94.10
162.5	0.76	2.72	2.41	94.11
165.0	0.87	2.22	2.30	94.60
167.5	0.61	2.68	2.57	94.14
170.0	0.46	2.58	2.38	94.58
172.5	1.12	3.60	2.42	92.86
175.0	0.69	2.90	2.57	93.84
177.5	1.03	3.29	2.51	93.17
180.0	4.26	3.67	2.37	89.70
182.5	0.72	3.09	2.70	93.50
185.0	5.57	3.42	2.41	88.60
187.5	9.99	3.33	2.36	84.33
190.0	0.85	3.17	2.60	93.39
192.5	0.81	3.21	2.84	93.13
195.0	0.67	3.77	2.85	92.71
197.5	1.15	3.38	2.51	92.96
200.0	0.96	3.83	2.66	92.55
202.5	0.89	3.54	2.61	92.97
205.0	1.28	4.50	2.89	91.34
207.5	1.08	4.87	3.44	90.61
210.0	0.84	4.52	2.95	91.69
212.5	1.40	4.45	2.73	91.42
215.0	1.36	4.01	2.86	91.76

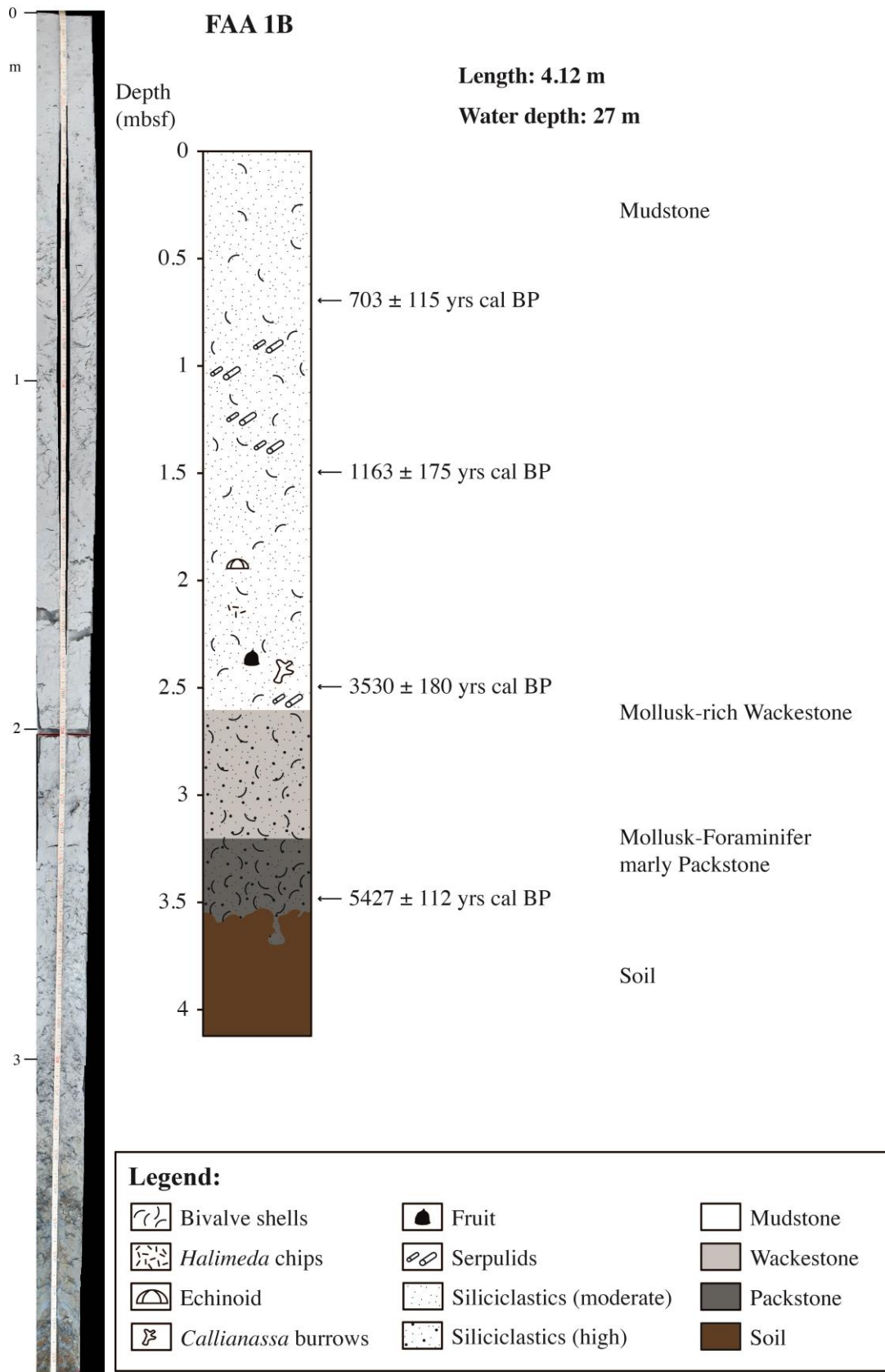
continue on next page

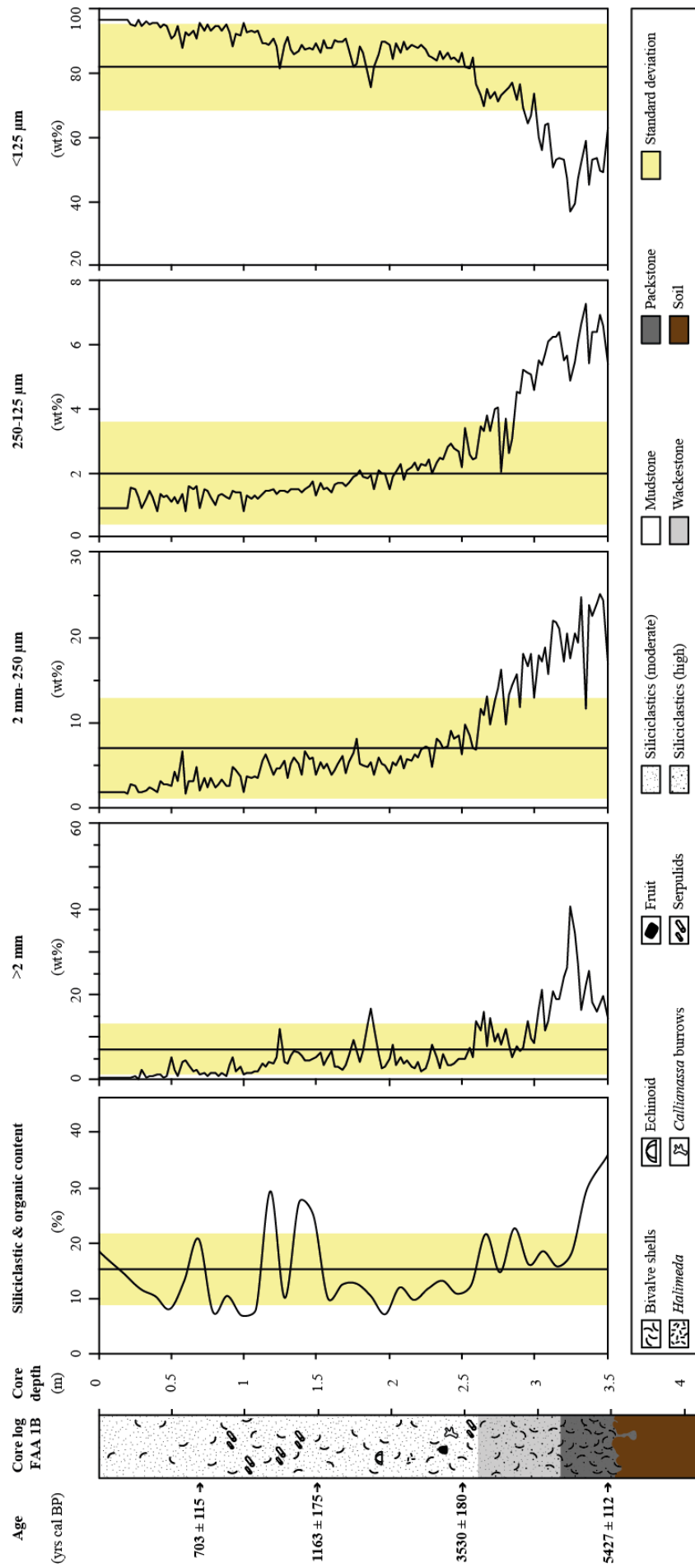
core depth (cm)	>2 mm (wt%)	2-0.25 mm (wt%)	0.25-0.125 mm (wt%)	<0.125 mm (wt%)
217.5	2.20	4.87	2.88	90.05
220.0	1.12	4.22	3.01	91.65
222.5	2.59	3.99	2.96	90.46
225.0	1.14	4.24	3.05	91.58
227.5	1.67	4.78	3.34	90.22
230.0	2.72	3.89	2.97	90.42
232.5	0.62	4.43	3.37	91.57
235.0	0.73	4.76	3.21	91.30
237.5	3.41	5.80	3.30	87.50
240.0	3.04	6.72	3.68	86.55
242.5	1.58	6.38	3.86	88.18
245.0	1.86	5.35	3.68	89.11
247.5	0.99	5.72	3.54	89.76
250.0	1.93	5.79	3.78	88.50
252.5	1.72	6.23	3.99	88.07
255.0	1.95	5.70	4.07	88.28
257.5	1.18	5.86	3.96	89.00
260.0	1.18	5.52	3.92	89.39
262.5	1.00	6.16	4.22	88.62
265.0	1.29	5.91	4.08	88.72
267.5	1.53	5.34	4.17	88.96
270.0	0.66	6.15	4.61	88.58
272.5	1.36	6.25	4.19	88.19
275.0	1.42	6.10	4.36	88.12
277.5	1.40	7.09	5.31	86.19
280.0	0.93	6.62	4.67	87.77
282.5	1.79	7.21	4.45	86.55
285.0	1.23	8.22	4.93	85.62
287.5	1.46	8.71	4.97	84.86
290.0	2.16	6.98	5.24	85.62
292.5	4.57	7.63	5.17	82.62
295.0	0.91	6.77	5.40	86.91
297.5	1.14	7.52	5.40	85.94
300.0	0.45	6.08	5.03	88.44
302.5	1.65	7.47	5.66	85.21
305.0	0.85	7.12	5.45	86.58
307.5	0.40	5.63	5.18	88.79
310.0	0.44	7.58	5.31	86.67
312.5	0.72	10.76	6.40	82.12
315.0	0.91	7.71	6.28	85.10
317.5	0.90	7.78	7.33	83.99
320.0	2.03	7.38	7.12	83.47
322.5	1.73	7.40	7.81	83.06
325.0	0.48	7.82	8.44	83.26

continue on next page

core depth (cm)	>2 mm (wt%)	2-0.25 mm (wt%)	0.25-0.125 mm (wt%)	<0.125 mm (wt%)
327.5	1.38	7.29	7.88	83.46
330.0	1.14	8.79	9.07	81.00
332.5	0.59	10.03	10.66	78.72
335.0	1.18	8.88	10.29	79.65
337.5	1.15	10.76	11.95	76.13
340.0	0.87	11.10	12.28	75.75
342.5	1.53	11.68	12.21	74.58
345.0	1.21	12.45	11.92	74.42
347.5	0.64	9.82	12.07	77.48
350.0	5.30	11.61	11.23	71.86
352.5	1.87	10.11	10.95	77.07
355.0	4.24	10.81	10.12	74.83

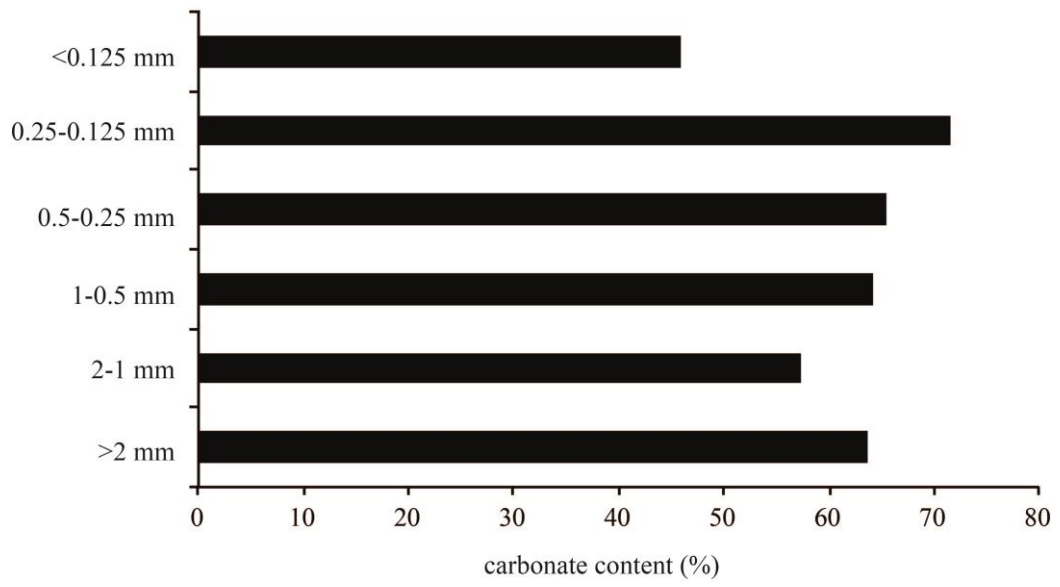
Core FAA 1B





Core FAA IB: Corelog, texture and siliciclastics

FAA 1B 349-351



Core FAA 1B: Carbonate content of different grain sizes, sample FAA 1B 349-351

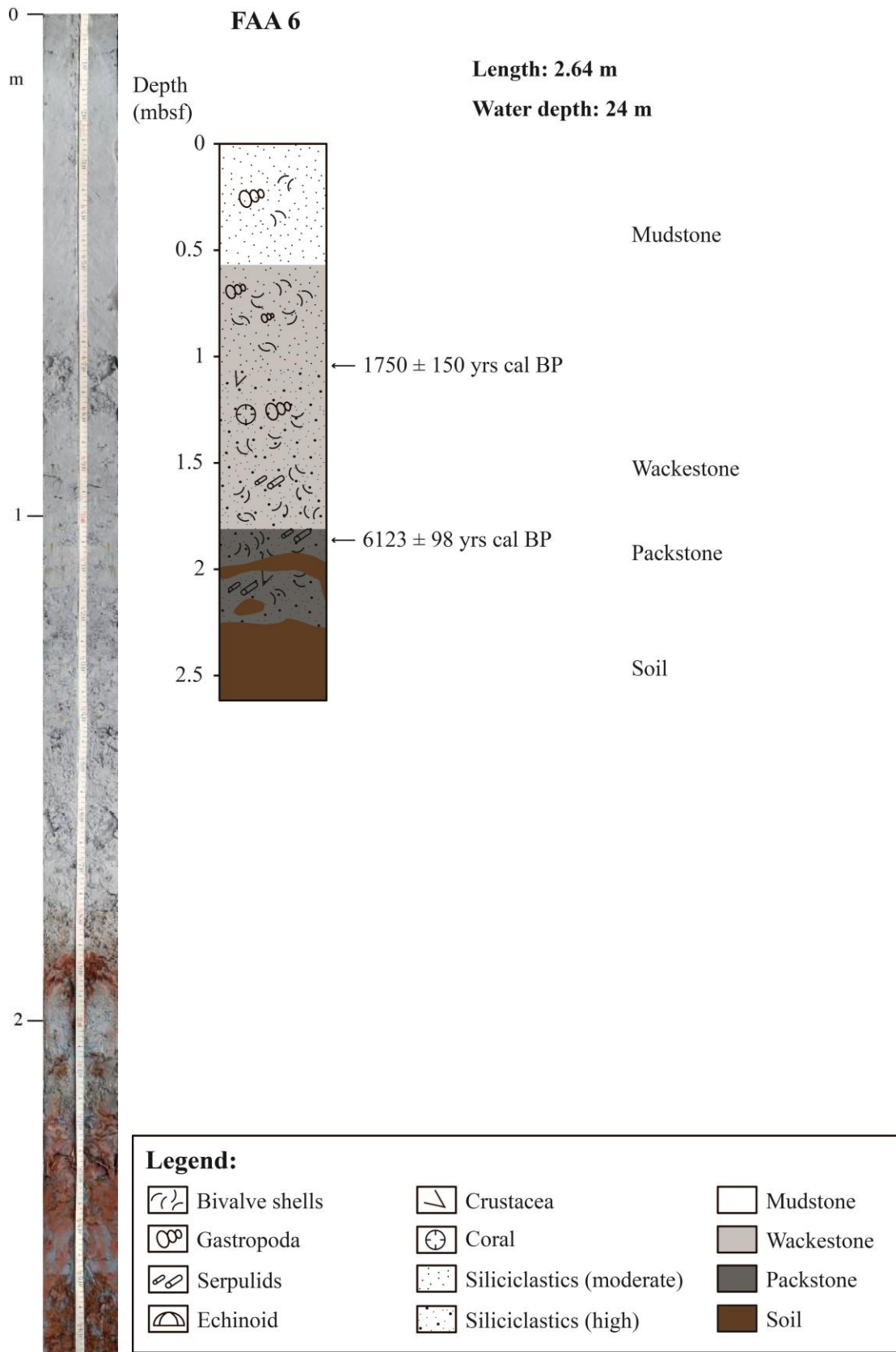
Core FAA 1B: Grain-size analyses

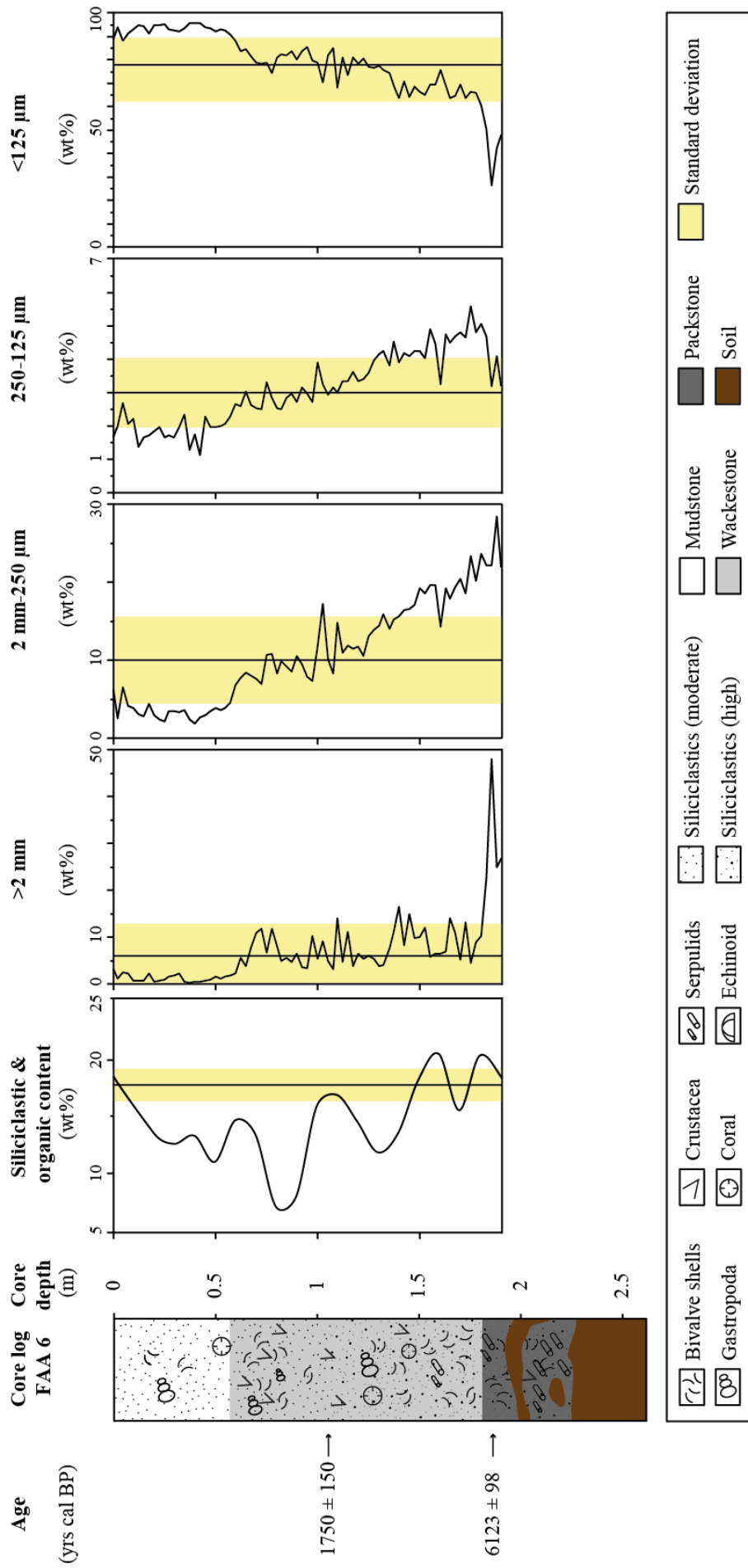
core depth (cm)	>2 mm (wt%)	2-0.25 mm (wt%)	0.25-0.125 mm (wt%)	<0.125 mm (wt%)
22.5	0.50	2.80	1.57	95.13
25.0	0.85	2.59	1.52	95.04
27.5	0.30	1.86	1.26	96.58
32.5	0.47	2.12	1.18	96.23
35.0	0.74	2.52	1.44	95.31
37.5	0.86	2.25	1.25	95.63
42.5	1.16	3.19	1.37	94.28
45.0	0.42	2.80	1.26	95.52
47.5	0.89	2.91	1.28	94.92
52.5	2.42	4.36	1.24	91.98
55.0	1.04	3.19	1.04	94.74
57.5	4.07	6.64	1.33	87.97
62.5	3.45	3.28	1.60	91.67
65.0	1.95	3.22	1.48	93.34
67.5	2.38	4.90	1.58	91.14
72.5	1.51	3.67	1.51	93.31
75.0	0.75	2.54	1.45	95.26
77.5	1.52	3.68	1.26	93.55
82.5	0.91	2.82	1.31	94.97
85.0	1.74	3.34	1.37	93.55
87.5	0.95	2.58	1.26	95.21
92.5	5.24	4.86	1.43	88.47
95.0	1.94	4.42	1.40	92.25
97.5	3.15	3.79	1.39	91.66
102.5	1.78	3.85	1.32	93.06
105.0	1.68	3.65	1.18	93.49
107.5	2.13	3.75	1.32	92.80
112.5	3.75	5.63	1.34	89.28
115.0	2.97	6.28	1.44	89.32
117.5	4.29	5.38	1.44	88.88
122.5	5.37	4.65	1.37	88.61
125.0	11.97	4.76	1.45	81.82
127.5	4.28	5.53	1.46	88.73
132.2	5.78	5.30	1.48	87.45
135.0	6.64	6.07	1.48	85.81
137.5	6.36	5.31	1.49	86.85
142.5	4.44	6.71	1.48	87.37
145.0	4.57	5.85	1.61	87.98
147.5	4.91	5.90	1.74	87.45
152.5	6.49	5.40	1.67	86.44
155.0	3.65	4.62	1.52	90.21
157.5	5.10	5.17	1.54	88.19
162.5	3.26	4.57	1.62	90.55
165.0	3.15	5.19	1.70	89.96
167.5	2.44	6.08	1.68	89.80
172.5	5.57	5.39	1.70	87.35
175.0	9.51	6.47	1.90	82.11
177.5	6.89	8.24	1.92	82.96
182.5	6.74	5.04	1.88	86.34
185.0	12.93	4.88	1.83	80.35
187.5	16.78	5.42	1.96	75.84
192.5	6.10	6.00	2.09	85.81
195.0	2.84	5.29	2.00	89.88

continue on next page

core depth (cm)	>2 mm (wt%)	2-0.25 mm (wt%)	0.25-0.125 mm (wt%)	<0.125 mm (wt%)
197.5	2.97	5.09	2.00	89.94
202.5	8.38	5.38	1.90	84.34
205.0	3.57	5.15	2.04	89.24
207.5	5.22	6.10	2.28	86.41
212.5	4.43	5.81	2.11	87.65
215.0	3.25	5.69	2.19	88.87
217.5	2.77	6.42	2.31	88.51
222.5	1.96	6.96	2.30	88.78
225.0	2.72	7.35	2.25	87.68
227.5	4.92	7.15	2.41	85.52
232.5	5.51	8.10	2.34	84.06
235.0	2.84	7.80	2.46	86.90
237.5	6.09	7.09	2.41	84.41
242.5	3.38	9.04	2.94	84.64
245.0	4.01	8.28	2.78	84.92
247.5	5.07	8.65	2.66	83.62
252.5	4.89	9.82	3.40	81.90
255.0	7.45	8.48	2.57	81.50
257.5	5.38	7.15	2.45	85.03
262.5	11.62	11.66	3.44	73.28
265.0	16.11	10.93	3.33	69.63
267.5	7.85	13.19	3.82	75.14
272.5	9.11	12.69	4.01	74.19
275.0	10.68	14.14	4.05	71.13
277.5	8.33	16.29	2.02	73.36
282.5	8.12	13.37	2.62	75.89
285.0	5.44	14.46	3.07	77.03
287.5	7.81	15.67	4.52	72.00
292.5	7.47	18.15	5.23	69.16
295.0	13.87	16.62	5.12	64.39
297.5	9.81	18.06	5.09	67.03
302.5	16.65	18.00	5.53	59.83
305.0	21.11	17.28	5.38	56.22
307.5	11.56	18.84	5.71	63.89
312.5	20.94	21.96	6.28	50.82
315.0	18.80	21.90	6.25	53.06
317.5	19.10	21.08	6.41	53.41
322.5	26.24	20.58	5.69	47.48
325.0	40.81	17.58	4.88	36.72
327.5	34.41	20.53	5.47	39.59
332.5	16.29	24.69	6.65	52.37
335.0	22.15	11.67	7.29	58.89
337.5	25.44	23.88	5.43	45.24
342.5	15.97	24.03	6.41	53.59
345.0	18.02	25.12	6.95	49.91
347.5	19.72	24.46	6.61	49.21

Core FAA 6





Core FAA 6: Corelog, texture and siliciclastics

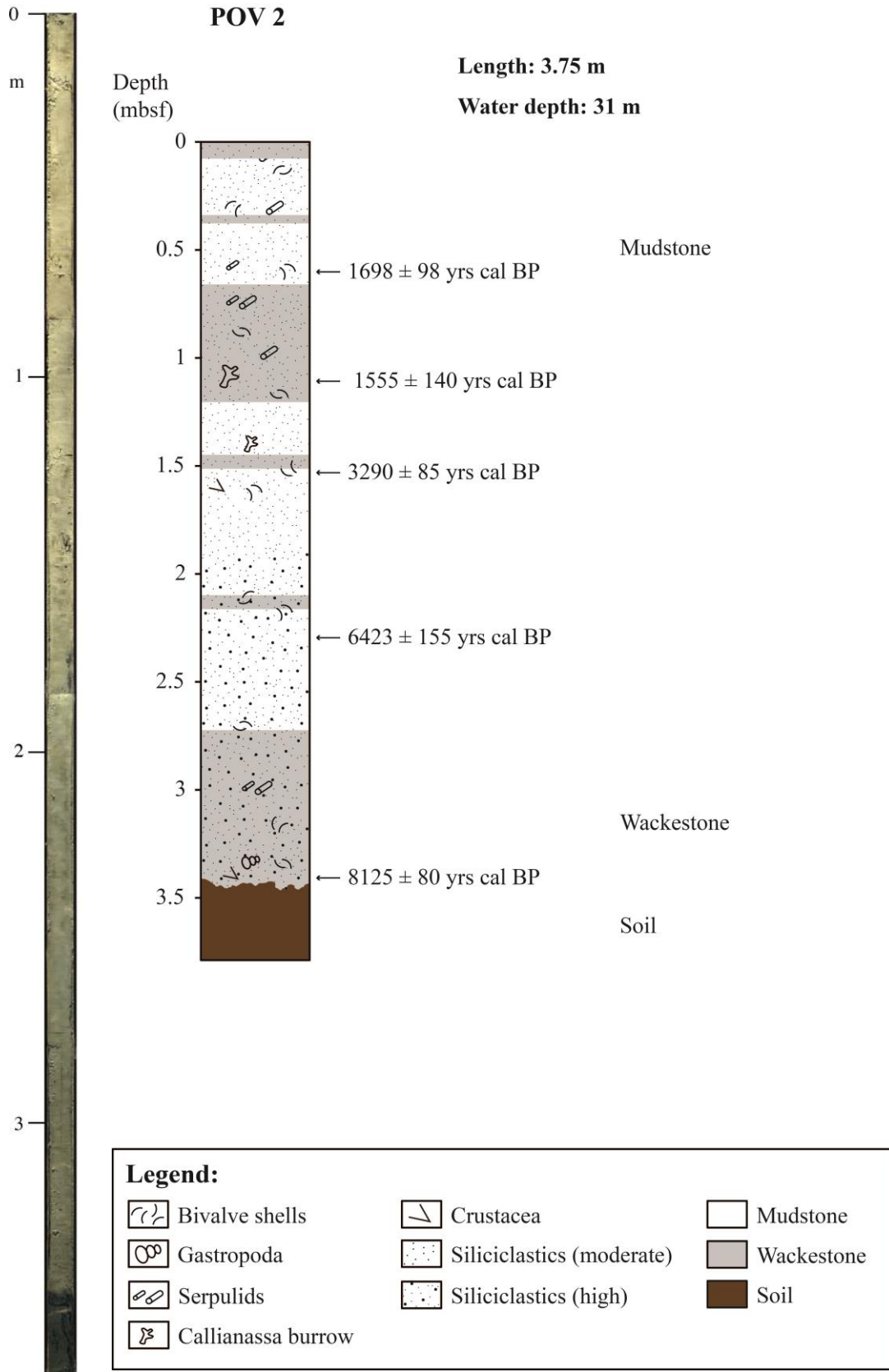
Core FAA 6: Grain-size analyses

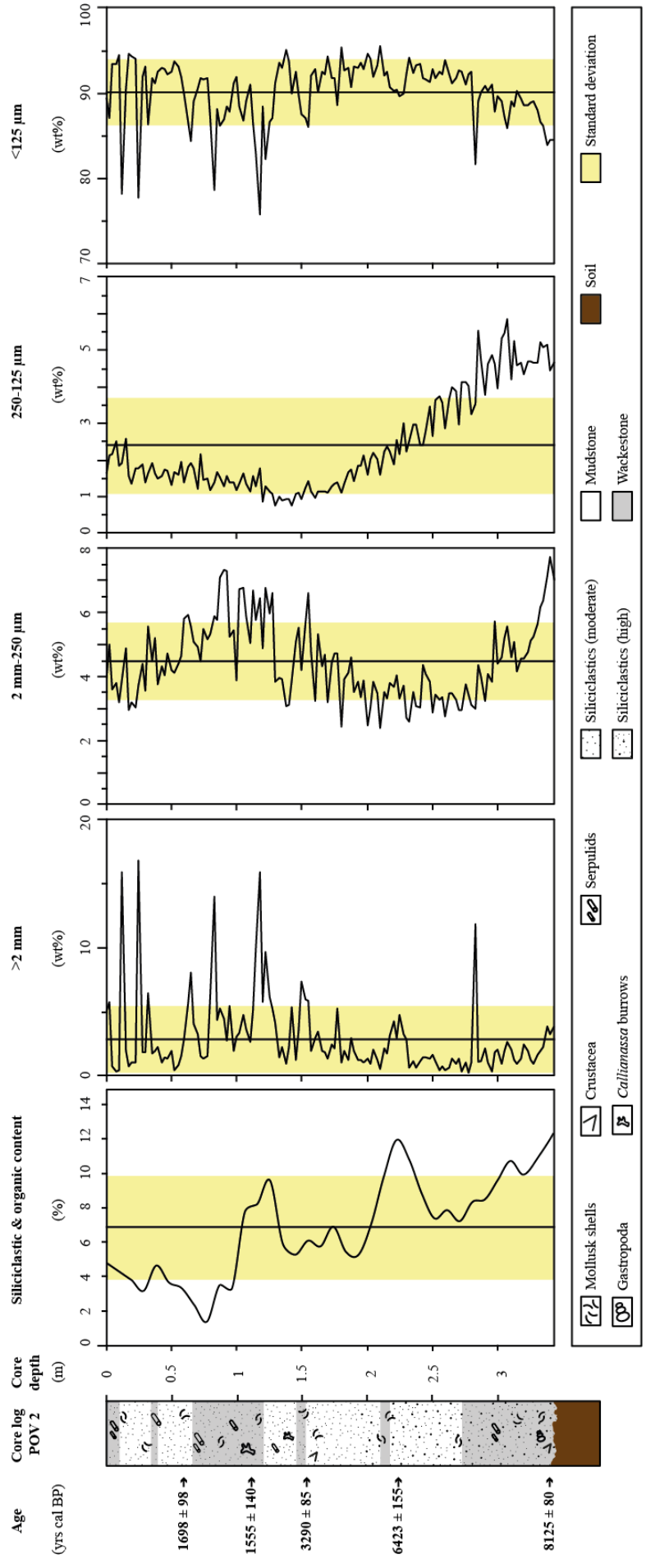
core depth (cm)	>2 mm (wt%)	2-0.25 mm (wt%)	0.25-0.125 mm (wt%)	<0.125 mm (wt%)
0	3.15	6.16	1.70	88.99
2.5	1.27	2.66	2.02	94.05
5.0	2.66	6.58	2.69	88.07
7.5	2.26	4.25	2.08	91.40
10	0.80	3.93	2.23	93.04
12.5	0.77	3.09	1.37	94.76
15.0	0.80	2.92	1.65	94.63
17.5	2.23	4.51	1.74	91.52
20	0.48	2.97	1.86	94.69
22.5	0.74	2.41	1.97	94.88
25.0	0.93	2.20	1.66	95.22
27.5	1.59	3.54	1.73	93.14
30	1.96	3.58	1.66	92.80
32.5	2.24	3.39	1.98	92.39
35.0	0.59	3.65	2.34	93.42
37.5	0.27	2.48	1.28	95.97
40	0.65	1.95	1.75	95.66
42.5	0.45	2.70	1.15	95.70
45.0	0.86	3.00	2.29	93.85
47.5	0.92	3.51	1.96	93.61
50	1.68	3.88	1.99	92.44
52.5	1.15	3.64	2.02	93.20
55.0	1.56	3.90	2.06	92.48
57.5	1.99	4.64	2.28	91.09
60	2.28	6.90	2.66	88.16
62.5	5.73	7.76	2.61	83.89
65.0	3.94	8.48	3.02	84.57
67.5	7.85	8.07	2.62	81.47
70	10.96	7.66	2.53	78.85
72.5	11.93	7.02	2.52	78.53
75.0	6.84	10.73	3.32	79.10
77.5	11.93	10.93	2.86	74.28
80	8.04	8.27	2.53	81.17
82.5	5.04	9.91	2.52	82.53
85.0	5.74	9.27	2.86	82.13
87.5	4.72	8.58	2.98	83.72
90	6.46	10.64	2.73	80.17
92.5	3.58	9.51	3.17	83.74
95.0	3.52	7.87	2.98	85.64
97.5	10.30	7.36	2.71	79.63
100	5.38	11.74	3.89	78.99
102.5	9.24	17.22	3.24	70.31
105.0	5.01	10.22	2.95	81.82
107.5	3.22	8.30	3.16	85.32
110	14.10	14.84	3.00	68.06
112.5	4.71	10.99	3.34	80.96
115.0	11.22	11.98	3.33	73.47
117.5	3.89	11.49	3.63	80.99
120	6.62	11.75	3.34	78.29
122.5	5.34	10.56	3.41	80.69
125.0	6.08	13.09	3.58	77.26
127.5	5.52	13.99	3.97	76.52
130	3.91	14.50	4.14	77.45

continue on next page

core depth (cm)	>2 mm (wt%)	2-0.25 mm (wt%)	0.25-0.125 mm (wt%)	<0.125 mm (wt%)
132.2	4.22	15.87	4.25	75.66
135.0	7.65	14.05	3.82	74.48
137.5	11.18	15.27	4.54	69.02
140	16.54	15.60	3.89	63.97
142.5	8.29	16.47	4.19	71.05
145.0	14.93	16.60	4.10	64.38
147.5	9.87	17.18	4.26	68.69
150	10.01	19.33	4.24	66.42
152.5	12.14	18.55	4.04	65.28
155.0	5.82	19.66	4.91	69.62
157.5	6.51	19.61	4.46	69.42
160	6.57	14.34	3.26	75.83
162.5	7.01	19.30	4.73	68.96
165.0	14.02	17.91	4.49	63.58
167.5	11.09	19.43	4.67	64.81
170	5.25	20.45	4.81	69.49
172.5	13.22	18.55	4.66	63.56
175.0	4.64	23.46	5.60	66.30
177.5	9.00	20.18	4.80	66.02
180	10.42	23.71	5.05	60.82
182.5	22.73	22.18	4.68	50.41
185.0	48.16	22.26	3.18	26.40
187.5	25.06	28.41	4.10	42.42
180.0	26.78	22.13	3.23	47.86

Core POV 2

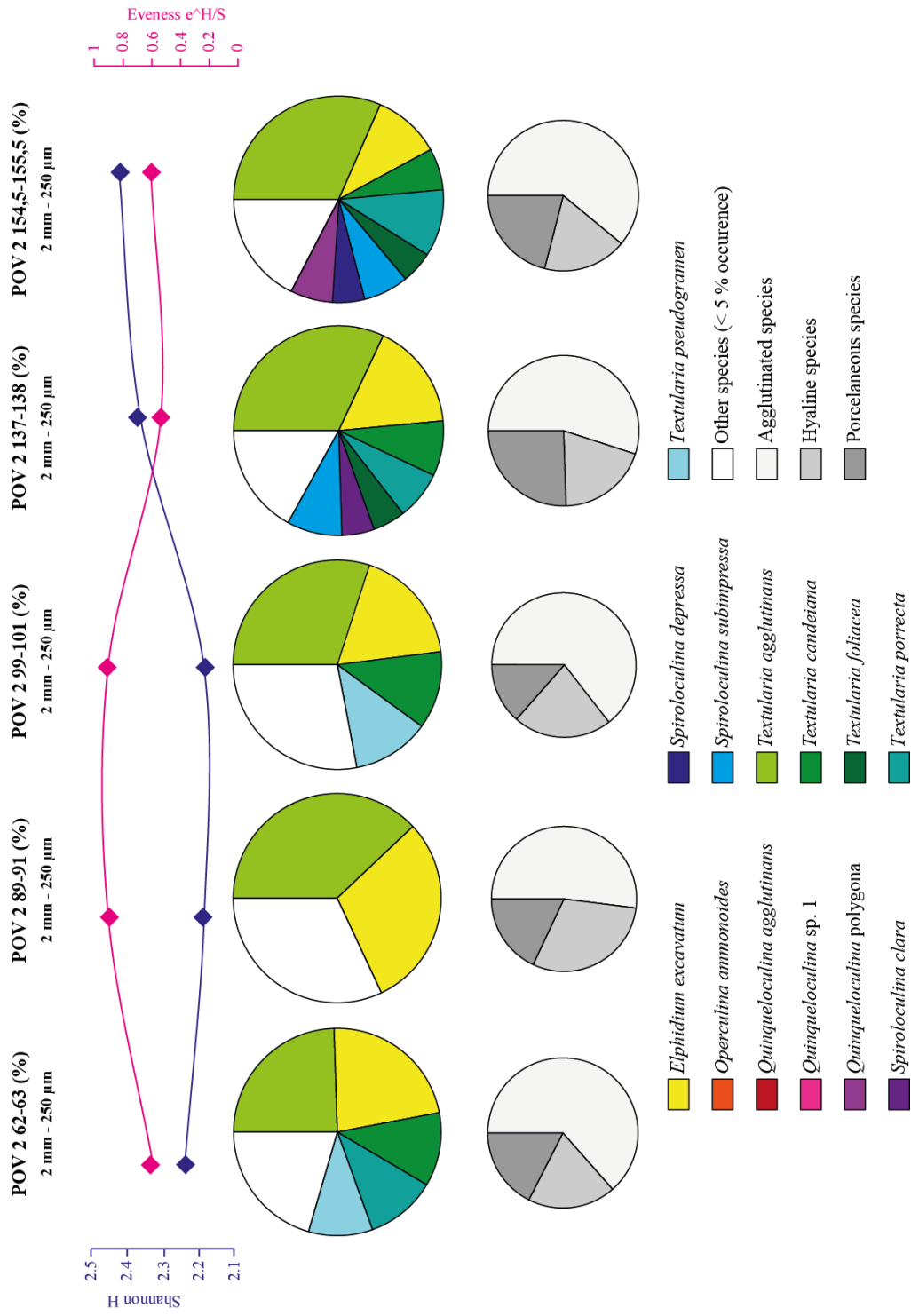




fff

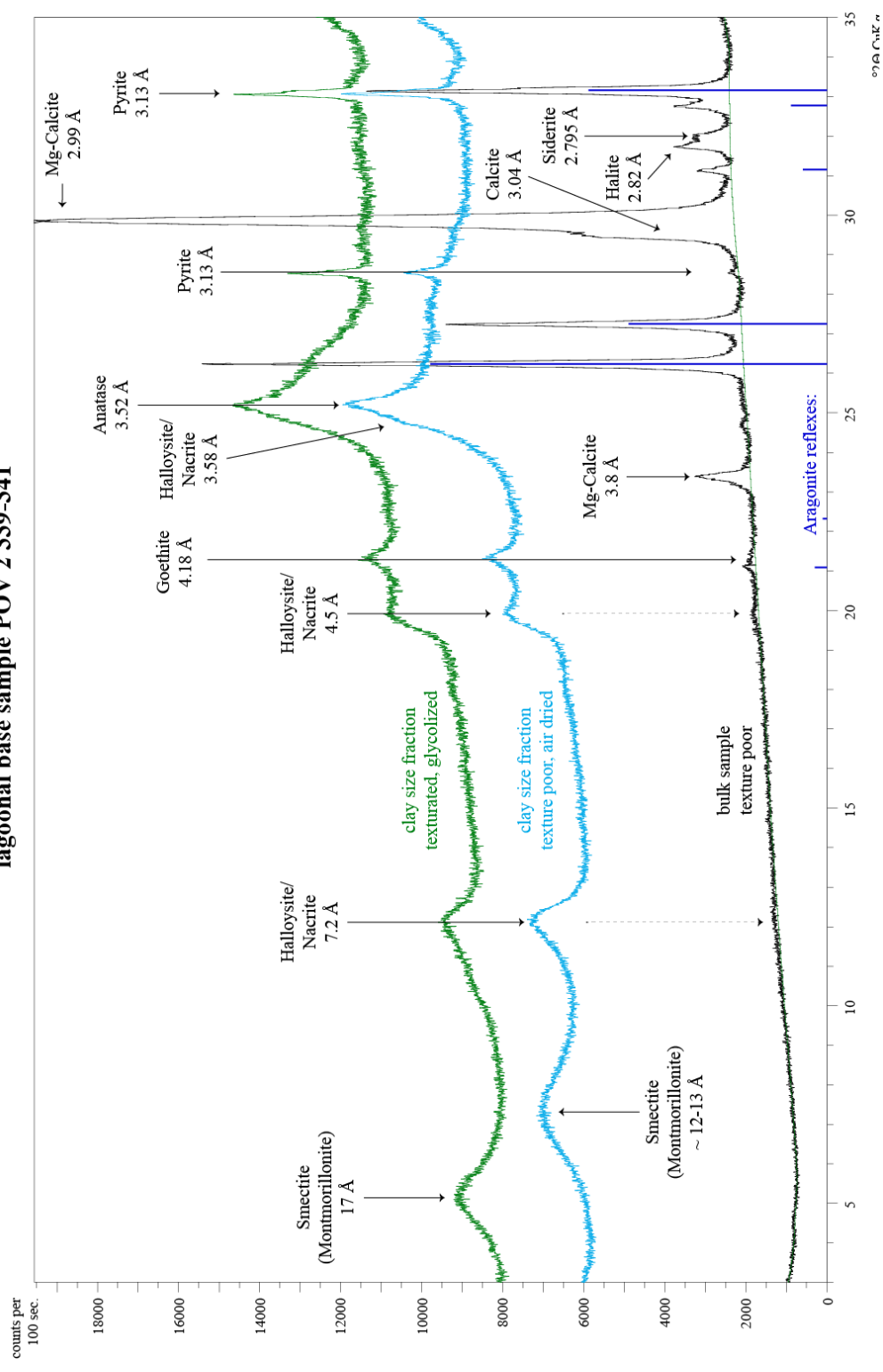
Core POV 2: Corelog, texture and siliciclastics

potentially redeposited potentially redeposited background sediment background sediment potentially redeposited



Core POV 2: Foraminifera assemblages and diversity indices

lagoonal base sample POV 2 339-341



Core POV 2: X-ray diffractogram of sample POV 2 339-341

Core POV 2: Grain-size analyses

core depth (cm)	>2 mm (wt%)	2-0.25 mm (wt%)	0.25-0.125 mm (wt%)	<0.125 mm (wt%)
2.5	5.80	5.02	2.14	87.04
5.0	0.76	3.59	2.18	93.47
7.5	0.31	3.80	2.50	93.39
12.5	15.97	3.87	1.90	78.27
15.0	2.01	4.89	2.58	90.52
17.5	0.76	2.96	1.56	94.72
22.5	1.08	3.02	1.78	94.12
25.0	16.83	3.71	1.76	77.70
27.5	1.85	4.40	1.88	91.87
32.5	6.49	5.55	1.62	86.34
35.0	1.79	4.49	1.90	91.83
37.5	1.93	5.21	1.64	91.22
42.5	1.05	4.31	1.58	93.06
45.0	1.42	4.03	1.75	92.81
47.5	1.36	4.71	1.70	92.23
52.5	0.44	4.14	1.67	93.75
55.0	0.88	4.42	1.61	93.09
57.5	1.51	4.64	1.96	91.89
62.5	5.66	5.91	1.81	86.62
65.0	8.07	5.55	1.93	84.44
67.5	4.09	5.10	1.79	89.01
72.5	1.57	4.47	2.16	91.80
75.0	1.37	5.49	1.46	91.68
77.5	1.59	5.16	1.51	91.74
82.5	14.01	5.88	1.40	78.72
85.0	4.39	5.78	1.68	88.15
87.5	5.25	7.09	1.53	86.14
92.5	2.74	7.31	1.55	88.40
95.0	5.47	5.26	1.38	87.89
97.5	1.96	5.44	1.40	91.21
102.5	3.41	6.75	1.37	88.47
105.0	4.77	6.78	1.64	86.81
107.5	3.66	5.88	1.34	89.11
112.5	5.18	6.68	1.58	86.56
115.0	9.87	5.76	1.29	83.08
117.5	15.95	6.45	1.77	75.82
122.5	9.68	6.78	1.27	82.27
125.0	6.22	5.98	1.13	86.67
127.5	5.24	6.60	1.09	87.07
132.2	1.50	3.95	1.01	93.53
135.0	2.25	3.93	0.90	92.92
137.5	0.92	3.09	0.92	95.06
142.5	5.35	3.87	0.74	90.04

continue on next page

core depth (cm)	>2 mm (wt%)	2-0.25 mm (wt%)	0.25-0.125 mm (wt%)	<0.125 mm (wt%)
145.0	1.30	5.10	1.09	92.51
147.5	3.55	5.52	1.12	89.81
152.5	5.95	5.68	1.26	87.11
155.0	5.85	6.60	1.43	86.11
157.5	1.93	4.78	1.14	92.16
162.5	3.46	5.32	1.14	90.08
165.0	2.00	4.34	1.15	92.51
167.5	1.90	4.69	1.13	92.28
172.5	2.43	4.43	1.29	91.85
175.0	2.17	4.73	1.35	91.75
177.5	5.29	4.74	1.40	88.57
182.5	2.00	3.91	1.34	92.75
185.0	1.22	4.14	1.67	92.97
187.5	2.94	4.60	1.74	90.72
192.5	1.30	3.83	1.85	93.01
195.0	1.25	3.36	1.85	93.54
197.5	1.10	3.89	2.12	92.89
202.5	0.91	3.04	2.04	94.01
205.0	2.07	3.84	2.21	91.87
207.5	1.24	3.49	2.02	93.25
212.5	2.20	3.50	2.23	92.06
215.0	1.77	3.31	2.39	92.54
217.5	3.19	3.79	2.23	90.78
222.5	2.96	4.06	2.54	90.43
225.0	4.82	3.33	2.15	89.71
227.5	3.31	3.70	3.01	89.97
232.5	0.62	2.59	2.52	94.26
235.0	1.17	3.50	2.98	92.36
237.5	0.65	3.08	2.96	93.31
242.5	1.44	4.35	2.42	91.78
245.0	1.44	4.07	2.81	91.68
247.5	1.33	3.84	3.46	91.37
252.5	1.12	3.45	3.64	91.79
255.0	0.43	3.27	3.73	92.57
257.5	0.80	3.37	3.58	92.25
262.5	0.61	3.49	3.69	92.20
265.0	1.36	3.47	3.98	91.20
267.5	0.97	3.29	3.89	91.84
272.5	0.31	2.95	4.13	92.60
275.0	1.08	3.77	4.12	91.03
277.5	0.29	3.43	4.04	92.24
282.5	11.81	2.99	3.53	81.67
285.0	1.02	4.37	5.55	89.06
287.5	1.15	3.98	4.74	90.13

continue on next page

core depth (cm)	>2 mm (wt%)	2-0.25 mm (wt%)	0.25-0.125 mm (wt%)	<0.125 mm (wt%)
292.5	1.03	4.07	4.63	90.26
295.0	0.33	3.82	4.86	90.99
297.5	1.87	5.72	4.62	87.79
302.5	0.95	4.62	5.34	89.09
305.0	1.99	5.21	5.47	87.33
307.5	2.64	5.58	5.85	85.93
312.5	1.21	5.10	5.26	88.43
315.0	0.97	4.18	4.60	90.26
317.5	1.37	4.57	4.67	89.39
322.5	1.93	4.77	4.71	88.58
325.0	1.25	5.11	4.68	88.96
327.5	0.97	5.25	4.65	89.13
332.5	1.96	6.17	5.24	86.63
335.0	2.29	6.38	5.08	86.24
337.5	3.88	7.12	5.14	83.87
342.5	3.73	7.11	4.61	84.55

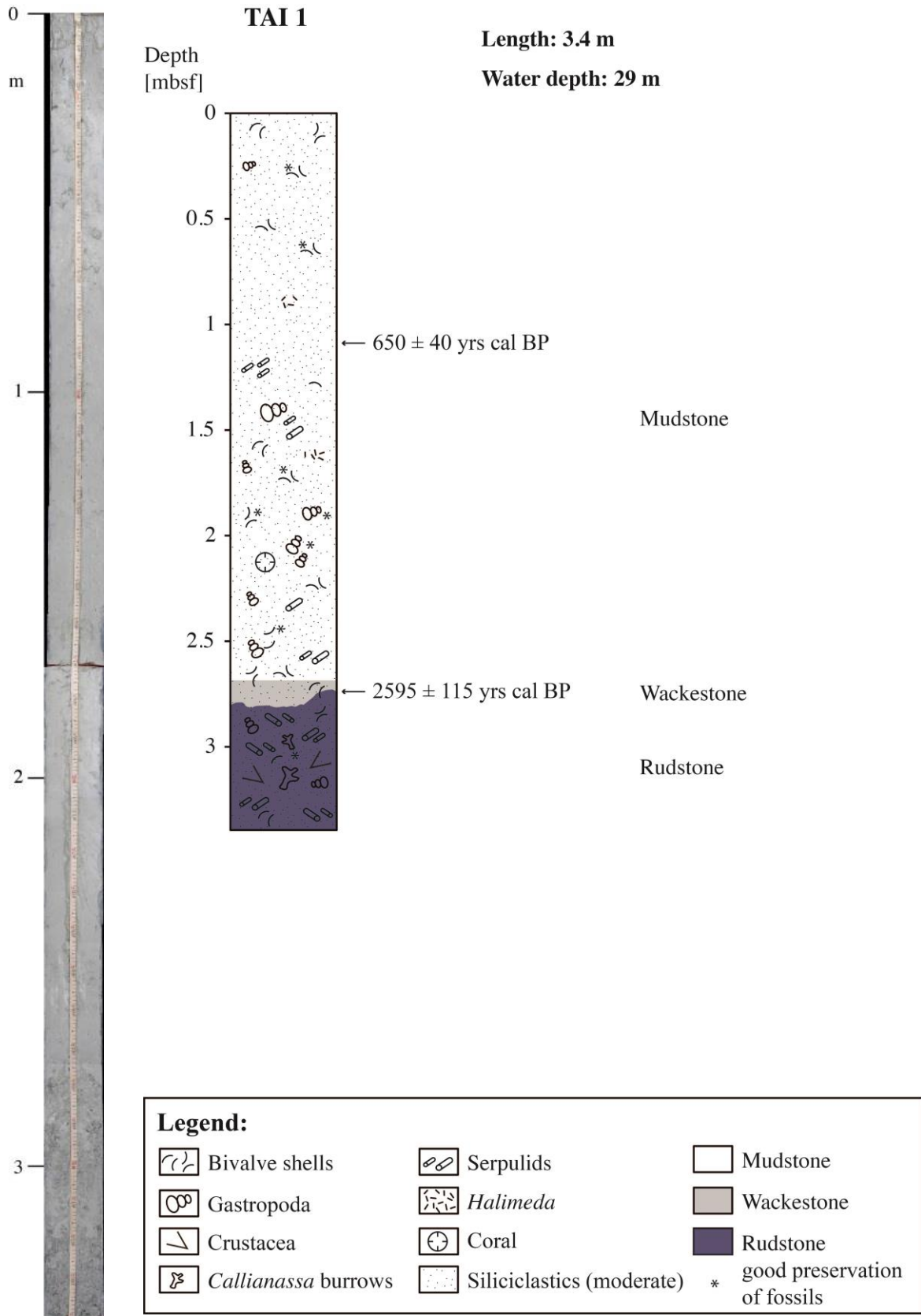
Core POV 2: List of foraminifera species

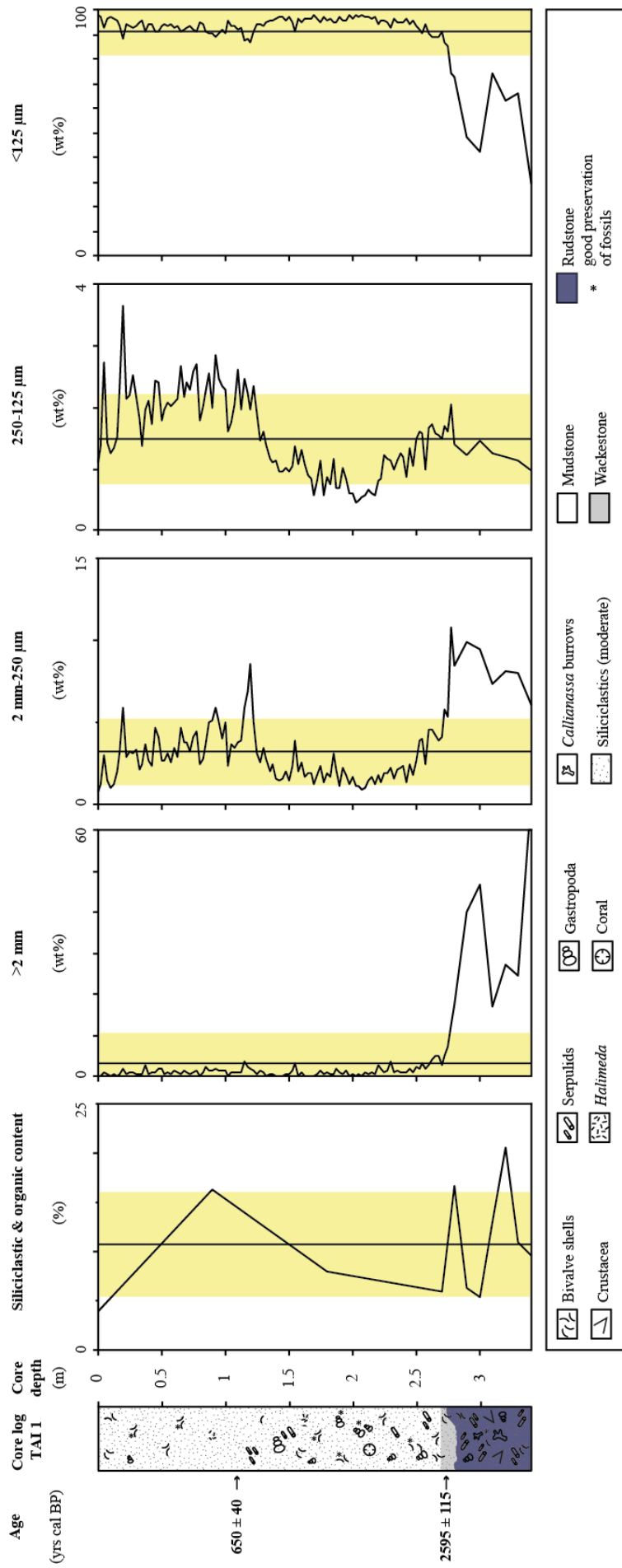
Foraminifera	*POV 2 62-63	*POV 2 89-91	POV 2 99- 101	POV 2 137-138	*POV 2 154,5-155,5
<i>Textularia agglutinans</i>	49	76	60	64	63
<i>Elphidium excavatum</i>	45	60	36	33	21
<i>Textularia candeiana</i>	23		24	17	13
<i>Textularia pseudogramen</i>	20		24		
<i>Textularia porrecta</i>	22			15	21
<i>Textularia foliacea</i>				10	10
<i>Spiriloculina. clara</i>				10	
<i>Spiriloculina subimpressa</i>				17	14
<i>Spiriloculina depressa</i>					10
<i>Quinqueloculina polygona</i>					13
Other species (<5 % occurrence)	41	64	56	34	35
sum	200	200	200	200	200

*** peak layer**

Agglutinated species	127	104	129	110	122
Hyaline species	38	36	27	39	36
Porcelaneous species	35	60	44	51	42
sum	200	200	200	200	200

Core TAI 1





Core TAI 1: Corelog, texture and siliciclastics

Core TAI 1: Grain-size analyses

core depth (cm)	>2 mm (wt%)	2-0.25 mm (wt%)	0.25-0.125 mm (wt%)	<0.125 mm (wt%)
0	0.18	0.85	1.10	97.86
2.5	0.14	1.32	1.39	97.15
5.0	1.20	3.08	2.74	92.98
7.5	0.75	1.50	1.45	96.30
10	0.12	1.00	1.25	97.63
12.5	0.60	1.30	1.35	96.75
15.0	0.30	2.04	1.54	96.12
17.5	0.66	3.28	2.36	93.71
20	1.95	5.93	3.67	88.45
22.5	0.53	2.94	2.14	94.40
25.0	1.10	3.26	2.20	93.44
27.5	1.08	3.12	2.54	93.26
30	0.72	3.38	2.17	93.73
32.5	0.65	2.13	1.82	95.40
35.0	0.53	2.45	1.39	95.62
37.5	2.70	3.73	1.98	91.60
40	0.69	2.70	2.11	94.50
42.5	1.06	2.44	1.73	94.76
45.0	1.18	4.72	2.44	91.66
47.5	2.22	4.22	2.42	91.14
50	1.96	2.67	1.79	93.58
52.5	0.72	2.76	1.97	94.55
55.0	1.29	3.13	2.08	93.50
57.5	0.69	2.56	2.03	94.72
60	1.73	3.47	2.10	92.70
62.5	1.06	2.95	2.16	93.83
65.0	0.82	4.75	2.69	91.74
67.5	1.52	3.83	2.18	92.47
70	1.01	3.85	2.41	92.74
72.5	0.77	3.28	2.30	93.66
75.0	1.18	4.15	2.60	92.06
77.5	1.34	4.47	2.71	91.47
80	0.34	2.48	1.79	95.38
82.5	1.00	2.79	2.04	94.17
85.0	2.66	3.69	2.27	91.38
87.5	1.47	5.02	2.57	90.94
90	1.74	5.16	2.01	91.09
92.5	2.08	5.98	2.86	89.07
95.0	1.53	5.10	2.46	90.91
97.5	1.58	4.04	2.37	92.02
100	1.72	5.08	2.31	90.89
102.5	0.39	2.44	1.61	95.56
105.0	1.16	3.71	1.77	93.36
107.5	1.06	3.51	2.07	93.37
110	1.09	3.81	2.62	92.49
112.5	1.13	3.97	1.96	92.94
115.0	3.81	5.89	2.48	87.82
117.5	2.36	6.92	2.24	88.48
120	2.02	8.61	1.97	87.39
122.5	1.34	5.09	2.35	91.21
125.0	0.84	3.13	1.92	94.11
127.5	1.35	2.66	1.48	94.51
130	1.04	3.48	1.62	93.87

Continue on next page

core depth (cm)	>2 mm (wt%)	2-0.25 mm (wt%)	0.25-0.125 mm (wt%)	<0.125 mm (wt%)
132.2	0.36	2.85	1.40	95.39
135.0	0.51	2.10	1.17	96.21
137.5	0.68	2.46	1.11	95.75
140	0.38	1.63	1.14	96.86
142.5	0.43	1.49	0.96	97.11
145.0	0.19	1.65	0.97	97.18
147.5	0.72	2.02	1.03	96.24
150	0.50	1.49	0.95	97.06
152.5	1.52	2.34	1.06	95.09
155.0	3.31	3.98	1.39	91.32
157.5	0.19	2.11	1.08	96.62
160	0.89	2.57	1.31	95.24
162.5	0.40	1.75	1.07	96.78
165.0	0.25	1.94	0.90	96.91
167.5	0.42	1.91	0.85	96.82
170	0.10	1.28	0.59	98.04
172.5	0.63	1.80	0.81	96.76
175.0	1.35	2.34	1.15	95.16
177.5	0.53	1.38	0.58	97.50
180	1.25	1.89	0.86	96.00
182.5	0.88	1.73	0.75	96.63
185.0	0.49	3.16	1.18	95.18
187.5	1.80	2.21	0.71	95.29
190	0.96	1.16	0.70	97.19
192.5	0.50	2.23	1.01	96.27
195.0	1.51	1.86	0.83	95.81
197.5	0.21	1.23	0.60	97.97
200	0.86	1.68	0.60	96.86
202.5	0.30	1.14	0.47	98.09
205.0	0.66	1.18	0.49	97.68
207.5	0.27	0.90	0.54	98.29
210	0.93	1.05	0.57	97.45
212.5	0.60	1.50	0.67	97.23
215.0	1.10	1.71	0.61	96.57
217.5	0.55	1.24	0.59	97.62
220	2.75	1.83	0.80	94.62
222.5	2.09	1.36	0.84	95.71
225.0	1.20	1.98	1.23	95.59
227.5	1.39	1.92	1.16	95.53
230	3.95	2.25	1.14	92.66
232.5	0.92	1.58	1.00	96.49
235.0	1.51	2.21	1.15	95.12
237.5	1.09	2.26	1.26	95.40
240	0.98	2.43	1.19	95.40
242.5	1.07	1.36	0.87	96.71
245.0	1.79	2.45	1.35	94.41
247.5	1.15	1.87	1.06	95.92
250	2.39	2.74	1.49	93.37
252.5	2.03	3.91	1.60	92.46
255.0	3.51	4.05	1.59	90.85
257.5	2.06	2.52	1.00	94.42
260	2.82	4.62	1.67	90.89
262.5	4.29	4.58	1.73	89.40
265.0	5.04	4.24	1.58	89.13
267.5	5.32	3.90	1.57	89.20

Continue on next page

core depth (cm)	>2 mm (wt%)	2-0.25 mm (wt%)	0.25-0.125 mm (wt%)	<0.125 mm (wt%)
270	3.02	4.19	1.50	91.30
272.5	5.19	5.79	1.70	87.32
275.0	7.51	5.37	1.60	85.53
277.5	12.85	10.86	2.05	74.24
279-281	17.45	8.49	1.42	72.63
289-291	40.30	9.99	1.23	48.48
299-301	46.73	9.52	1.48	42.27
309-311	17.08	7.35	1.27	74.29
319-321	27.17	8.15	1.21	63.46
329-331	24.46	8.07	1.14	66.33
338-340 cc	63.28	6.12	0.98	29.63

CURRICULUM VITAE

Anja Isaack

Personal Details

Date of Birth: ■■■■■■■■■■

Place of Birth: Tübingen, Germany

Citizenship: German

Work Experience

- Since 06/2014** Research associate at the Institut für Geowissenschaften, Goethe Universität Frankfurt in the working group of Prof. Dr. Eberhard Gischler; DFG-Project Gi222/23: „Holocene development of reefs and lagoons of Bora Bora, Darwin’s type barrier reef (French Polynesia): the influence of sea level, antecedent topography and subsidence“
- 01/2014 – 05/2014** Research associate at the Institut für Geowissenschaften, Goethe Universität Frankfurt in the working group of Prof. Dr. Eberhard Gischler
- 10/2013 – 12/2013** Temporary job at Thomson Linear Motion GmbH, Wolfschlugen
- Since 08/2013** Foundation of a small scale enterprise (promotion and office services)
Former employers: media one GmbH Communication Group Frankfurt Berlin; HIC for FAIR (Helmholtz International Center for Facility for Antiproton and Ion Research), Frankfurt am Main; Thomson Linear Motion GmbH, Wolfschlugen
- 04/2010 – 06/2011** Student assistant at the Institut für Geowissenschaften, Goethe Universität Frankfurt am Main in the Emmy–Noether Research Group, PD Dr. Oliver Friedrich
- 07/2009 – 07/2013** Student assistant at the Institut für Geowissenschaften, Goethe Universität Frankfurt am Main in the working group of Prof. Dr. Eberhard Gischler

Education

- 04/2012 – 11/2013** Institut für Geowissenschaften, Goethe Universität Frankfurt am Main
Master of Science Geology and Paleontology
Thesis: “*Recent Sedimentary Facies of the Dry Tortugas, Gulf of Mexico, South–Florida, USA*”
- 03/2008 – 03/2012** Institut für Geowissenschaften, Goethe Universität Frankfurt am Main
Bachelor of Science in Geoscience
Thesis: “*Holocene development of the southern lagoons of two atolls Lighthouse Reef and Turneffe Islands, Belize, Centralamerica*”